Digital Photogrammetric Mapping of Canopy Height in a Radiata Pine Plantation

Antonius Bambang Wijanarto

Submitted in fulfillment of the requirements for the degree of

Doctor of Philosophy

Centre for Spatial Information Science

School of Geography and Environmental Studies

UNIVERSITY OF TASMANIA

October 2000

Declaration

Except as stated herein, this thesis does not contain any material which has been accepted for the award of any other degree or diploma in any university nor, to the best of my knowledge and belief, does it contain any copy or paraphrase of material previously published or written by another person, except where due reference is made in the text of this thesis.

signed: 

FOR MUM and DAD,

Novi, Sigit, Andri and Dedi

Abstract

Tree height is a crucial stand characteristic in forest inventories and has been used widely to estimate timber volume, to monitor growth rate, and as an indicator of site quality. Current tree heighting relies on field measurements, with sampling rates, which are typically less than one percent. Low sampling rates produce high variation in measured parameters and reduce statistical reliability. Digital photogrammetry provides an opportunity to automate the measurement of tree heights and to generate digital models of forest canopies. A sufficiently dense canopy model, with tree height data at nearly 100% sampling rates, has the potential to improve significantly the reliability of strategic and operational forest inventory. This study investigates the utility of digital photogrammetric techniques to map tree height within radiata pine plantations.

A digital photogrammetric workstation, the Leica Helava DPW 770, was used to generate digital canopy models of both closed canopy and thinned stands. The performance of the image-matching algorithm was assessed using scanned aerial photos of different film types and scales, including colour, black and white, colour infrared, and black and white infrared, at 1:5,000, 1:10,000, and 1:15,000 scales.

Canopy height data were obtained by subtracting a DTM from the photogrammetric data. Various filtering strategies were used to process the canopy height data including median, mean tallest tree, adaptive wavelet, adaptive Fourier filtering, and NDVI–thresholding techniques. A method for improving automatically derived tree height using a limited number of manually measured tree heights using a DPW was also developed. The reliability of the derived data was assessed by comparing it with a reference DCM produced using an analytical stereoplotter at a 10m grid, and field measurements.

The study demonstrates that tree heights in a coniferous forest can be mapped using digital photogrammetric methods and appropriate post–processing. Filtered digital photogrammetric data are shown comparable to analytical stereoplotter data and field-measured data, particularly for dense stand. With the efficiency and high sampling rates afforded by digital photogrammetric techniques, this study demonstrates the potential application of photogrammetrically measured tree height data to forest inventory.

Table of Contents

Acknowledgments

I would like to extend my special thanks to the following people for their contribution to this thesis.

The research was completed under the supervision of Dr. Jon Osborn, who patiently kept me on track, and facilitated my interaction with many people and organisations who directly or indirectly have supported the project.

The digital photogrammetric workstation, the Leica–Helava DPW 770, was made available by the Hydro Electric Commission (HEC) of Tasmania, Survey and GIS Division. My thanks to Mr. Keith Stove and Mr. Graham Humphries.

Access to the study area and aerial photography was provided by Fletcher Challenge Paper Australia through Mr. Tim Osborn, Mr. Andrew Dickinson, and Mr. John Webb. These people provided a great assistance, particularly in the early stages of the research.

The GPS fieldwork was completed with assistance from Nguyen Ngoc Lau, Murray Webster, Mark Morffew, Anthony Mewengkang, and Bambang Rudito. Mark Morffew generated the colour infrared orthoimage for the NDVI–thresholding described in Chapters 5 and 6, and assisted with the GPS processing.

Finally, this research was made possible through the financial support of the Tasmanian Forest Research Council and an Australian Government Overseas Postgraduate Research Scholarship.

Chapter 1. Introduction

1.1. The Importance of Forest Inventory

Forest management is concerned with ensuring a sustainable supply of timber and other forest products while maintaining sound ecological practices. Economically viable and ecologically sound forest management can only be achieved by careful planning. The steps involved in the management of a forest usually include [Susilawati and Weir 1990]:

- *forest inventory*, in which information is gathered about the environment to identify where decisions and action are needed;
- *planning*, which permits the analysis of alternative courses of action when models are developed;
- *policy–making*, during which a particular course of action is selected;
- *operation,* in which the chosen action is implemented; and
- *monitoring,* in which the results of the operation are reviewed.

Extensive data collection and monitoring are required to evaluate the rate and course of early plant succession, and to prescribe the necessary vegetation management treatment to fulfil the objectives of forest management. New technology such as geographic information systems can enhance decision–making, but require comprehensive and high–quality data as inputs. Therefore, data collection methods must be capable of delivering objective, quantitative, multi–dimensional, multi–scale, spatially accurate, and cost–effective data for forest management decision making and monitoring [Pitt *et al.* 1997].

Accurate and efficient data collection has been one of the most important and difficult tasks faced by forest managers. Most of the established inventory methods

involve very time consuming and expensive field measurements of a large number of sample plots. Surveys range from simple visual observations made from an aircraft, road vehicle, or by foot, to installation of field plots to measure variables such as vegetation height, cover, and health [Congalton and Biging 1992, Gillis and Leckie 1996].

Recognition of the importance of efficient forest inventory methods has led to extensive research and the development of various different methods for forest classification and forest size measurement. These include the applications of photogrammetry, remote sensing, geographic information systems, and other computer–aided analysis and mapping techniques.

1.1.1. Forest Parameters and Stand Variables

Forest inventories are generally defined in terms of their function, which is to determine the extent, scale, quantity, quality and the location of both forest and non-forest parameters (Table 1.1) [e.g. Biging *et al.* 1991, Congalton and Biging 1992, Long 1994].

Forest	Stand (forest) types	
	Stand boundaries	
	Stand structure variables	Species composition, height classes, age classes, density (canopy closures and stocking), diameter (basal area), timber defect, volume, leaf area index (LAI) and other stand variables
	Location	
	Status	Conditions, Thinned Unthinned alive/cut
Non–forest	Farm land, Water, rocks, roads and tracks etc.	

Table 1.1. Components of a forest inventory [adapted from Congalton and Biging 1992, Long 1994].

In plantation forests, the number of forest parameters collected may be reduced since some of the parameters are already known or have been measured prior to

plantation, for example, age and type of plantation (often homogeneous), and terrain characteristics. Other parameters such as diameter at breast height (DBH) and tree height must however be measured. Generally, forest managers collect these parameters using statistical sampling methods and rely heavily on measurements of individual trees within sample plots.

1.1.2. The Need to Measure Tree Height

Tree heights are a crucial stand characteristic in forest inventory. Tree height:

- contributes to estimated timber volume;
- is used to monitor growth rate; and
- is used as an indicator of site quality.

Tree heights are often represented using the parameters stand mean height and stand mean dominant height (MDH) [e.g. Carron 1968, Candy 1989a and 1989b]. Stand mean height is normally not the average of individual tree heights, but an approximation to it, associated with the arithmetic stand mean basal area. Fletcher Challenge Paper Australia (FCPA), who manage the plantation used in this research, defines mean dominant height as the mean height of the sixty trees with the largest diameter at breast height (DBH) per hectare.

The major objective of forest inventory is to estimate timber yield of harvesting events over time. Individual tree volume is a function of diameter at breast height (DBH), tree height and age [Candy 1989a]. Total standing timber volume for stands is a function of mean dominant height and stand basal area [Candy 1989b].

1.2. Photogrammetric Measurement of Tree Height

Tree height is a parameter that has the potential to be measured and exploited using remote sensing techniques including radar [e.g. Hagberg *et al.* 1995, Hyyppä and Hallikainen 1996], airborne laser [e.g. Aldred and Bonnor 1985, Nelson *et al.* 1988, Jacobs *et al.* 1993, Nilsson 1996, Naesset 1997a and 1997b, Means *et al.* 1999], and aerial photography.

Aerial photography has previously been used to measure tree height using medium to large–scale aerial photographs from parallax measurements [e.g. Andrews 1936, Worley and Landis 1954], tree shadows [e.g. Johnson 1954],

stereoplotters [e.g. Johnson 1958, Kippen and Sayn–Wittgenstein 1964, Aldred and Kippen 1967, Sayn–Wittgenstein and Aldred 1967, Avery and Canning 1973, Titus and Morgan 1985, Nielsen 1997, Reutebuch and Ahmed 1997], and manually using a digital photogrammetric workstation [e.g. Gagnon *et al.* 1993, Kovats 1997]. More detailed descriptions are included in Section 2.4.2.

The shift from analytical to digital photogrammetry offers an opportunity to automate the measurement of tree heights. Digital photogrammetric workstations include modules to generate digital elevation models (DEMs) automatically by image matching techniques in stereo pairs of scanned aerial photographs. Over forested terrain the DEM will include tree height data. Automation has the potential to provide tree height data at nearly 100% sampling rates, with consequent potential to improve the reliability of timber volume estimates.

The use of digital photogrammetry for automatic terrain extraction has been an important innovation in topographic mapping and related applications. To date, however, very few organisations have attempted to use this advanced technology to measure forest parameters automatically, relying instead on conventional methods of field inventory and film–based aerial photo–interpretation. This suggests a need for further study to determine the potential of digital photogrammetry to contribute to forest inventory, in particular tree height.

1.3. Research Objectives

The objectives of this study were to determine whether high resolution scanned aerial photography can be used to estimate canopy height in a Radiata pine plantation, and to develop methods to represent the extracted data in a form that can contribute to forest inventory and management. Specific objectives were as follows:

(1) to test the application of the image matching algorithms in a digital photogrammetric workstation to estimate canopy height over various canopy types, using different scales of aerial photography and different types of film;
(2) to determine the most suitable scale and film type to measure canopy height;
(3) to develop, test and compare various data filtering methods to extract data reliably which has been generated from the DPW;

(4) to compare data derived from a DPW with tree heights measured using an analytical stereoplotter, and to quantify the accuracy of the automatic methods;

(5) to develop a method for ground truthing or improving automatically derived digital photogrammetric tree heights using a small number of manually measured photogrammetric tree heights.

1.4. Thesis Outline

This thesis is divided into eight chapters. In this chapter the importance of forest inventory, the need to measure tree height and the objectives of the research have been introduced.

Chapters 2 and 3 provide the necessary background information for photogrammetrists and foresters. Chapter 2 is a review of relevant background information concerning forest inventory methods and Chapter 3 is a review of image matching methods employed by digital photogrammetric workstations.

Chapter 4 presents the methods and procedures used to collect field data, including tree heights, DTM data, and ground control for photogrammetric measurement. Chapter 4 also describes the acquisition of aerial photography, and the generation of a tree height model from aerial photographs using an analytical stereoplotter.

In Chapter 5, methods of measuring tree height using the digital photogrammetric workstation and methods of processing the data into useful and meaningful information are presented. The DTM extraction strategies and image processing filtering strategies are described.

Chapter 6 presents an analysis of the different tree heighting methods for both the closed canopy stands and thinned stands. In this chapter, data derived from a DPW are compared with data derived from an analytical stereoplotter. The analysis includes visual inspections and comparisons of statistical results, distributions and image profiles.

Chapter 7 presents methods for improving the automatically derived digital photogrammetric data using manually measured photogrammetric data.

Chapter 8 provides a summary, conclusions, and recommendations for future work.

Chapter 2. Measuring Forest Inventory

2.1. Introduction

Remote sensing techniques have been used with varying degrees of success in forest inventory to measure forest parameters. Remote sensing techniques can offer high repeatability, multi–dimensional, multi–spectral, multi–resolution and GIS compatible data. Field measurement remains, however, the principal mean of data acquisition for forest inventory. Most studies have focused on coniferous forests, such as pine plantations, which tend to be more uniform and more distinguishable from other vegetation types.

There is a range of remote sensing systems capable of providing data useful to forest inventory. These include aerial photography, airborne video, line imagers, airborne laser, airborne radar, Landsat TM, Landsat MSS, SPOT and Radarsat. The characteristics of these sensors are summarised in Table 2.1.

This chapter provides a general review of methods used to measure forest parameters over coniferous forests, focusing on methods of measuring tree height. For tree height measurement in particular, three competing technologies are discussed in detail. These technologies are photogrammetry, airborne laser, and radar. Advantages and disadvantages of laser and radar technologies are identified in comparison to photogrammetric techniques.

Sensor	Pixel size	Image swath	Stereo viewing	Spectral Characteristics	Image form	Geometric correction	Weather Requirement	Potential uses
Aerial photos	Depends on flying height, lens' focal length, and sensor format. Typically, resolution of aerial photo > digital camera > airborne video		Easy	Visible and near IR	Film or scanned digital	Easy	Clear to light cloud cover	Mapping Stratification Sampling
Digital camera			Easy	Visible and near, mid and thermal IR (3 to 8 bands)	Digital	Easy	Clear to light cloud cover	Mapping Stratification Sampling
Airborne Video			Moderate	Visible and near, mid and thermal IR (3 to 8 bands)	Analog or digital	Moderate	Clear to light cloud cover	Stratification Sampling
CASI	No. of bands and flying height influence the spatial resolution, e.g. 30cm can be achieved from 1 band, 60cm from 5 bands and 1m from 10 bands at same flying height	150m to 5km	Difficult	Visible to near IR (1 to 19 bands)	Digital	Difficult	Clear to light cloud cover	Stratification Sampling
Landsat MSS	79m and 82m	185km	No	Visible + near IR (4 bands)	Digital	Easy	Cloud–free	Mapping Stratification
Landsat TM	30m	185km	No	Visible, near and mid IR (6 bands) + thermal IR @ 120m	Digital	Easy	Cloud–free	Mapping Stratification
SPOT	10m or 20m	65km	Difficult	Panchromatic visible, near IR (3 bands)	Digital	Easy	Cloud–free	Mapping Stratification
Airborne radar	>1m	>4km	Difficult	Microwave	Digital	Difficult	None	Mapping Stratification Sampling
Radarsat	>10m	50–500km	Easy	Microwave	Digital	Moderate	None	Mapping Sampling
Laser, LIDAR	10–50cm	Point	N/A	Generally near IR	Digital	Moderate	No rain	Sampling

Table 2.1: Typical sensor characteristics [adapted from Pitt *et al.* 1997].

2.2. Field Survey

2.2.1. Introduction

Field survey is currently still the principal means of collecting forest parameters. In a forest inventory that involves remotely sensed data, it is necessary to check the data with the field measurements. The field–measured data (ground truth data) can be used to overcome any confusion in forest measurement or classification, and to improve forest inventory results. The following are two approaches to collecting ground data [e.g. Congalton and Biging 1992, Gillis and Leckie 1996]:

(i) *Visual census*

In this approach, a field crew will visually carry out a census of dominant species, size class of dominant species, crown closure of dominant size class, and crown closure of all tree species combined. This type of survey can be made from an aircraft, road vehicle, or by foot.

(ii) *Plot measurement*

A plot is a permanent or temporary-sampling unit established in forests to collect forest parameters. The size and shape of plots may vary with forest conditions. The shapes may be regular, for example, rectangular, square, circular, narrow–width rectangular; or they may be irregular, for example, basal–area sweeps. The relative efficiency of different sizes and shapes is influenced by the purpose of the inventory, and can be compared by estimating the respective sampling errors [Gambill *et al.* 1985]. As a guiding principle, the size of a plot must be related to the elements of the population. A typical plot size for a coniferous plantation forest is between 0.005 and 0.01 hectares [e.g. Gambill *et al.* 1985].

In plot measurement, there are two types of variables: *estimated* and *measured.* The estimated variables include:

- species,
- timber product (sawlog, pulp),
- habitat value (for native forest), and
- timber defect.

The measured variables include:

- diameter at breast height (DBH),

- height,
- leaf area index (LAI),
- crown closure, and
- crown size.

The most difficult variables to measure are usually crown closure and tree height, which require considerable experience to obtain adequate precision [Congalton and Biging 1992].

2.2.2. Tree Height Measurement

There are three representative methods of measuring tree height in the field: *height–matching* method, *distance–measure* method, and *angle–measure* method [e.g. Korning and Thomsen 1994].

(i) Height–matching method

This method involves one observer at a point where the entire tree can be seen, who matches the top and the base of the tree to the ends of a hand–held object of length l (Figure 2.1). From the base of the object, a portion of length p is marked. A second person at the base of the tree lifts a rod (height = f) until the observer sees its top matching with the mark of p seen by the observer. The tree height is

$$h = \frac{f \times l}{p}.$$

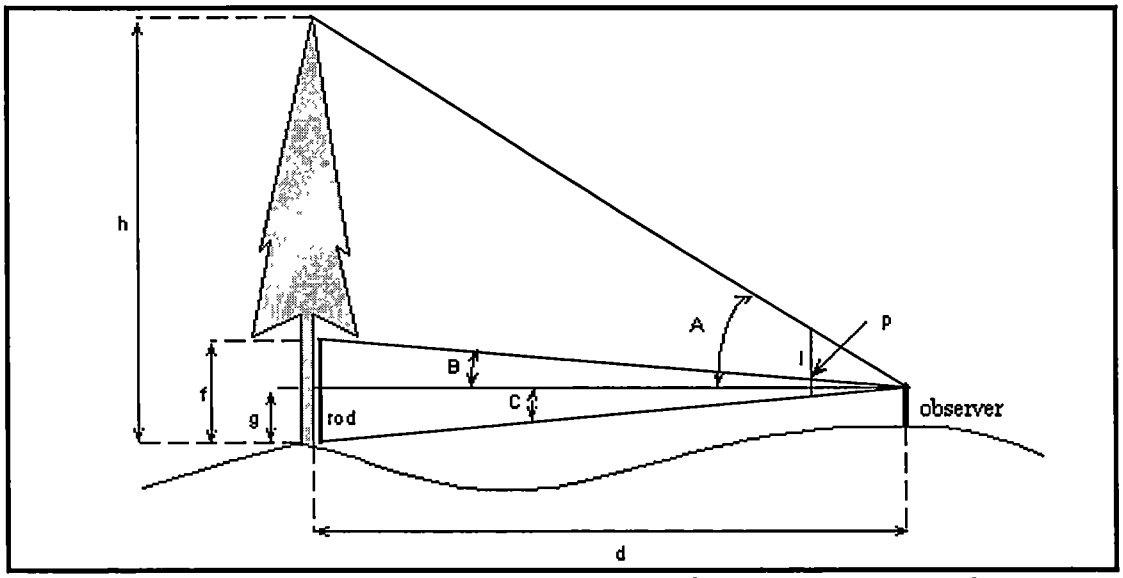

Figure 2.1: Angles and distances employed in the measurement of tree heights [Adapted from Korning and Thomsen 1994].

(ii) Distance–measured method

In this method, one horizontal distance (d) and two angles (A and C) are measured (Figure 2.1). The horizontal distance (d) is measured from the tree to an observation point. The angles are measured using a clinometer. These are the angle between the horizontal plane and the treetop (A) and the angle between the horizontal plane and the tree base (C). The height h is calculated as

$$h = d(\tan A + \tan C).$$

(iii) Angle–measured method

In this method, three angles A, B and C are measured (Figure 2.1). B is the angle to the top of a pole of length *f*, placed at the base of the tree. The tree height *h* can be calculated from

$$h = \frac{(\tan A - \tan C)}{(\tan B - \tan C)}.$$

The accuracy of tree height measurements using the methods described depends on several factors including the accuracy of the vertical angle and/or distance measurements, and the visibility of the tree. Vertical angles are usually measured using a clinometer, and distances are measured using a tape or an electronic device. Measurement of distance using a tape is not as efficient as using an electronic device. However, measurement using an electronic device requires a good visibility or clearance to the tree being measured. Further, angle measurements require good visibility to the top and the bottom of a tree, which can be difficult especially in dense forests.

Examples of modern electronic instruments commonly used to measure tree height in forest inventory are the Forestor Vertex, which measures distance using ultrasonic pulses, and the Impulse Laser 200 (now called Impulse Laser Rangefinder and Hypsometer), which uses a near infrared laser beam. Both devices have a built–in clinometer to measure vertical angle. Typical specifications for these devices are a distance precision of ±1% and an angular precision of ±0.1 degree. No published papers have been found indicating the typical tree height accuracy that can be achieved in practice. According to Fletcher Challenge Paper personnel [Dickinson and Webb 1999], an accuracy of ±0.5m can be achieved in good conditions, reducing to ±1.5m in less satisfactory conditions.

2.3. Aerial Photographs

2.3.1. Introduction

Aerial photography is regarded as a reliable method to measure some forest parameters and has played a key role in forest mapping and inventory systems. It is the most frequently utilised remote sensing tool for forest assessment [Gillis and Leckie 1996]. Aerial camera performance has been improved by computer designed lenses, forward motion compensation, angular motion stabilisation, and integrated geopositioning and exposure control systems [Fent *et al.* 1995, Light 1996]. Aerial films have also been improved to address issues such as film speed, spectral sensitivity, resolution, colour rendition, and processing [Fent *et al.* 1995]. Factors that influence the reliability of aerial photography are described in the following Sections.

2.3.2. Considerations in the Use of Aerial Photographs

The most important consideration when preparing specifications for aerial photography is the photographic scale. Photographic scale is a critical determinant of photo–interpretability. Therefore, the choice of scale can maximise the utility of photographs for particular projects.

A wide range of photographic scales has been used for forest inventory. Usually, the smaller scales have been used for mapping forest types and estimating stand volumes, whereas large–scale photographs have been used for tree volume estimation and regeneration assessment. Table 2.2 summarises several information thresholds according to the photographic scale or image resolution. Other factors include:

(1) **Camera geometry**: The geometry of a camera system affects the visual penetration of forest canopies. For a given camera format, longer focal lengths provide greater penetration than shorter focal lengths for photographs at the same scale, but result in weaker vertical geometry and less ground coverage for a given flying height.

(2) **Film type**: There are four film types available: colour, black and white, colour infrared, and black and white infrared. Colour photographs have been used

extensively in API for forest inventory and they are generally superior to black and white photographs for forest mensuration from aerial photographs. Black and white film may offer some advantages including, for example, high spatial resolution and smaller file size when scanned. Infrared films (colour or black and white) are also used in forest inventory. The advantages of using IR film include the ability to interpret and measure energy spectra which are not visible to the human eye, and the ability to measure forest parameters which depend on spectral sensitivity in the near infrared, for example, tree health and species [e.g. Elvidge 1990].

	Photo–scale	Forest characteristics	Remarks
1	<1:30,000	Forest/non–forest, evergreen /deciduous /mixed, some size classes, occasional forest types, stand size classes, stand physiognomy, some forest types	Tone, colour contrast, textural contrast, site, stand height, crown cover, crown size (qualitative)
2	1:30,000 to 1:25,000	As 1, more details	As 1, API easier
3	1:20,000 to 1:10,000	As 1, forest types, stand volumes, tree volumes, some tree species, and understorey data	As 1, but quantitative, photogrammetric measurement (E.g. Tree height)
4	1:10,000 to 1:8,000	As 3, stand composition by tree species	As 3, colour/tone contrast within tree crowns
5	1:5,000 to 1:4,000	As 4, individual tree species	As 4, branching habit
6	>1:2,000	As 5, tree species identification, more reliable tree volumes, improve shrub characteristics	As 5, crown details

Table 2.2: Forest information thresholds over a range of aerial photographic scales [adapted from Howard 1990: 270].

(3) **Sun angle and illumination**: Appropriate sun angle and illumination conditions can provide aerial photographs with reduced shadow: shadowless photography results in significant advantages when understorey and ground conditions are to be interpreted [e.g. Bradshaw 1974, Bradshaw and Chandler 1978], and when tree heights are to be measured [e.g. Lyons 1967, Spencer 1979].

(4) **Film exposure and processing**: Film exposure and processing affect the image quality and must be monitored to ensure that the best results for interpretation are achieved. Interpretation from transparencies viewed by transmitted light is

superior to prints [Welch 1968] with film diapositives widely used in photogrammetric applications. For digital processing, the films are scanned. The choice of scanning resolution affects the interpretability of digital images and the file size.

Photogrammetric scanners must provide high spatial resolution and high radiometric and geometric accuracy. The typical specifications of ten photogrammetric scanners are summarised in Table 2.3.

Brand	Model	Geometric accuracy (μm)	Radiometric accuracy (DN)	Price (US$)
LH System	DSW 300	2	1–2	145,000
Zeiss	SCAi	2	±1.5	138,000
XL Vision, ISM	OrthoVision, XL–10	<3	–	95,000
Vexcel Imaging	VX 4000	±2	±2	60,000
Wehrli and Assoc. Inc	RM–2 Rastermaster	–	–	55,000
Zeiss/ Intergraph	PhotoScan 1	<2	±2	147,000
Int'l Systemap	DiSC	5	–	75,000
Lenzar	Lenzpro 2000 Multimedia	<3 or 0.1 pixel	±2.5	165,000
DBA System Inc.	DFS	1	–	350,000
GeoSystem	Delta–Scan	3	–	25,000

Table 2.3: Photogrammetric scanners (status January 1998) [Adapted from Baltsavias 1998].

2.3.3. Tree Height from Aerial Photographs

2.3.3.1. Photo Measurement

Photo interpretation and measurement may be grouped into two categories: *direct* and *indirect* measurements. Direct measurements are taken directly from the photograph, and these include stand height, visible crown diameter, and degree of stocking (individual crown count and percent crown cover). The only errors considered in direct measurements are sampling errors and related measurement errors. Indirect measurement, such as stem diameter at breast height, form class, site index, growth, age, stand structure, volume and basal area, are obtained through regression and correlation procedures and include additional variation resulting from imperfect correlation [Paine 1981: 418–420].

Determination of the height of an individual tree, or mean height of a stand of trees, is one of the most important operations in the measurement of standing

timber. Conventionally, there are three methods of height measurement:

(i) measurement of displacement using a single photograph,

(ii) measurement of shadow length, and

(iii) measurement of parallax differences on stereophotography.

The main difficulty is finding the ground in a dense forest. The measurement of tree heights using stereophotography is commonly still based on conventional methods in which the operator places a floating mark onto the ground as close as possible to the base of a tree and then places the floating mark on top of the tree. In a dense forest, the photo interpreter must look for a hole in the canopy and then decide whether the surface seen at the bottom is the ground or vegetation with a significant height. Measurement is usually easier when the aerial photographs are taken after the forest has been thinned or cleared.

2.3.3.2. Tree Height from Large–scale Photography

Large–scale photographs have been used to measure tree height using simple parallax heighting methods [e.g. Andrews 1936, Johnson 1958], analogue stereoplotters [e.g. Kippen and Sayn–Wittgenstein 1964, Aldred and Kippen 1967, Sayn–Wittgenstein and Aldred 1967, Avery and Canning 1973], analytical stereoplotters [e.g. Titus and Morgan 1985, Nielsen 1997, Reutebuch and Ahmed 1997], and digital photogrammetric systems [e.g. Gagnon *et al.* 1993, Kovats 1997].

Various large–scale camera systems have been designed such that the photoscale can be calculated without reference to ground control so that reliable measurements can be obtained at low cost. Two such methods are:

(i) sequential photography with known flying height, and

(ii) fixed–based photography.

Sequential photography involves a single camera. Photographic scales for the sequential photography method are calculated from the flying height determined with a precise altimeter. Fixed–based photography involves simultaneous exposure of two cameras, mounted on supports at a fixed and known separation and orientation. Photographic scales are calculated from the known separation and orientation of the stereo camera.

Using sequential photography and a digital photogrammetric system, the

relationship between scanning resolution and tree height accuracy over a coniferous plantation forest (black spruce and white pine) has been investigated by Gagnon *et al.* (1993). Aerial photography was acquired at 1:1,100 scale with 100m flying height, a base/height ratio of 0.1, and a stereo overlap of 80%. The camera used was a 70mm format Hasselblad with 100mm focal length lens. The photographs were scanned at three resolutions: 300, 450 and 600 dots per inch (equivalent to approximately 80, 55 and 40μm, respectively). Tree heights were measured manually using a floating mark in the stereo display. A point on the ground, which also appeared on the photograph, was used as the datum. Twenty-four trees (12 black spruce and 12 white pine) were measured and the results were compared against ground truth data. Standard deviations of ±0.48m, ±0.32m and ±0.24m were achieved for scanning resolutions of 300, 450 and 600 dpi, respectively.

The investigation conducted by Gagnon *et al.* (1993) demonstrates that scanning resolution affected the accuracy of tree height measurement, at least for manual measurement using a floating mark on the screen. The results also indicate that precision comparable to field measurements can be achieved using scanned, large–scale photography. In practice, the method could be used to replace field–measured tree height for small areas, such as for plot measurement. The method is relatively inexpensive since it employs small format photography and a low precision scanner. A disadvantage of the method is the problem of finding a visible ground surface.

A similar method was developed using a helicopter mounted with a pair of 70mm format cameras and 100mm focal length lenses, and using a fixed wing aircraft with 230mm format camera and 152mm focal length lens [Kovats 1997]. The photographs were acquired at several photoscales (1:800, 1:1,000 and 1:1,200) over a coniferous plantation forest of 3000 sample trees. Permanent ground control was placed across the study area prior to photography. The photogrammetric results were compared against ground truth data. Standard deviations of the differences from the ground truth data were ±0.34m at 1:800 scale for the helicopter photography and ±0.80m at 1:1,200 scale for the fixed wing photography.

Similar to Gagnon *et al.* (1993), the method developed by Kovat (1997)

demonstrates that large–scale photography can be used to measure tree heights with precision comparable to field measurement techniques. However, the method relies on many permanent targets over a large area, which must remain visible even when the trees have grown taller. On-board integrated GPS-inertial navigation systems at reasonable costs are not sufficiently accurate to replace ground control at these photoscales.

Other large–scale applications have been the use of small–format aerial photography to acquire detailed forest data [e.g. Nielsen 1997] and to monitor stand development using a twin camera helicopter boom [e.g. Reutebuch and Ahmed 1997].

2.3.3.3. Tree Height from Medium and Small–scale Photography

Tree heights have been measured using a pocket stereoscope and a parallax bar in the study by Allison (1956). Photographs were acquired at 1:10,000 and 1:20,000 scales from a combination of flying heights and 3.25-inch and 8-inch lenses. The photo–measured tree heights were compared against ground truth data. Under ideal conditions, tree heights were measured to within ±1.5m and ±3m from the ground truth data on 1:10,000 and 1:20,000 scale photography, respectively.

A similar technique was investigated by Johnson (1958) using both a parallax wedge and a parallax bar on 1:5,000, 1:10,000, 1:15,000 and 1:20,000 photographs. The method employed three different operators and various combinations of instruments, photographic scales and operators. In contrast to the finding of Allison (1956), Johnson found that errors in measured tree height were not associated with photographic scales, at least in the range from 1:5,000 to 1:20,000, but more likely associated with tree characteristics such as crown shape and tree size, and instrument operator skills.

Tree characteristics and instrument operator skills are important and can cause errors in tree heighting; however, the degree of interpretability of tree characteristics by an operator is greatly influenced by photographic scales. Measurements by different operators often produce different results at a given scale, but the differences are usually systematic. Johnson did not compare results in which each operator measured all of the tested photographs, and hence, the relationship between tree height accuracy and photographic scale for each operator.

No published research has been found that indicates the accuracy of tree height measurement from medium to small-scale photographs using analogue or analytical stereoplotters.

2.3.3.4. Mapping Tree Height Using a DPW – Previous Research

Carson *et al.* (1996) used a digital photogrammetric workstation to generate digital canopy models of forested areas in New Zealand using aerial photographs at four epochs: 1971, 1981, 1988 and 1994. The photographs were acquired at a scale of 1:25,000. The 1994 photography was in colour, whereas the previous photography was in BW. The images were scanned at 12.5μm to give a pixel size of approximately 0.31m. The areas consisted of mainly Radiata pine plantations, which were planted in 1973 and 1980. The different–epoch photographs provided different types of canopy closures (Table 2.4).

Area	Acres	1971	1981	1988	1994
1	40.0	Bare	Good crown closure (planted in 1973)	Thinned	Thinned again
2	10.6	Bare	Planted in 1980	Good crown closure	Heavily thinned
3	17.0	Bare	Good crown closure (planted 1973)	Good crown closure	Good crown closure but thinned

Table 2.4: Test areas [Carson *et al.* 1996].

A Leica–Helava DPW 770 was used to generate a canopy model of the forested areas. The DEMs were produced at 2m spacing using a variety of strategies. The strategies applied in this study were not described. The 1971 photography was used to generate a DTM of each area. The canopy height models were generated by subtracting the DTM of the 1971 photography from the canopy models of the 1981, 1988 and 1994 photography. The results are summarised in Table 2.5.

Area	Period	Mean (m)	Standard Deviation (m)
1	1971–1981	12.37	2.22
	1971–1988	10.80	10.10
	1971–1994	18.45	9.70
2	1971–1981	0.17	0.95
	1971–1988	11.29	2.10
	1981–1994	2.39	6.37
3	1971–1981	12.30	2.42
	1971–1988	20.90	3.04
	1971–1994	9.49	15.85

Table 2.5: Differences in heights between epochs [Carson *et al.* 1996].

As indicated in Table 2.5, the results were encouraging in areas of good canopy closure, but less encouraging in areas where the plantations had been thinned. In the thinned areas, the errors, as reported by Carson *et al.* (1996), were associated with the more irregular canopy structures produced from the thinning, in which more of the ground surfaces and long dark shadows of the trees were visible.

The 2m grid spacing used by Carson *et al.* (1996) was sufficient to create canopy models but not to model individual trees, especially for a coniferous shape. Further, with a 2m grid spacing the probability of any grid point falling on or very close to the top of a tree is reduced. This suggests a need to investigate a higher sampling rate or a denser grid spacing particularly over thinned canopies.

2.4. Radar

2.4.1. Introduction

Radar is an active remote sensing device that has developed rapidly for topographic mapping. Radar data can be collected from an aircraft (airborne radar systems) or from a satellite (spaceborne radar systems). Radar is able to penetrate cloud, operate in all weather conditions, and cover large areas in a single flight [e.g. Elhassan and Ali 1995].

A radar instrument emits microwave pulses to a surface via a transmitter. These pulses are reflected by the surface and a small part of this reflection can be detected by the radar antenna. Radiation reflected in the direction of the radar sensors is called backscatter. The amplitude and phase of the signal received by the antenna depend on the reflection at the surface. Variations in the intensity of backscatter, the time taken to return to the radar sensor, and the phase information, provide the fundamental data for Radar remote sensing [van Halsema and Hansen 1996].

2.4.1.1. Radar Wavelength and Polarisation

Radar is classified by its wavelength and polarisation. Radar wavelengths are classified into bands (Table 2.6).

There are two types of radar polarisation: horizontal (H) and vertical (V). Polarisation is horizontal if the electric vector is perpendicular to the plane of incidence and vertical if the electric vector is in the plane of incidence [Elachi

1987]. Polarisation in radar is also divided into two types: like polarisation and cross polarisation. Radar is said to be like polarised (or co-polarised) when the send and receive polarisation have the same orientation, and cross-polarised when the two polarisations are opposite. The send and receive polarisation are usually denoted as two letters: H for horizontal and V for vertical; for example, VH indicates the vertical send and horizontal receive.

Band	Wavelength (cm)	Frequency (MHz)
K_a	0.75–1.10	40,000–26,500
K	1.10–1.67	26,500–18,000
K_u	1.67–2.40	18,000–12,500
X	2.40–3.75	12,500–8,000
C	3.75–7.50	8,000–4,000
S	7.50–15	4,000–2,000
L	15–30	2,000–1,000
P	30–100	1,000–300

Table 2.6: Radar bands, wavelengths and frequencies [Adapted from Lillesand and Kiefer 1994: 668].

2.4.1.2. Imaging and Non–Imaging Radar

Radar may also be classified into imaging and non-imaging radar. Non-imaging radar systems are generally used for non-topographic mapping. The systems utilise low look angles and use Doppler shift to measure distance. Imaging radar systems use higher look angle (usually >20°). The systems are also referred to as side looking radar (SLR) or side looking airborne radar (SLAR). The backscatter signals detected by the radar sensor are recorded as pixel gray level values. One advantage of imaging radar is that the images produced can be viewed stereoscopically.

Synthetic aperture radar (SAR) is an imaging radar device developed to overcome the technical difficulties of constructing a very long antenna. In radar systems, longer antennas provide higher ground resolution and satellite radar would require a very long antenna in order to achieved desirable ground resolution. Modern spaceborne SAR now has multi–wavelength polarimetry (HH, HV, VH, and VV polarisation).

2.4.1.3. Radar Interferometry

Radar interferometry is a method of processing radar backscatter data of two

different SAR images of the same terrain, taken from slightly different positions or at different times. The changes of the path length can be measured and related to either surface topography or topographic deformation. A specially designed interferometry SAR would usually consist of two antennas. One antenna both transmits and receives the radar signal, while the second receives only. A spaceborne SAR has only one antenna; therefore, the repeatability of the satellite's orbit must be used. This method is called 'repeat pass interferometry' or 'across track interferometry' [Hagberg *et al.* 1995, van Halsema and Hanssen 1996].

The technique has some similarities to stereoscopic photogrammetry [van Halsema and Hanssen 1996], however there are two significant differences. In photogrammetry, the two overlapping images or photos have a baseline in the order of 60% of the height of the sensor (somewhat greater in the case of a superwide angle lens and less in the case of a normal angle lens), but for the SAR interferometry technique the baseline should be small since the scattering pixel can no longer be compared if the sensors are too far apart. The other significant difference is the definition of vertical resolution. The vertical resolution in photogrammetric techniques is usually a function of base to height ratio, whereas the vertical resolution in the interferometry technique is a function of wavelength.

Interferometric SAR (INSAR) is a promising technique for the production of detailed and accurate three-dimensional relief data of the Earth's surface, and detection of cm-scale movement of land surface features [Coulson 1996]. The technique has been used to measure mm-scale ground motion in agricultural fields using SEASAT data [e.g. Gabriel *et al.* 1989], and cm-scale to m-scale co-seismic displacement [e.g. Massonnet *et al.* 1993, Massonnet *et al.* 1995].

2.4.2. Applications of Radar in Forestry

There have been a number of attempts to use radar for forest inventory, using single or repeat pass interferometry and single or multi–frequency radar data. For example, forest biomass, tree geometry, and canopies have been measured using P band [e.g. Rignot *et al.* 1995], L band [e.g. Reich and Hussin 1993], and multi–frequency (bands P, L and C) [e.g. Ranson and Sun 1994, Ferrazzoli and Guerriero 1995, Imhoff 1995, Sun and Ranson 1995, Milne *et al.* 1996], and there have been

attempts to measure tree height using multi–frequency radar [e.g. Hagberg *et al.* 1995, Dobson *et al.* 1995, Hyyppä and Hallikainen 1996].

There are some important characteristics of radar, which may be useful when applied to forestry:

- Radar response is strongly influenced by the surface roughness characteristics of the object being mapped, incidence angle and the dielectric properties of the object [e.g. Bryan 1981, Brown 1987, Weishampel *et al.* 1994, Wilson 1996].
- Radar backscatter is a function of both the vertical and horizontal distribution of vegetation. The return signal strength is determined by tree height, trunk diameter, branching pattern and canopy characteristics as well as the distribution and size of plants within the resolving element of the radar system [e.g. Milne *et al.* 1996].
- The amount of penetration into the vegetation is a function of the radar frequency, as well as vegetation density and moisture content [e.g. van Zyl 1996].

2.4.3. Tree Height from Radar

There are two techniques that can be used to measure tree height for inventory using a radar system. These are interferometric and polarimetric techniques. Digital elevation models (DEM's) over forested terrain can be produced from repeat pass SAR interferometry. Tree heights can be measured in combination with another DEM or by combining interferograms at two different frequencies, for example using C and P bands (P band penetrates the canopy more than C band). The like polarisation gives a clear radar return both from the treetops and the ground. The ground reflections are partly due to penetration and partly due to gaps in the canopy.

Hagberg *et al.* (1995) used repeat pass interferometric techniques with ERS–1 SAR at C band to measure tree heights of fir canopies over relatively flat terrain. The ERS–1 SAR has a typical image coverage of 80×80 km and a pixel spacing of 12.5m×12.5m. The accuracy of tree height was investigated using various interferograms, created with combinations of images taken with baselines ranging from 12 to 303m and time intervals from 3 to 12 days. These were related to

weather conditions such as temperature and wind. The results from radar measurements were compared to tree heights obtained with conventional field measurements. Hagberg *et al.* found that over a dense forest with an average height of 15.6m measured in the field, the interferometric method measured the forest at an average height of 14.9±1.6m and that over more sparse forest with an average height of 9.9m measured in the field, the interferometric method measured the forest at an average height of 4.9±1.6m. Both results were obtained from baselines longer than 100m. In terms of weather conditions, the interferograms were found to be sensitive to air temperature, but not to wind condition. This was because of the stiffness of the fir canopy. Other types of forests may have different responses to wind.

Dobson *et al.* (1995) used polarimetric data derived from SIR–C/X–SAR data at L and C bands to estimate tree height in mixed forests including some types of coniferous trees. The fully polarimetric SIR–C data at L and C bands (VV polarised X–SAR data at X band) were processed. The pixel resolutions were 24.6m×26.9m for the L and C bands, and 25.5m×22.5m for the X band. Ground control points were used to co–register X band to the L and C bands of the SIR–C data, with an accuracy of ±25m.

Group	Local Species Name	Polarisation components	No. of Cases	Correlation (R^2)	RMSE (m)
Long needle	Upland conifers	L,vv	40	0.78	4.14
Short needle	Lowland conifers	L,vv–C,vv	4	0.63	0.62
Small branches, small needle	Lowland conifers	L,vv–C,hv	4	0.95	4.21
Small branches, medium needle	Upland conifer (Jack pine)	L,vv/L,hv	20	0.78	1.47
Large branches, long needle	Upland conifer (Red pine)	L,vv	19	0.89	3.45

Table 2.7: Accuracy of tree heighting using polarimetric SIR–C data over coniferous forests [adapted from Dobson *et al.* 1995].

The mean backscattering coefficients (σ^o) for each of the three linear polarisation combinations (HH, HV, VV) were used to estimate the mean height. Several models were used to estimate mean height of conifers, but using only the SIR–C data because of the misalignment between the SIR–C and X–SAR antennas. The results from radar measurements were compared to tree heights obtained with

conventional field measurements (Table 2.7). The recorded heights in the area ranged from 0–23m.

Hyyppä and Hallikainen (1996) used an airborne profiling radar system to measure tree height of pine and spruce dominated forests of variable density. In sparse stands, for example, there were less than 12 trees per plot (20m × 20m). The radar stand profiles were collected using a helicopter–borne ranging scatterometer, HUTSCAT (Helsinki University of Technology SCATterometer). HUTSCAT is non-imaging radar, which has a multi–channel capability (VV, HH, VH and HV polarisations at C and X band). Radar data were collected with a dual antenna configuration at incidence angles of 3, 20, 30 and 40 degree off nadir. The flying height was between 50m and 70m, providing a microwave footprint at tree top level of 5m approximately. Tree height was calculated along the flight lines. The results from radar measurements were compared to tree heights obtained with conventional field measurements, which indicated a mean height of 17.9±0.57m. Hyyppä and Hallikainen found that the response of all polarisation modes were equal, but that accuracy of the mean height and mean dominant height and their correlation values with the ground truth data were influenced by the incidence angles (Table 2.8). They found that radar derived mean height underestimated the field measured tree height for tree of more than 10.2m, whereas radar derived MDH overestimated field measured MDH for tree of more than 40m. The size of underestimation or overestimation depended on the height of trees for example, at 50m height radar mean height underestimated field mean height by 6% (3m) and overestimated field MDH by 0.2% (0.1m).

Predictor variable	Correlation (R^2) Standard Deviation.	Incidence angle (^{0})			
		3	20	30	40
Mean height	R^2	0.977	0.969	0.950	0.951
	Std. Dev.	1.04m	1.17m	1.43m	1.50m
Dominant height	R^2	0.976	0.964	0.940	0.940
	Std. Dev.	1.06m	1.28m	1.57m	1.64m

Table 2.8: Accuracy of estimated mean height and dominant height for pine trees [adapted from Hyyppä and Hallikainen 1996].

The investigations described above provide three important examples: spaceborne interferometry, spaceborne polarimetry, and airborne polarimetry. No published research has been found that describes the application of airborne radar

interferometry to tree height measurement. Spaceborne radar has been shown to be reliable, but only for measuring mean stand height. This is because of its low horizontal resolution (>10m, see also Table 2.1), which limits its integration with other geographic data. Airborne radar provides better horizontal resolution and higher sampling rates and consequently, tree height may be measured at the individual tree level. However, it requires substantially more intensive data collection and processing.

2.5. Airborne Laser

2.5.1. Introduction

Laser profiling and scanning systems transmit a laser pulse and determine the distance to the surface according to the time taken for the pulse to travel back to the sensor. In a profiling mode, only a single line of data directly beneath the aircraft is recorded. In scanning mode, strips of laser data are recorded orthogonally to the flight line. The width of the strip is a function of the scan angle and flying height. More detailed description can be seen in for example, Wehr and Lohr (1999).

In forestry, airborne laser technology has been used to measure forest canopy characteristics [e.g. Nelson *et al.* 1984], to create digital terrain models of forested areas [e.g. Krabill *et al.* 1984, Ackermann 1988, Blair *et al.* 1999], to estimate forest biomass and volume [e.g. Naesset 1997a], and to measure tree height in forest inventory [e.g. Aldred and Bonnor 1985, Nelson *et al.* 1988, Jacobs *et al.* 1993, Nilsson 1996, Naesset 1997b, Blair *et al.* 1999, Means *et al.* 1999].

2.5.2. Tree Height from Airborne Laser

Nilsson (1996) describes a helicopter borne Lidar profiling system. The system acquired and recorded data at a rate of 62 or 160 laser pulses per second. Four different beam divergences were tested: 2.5, 5.0, 7.5 and 10.0 mrad. The helicopter was flown over an even-aged Scots pine (*Pinus sylvestris*) stand at a flying height of approximately 300m above terrain. The ground data comprised tree height collected before and after a partial thinning, with mean heights of 12.3m and 12.4m, respectively. The laser was used to collect data before and after the

thinning, as shown in Table 2.9.

Tree heights were estimated using an algorithm that was initially developed for depth sounding. The results of the laser measurements were compared with the ground truth data. Both laser and ground data were transformed to a grid with a 0.5m resolution. To match both data sets, two methods were used. The first method used a correlation algorithm, which defined the correct position as the location with the highest correlation between the laser and field data (June data sets), whereas the second method used white plastic targets prior to laser data collection (October and December data sets).

Measurement	Beam divergence (mrad)	Footprint diameter (m)	Sampling distance (m)	Pulse repetition freq. (Hz)
June, Data #1	2.5	0.75	0.8	160
#2	5.0	1.5	1.5	160
#3	10.0	3.0	3.0	160
#4	5.0	3.0	1.5	62
#5	10.0	3.0	3.0	62
October, #1	2.5	0.75	1.0	160
#2	5.0	1.5	1.5	160
#3	7.5	2.25	1.5	160
December, #1	2.5	0.75	1.0	160
#2	7.5	2.25	1.5	160
#3	10.0	3.0	3.0	160

Table 2.9: The Lidar setting for the laser data sets used in the study [adapted from Nilsson 1996].

		Beam Divergence (mrad)							
		2.5		5.0		7.5		10.0	
		Field	Laser	Field	Laser	Field	Laser	Field	Laser
Mean (m)	June	12.6	8.9	12.5	9.3	–	–	12.7	9.5
	Oct.	12.6	10.2	12.5	10.0	12.7	10.0	–	–
	Dec.	12.6	9.5	–	–	12.5	10.4	12.7	9.9
Std Dev (m)	June	1.5	2.1	1.4	2.4	–	–	1.3	2.3
	Oct.	1.3	1.7	1.0	2.2	1.2	2.1	–	–
	Dec.	1.2	1.7	–	–	1.1	1.4	1.5	1.8

Table 2.10: Summary of results for field and laser tree height data [adapted from Nilsson 1996].

One of the problems reported in the study was to locate the test area from the helicopter, although it was marked with white targets. Aircraft geo–referencing such as differential GPS was not used in this investigation. The overall mean height measured using the Lidar system was reported to underestimate the true height by 2.1–3.7m. The results of using different footprints are summarised in

Table 2.10. For the June data sets, the use of a larger footprint produced a higher mean height but this efect was not apparent for the October and December data sets.

Naesset (1997b) describes an investigation of the Optech ALTM 1020 laser scanning system. The aircraft was flown over an area of spruce and pine dominated forests (age ranging from 31 to 145 years) at 640–825m above the ground and at a speed of 80m/s approximately. Laser data were collected with a maximum scan angle (off nadir) of 20°, which gave an average swath width of about 460–600m and side overlap between 70–425m. A beam divergence of 0.25 mrad was used, producing footprints with a diameter of approximately 13–16cm. The laser data were geo–referenced using differential GPS mounted on the plane, and were transformed into a local coordinate system to match with the digitised stand boundaries. The results from laser measurements were compared with data obtained with conventional field measurements (Table 2.11).

Test site	No. of stands	Stand area (ha)		Tree species distribution (%)		Height (m)	
		Range	Mean	Spruce	Pine	Range	Mean
1	18	0.7–4.6	1.5	3	97	8.1–24.3	17.5
2	18	0.5–3.4	1.5	69	28	8.2–20.1	14.9

Table 2.11: Summary of ground truth data [adapted from Naesset 1997b].

Test site	Comparison	*D* (m)	*SD* (m)
1	At 15m×15m	–0.4 (P≈0)	1.3
1	At 20m×20m	0.3 (P≈0)	1.3
1	At 30m×30m	1.1 (P<0.01)	1.3
2	At 15m×15m	0.1 (P≈0)	1.2
2	At 20m×20m	0.9 (P<0.01)	1.2
2	At 30m×30m	1.9 (P<0.001)	1.3

Table 2.12: Mean difference (*D= laser–ground data*) between laser and ground data and the standard deviation (*SD*) of the difference [adapted from Naesset 1997b].

The analysis was divided using two methods: original data analysis and grid analysis. For original data analysis, the laser mean height underestimated the ground height by 2.1–3.6m. For the grid analysis, both data sets were transformed into 15m×15m, 20m×20m, and 30m×30m grid cells. The results were more encouraging than the original analysis (Table 2.12).

A pulsed near infrared laser system developed by NASA, and called SLICER (scanning lidar imager of canopies by echo recovery) was used to measure tree height of coniferous forests in the Pacific Northwest of the United States [Means *et al.* 1999]. The aircraft was flown approximately 5000m above the ground, producing large laser footprints, nominally 10m in diameter. A differential GPS receiver was mounted on the aircraft to determine aircraft position, allowing the horizontal position of the first reflecting surface of each pulse to be determined to within ±5 to ±10m. SLICER data were compared with conventional field plot measurements (Table 2.13). The accuracy of matching the field plot and SLICER footprints was estimated to be 5–20m.

Forest type	No. of plots	Density (trees/ha)	Mean height (m)
Young	7	1975	17
Mature	5	948	33
Old–growth	9	689	43

Table 2.13: Summary of field plot data [adapted from Means *et al.* 1999].

Using a regression analysis, SLICER data correlated well with the field measured data (r^2=0.95), with a RMSE of 3.8m. For tree heights more than about 3m, heights derived from SLICER overestimated heights measured on the ground. Based on the given equation model, the amount of overestimation depends on tree height, from zero at 3m to about 9% at 50m (tree heights measured on the ground) [Acker 2000].

Laser systems have demonstrated potential for measuring terrain data and some forest parameters. In the case of tree heighting, depending on the size of the footprint, the data-recording rate is capable of measuring individual trees. Laser scanning techniques provide a high sample rate from the canopy but ground surface sampling near the edges of the scanning strips is limited because of its low penetration through vegetation [Pitt *et al.* 1997]. Georeferencing can be a problem in airborne laser systems [eg Nilsson 1996, Means *et al.* 1999]; however, this can be resolved with sophisticated GPS and inertial systems.

2.6. Optical Satellites

Various spaceborne imaging spectrometers produce repetitive, small–scale synoptic images for measuring biophysical parameters and monitoring landscape change; for example, Landsat MSS and TM, SPOT, the Japanese Earth Resource Satellite (JERS–1), and the Indian Resource Satellite (IRS–1A, 1B, and 1C).

Landsat MSS data has been used to develop regression models for timber volume estimation in Scots pine dominated forest stands [Jaakkola and Saukkola 1979], to estimate stocking in sparse to moderately stocked ponderosa pine forests [Strahler and Li 1981], to estimate the age and volume of stands [Poso *et al.* 1984, 1987], and to assess continental or sub–continental forest resources in a stratified sampling design [Nelson *et al.* 1987].

Landsat TM data has been used to estimate volumes and age of stands [Poso *et al.* 1984, 1987], to relate biomass and successional age to vegetation index derived from TM data [Sader *et al.* 1989], and to estimate above ground biomass on semiarid rangelands [Anderson *et al.* 1993].

SPOT–1 data has been used to estimate the stand age of radiata pine in Canberra, Australia [Turner *et al.* 1987], and to estimate five stand variables (tree density, mean DBH, mean tree height, mean density and age) of Corsian pine in northern England [Danson 1987]. In the case of measuring tree height, Danson (1987) found that the SPOT NIR data had strongly negative correlation with mean height (R=–0.83) but did not provide a detailed statistical summary.

2.7. Airborne Line Imagers

Line imagers are electro–optical imaging systems that collect data along a single line on the ground, perpendicular to the direction of flight [Schott 1997]. Airborne line imagers include the multi–spectral electro optical imaging scanner (MEIS) [McColl *et al.* 1983], the wide angle high resolution line imager (WhiRL) [Neville *et al.* 1992], and the compact airborne spectrographic imager (CASI) [Babey and Anger 1993, Anger *et al.* 1994]. CASI is the most recent and widely discussed system applied to forest inventory. CASI is a single, video resolution, solid state array sensor and operates in imaging mode with up to 15 programmable bands or spectrometer mode with 288 bands.

In forestry, CASI has been applied to the discrimination of forest species and canopy density [e.g. Franklin 1994], tree crown recognition and counting [e.g. Held and Billings 1998], and forest moisture stress mapping [e.g. Chisholm and Louis 1998]. The advantage of CASI over an airborne optical array sensor is its higher spectral resolution. Stereo viewing is possible but less convenient because it can only use viewing of side–lap between adjacent flight lines. No published applications of airborne line imagers to tree heighting have been found.

2.8. Airborne Videography

Airborne video is captured continuously along a flight line, usually at 25 or 30 frames per second. The analog data in individual frames can be converted into digital data using a video frame grabbing board with image resolution limited to about 792×480 pixel [Pitt *et al.* 1997], or stored digitally in the case of a digital video camera.

Compared to a film camera, videography provides much lower spatial resolution and requires a large number of frames for comparable results [Wright 1993]. Other limitations, depending on the method of image plane scanning, are poor and inconsistent image geometry and the addition of electronic noise [King and Vlcek 1990]. However, in some applications where the high resolution of photographic film is not required, video offers an affordable alternative because of its low cost, convenience, and immediate availability [King and Vlcek 1990].

In forestry, airborne video has been used to provide descriptions of, for example, species composition, forest condition, crown density, vertical stratification and foliage density [Bercha *et al.* 1990]. It has also been used to complement aerial photographs for updating forest maps [Hosking 1994, Pitt *et al.* 1997]. Multispectral video has been used in forestry with varying success, for example, to classify conifer stands from other forest types in mixed forest groups [King and Vlcek 1990], to classify forest vegetation [Lowe *et al.* 1995], and to acquire reference data for Landsat mapping [Slymaker *et al.* 1995]. No reference has been found of airborne video being used to estimate tree height in forests.

2.9. Summary

Remote sensing techniques have been used to measure a range of forest parameters for inventory purposes using various methods and approaches. The techniques range from large-scale vegetation classification to measurement of individual tree characteristics.

In the case of measuring tree height, there are three competing technologies: aerial photography using photogrammetric techniques, airborne laser, and radar. These three technologies have a demostrated potential to compete with field measurement techniques. However, for inventory purposes, large format aerial photographs and photogrammetric techniques offer some important advantages to forest managers:

i. higher spatial resolution and accuracy,
ii. superior stereo capability;
iii. potential to provide additional inventory data; and
iv. lower cost, with the photography already routinely acquired and used intensively by forest managers.

Techniques developed for aerial photography also offer the possibility to measure historical data (e.g. Long-term growth) using the extensive collections of large format aerial photographs held by most forestry organisations.

Previous research has demonstrated the potential of photogrammetric techniques to provide tree height data. This research focuses on the utility of aerial photography and digital photogrammetric techniques to reliably measure tree height.

Chapter 3. Image Matching Techniques

3.1. Introduction

Image matching plays a key role in the automation of digital photogrammetry. The technique can be used to supplement, complement or replace the human operator. In photogrammetry, matching is essential for two separate procedures; the first is image orientation, and the second is three-dimensional object reconstruction. The orientation processes require measurements of fiducial marks for interior orientation, pass points for relative orientation, and ground control points in absolute orientation. The second procedure is the determination of position and elevation of image points in the overlap area.

A digital photogrammetric workstation (DPW) consists of hardware and software to carry out photogrammetric tasks in an interactive and automated way using digital image data as input. The resulting photogrammetric products include three-dimensional coordinates, geometric and radiometric object surface descriptions, structured vector data, and transformed digital imagery (e.g. orthoimages and perspective views) [e.g. Grün 1989].

The characteristics and advantages of a DPW in comparison to analogue and analytical methods are [Grün 1989, Lohmann *et al.* 1990]:

- no need for high precision opto–mechanical parts,
- robust measurement system,
- stable image geometry, no deformation over time,
- no instrument calibration, no manual image handling,
- automatic, semi automatic or manual operation,
- high degree of interactivity,

- data acquisition, storage and processing in one system,
- online and real time capabilities, and
- direct three-dimensional graphic superimposition possibilities.

Leading DPWs such as the Leica–Helava, ERDAS Imagine OrthoMAX, Autometric Softplotter, INPHO, Zeiss PHODIS, VirtuoZo, and Intergraph ImageStation (now Z/1 Imaging) systems offer complete photogrammetric functionality including orientations, aero triangulation, automatic DEM generation and orthophoto production. This chapter reviews the image matching algorithms employed in these leading digital photogrammetric workstations. Comparative studies of their performances are reviewed, focusing on the performance of automatic DEM extraction.

3.2. Classification of Image Matching Techniques

Before discussing the matching techniques employed by different digital photogrammetric systems, it is appropriate to describe the range of matching techniques that have been developed. The following classification is based on four fundamental questions (see Vosselman 1992 for a similar approach):

(1) What primitives are being matched?

(2) What models are used to define the geometric and radiometric mapping between primitives?

(3) How is the match measured?

(4) How is the best match found?

3.2.1. What Primitives are Being Matched?

There are two broad categories of matching primitives: windows composed of grey values, and features extracted from an image prior to matching. These two distinct categories lead to two different approaches to image matching: area based matching and feature based matching [Heipke 1992].

In both cases, local or global support for the primitives can be used [Medioni and Nevatia 1985]. Local matching associates each primitive of one image to one or more primitives of the other image based on the neighbouring area, seldom larger than 51 by 51 pixels. Global matching employs a larger area and can

comprise the whole image.

3.2.1.1. Area Based Matching

In area based matching, small windows composed of grey values are used as matching primitives. The windows are normally square. The window on one image is used as a reference window (called the template window), while the corresponding window on the other image is called the search window. The template window centre, possibly weighted with respect to the grey value gradient, defines the point to be matched.

The advantage of area based matching is that high accuracy can be achieved in well-textured image regions. Accuracy comparable to human operator based measurements have been reported [e.g. Pertl 1985, Grün and Baltsavias 1987, Rosenholm 1987a]. The disadvantages of area based matching include the sensitivity of the grey values to changes in radiometry, and the time required for searching for the best match.

3.2.1.2. Feature Based Matching

Feature based matching determines the correspondence between image features. In feature based matching, features such as points, lines and regions are extracted from both images prior to matching. Features selected for matching must have the following characteristics [Förstner 1986]:

- *Distinctness*: The selected point should be distinct from the neighbouring points, ensuring local separability.
- *Invariance*: The distinct point position should be invariant with respect to the expected geometric and radiometric distortions.
- *Stability*: The selected point should be robust with respect to noise and be expected to appear in the other image.
- *Seldomness*: Seldomness aims at global separability.
- *Interpretability*: The selection should be interpretable, for example, identifying edges, corners or other simple features.

Feature primitives are described by their characteristics, called attributes. A point can be described for example, by pixel number, row and column numbers, and its intensity. A polygon can be described by its length, shape and closure.

Beside the attributes of features, the relationship between local features is introduced to characterise global features. These can be geometric or radiometric. Geometric relationships can be, for example, the angle between two adjacent polygons or the minimum distance between two edges. Radiometric relationships can be, for example, the difference in grey value between two adjacent polygons. A description of primitives and their interrelationship is called a relational description [Vosselman 1992: 7].

Local features have been used for matching by, for example, Förstner (1986) and Hannah (1989), where in each case, points were selected as features. Global features are usually composed of local features. Matching with global features is referred to as relational matching [Shapiro and Haralick 1987]. Relational matching using global features has been described by, for example, Vosselman (1992). A combination of global and local features is described by Schenk *et al.* (1991).

One of the advantages of feature based techniques are that they are faster than area based techniques, because the number of matched elements is generally lower. The other advantage is that they have a reduced sensitivity to light variations and, in general, to all radiometric differences between images of the stereo pair, because the criteria for matching are mainly geometric and structural rather than based on similarity of the neighbouring pixels [Cappelini *et al.* 1991]. The disadvantages are lower accuracy, and poorer indication of the quality of the match.

3.2.2. What Models are Used to Define the Geometric and Radiometric Mapping Between Primitives?

The mapping between the primitives of the various images can be defined using a sensor model, an object surface model or a combination of the two.

3.2.2.1. Sensor Models and the Epipolar Constraint

Looking for the mapping with the best similarity value often results in a very time consuming search. To reduce this, constraints are applied. These can be hard constraints such as the limit of the search space or soft constraints such as the methods more likely to find the best mapping. An example of the latter is a smoothness constraint – points that are adjacent in one image are adjacent in the

other image, since the recorded objects generally have piecewise smooth surfaces.

Sensor models represent the geometric definition of the aerial photographs at the time of exposure. The central perspective projection in photographic imagery allows the epipolar geometry to be used as a constraint. Given two images, the epipolar plane for a point in a three-dimensional space is defined as the plane containing this point and the two projection centres of both images. The plane intersects both images in straight lines – the epipolar lines. If the relative orientation of two images is known, for a given point in one image the epipolar line in the other image can be calculated, and the conjugate image point must lie on this epipolar line. The epipolar constraint is vital in reducing ambiguity problems and computational cost.

Epipolar resampling is a common pre–processing stage in matching algorithms. Once the image pair is oriented, the area of interest in the individual images is selected and resampled to reflect the epipolar geometry. Epipolar resampled images improve the performance of the image matching (and enhances the stereo viewing).

3.2.2.2. Object Surface Models

Geometric models for the object surface used in image matching range from horizontal and tilted planes to models describing discontinuities in the surface slope or the surface itself. An important difference between images in a stereopair is the geometric distortion caused by ground slope. This produces different effective pixel sizes in the conjugate image windows. Matching in object space is accomplished by resampling the images from pixel space to ground elements (groundels). Each groundel has three-dimensional centre coordinates.

Radiometric models of the object surface are used to describe the brightness of the groundels. Due to reflection effects, shading, and other factors such as noise, a groundel usually has different brightness when viewed from different directions. In image matching these differences are normally modelled by means of a local linear radiometric transformation.

The advantage of mapping primitives in terms of object space parameters is that multiple images can be matched simultaneously. This results in a higher redundancy and thus greater reliability.

3.2.3. How is the Match Measured?

The best match between two descriptions is the mapping for which the corresponding primitives of the descriptions show the best similarity in their attributes and their relations. For area based matching, the similarity of two descriptions is usually defined by a covariance, correlation, or least squares function of the differences between corresponding grey values [e.g. Wang 1990]. For feature based matching, defining a similarity measure is more complicated, and must be based on the attributes of the features. To measure similarity for feature based matching, the differences in geometric and radiometric attribute values are combined using a measure called a cost function.

3.2.3.1. Similarity Measures for Area Based Matching

3.2.3.1.1. Covariance Function

The maximum of a covariance function defines the position of the best match between the template window and the search window, with the function typically defined by [e.g. Wang 1990]:

$$\sigma^2 = \frac{\sum_{r=1}^{R}\sum_{c=1}^{C}(g_1(r,c)-\mu_1)(g_2(r,c)-\mu_2)}{RC}$$

where $g_1(r,c)$ is the individual grey values of the template matrix;

μ_1 is the average grey value of the template matrix;

$g_2(r,c)$ is the individual grey values of the conjugate part of the search matrix;

μ_2 is the average grey value of the conjugate part of the search matrix; and

R,C are the dimensions of the template matrix.

3.2.3.1.2. Correlation Coefficients

A correlation coefficient is a normalised covariance function. The maximum correlation coefficient also defines the position of the best match between the template window and the search window. The function is typically defined by [e.g. Wang 1990]:

$$\rho = \frac{\sum_{r=1}^{R}\sum_{c=1}^{C}(g_1(r,c)-\mu_1)(g_2(r,c)-\mu_2)}{\sqrt{\sum_{r=1}^{R}\sum_{c=1}^{C}(g_1(r,c)-\mu_1)^2 \sum_{r=1}^{R}\sum_{c=1}^{C}(g_2(r,c)-\mu_2)^2}}; \qquad -1 \le \rho \le 1$$

where $g_1(r,c)$, μ_1, $g_2(r,c)$, μ_2, and R,C are defined as in the covariance function.

3.2.3.1.3. Least Squares

The minimum value of the sum of the squares of the differences between the search and template windows defines the position of the best match. The function is typically defined by:

$$d = \sum_{r=1}^{R}\sum_{c=1}^{C}((g_1(r,c)-\mu_1)-(g_2(r,c)-\mu_2))^2$$

where $g_1(r,c)$, μ_1, $g_2(r,c)$, μ_2, and R,C are as defined in the covariance function.

In digital photogrammetry, considerable attention has been paid to area based matching using least–squares methods, since they were first introduced [e.g. Helava 1976, Förstner 1982, Förstner 1982, Rosenholm 1987a and 1987b, Helava 1988, Wrobel 1991]. There are three main reasons for this [Heipke 1992]:

- extremely high accuracy potential,
- high degree of invariance against geometric image distortions, and
- relatively simple possibilities for statistical analysis of the results.

Compared to other matching techniques, area based least squares matching is very precise, but for surface reconstruction and point mensuration it requires good approximate values for the transformation parameters [Vosselman 1992: 28].

3.2.3.2. Similarity Measures for Feature Based Matching

A similarity definition for primitives having an attribute with a numerical value is straightforward. For example, if the grey value is a pixel primitive, then two pixels may be said to be similar if the absolute difference of their grey values is small. Similarity definition becomes more complicated if two or more attributes are involved. In most feature based matching, the similarity measure is defined using a cost function. Costs are to be minimised and are zero only if both descriptions are identical. Vosselman (1992) describes the cost function as

follows.

Suppose that two feature based descriptions P and Q are to be matched, where both descriptions are sets of primitives $\{p_1,p_2,\ldots,p_N\}$ and $\{q_1,q_2,\ldots,q_N\}$, respectively. Further suppose that all primitives are described by N_a attributes a_k with values v_k and that a mapping is given by h which maps the primitives of P to the primitives of Q, such that, when $h(p_i)=q_j$, primitive q_j is considered to correspond with primitive p_i. Then the costs are defined as the sum of the attribute correspondence costs over all attributes:

$$\text{costs}(p_i,q_j)=\sum_{k=1}^{N_a}\text{costs}(v_k(p_i),v_k(q_j))$$

where $v_k(p_i)$ denote the value of the kth attribute of the ith primitive of description P. The costs of the mapping h is defined by:

$$\text{costs}(h)=\sum_{i=1}^{N}\text{costs}(p_i,h(p_i)).$$

The costs can be defined using three approaches: the absolute of the attribute value difference, the square of the attribute value difference, or using probability theory. The first two approaches are similar to the absolute difference and square of the difference method in area based matching. Probability theory requires that the conditional probability functions are known for all attributes. The conditional probability function $P_a(v_2|v_1)$ of attribute a defines how likely it is that v_2 corresponds to v_1. This conditional probability can be converted to a cost function by taking the negative of the logarithm [Vosselman 1992]:

$$\text{costs}(v_1,v_2)=-\log P(v_2\mid v_1).$$

Summing up these costs means multiplying of probabilities under logarithms. Hence, minimising the costs is equivalent to maximising the product of all probabilities.

3.2.4. How is the Best Match Found?

Methods are required which will allow the similarity measures to be computed efficiently and reliably. The following methods are representative of the range of techniques employed.

3.2.4.1. Search Methods for Area Based Matching

3.2.4.1.1. Conjugate Template and Search Windows

In order, for example, to compute the cross correlation function of two windows, a template window is shifted pixel by pixel across a search window (Figure 3.1). In each position the function is computed, and the maximum of this function defines the position of the best match between the template and search windows.

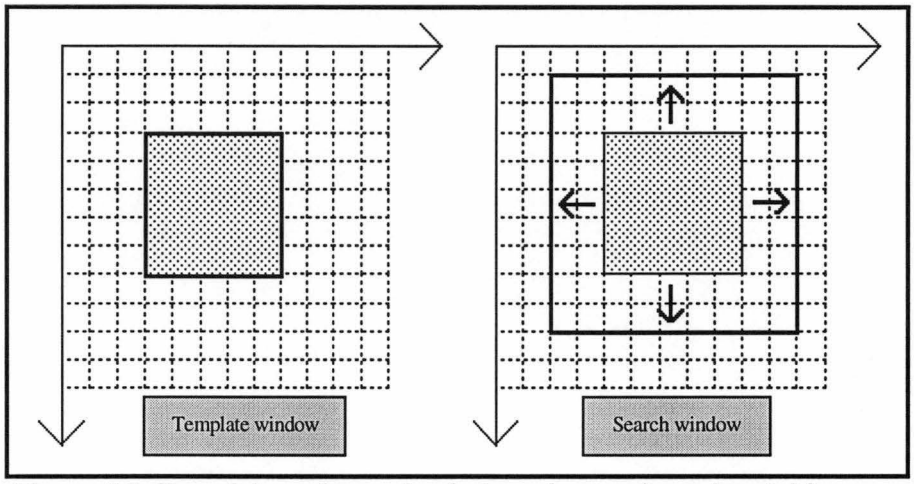

Figure 3.1: Template and search windows in area based matching.

3.2.4.1.2. Vertical Line Locus (VLL)

Rather than search along the x–axis in an epipolar resampled image, the VLL method begins with a point, the X,Y object space coordinates of which are fixed. A vertical line is made to pass through that point, and an odd number of rectangular windows with equal interval are taken along that vertical line. These windows are projected onto both photographs. The correlation coefficients are computed based on the grey value matrices of the corresponding windows on the left and right photographs, and the results representing different Z values in the object space. By interpolating from the coefficients, the maximum correlation is obtained and the corresponding Z value is taken as the estimated elevation [Wang 1990, Wang *et al.* 1993].

3.2.4.1.3. Hierarchical Approach

Hierarchical methods are used in many matching algorithms in order to reduce the ambiguity problem and to extend the pull–in range.

In area based matching, the most common approach derives a series of increasingly smoothed images from the original images and uses these images or features detected in them for the matching. The search is started from the coarser level. These measurements are then used as the starting points to find matches for the higher resolutions images. To search for a match at a given starting point and at a given resolution, area based cross correlation is used. This approach uses the same kind of primitives at each level (Figure 3.2, third column).

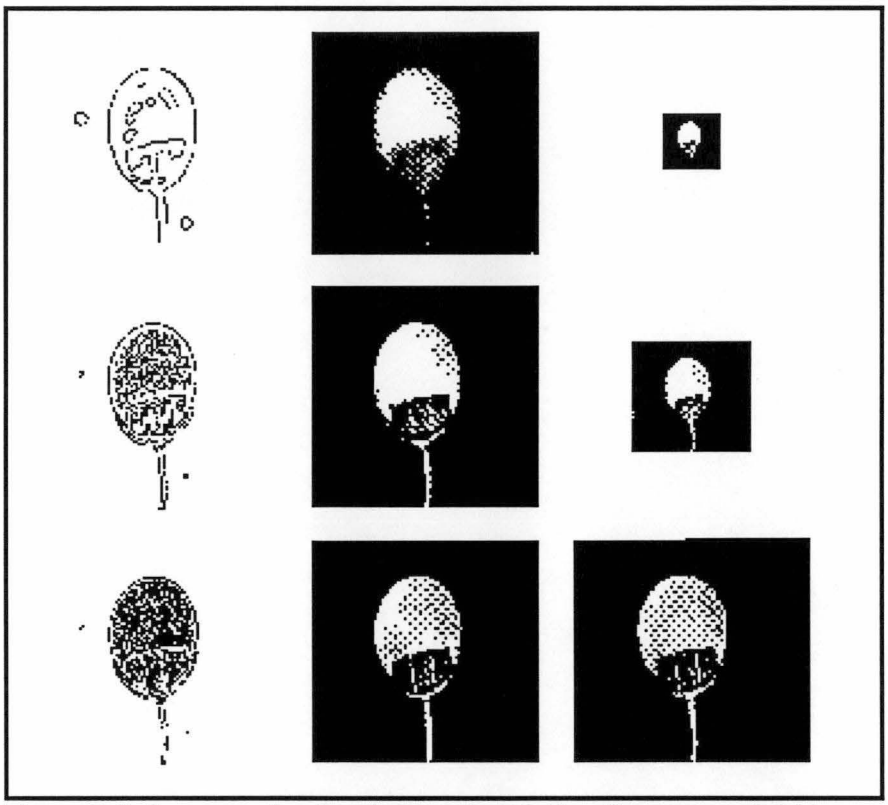

Figure 3.2: An example of an image description (image pyramid in first and third columns) derived from increasingly smoothed images (second column) [Vosselman 1992: 21].

3.2.4.2. Search Methods for Feature Based Matching

Feature based matching starts with discrete features. In local feature based matching, each given feature in one image is defined in the conjugate image using a transformation. To achieve global consistency, alternate schemes are available including a tree search [Vosselman 1994], dynamic programming [Wang 1990, Zhang *et al.* 1996], and hierarchical approach. Others will only be mentioned here, including simulated annealing [Kirkpatrick *et al.* 1983, Davis and Steentrup 1987] and relaxation labelling [Barnard and Thompson 1980].

3.2.4.2.1. Tree Search

Tree search methods find solutions using a search space, which can be represented by a tree [Vosselman 1994]. The root node of the tree represents the initial problem state, where the mapping is undefined. The tree search can be divided into two categories: *blind* methods [Nilsson 1982] and *informed* methods [Pearl 1984]. Blind methods have no *a priori* knowledge of where to search for a solution. These methods are suitable for tasks where no such information is available, e.g. object location and recognition. The informed search methods have a function by which the nodes of the trees can be evaluated. The function gives a measure for the quality of the path from the root node to the current node.

3.2.4.2.2. Dynamic Programming

Dynamic programming is a method used to solve problems in optimisation of multi–stage decision making, in which the activity is divided into several interrelated stages, and in each stage a decision has to be made. After a decision is made for each stage, a decision sequence is formed. Multi–stage decision making provides many decision sequences and allows an optimal decision sequence to be chosen from among many decision sequences [Wang 1990: 442].

3.2.4.2.3. Hierarchical Approach

In feature based matching, the hierarchical approach describes models at different levels of abstraction. Starting from a detailed model description, more abstract descriptions are obtained by generalisation. This more qualitative approach may use different kind of primitives at each description level (Figure 3.2, first column).

3.3. Matching Algorithms Employed by Leading DPWs

Automated three-dimensional reconstruction by image matching is the most important function of a digital photogrammetric workstation. The image matching algorithms for three-dimensional object reconstruction that have been employed by some leading digital photogrammetric workstations, namely the Leica–Helava, VirtuoZo, Intergraph ImageStation, INPHO, PHODIS, Autometric Softplotter, and ERDAS Imagine OrthoMAX systems, are described in the following sections.

3.3.1. Leica–Helava DPW 770

In the Leica Helava DPW 770 used for this research, the SOCET SET® software employs an algorithm called Automatic Terrain Extraction (ATE) to measure automatically a DEM covering the region of interest. ATE uses *Hierarchical Relaxation Correlation* [Helava 1988, Miller and de Venecia 1992]. The matching algorithm employs least squares area based matching.

After epipolar resampling, image pyramids are formed (usually 8 levels). Correlation is begun on the coarsest level of the pyramids. Before comparing the similarity of areas to be matched, groundel resampling (described in Section 3.2.2.2) is applied. The objective is to resample the image areas to be matched to an equal scale, which may include terrain slope effects, radiometric and geometric characteristics [Miller and de Venecia 1992]. The results of the matching, defined by area-based cross correlation coefficients, are used as seed points to find matches in succeeding, higher resolution, images.

DEM collection in the Leica Helava DPW 770 uses a regular grid in object space. Users are given flexibility to input the DEM grid spacing, the object space coordinate system, and the boundary of the area of interest. The DEM can be measured using one or more of many different strategies. Each strategy comprises several passes, each working on images at a certain pyramid level. The strategies are chosen according to the terrain conditions. Table 3.1 lists the strategies that can be used.

Maximum Terrain Slope	High–Speed Extraction	High–Accuracy Extraction	High–Accuracy and Removes Artefacts such as building and trees	High–Accuracy and High–Speed for Very Dense DEM
20 degrees	Flat	Flat_1	Flat_plus	Flat_dense
30 degrees	Rolling	Rolling_1	Rolling_plus	Rolling_dense
50 degrees	Steep	Steep_1	Steep_plus	Steep_dense

Table 3.1: Automatic Terrain Extraction Strategies in the Leica Helava DPW 770 [SOCET SET User Manual].

3.3.2. VirtuoZo

VirtuoZo is a digital photogrammetric system developed by the Wuhan Technical University, China and Geonautics Pty. Ltd., Australia. The matching

algorithm within VirtuoZo is area and feature based, using least squares matching techniques and dynamic programming.

After epipolar resampling, image pyramids are formed (usually 4 levels) and matching is conducted from the coarsest level in the image pyramids. In each level, features are extracted. The results of the matching of the coarser level are used as seed points to find matches in succeeding, higher resolution, images. Using one–dimensional epipolar line correlation, the windows of the target and search areas are each placed between two feature elements, with one already matched feature element located at one end (left), and the feature element to be determined on the other end (right). Before comparing the similarity of areas being matched, the effect of geometric distortion caused by ground slope is overcome using a method called bridge mode resampling [Zhang 1989, 1990], in which the size of the search window is always made equal to the template window. To optimise the search for global consistency, least squares matching is employed in the case of area based matching, and the dynamic programming method is employed in the case of feature based matching.

To compute a DEM, VirtuoZo uses a regular grid in image space, which generates a non-uniform grid in object space. Users are given the flexibility to input the DEM grid spacing and the size of windows (search and template windows) for matching. The DEM can be measured using one of five different collection strategies, mainly depending on terrain slope and form. The types of terrain set for the matching strategies include flat, undulating, hillock, broken, and rugged.

3.3.3. INPHO, Intergraph ImageStation, and Zeiss PHODIS

INPHO, ImageStation, and PHODIS uses an algorithm called *Match–T* for automatic DEM generation [Ackermann and Krzystek 1995, Ackermann 1996].
After epipolar resampling, image pyramids are formed (usually 8 or 9 levels). On each level features are extracted to build feature pyramids. Feature matching is performed starting from the coarser level and using bounded search spaces. The matched image points are processed analytically to three-dimensional (terrain) points from which a finite element fitting is derived in tiles representing the DEM.

The final DEM is edited as a rectangular grid, defined by the finite elements. Refinements are introduced by additional break lines and excluded areas which are determined interactively.

To compute a DEM, *Match–T* uses a regular grid in image space. The spacing of the DEM posts is automatically adapted to the local terrain curvature of the terrain surface. The types of terrain set for the matching strategies include plain, slightly undulating, undulating, and mountainous.

3.3.4. Erdas Imagine OrthoMAX and Autometric Softplotter

Both these systems employ an iterative image/object space matching procedure for DEM extraction. The algorithms employed are area based cross correlation matching and least squares matching. The cross correlation matching is employed first and the results are used as an approximation for the least squares matching. Image pyramids are created for both images in the stereo pair and the matching is performed at each level of the pyramid starting from the coarser level. A vertical line locus method is used to establish initial approximations.

Before a correlation coefficient is determined, the template and search windows are orthorectified to produce image patches on the left and right imagery. A 'shaping' technique is employed to rotate the image patches so as to remove the rotation effects of the cameras and to remove any apparent relief displacement. With the left template fixed, the right search window shifts in the x image direction along the epipolar line. The steps are repeated within the range of allowed maximum x and y parallax.

The pair of image points with the largest correlation coefficient are projected to the ground surface. The differences between the estimated elevation and the initial approximation and between the newly derived XY coordinates and the XY coordinate of the grid point are computed and analysed. The solution is iterated until XYZ coordinates lie within specified limits.

3.4. Accuracy of DEM Extraction: Comparative Studies

There have been a number of studies to assess the performance of digital photogrammetric workstations, especially for automatic generation of digital terrain

models. The studies include comparisons between several DPWs [e.g. Baltsavias *et al.* 1996, Smith and Smith 1996, Baltsavias and Käser 1998]; and assessment of individual DPWs [e.g. Ackermann and Krzystek 1995, Stojic *et al.* 1998, Gooch *et al.* 1999].

The evaluation and comparison of DEMs generated by DPWs can be used to indicate the quality or performance of the matching algorithms and the strategy parameters employed. There is no study that has evaluated all mentioned matching algorithms, but comparative studies which involved at least two or three of the algorithms are available. These include, for example, Leica Helava and VirtuoZo [Baltsavias *et al.* 1996], Erdas Imagine and ImageStation [Smith and Smith 1996], and Leica Helava, PHODIS, Softplotter and INPHO [Baltsavias and Käser 1998].

Baltsavias *et al.* (1996) compares the accuracy of the Leica Helava DPW 770 and VirtuoZo. The study assessed DEM generation in a mountainous region that includes glaciers. A strip of three photographs with 85% overlap at 1:10,000 scale were used, and scanned at 15 microns, but then resampled at 30 microns due to image size. In order to assess the DEM accuracy of the digital systems, a reference DEM was measured on an analytical stereoplotter. From both digital systems, DEMs were measured on a 2.5m grid. Interpolation was required for VirtuoZo because of its image space matching.

In the LH DPW 770, the patch size used was 15×15 pixels and the DEM collection strategy was the "steep_1 strategy". In this study, it was reported that the modification of the parameters to suit the terrain conditions required further investigation. In VirtuoZo the patch size used for correlation was 9 × 9 pixels and the DEM collection strategy was the "rugged terrain". The differences between manual and automatic measurements are listed in Table 3.2 and Table 3.3.

Version	Number of points	Maximum absolute (m)	Average (m)	RMS (m)
DPW 770 (whole image)	8728	87.0	0.28	3.53
DPW 770 (region without large blunders)	3997	16.5	0.15	1.08
VirtuoZo (whole image)	8594	103.5	0.27	4.13
VirtuoZo (region without large blunders)	3997	14.6	0.21	0.96

Table 3.2: Statistics of height differences between the analytical and automatic measurements [adapted from Baltsavias *et al.* 1996].

Version	0–2m	2–3m	3–4m	4–6m	6–9m	9–15m	>15m
DPW 770 (whole image)	85.6	5.4	2.8	2.7	1.9	0.9	0.7
DPW 770 (region without large blunders)	96.8	1.7	0.6	0.4	0.3	0.2	0.1
VirtuoZo (whole image)	89.2	4.0	2.3	1.9	1.1	0.8	0.9
VirtuoZo (region without large blunders)	97.7	1.4	0.4	0.3	0.2	0.2	–

Table 3.3: Percentage of points for various classes of absolute differences between the analytical and digital measurements [adapted from Baltsavias *et al.* 1996].

The accuracy of the systems were found to be very similar with the DPW 770 achieving slightly lower RMS and maximum error in the whole image. Blunders were found in the DEMs measured by both systems, caused by difficult regions such as those with minimal features and those with abrupt terrain discontinuities. These were large and significantly influenced the statistical results. Some differences between the results were attributed to the smaller patch size used in the VirtuoZo solution.

Baltsavias *et al.* (1996) emphasise that the selection of appropriate strategies and modification of parameters were more important than the choice of software. VirtuoZo offers five strategies but only permits the user to change the grid spacing and the patch size. The DPW 770 offers more strategies and greater flexibility to change matching parameters, but the effect of changing these parameters may be difficulty for the user to predict.

Smith and Smith (1996) compare the performance of automatic DEM generation for Erdas OrthoMAX and ImageStation. The performance of DEM generation was tested for mapping in both urban and rural areas. For the urban area, the imagery comprised a pair of black and white photographs at 1:3,000 scale containing a mixture of residential and industrial areas. For the rural area, a pair of colour photographs taken at 1:10,000 scale were used. The accuracy of the DEMs was analysed by comparing them with analytical stereoplotter data.

The results for urban area were reported only for the Erdas system. The parameters: block and stereopair options and minimum and maximum template sizes were tested. In the case of the block and stereopair options, the results differed significantly, with approximately 8% of points of the DEM measured using the block option were outside ±1m of the DEM measured using the stereopair

option. In the case of template size, the default minimum and maximum template size of 7 and 9 were compared with a minimum and maximum template size of 7 and 11. Although this change appears to be quite small, the results differed significantly, with 10.5% of points generated using the minimum and maximum template size of 7 and 11 falling outside ±1m of the surface generated using the default template size.

In the rural area, each of the three colour bands (red, blue and green) was separately used to perform the image correlation. For both systems, DEMs generated from the blue band were significantly different (higher) from DEMs generated from the red or green bands. For the Erdas system, red and green bands produced similar results and both results were reported to compare well with the analytical data, although detailed statistics were not provided. For the ImageStation system, three DEM collection strategies were tested: flat, hilly and mountainous, which in the selection were influenced by two parameters: parallax bound and epipolar line distance. DEMs generated using the flat and mountainous strategies differed significantly. All three strategies resulted in approximately 64% of points falling within ±1m of the analytical data. The magnitude of the errors for the remaining points for the three strategies were not provided. Smith and Smith (1996) also emphasise that the selection of system was not as important as selection of appropriate matching strategies and parameters.

Baltsavias and Käser (1998) describe a comparison of four digital photogrammetric systems: LHS DPW 770, Autometric Softplotter, Zeiss PHODIS, and INPHO, to generate DEMs (and orthoimages) using a pair of black and white photographs, which included forests, rivers, creeks, and urban areas. The photographs were acquired at 1:24,000 scale and scanned at 15μm. Two versions of Softplotter were used (old and new), with newer version generating a denser DEMs. Images scanned at 30μm were also processed (INPHO software only) to indicate the effect of different image resolutions. To assess the accuracy of DEMs generated from the DPWs, reference data was generated using an analytical steroplotter.

In this study, the DPW 770 employed the "steep_plus" strategy with 8 pyramid levels and 15×15 pixel patch size. Steep_plus is intended for steep terrain and is

intended to remove building and trees, and perform smoothing at "non critical" DEM points. Softplotter employed 6 pyramid levels and an adaptive patch sizes of 7×7 or 9×9 pixels. PHODIS employed points in every fourth epipolar line, used 6 pyramid levels, 8 pixels parallax bound, and terrain smoothing for rolling terrain. INPHO employed points in every epipolar line, used 10 pyramid levels, 15 pixel parallax bound, and terrain smoothing for mountainous terrain. All systems produced a 10m regular grid. The results are summarised in Table 3.4.

	DPW 770	Softplotter (old)	Softplotter (new)	PHODIS	INPHO (15μm)	INPHO (30μm)
No. of points	16236 / 1102	15659 / 1065	15085 / 1037	16357 / 1108	16357 / 1108	16357 / 1108
Mean	–0.73 / –1.68	–0.17 / –0.88	0.1 / –0.46	–0.82 / –1.52	0.17 / –0.28	0.13 / –0.37
Max. Abs.	18.46 / 8.18	11.55 / 8.81	18.11 / 6.24	65.17 / 6.52	8.03 / 3.73	6.30 / 4.32
RMS	1.51 / 2.42	0.87 / 1.72	0.78 / 1.21	1.60 / 2.16	0.58 / 0.95	0.67 / 1.14

Table 3.4: Statistical differences for mass points / breaklines between reference data and automatically generated DEMs (in metre) [adapted from Baltsavias and Käser 1998].

The main finding of the study were that the DEM's deteriorated if the DEM resolution was too low (PHODIS and Softplotter–old version), or if the correlation patch size was too large (DPW 770). INPHO produced similar results to those of the new Softplotter. The poorest of all systems was the LH DPW 770, attributed to the large correlation patch size, but no further investigation of smaller patch sizes was conducted.

Baltsavias and Käser (1998) also conducted a visual inspection by overlaying the resulting DEMs on an orthoimage to check the positions of points with large errors. It was found that large errors were likely to occur (as expected) at or close to surface discontinuities, large perspective differences, low texture, and where edges were parallel to the epipolar lines.

Regarding DEM generation using these systems, Baltsavias and Käser (1998) emphasise some important points:

- the main limitation of the systems is their inability to reliably detect blunders;
- setting up appropriate matching strategies and parameters influences the final DEM results, but the available choices of all systems vary and are not easy to set, and hence,
- the sensitivity of the DEM to changing parameters requires investigation and

may require adaptive techniques within the software; and

- denser DEM collection provides better results because it includes more detail (trees and buildings), better represents terrain, and provides more redundancy for blunder detection.

Under what circumstances one algorithm may perform better than another depends on many factors, including the nature of the images being mapped, the purpose of mapping, and the ability of the user to obtain the optimised parameter setting within the software.

The comparative studies described above emphasise the importance of understanding how each matching parameter can affect the accuracy of DEMs and how, for a particular project, the setting of available parameters needs to be optimised. It is not easy to set the parameters given in each DPW to obtain optimum results, because of the large number of possible combinations and the lack of independent data against which to assess the resultant DEM under normal circumstances.

3.5. Measuring DEMs Over a Pine Forest

For forestry applications, particularly mapping tree height in pine forests, there are two other important factors that need to be considered: the density of the canopy and the shape of the trees. The density of the canopy influences whether abrupt changes in the canopy surface caused by the visible ground are present, and the shape of the trees influences the visibility of the treetops and the DEM point density required in order to facilitate treetop measurement. Consequently, it can be expected that:

- the aerial photographs should be scanned at very high resolution; and
- a high DEM collection density should be employed.

It follows that the selected digital photogrammetric workstation must have the capability to process large amounts of data resulting from the high image resolution and high DEM point density.

In the case of a dense canopy, it might be expected that both area and feature based image matching will perform well because the plantation is rich in features and texture. In the case of a sparser canopy, such as the thinned canopy, the feature

based algorithms might be advantageous because of the presence of abrupt surface changes caused by visible ground. However, both the area and feature based approaches may be expected to fail if the forest structure is too complex, too variable between the photos, or highly repetitive.

3.6. Summary

A well-designed matching algorithm that uses an optimum combination of the matching modules described above provides a powerful solution to image matching in many photogrammetric operations. These operations are interior, relative orientation and, most importantly, automatic DEM generation. Leading digital photogrammetric workstations use a combination of matching methods, with the selection mainly characterised by whether they employ area based matching and/or feature based matching.

For automatic DEM generation, comparisons of some leading digital photogrammetric workstations indicate that the most important factor is an understanding of the matching parameters and optimisation of those parameters. For mapping tree height in pine plantation forests, high-resolution imagery and a high DEM point density is expected to be required.

Chapter 4. Data Acquisition

4.1. Introduction

In order to assess the accuracy of canopy height models derived from a digital photogrammetric workstation properly, careful consideration must be taken in selecting appropriate data sets. The selection of the data should have regard to the following [Long 1994: 81]:

- *representativeness* and *comprehensiveness*, in which the selected study areas must be representative of the variety of conditions within a radiata pine plantation and include parameters that characterise these conditions (e.g. different types of canopy closure); and
- *accessibility and recognisability*, in which the selected areas must be both easy to access and identify on the corresponding aerial photographs.

This chapter describes the acquisition and pre-processing of data used in the research, specifically:

- the selection of the study area;
- the acquisition of aerial photography and ground control data;
- the generation of digital terrain models, and the methods used to collect the DTM data; and
- the collection of reference tree height data, both the analytical stereoplotter data and ground truth data.

4.2. Study Area

Study sites were selected following ground visitation and assessment of

available aerial photography. The plantations are owned and managed by Fletcher Challenge Paper Australia (formerly Australian Newsprint Mills) and situated in the Uxbridge area (Latitude ≈ 42°53' S and Longitude ≈ 147°20' E), South Eastern Tasmania, Australia. The area has a mean altitude of approximately 400m above sea level, varying approximately from 200 to 600m above sea level. The topography of the area varies from 0° to 30° slope.

Within the study area, two types of canopy closures were selected: a 14–year old closed canopy stand and a 19–year old thinned stand. The establishment density of both plantations was approximately 1000–1200 trees per hectare. In the closed canopy stands there is good canopy closure, while in the thinned stands both ground and canopy surfaces are visible. Figure 4.1 shows the location of the two stands.

4.3. Aerial Photography

4.3.1. Initial Photography

Initially, a pair of existing overlapping colour aerial photographs were provided by Fletcher Challenge Paper. The photographs were taken in January 1996 using a normal angle lens (305mm) and a large format camera, but no forward motion compensator (FMC) was used. The flying height was 17,000 feet (5400 m) giving a scale of approximately 1:15,000 with 60% forward overlap. The original diapositives of the two aerial photographs were scanned at 15μm to give a pixel size on the ground of approximately 0.22m. The images occupied about 700 MB each.

4.3.2. New Photography

The first set of new photographs were acquired in April 1998 using colour film and at 1:5,000 and 1:10,000 scales, and large format camera, but again no FMC was used. Unfortunately, they were not flown to specification in which a wide–angle (152mm) lens rather than a normal–angle (305mm) lens was used, and the 1:10,000 scale photography had only 20% forward overlap. This resulted in large relief distortion on individual trees within the stereomodel.

The second set of new photographs were acquired between December 1998 and February 1999 using a 305mm lens. For each photographic scale, four types of film were used: colour, black and white, colour infrared, and black and white infrared. In order to store the images onto 650MB CDs, the diapositives of all new photographs were scanned at 16μm. For an uncompressed format, this produced a file size of approximately 650MB for a colour image and approximately 220MB for a black and white image. Table 4.1 shows the details of aerial photography of the study areas and Figures 4.1 to 4.4 show representative examples of each type of film used, including black and white, black and white infrared and colour infrared.

No	Date	Scale	Type	Pixel size	Remarks
1	26 Jan 1996	1:15,000	Colour	~ 0.22m	Good
2	7 Apr 1998	1:10,000	Colour	~0.16m	No adequate overlap (20%)
3	7 Apr 1998	1:5,000	Colour	~0.08m	Large relief distortion
4	2 Dec 1998	1:10,000	Colour	~ 0.16m	Hotspot[1]
5	2 Dec 1998	1:5,000	Colour	~ 0.08m	Hotspot
6	25 Feb 1999	1:10,000	Colour	~0.16m	Good
7	25 Feb 1999	1:5,000	Colour	~ 0.08m	Good
8	10 Jan 1999	1:10,000	BW	~ 0.16m	Good
9	10 Jan 1999	1:5,000	BW	~ 0.08m	Good
10	10 Jan 1999	1:10,000	BW IR	~ 0.16m	Good
11	10 Jan 1999	1:5,000	BW IR	~ 0.08m	Hotspot
12	25 Feb 1999	1:5,000	BW IR	~ 0.08m	Good
13	10 Jan 1999	1:10,000	Colour IR	~ 0.16m	Good
14	10 Jan 1999	1:5,000	Colour IR	~ 0.08m	Good

Table 4.1: Aerial photographs acquired over the study areas.

4.4. Ground Control Points

For precise photogrammetric measurement, a minimum of six control points were acquired for each model. The locations of control points were identified on the photographs, and included stumps, rocks, a track intersection, and tree logs. Two Leica 200 GPS receivers were employed to collect the data. Ski software version 3 was used to process the GPS data using WGS 84 as datum. The procedure for measuring the ground control data were as follows:

(1) *Establishment of base station*: To avoid solving the ambiguity problem for a

[1] A hotspot is an overexposed area that can occur on aerial photograhs when the sun's elevation exceeds a limiting angle [Mason 1953].

long baseline, a common base station was established adjacent to the study area. This base was used as a reference point for all other GPS measurements. Absolute coordinates of this base station were computed relative to a known GPS base station in Hobart, approximately fifty kilometres away. The solution was based on approximately 10 hours of 30-second interval observations (classic static method).

(2) *Measurement of ground control points*: There were 12 ground control points measured, which were used for the 1:15,000, 1:10,000 and 1:5,000 scale photography. Each control point was measured using classic static mode. The measurements were taken over approximately 30 to 120 minutes with a 10-second interval. This gave accuracies of approximately 10mm horizontally and 30mm vertically.

(3) *Transformation of coordinates*[2]: The Ski software version 3 was used to process the GPS data and produce XYZ coordinates in WGS 84 datum. All WGS 84 coordinates were then transformed into the Australian Map Grid (AMG) coordinate system for planimetric coordinates and Australian Height Datum (AHD) for vertical coordinates.

4.5. Digital Terrain Model

4.5.1. Introduction

The height of a tree is the difference in elevation between the top and bottom of that tree. In many cases, the bottom of a tree is hard to view stereoscopically from aerial photographs. Under heavy canopy cover for example, measurement of terrain elevation from aerial photographs is impossible. Photo–interpreters would usually measure any available open area close to the bottom of the measured tree, which often produces inaccurate results, particularly when ground elevation varies rapidly.

---

[2] Any degradation in the quality of the control points as a result of coordinate transformation has yet been studied. However, the degraded quality will not significantly affect the accuracy of photogrammetric measurements within the project but will significantly affect the accuracy when integrating the results into other map products. Therefore, it is necessary to implement the correct transformation parameters of a particular area in the future.

A good digital terrain model (DTM) was required in order to reliably estimate the accuracy of tree canopy height measurements. The DTMs available from local authorities were not of sufficient accuracy, so an accurate DTM over the areas of interest was created.

4.5.2. Closed Canopy DTM Data Collection

Under the closed canopy plantation, the DTM data were collected using dGPS observations. Two Leica 200 GPS receivers were used, one receiver used as a base station and the other for collecting the DTM data (rover). The DTM data were collected on an approximate 20×20m sampling grid, providing a DTM accuracy of ±0.15m or better [e.g. Li 1992].

The GPS receiver could not receive a signal under the closed canopy and so the antenna was extended so that it reached approximately to the top of the trees. In 1996, the average height of the pine trees in the closed canopy forest was only about six metres so that a six–metre pole could be used. To measure the sampled points, the antenna had to be kept stable if a stop-go mode was employed. Small movements would cause significant error in measurement. In order to overcome this problem, the antenna was braced against a tree and the measurements undertaken in calm wind conditions. Each sampled DTM point was measured for between 10 to 30 minutes depending on canopy cover and wind conditions. The ambiguity of eighty percent of collected points could be resolved. The unsolved ambiguity points were removed and remeasured. Accuracy of 10cm or better can be achieved using this method.

4.5.3. Thinned Area DTM Data Collection

The DTM data for the thinned area were collected on a 10m grid using photogrammetric techniques from the 1:10,000 black and white photographs. To check accuracy, the DTM was compared against the field data measured using a combination of GPS observations and conventional traversing techniques. The GPS receivers in the field measurements were used to locate reference points along the open areas and a theodolite and a prism were used to collect the DTM data along the thinned rows. The accuracy of GPS measurements on each control point

was about ±0.01m, measured using a classic static method with a period of approximately two hours. The total station used was a Sokkia, with linear and angular accuracy specifications of ±(5mm + 5ppm) and ±10", respectively.

The mean difference between the DTMs produced using the photogrammetric technique and using the field measurement was 1.0±0.85m with the photogrammetric data overestimating the field data. This is to be expected, because of debris on the ground between rows, but does indicate a systemetic error that needs to be considered in later analyses.

4.6. Reference Canopy Height Models

4.6.1. Introduction

As described in Chapter 2, any measurement or classification involving remotely sensed data should be checked using reference data. This could be data observed from field measurements or some other accepted method.

4.6.2. Analytical Stereoplotter Data

For the 1:15,000 photographs, digital canopy models over both thinned and closed canopy plantations were generated using a Zeiss Planicomp P2 analytical stereoplotter. The canopy heights and terrain heights were measured on an approximate 10m grid. For the new photography at 1:10,000 and 1:5,000 scales, the same analytical stereoplotter was used to generate canopy models for the thinned and unthinned plantations. The latter reference data were obtained from the 1:10,000 scale black and white photographs on a 10m-grid interval.

The analytical stereoplotter data were used as the primary evidence of tree height for the following reasons:

- there was a one year gap between the date of aerial photography and the time of photogrammetric processing (for 1:15,000 scale photos), and consequent tree growth prior to field measurement; and
- the analytical stereoplotter data is preferable because it allows all the DPW data to be tested, rather than just a sample.

The reliability of the analytical stereoplotter data was tested against some well-

distributed ground truth data. It was found that the tree heights generated from the analytical stereoplotter underestimated the measured tree height by 0.4m on average, with a standard deviation of ±0.5m. This confirms the reliability of the analytical stereoplotter data.

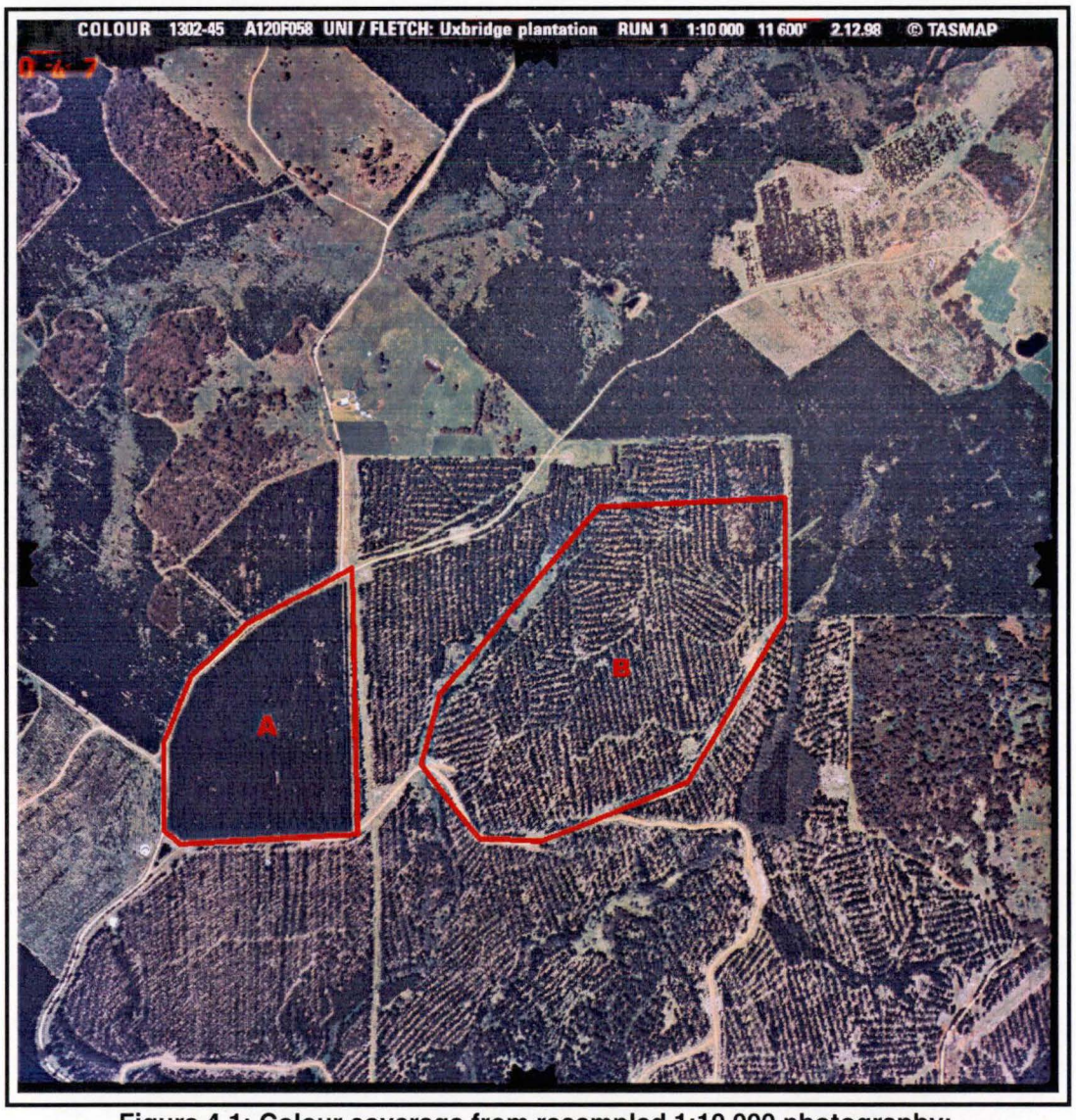

Figure 4.1: Colour coverage from resampled 1:10,000 photography; and location of study areas: (A) closed canopy stands and (B) thinned stands (scale 1:16,500 approximately).

Figure 4.2: Black and white coverage (from resampled 1:10,000 photography).

Figure 4.3: Black and white infrared coverage from resampled 1:5,000 photography.

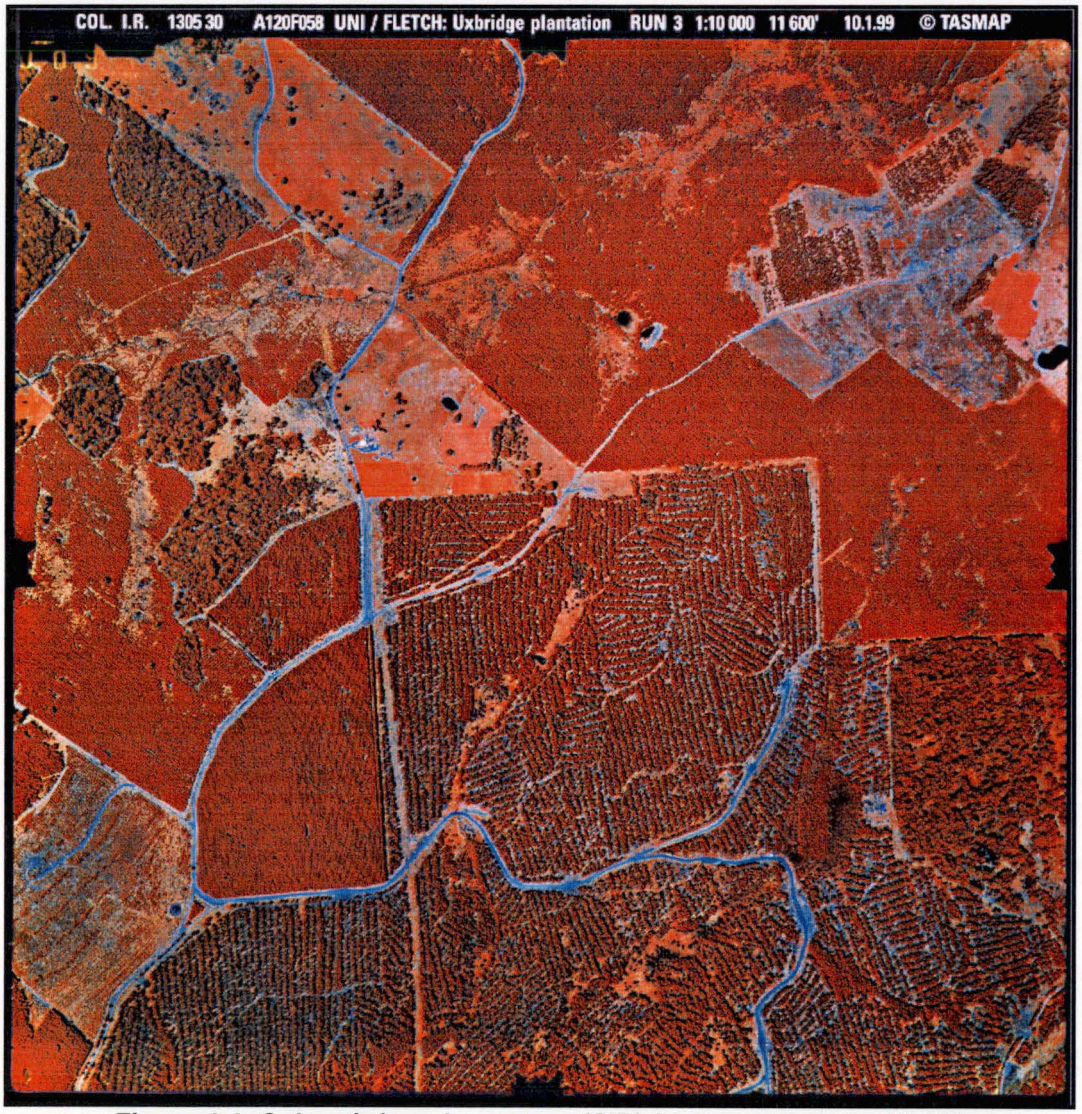

Figure 4.4: Colour infrared coverage (CIR) from resampled 1:10,000 photography.

Chapter 5. Methodology

5.1. Introduction

The research was completed in four stages:

(i) extraction of a digital canopy model using photogrammetric image correlation techniques (Section 5.2),

(ii) generation of digital elevation models (DEMs) (Section 5.3) including digital terrain models (DTMs), digital canopy models (DCMs) and digital canopy height models (DCHMs),

(iii) data filtering and processing (Section 5.4), and

(iv) statistical analysis (Section 5.5).

5.2. Extraction of Canopy Models

The procedure to generate a digital elevation model and orthoimages using SOCET SET® in the LH DPW 770 is illustrated in Figure 5.1.

5.2.1. Data Preparation and Project Creation

Nine projects were created (Table 5.1), with each project representing a unique combination of film type and scale.

5.2.2. Interior Orientation

The interior orientation determines the relationship between the image pixel coordinates and the calibrated fiducial coordinates. Camera calibration data (camera focal length, principal point offset in the x and y direction, radial lens distortion parameters and fiducial mark coordinates) were provided by the state

mapping agency.

The quality of interior orientation was measured in terms of error between the measured locations of the fiducial marks and the positions computed using an affine transformation derived from the calibrated and measured locations.

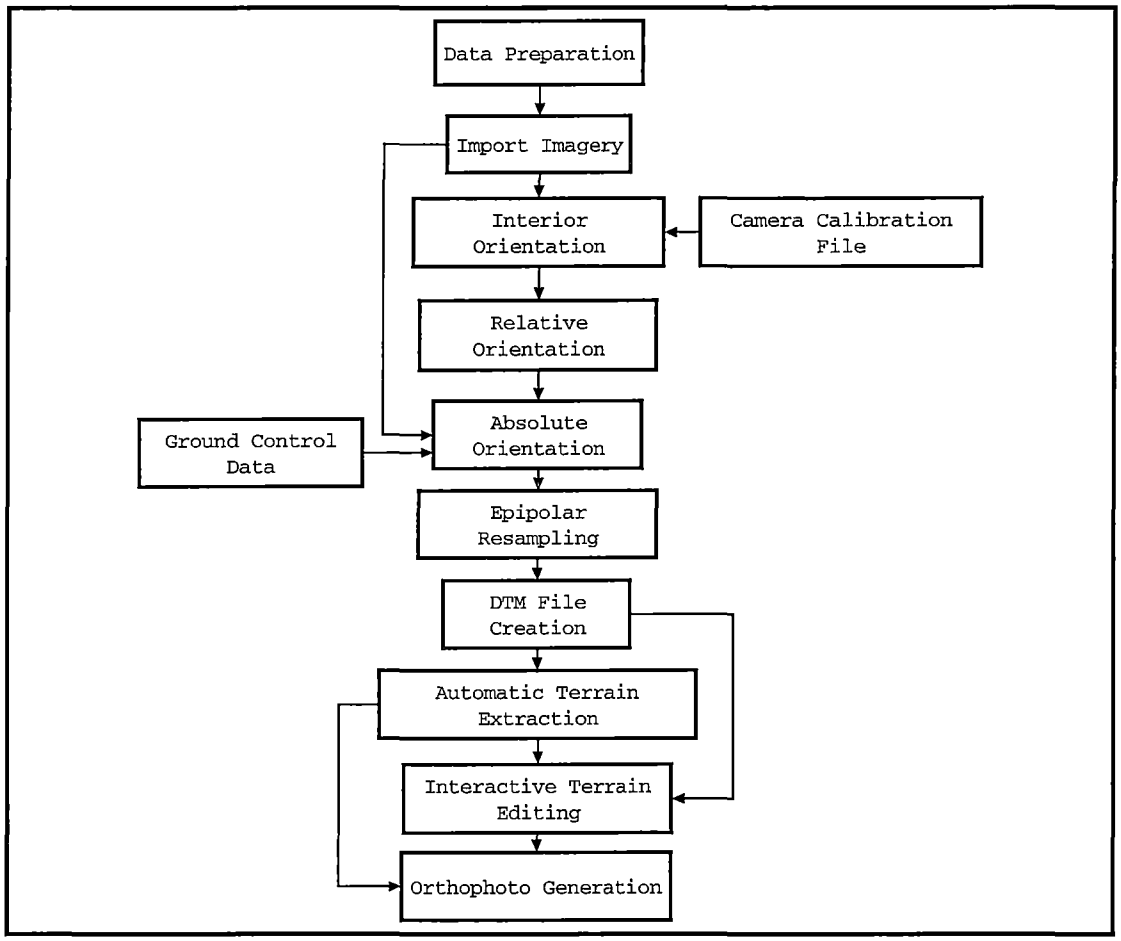

Figure 5.1: SOCET SET flowchart diagram.

Project No.	Scale	Film Type	Number of Photos
1	1:15,000	Colour (COL)	2
2	1:10,000	Colour	2
3	1:10,000	Black and white (BW)	2
4	1:10,000	Colour Infrared (CIR)	2
5	1:10,000	BW Infrared (BIR)	2
6	1:5,000	Colour	4
7	1:5,000	Black and white (BW)	4
8	1:5,000	Colour Infrared (CIR)	4
9	1:5,000	BW Infrared (BIR)	4

Table 5.1: List of projects created for this research.

5.2.3. Relative Orientation

The relative orientation determines the geometric relationship between two images. After several points are measured to establish an initial relationship between images, an automatic measurement utility uses image correlation in the stereo pair to assist in the location of conjugate image points. After completing the relative orientation, a stereo image can be viewed but, because the images have not been epipolar resampled, it may contain y–parallax that causes viewing discomfort.

5.2.4. Absolute Orientation

The absolute orientation relates the image or model coordinates to a ground coordinate system. The position and orientation of the camera is uniquely specified by six independent parameters, three positional elements (XYZ) and three rotational elements (Ω,Φ,K). At least six control points per stereomodel for the 1:10,000 photography and six control points per strip of four photographs were used in the absolute orientation. The method of measuring these points has been described in Chapter 4.

5.2.5. Epipolar Resampling

After completing the absolute orientation, the area of interest in the individual images is selected and epipolar resampled. Resampling to the epipolar format produces an equivalent vertical photograph, with the epipolar lines parallel to the x-axis of the image. Epipolar resampling incorporates any corrections the operator may have applied such as earth curvature, atmospheric refraction and lens distortion. Epipolar orientation simplifies the correlation process and greatly enhances the stereo viewing, significantly reducing eyestrain and therefore operator fatigue.

5.2.6. DTM Collection and Strategies

As described in Section 3.3.2, elevations can be measured automatically at any desired density. The area covered by a DEM can be defined precisely by a polygon outlining a specific region, which permits faster processing.

DEM points on a 0.5m grid were used to model the tree canopy surface. This

grid was applied to both unthinned and thinned plantations. For both areas, a modified *steep_1* strategy was employed. The window patch size used for the matching was reduced from 15×15 pixel to 11×11 pixel to anticipate the 0.5m grid, and all parameters that employed smoothing or filtering were switched off.

The automatic terrain extraction (ATE) software returns various statistics to indicate the status of the terrain extraction correlation algorithm. These include the correlation coefficient, signal power, shift and parallax, outside boundary points, and points thinned.

5.2.7. Output

SOCET SET can generate several different output formats. In this research the DEMs were exported into ARC/INFO grid ASCII files.

5.3. Generation of Digital Terrain Models and Digital Canopy Models

The GPS and analytical stereoplotter data were in the form of a list of XYZ coordinates, whereas the DPW data were in ARC/INFO ASCII grid format. This section describes the methods employed to generate uniformly formatted digital terrain models (DTMs) and digital canopy models (DCMs), including:

(1) definition of the boundary areas for the unthinned and thinned plantations;
(2) generation of the digital terrain models from GPS and photogrammetric data;
(3) incorporation of DPW data into ARC/INFO grid; and
(4) generation of the canopy height models.

The process involved GIS software (ARC/INFO version 7.0), operating in a Unix environment.

5.3.1. Boundary Definition

The aim of generating a boundary is to produce areas that have uniform size and orientation so that any mathematical operations involving two or more grids/lattices are possible.

The lines bounding the thinned and closed canopy plantations were measured using the LH DPW 770. The XY coordinates of the boundary lines were then

edited such that they could be imported into ARC/INFO to build a polygon coverage. The resulting files are in the form of a list of x,y coordinate pairs for each line. In this work, two polygon coverages were produced, one for the closed canopy stand and one for the thinned stand.

5.3.2. Derivation of DTMs and DCMs

The procedure for generating DTMs and DCMs from a list of XYZ coordinates is illustrated in Figure 5.2.

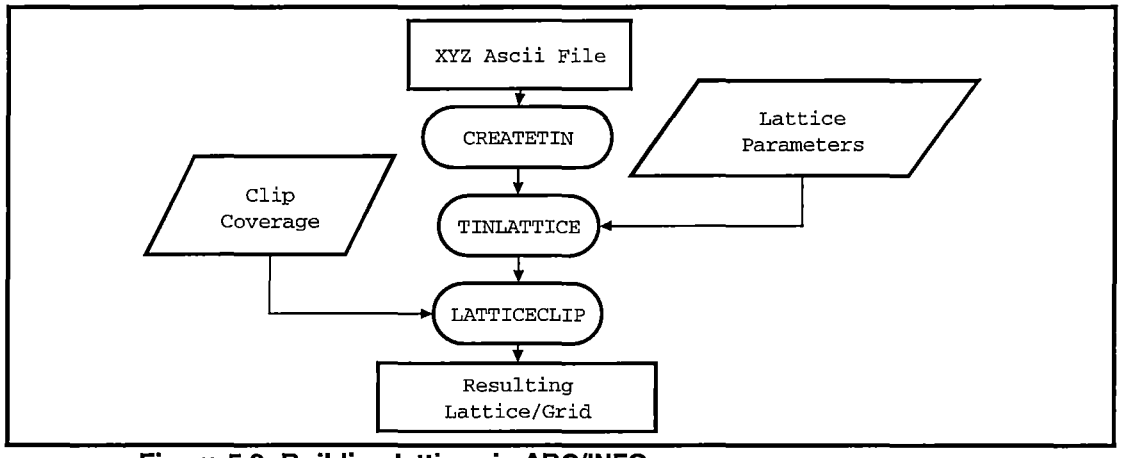

Figure 5.2: Building lattices in ARC/INFO.

The files containing XYZ coordinates derived from GPS and the analytical stereoplotter were edited in a point file format containing a list of x,y and z coordinates. The file was imported into ARC/INFO to build TINs (triangulated irregular networks) using the *CREATETIN* command. The TIN files were then converted into lattices using the *TINLATTICE* command. In this process, the resolution, size and orientation of the lattice were defined. A resolution of 0.5m was used, consistent with the grid produced by the DPW. The *LATTICECLIP* function clipped the lattices using the corresponding polygon coverage of the boundary.

5.3.3. Importing Digital Photogrammetric Data Into ARC/INFO

The DEM ASCII files generated of the DPW were already in ARC/INFO grid format. These files could be imported directly into ARC/INFO using the ASCII2GRID command. The resulting grids or lattices were also clipped using the corresponding boundary's polygon coverage.

5.3.4. Derivation of the DCHMs

The digital canopy height models (DCHMs) were extracted by direct subtraction of a terrain model (DTM) from the corresponding canopy model (DCM):

$$\mathbf{DCHM = DCM - DTM.}$$

The subtraction operation was done using the *LATTICEOPERATE* command in ARC/INFO.

5.4. Data Processing and Filtering

5.4.1. Introduction

The data generated from the DPW 770 contained errors due to incorrect image matching. Further processing was needed in order to produce reliable information. A number of issues were considered such as the definition of mean tree height (e.g. stand mean height, stand dominant height, or total height), possible method(s) that could used to extract these parameters, and determining the most reliable and effective method(s).

There are many methods of filtering digital data; the three most common are

(1) spatial domain algorithms,

(2) Fourier transforms, and

(3) wavelet transforms.

The following sections describe each method and how each method has been used to extract tree height data from data generated by the LH DPW 770. The algorithms were implemented using Matlab Version 5.3. A graphical user interface was developed to facilitate interactive assessment of the different data processing strategies. The graphical user interface is illustrated in Appendix A.

5.4.2. Spatial Domain Analysis

5.4.2.1. Introduction

In the spatial domain, the brightness or value of a pixel is represented as a function of its position in the image. Processing image data can be in a global, local or point operation [e.g. Rosenfeld and Kak 1982, Gonzalez 1987]:

- In global operations, pixels are modified by a transformation function based on

the gray levels of pixels distributed over an entire image. Some examples of global operations are image statistics, colour adjustment, and geometric operations such as rotation and resizing.

- In local operations, pixels are modified by a transformation function based on the gray level of pixels in the neighbourhood of that point. These local operations can be used to filter noisy data, to extract features (e.g. edge detection) and to smooth the image (e.g. local mean and median filters).
- In point operations, pixels are modified by a transformation function based on the gray level of the point. Point operations are usually used for gray scale manipulation and image segmentation by pixel classification.

5.4.2.2. The Spatial Domain Filters

Three spatial domain filters are used in this work. These are:

(1) a median filter,

(2) a mean tallest tree (MTT) filter, and

(3) an ortho threshold filter (for the thinned stand).

5.4.2.2.1. Median Filter

In a median filter the gray level of each pixel is replaced by the median of the gray levels in a neighbourhood of that pixel. A median filter is typically used to reduce "salt and pepper" type noise representing extreme values or outliers.

5.4.2.2.2. Mean Tallest Tree Filter

Mean dominant height (MDH), as defined in Section 1.1.2, cannot be derived from the photogrammetric data because the diameter at breast height (DBH) is not known. Instead, the parameter *mean tallest tree* (MTT) is used which is defined as the mean height of the tallest 60 trees per hectare. The number of sampled trees, plantation density and the size of the sampled area might vary among different forestry organisations. In this study, the plantation density is approximately 1000 trees per hectare. Hence, the MTT can be defined as the mean height of the tallest 6% of trees per hectare.

For computational efficiency, a block processing method is used. A block here represents a sampled plot in the field, which can be rectangular or square. In this method, the image is divided into smaller areas of the same dimension. Suppose

that the size of an image is m×n pixels and the size of a sampled plot is c×d pixels, then there are (m/c)×(n/d) blocks produced. In many cases however, the results of m/c or n/d may not be an integer number. To overcome this, zeros are added such that the results of m/c and n/d are integer – a process called zero padding.

The filter operates in each block. The first step is to arrange the matrix elements in the block into a vector matrix, having a dimension of 1 by (c×d). The matrix is then sorted. The next step is to find the values greater than zero. Here, only the heights above the ground are considered. The highest 6% pixel values above the ground are then averaged to get the MTT value of the block, and all values in this block are replaced with the resulting MTT value. The matrix is then reshaped to the original dimension, c×d.

5.4.2.2.3. Thresholding (Thinned Stand Only)

In the thinned stand, both canopy and ground cover are visible. Thresholding was used to extract canopy height data using a corresponding orthoimage that spectrally separates the ground cover from the canopy cover. The objective is to extract the heights for the canopy cover only and to investigate whether any mismatch was related to the measurement of points falling on the ground surface.

A method known to distinguish between the canopy and non-canopy covers of a forest is the normalised difference vegetation index (NDVI). The NDVI can be applied to the near infrared and red bands of a colour infrared (CIR) image. The NDVI can be calculated as [Schowengerdt 1997: 183]:

$$NDVI = \frac{\rho_{NIR} - \rho_{RED}}{\rho_{NIR} + \rho_{RED}}.$$

The result is an image in which the canopy surface is shown as brighter pixel values and the non-canopy surface darker darker pixel values. The canopy and non-canopy surfaces can then be separated by image segmentation. In this case, an NDVI image was produced from a 1:10,000 colour infrared orthoimage. The 1:10,000 scale photograph was used because it provides good ground visibility through the tree canopies, and an orthoimage was used because it allows NDVI and tree height data to be directly compared.

5.4.3. Fourier Analyses

5.4.3.1. Introduction

The Fourier transform is the most common frequency domain analysis used in image processing [e.g. Kreyszig 1972, Weaver 1983, Brigham 1988]. It produces a representation which, although different from the original data, is completely equivalent to it in terms of the information contained. The Fourier transforms exploit the fact that an arbitrary function may be constructed from the sum of many sine and cosine functions with different amplitudes, frequencies and phases. The image is stored as a set of spatial frequency values together with their associated amplitudes and phases. Instead of brightness as a function of position, the Fourier representation is essentially amplitude as a function of spatial frequency. The Fourier representation is said to be in the frequency domain.

A Fourier transform can be continuous or discrete. Because a digital computer works only with discrete data, numerical computation of the Fourier transform requires discrete sample values. The two-dimensional discrete Fourier can be expressed as

$$F(u,v)=\frac{1}{N}\sum_{x=0}^{N-1}\sum_{y=0}^{N-1} I(x,y)e^{-2\pi j(ux+vy)/N}$$

where $e^{-2\pi j(ux+vy)/N} = \cos(2\pi(ux+vy)/N) - j\sin(2\pi(ux+vy)/N)$,

and the inverse transform as

$$I(x,y)=\frac{1}{N}\sum_{u=0}^{N-1}\sum_{v=0}^{N-1} F(u,v)e^{2\pi j(ux+vy)/N}$$

where $e^{2\pi j(ux+vy)/N} = \cos(2\pi(ux+vy)/N) + j\sin(2\pi(ux+vy)/N)$.

Direct computation of the two-dimensional discrete Fourier equation above requires in the order of N^4 operations. The Fast Fourier transform (FFT) is a particular method of computing a discrete Fourier transform. The FFT ignores the computation of individual values of the exponential term. These can be computed once and stored in a suitable table. The number of operations can be reduced to being of order ($N^2\log_2 N$). For example, if an image has 512 pixel square, then the number of operations otherwise needed is approximately 6.9×10^{10}. Using the FFT this number can be reduced to about 2.4×10^6, an improvement factor of nearly 30,000 times [Lewis 1990: 156–160].

5.4.3.2. The Fourier Transform as an Image

A standard representation of the Fourier transform of an image is another image in which the X axis represents spatial frequency along the original image's x axis and the Y axis represents spatial frequency along the original image's y axis. The constant term is at the origin and the highest frequency term is at the other end of the axis. The highest frequency component has a period equal to the width of a single pixel, that is one cycle per pixel. The amplitude and phase of the sine and cosine waves with particular frequencies are coded as a complex value stored in the appropriate pixel of the image [e.g. Lewis 1990: 155–158].

Displaying the Fourier spectrum of an image can be very difficult if there is a wide dynamic range of the data in the frequency domain. The spectrum is a real image with a floating-point value at each pixel location. The values must be remapped to an integer range compatible to the chosen display device. It is common to reduce the complexity by eliminating many low amplitude components and the least informative zero frequency term. Another way to display the Fourier spectrum is using the logarithm of the spectrum. The example in Figure 5.3 illustrates this method.

5.4.3.3. Processing Images Using the Fourier Transform

Some useful filtering operations can be carried out on the Fourier transform of an image rather than on the image itself. Two important filters are low pass filters and high pass filters. Low pass filters attenuate the high frequency components and have a smoothing effect on the image but preserve the general trend of the image. High pass filters attenuate low frequencies and produce a sharper image [Lewis 1990: 160–167].

An ideal filter is one in which a certain set of frequencies is passed through unaffected whilst all other frequencies are completely blocked. Figure 5.4 and Figure 5.5 illustrate ideal low pass and high pass filtering of an image.

The ideal filter uses a simple but dramatic method of reducing the amplitude of high or low frequency components of the frequency domain image. Rather more subtle approaches reduce the amplitude of high frequency components in relation to the low frequency ones. This can be done, for instance, by scaling down the amplitudes of high frequency components by a constant.

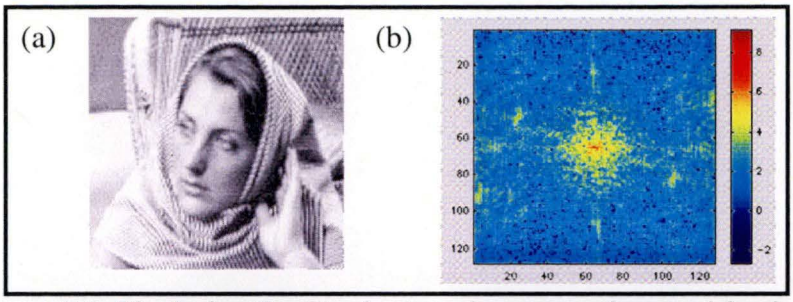

Figure 5.3: Displaying the Fourier transform as an image: (a) original image (Matlab 1998), and (b) its Fourier domain.

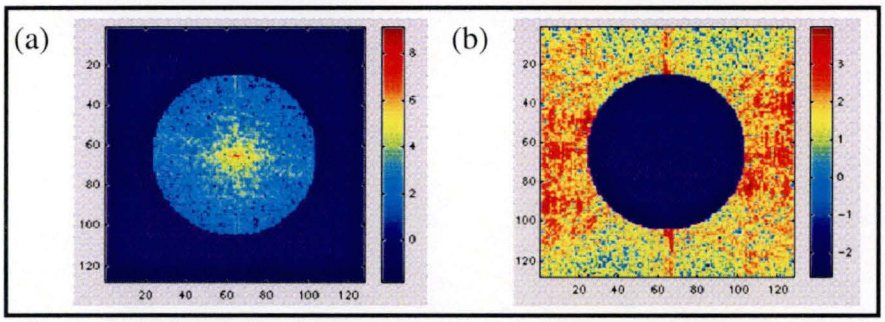

Figure 5.4: Example of a Fourier image (of Figure 5.3) after an ideal low pass filter (a) and an ideal high pass filter (b). The radius of the circle is 40 pixels.

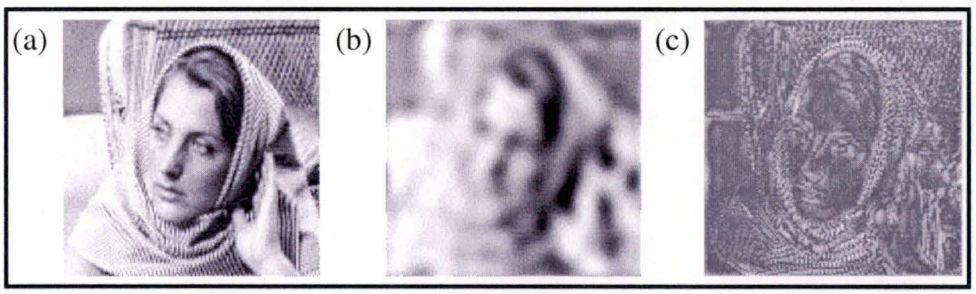

Figure 5.5: Example of an ideal filter: (a) Original image, (b) filtered version of (a) using an ideal low pass filter of radius 10 pixels; (c) filtered version of (a) using an ideal high pass filter of radius 10 pixels.

5.4.3.4. The Adaptive Fourier Filter

An adaptive, circular, low pass Fourier domain filter was developed to smooth the DPW derived tree heights. The filter has a fixed radius, R, defined as the shorter dimension of the image divided by four. For an image of dimension *m* by n, the resulting Fourier image also has a dimension of *m* by *n*. If *n* is less than *m* for example, then $R = n/4$. Figure 5.6 illustrates the iteration process used in the adaptive Fourier filter.

A number of well-distributed tree height data measured manually using the DPW are used as reference points for the iteration. The aim of the iteration process

is not to correct the original data based on manually measured data, but to smooth DPW data and remove any outliers. The algorithm adaptively filters the tree height data by assessing the mean differences between the reference points and the tree height model.

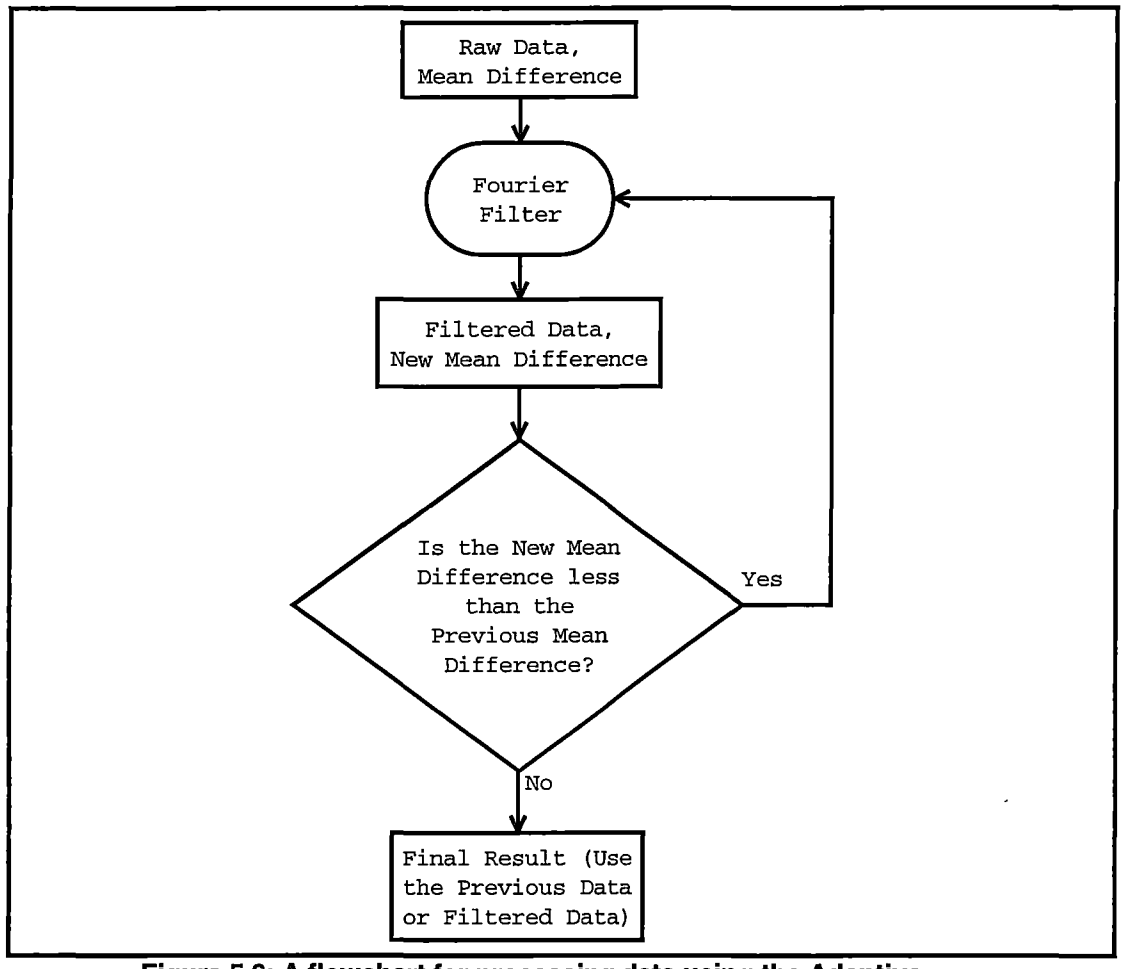

Figure 5.6: A flowchart for processing data using the Adaptive Fourier filter method.

Firstly, the mean difference between the reference points and the raw data is calculated. The raw data is then transformed into the frequency domain and the filter is applied. Next, the filtered data is transformed into the spatial domain, and the mean difference between the reference points and the filtered data is calculated. If the mean difference increases then the raw data is used, but if the mean difference is reduced then the filter is reapplied until there is no further significant reduction.Applying the adaptive Fourier filter consistently reduced the mean difference for all data sets. The number of iterations was recorded between 1 and 3 in the closed canopy stand and between 2 and 4 in the thinned stand.

5.4.4. Wavelet Transform

5.4.4.1. Introduction

Wavelets are mathematical functions that divide data into different frequency components, allowing data to be processed at different scales or resolution. Over recent years, wavelets have proven to be a versatile tool for various image processing tasks [Mallat 1989a]. They have been used for applications such as image compression [e.g. DeVore *et al.* 1992], feature detection [e.g. Mallat and Zhong 1992], image enhancement, and noise removal [e.g. Donoho and Johnstone 1994].

5.4.4.2. Basis Functions

A commonly used approach to analyse a signal $f(x)$ is to represent it as a weighted sum of simple building blocks, called *basis functions*:

$$f(x) = \sum_i c_i \Psi_i(x)$$

where Ψ_i are basis functions and the c_i are coefficients, or weights. Since the basis functions Ψ_i are fixed, it is the coefficients, which contain the information about the signal.

A useful analogy is to consider a digital vector rather than an analog function [Strang 1992]. Every two-dimensional vector (x,y) is a combination of the vectors (1,0) and (0,1). These two vector are the basis vector for (x,y). The best basis vectors have the valuable property that they are orthogonal to each other. The basis vectors (1,0) and (0,1) satisfy this criterion. A basis function varies in scale by chopping up the same function using different scale sizes.

5.4.4.3. The Wavelet Transform

A wavelet is defined as a family of functions that are generated by translating and dilating a single function [Mallat 1989b]. For a one dimensional signal $f(x) \in L^2(R)$, this is given by

$$W(a,b) = \frac{1}{\sqrt{a}} \int_{-\infty}^{+\infty} f(x) \Psi^* \left(\frac{x-b}{a} \right) dx$$

where $\Psi^*(x)$ is the analysing wavelet;

a(>0) is the scale parameter; and

b is the position parameter.

The transformation is characterised by the following properties [e.g. Starck and Bijaoui 1994]:

- it is a linear transformation;
- it is covariant under translations: $f(x) \rightarrow f(x-u)$; $W(a,b) \rightarrow W(a,b-u)$;
- it is covariant under dilations: $f(x) \rightarrow f(sx)$; $W(a,b) \rightarrow s^{-0.5}W(sa,sb)$.

The last property makes the wavelet transform very suitable for analysing a hierarchical structure. By performing the wavelet transform with multiple values of *a,* a representation of an image that has good local resolution in both the space and frequency domains can be obtained.

Wavelet analysis may be extended to m–dimensions [Daubechies 1988, Mallat 1989a]. For the two-dimensional case of interest to image processing, it is desirable to find the best approximation of the image $f(x,y)$ in the vector space ν. Lower resolution approximations, $A_i(x,y)$, may be expressed in terms of the vector space ν_i. The difference between the approximation signals at resolution i and $i+1$ is expressed in terms of an orthonormal basis of sub–space ω_i. This basis may be built by scaling and translating the following three wavelets [Henke–Reed and Cheng 1993]:

$$\psi^1(x,y) = \phi(x)\,\psi(y);$$
$$\psi^2(x,y) = \psi(x)\,\phi(y);$$
$$\psi^3(x,y) = \psi(x)\,\psi(y).$$

Any given image, $A_i(x,y)$, may be decomposed into one approximation and three difference signals that fully represent the original image. The difference signals contain high frequency components of the image, and therefore are also called detailed signals [Henke–Reed and Cheng 1993], and can be found in the following manner:

$$A_{i+1}(x,y) = \langle A_i(x,y), \phi_i(x)\phi_i(y) \rangle;$$
$$D^1_{i+1}(x,y) = \langle A_i(x,y), \phi_i(x)\psi_i(y) \rangle;$$
$$D^2_{i+1}(x,y) = \langle A_i(x,y), \psi_i(x)\phi_i(y) \rangle;$$
$$D^3_{i+1}(x,y) = \langle A_i(x,y), \psi_i(x)\psi_i(y) \rangle.$$

The forward and inverse wavelet transforms can be efficiently implemented by using a set of appropriately designed Quadrature Mirror Filters (QMFs): *G, H, G',*

and H'. The filter H is a low pass filter and G is high pass filter. The filters H' and G' are time–reversed versions of H and G, respectively. Using this notation, the above equations become:

$$A_{i+1}(x,y) = A_i(x,y)*H'(x)H'(y);$$
$$D^1_{i+1}(x,y) = A_i(x,y)*H'(x)G'(y);$$
$$D^2_{i+1}(x,y) = A_i(x,y)*G'(x)H'(y);$$
$$D^3_{i+1}(x,y) = A_i(x,y)*G'(x)G'(y).$$

The convolution products of QMFs are separable in the x and y directions which leads to a simple algorithm for the two-dimensional wavelet transform. A single (i=0) two-dimensional wavelet transform of an image is accomplished by two separate one dimensional transforms. The image $f(x,y)$ is first filtered along the x dimension, resulting in a low pass image $f_{Lo}(x,y)$ and a high pass image $f_{Hi}(x,y)$. Since the bandwidth of f_{Lo} and f_{Hi} along the x dimension is now half of f, each of these filtered images can be down sampled in the x dimension by 2 without loss of information, accomplished by dropping every other filtered value. Both are then filtered along the y dimension and down sampled in the y dimension by two, resulting in four sub images: f_{LoLo}, f_{LoHi}, f_{HiLo}, and f_{HiHi}.

A two-dimensional filtering decomposes an image into an *average signal* f_{LoLo}, and three detail signals which are directionally sensitive: f_{LoHi} emphasises the horizontal image features, f_{HiLo} the vertical features, and f_{HiHi} the diagonal features. This version of the two-dimensional wavelet transform is therefore sensitive to spatial orientation of an image.

In the two-dimensional inverse wavelet transform, the average and detail images are first up sampled by two along the y dimension, accomplished by inserting a zero between each pair of values in the y dimension. This is necessary to recover the proper bandwidth required to add the signals back together. After up sampling, the signals are filtered along the y dimension and added together appropriately. The process is then repeated in the x dimension to produce the final reconstructed image.

5.4.4.4. Examples of Applications

The most interesting difference between the wavelet transform and the Fourier

transform is that the individual wavelet functions are *localised in space*. Fourier sine and cosine functions are not. This localisation feature makes many functions and operators using wavelets "sparse" when transformed into the wavelet domain which results in a number of useful applications: data compression [e.g. Antonini *et al.* 1992], image classification [e.g. Henke–Reed and Cheng 1993], feature extraction [e.g. Simhadri *et al.* 1998], and noise removal or reduction from time series [e.g. Donoho 1993 and 1995, Liew *et al.* 1997, Pillard and Epelboin 1998].

5.4.4.5. The Adaptive Wavelet Filter

Wavelet shrinkage, resulting from the down sampling, can be used to smooth images. At each resolution level, the coefficients for the products of scaling and wavelet functions in the horizontal and vertical directions are obtained. If only the approximation image were up sampled then the result would be the smoothed version of the original image, where the horizontal, vertical and diagonal high frequency components have been eliminated.

The major problem is to select the most appropriate wavelet and its resolution level. There are a number of wavelet families: Haar, Daubechies, Biorthogonal, Meyer, Morlet, Symlet, Mexican hat, and Coiflet, and all of these have been discussed in many standard texts [e.g. Young 1993]. The Daubechies wavelets are a commonly used family, the only family that has continuous scaling functions and wavelets with full scaling and translation orthogonality [e.g. Horgan 1998].

Smoothing by the Daubechies wavelets produce a smoother and more satisfying image than other wavelets [e.g. Horgan 1998], and the field boundary are better preserved. In this experiment, Daubechies–6 at resolution level 2 was used. Preliminary investigation indicated that Daubechies–6 at resolution level 2 produced a smoothed image without loosing significant detail, whereas, although continuous, Daubechies–4 was differentiable nowhere and Daubechies–8 over smoothed the images.

To find the best result, an iterative algorithm was developed. Figure 5.7 illustrates the iteration process for the adaptive Wavelet filter. The iteration process was applied in the same way as for the adaptive Fourier filter, and filter used the same reference data. The number of iterations was recorded between 1 and 3 in the closed canopy stand and between 2 and 5 in the thinned stand.

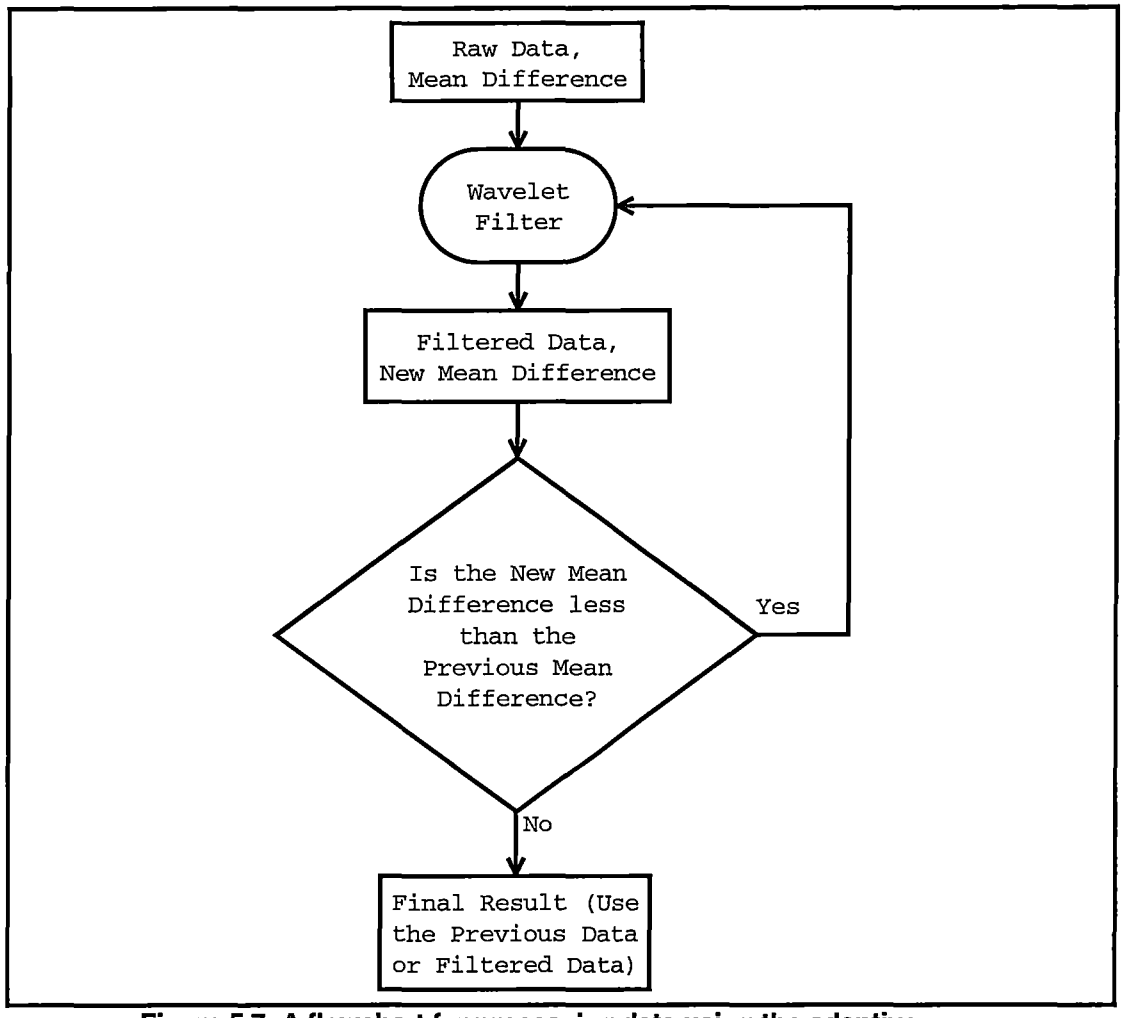

Figure 5.7: A flowchart for processing data using the adaptive wavelet filter.

5.4.5. General Computational Procedures

The computational procedures involve three stages. Figure 5.8 shows the steps used to generate clean data using the three stages.

The process for generating clean data began with exporting an ARC/INFO grid ASCII file from the DPW 770. The headers of this file contained information about the numbers of rows and columns, the geo–reference coordinates, the pixel resolution, and the NODATA value, usually –9999. This file was then imported into ARC/INFO to produce a uniform grid format to enable the derivation of a canopy height model. An ASCII grid file was exported from this grid data. The headers were deleted to form a matrix and saved into a different file for later use to enable processing in Matlab software. Image processing in Matlab could then be undertaken. The final image was then saved as an ASCII file for further processing

in ARC/INFO. The headers of the original ASCII file were simply copied onto the new ASCII file to geo–reference the coordinates.

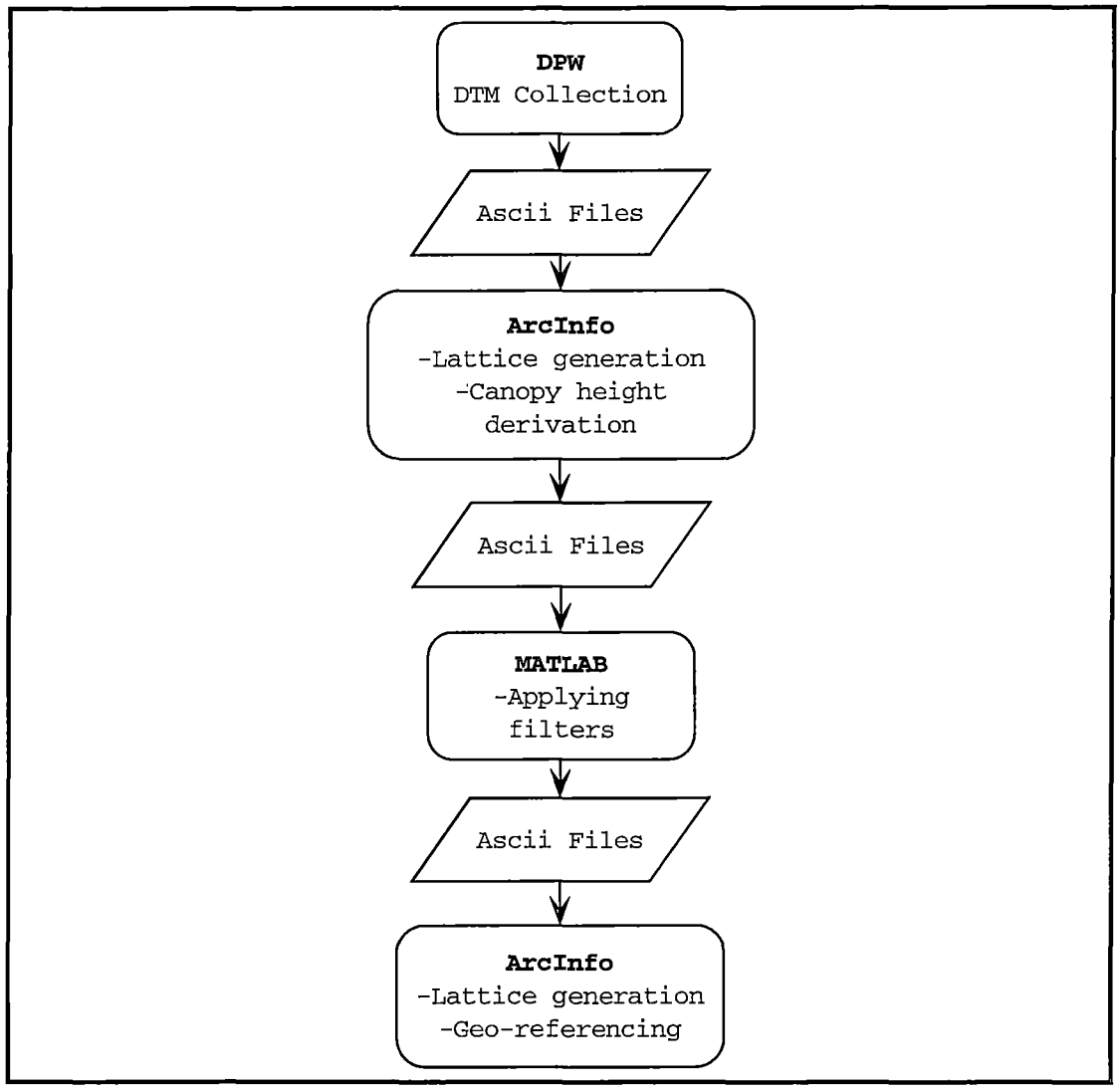

Figure 5.8: Flowchart for generating smoothed tree height data.

5.4.6. Filtering Strategies

Fourteen strategies have been tested, with each strategy applied to every image type (colour, black and white, colour infrared, black and white infrared, 1:15,000, 1:10,000 and 1:5,000 photoscale). The strategies and the analytical stereoplotter data against which they were compared are listed in Table 5.2.

No		Filter 1	Filter 2	Filter 3	Area	Vs	Analytical
Strategy 1	Raw Data	–	–		C,T	Vs	AP Raw data
Strategy 2	Raw Data	Median	–		C,T	Vs	AP Raw data
Strategy 3	Raw Data	Wavelet	–		C,T	Vs	AP Raw data
Strategy 4	Raw Data	Fourier	–		C,T	Vs	AP Raw data
Strategy 5	Raw Data	Median	MTT		C,T	Vs	AP MTT
Strategy 6	Raw Data	Wavelet	MTT		C,T	Vs	AP MTT
Strategy 7	Raw Data	Fourier	MTT		C,T	Vs	AP MTT
Strategy 8	Raw Data	Threshold	–		T	Vs	AP Threshold
Strategy 9	Raw Data	Median	Threshold		T	Vs	AP Threshold
Strategy 10	Raw Data	Wavelet	Threshold		T	Vs	AP Threshold
Strategy 11	Raw Data	Fourier	Threshold		T	Vs	AP Threshold
Strategy 12	Raw Data	Median	Threshold	MTT	T	Vs	AP MTT
Strategy 13	Raw Data	Wavelet	Threshold	MTT	T	Vs	AP MTT
Strategy 14	Raw Data	Fourier	Threshold	MTT	T	Vs	AP MTT

Table 5.2: Filtering strategies (C = closed canopy and T = thinned) and comparing the results against the analytical stereoplotter data.

5.5. Statistical Analyses

There are several analysis methods that can be applied to compare two or more digital elevation models. These include:

5.5.1. Statistical Measures

The first and easy method of analysing two surface models is by comparing the global statistics of each data set; specifically means and standard deviations as well as the absolute differences between the two data sets [e.g. Bosltad and Stowe 1994, Rieger 1996].

5.5.2. Histogram Distributions

In this case, the histogram distributions of tree heights for two or more DEM data are compared. The distributions are tested by examining their mean and variance the skewness and kurtosis tests [Kendall and Stuart 1969], and by visual inspection.

5.5.3. Correlation Coefficients

Comparison of two-dimensional data can also be examined by computing the correlation coefficient of the two images. The correlation coefficient (ρ) of two images or matrices A, B of the same size can be defined as

$$\rho = \frac{\sum_{n1}\sum_{n2} A(n_1,n_2)B(n_1,n_2)}{\sqrt{\sum_{n1}\sum_{n2} A^2(n_1,n_2)\sum_{n1}\sum_{n2} B^2(n_1,n_2)}}$$

where ρ has a value between 0 to 1 (indicating low to high correlation),

n_1 is the number of row in the image

n_2 is the number of column in the image

5.5.4. Image Profiles

Image profiles can be used to support the correlation coefficient results. Vertical and horizontal profile data of two DEMs are compared in this method. This is also a visual method to examine the degree of surface roughness of the two DEMs, the analytical stereoplotter data and the DPW data. It should be noted that the difference in data sampling between the test data (DPW data) and the reference data (analytical stereoplotter data) must be considered.

5.5.5. Visual Inspection

The images of the DCHMs can be transformed into gray scale images. Characteristics of the distributions, which may not be evident in the previous analyses, may become evident upon visual inspection.

Chapter 6. Comparison Between Digital and Analytical Photogrammetric Data

6.1. Introduction

This chapter presents a comparison between the digital photogrammetric data and the analytical stereoplotter data. The first part of the chapter (Section 6.2) deals with the closed canopy stand; the second part (Section 6.3) deals with the thinned stand. Each canopy height model of both the closed canopy and thinned stand was compared against the reference canopy models derived from the analytical stereoplotter. The method of comparing these models has been outlined in Section 5.4.6. In the case of the closed canopy stand, the analysis is classified into two parts: before and after applying a mean tallest tree filter. In the case of the thinned stand, more filtering strategies were applied to the canopy height models, comprising seven additional strategies. Similar to the closed canopy stand, the analysis is classified into two parts: before and after applying a mean tallest tree filter.

All digital canopy height models (DCHMs) and images included in this chapter can be viewed at high resolution using the enclosed CD. The DCHMs are all in Windows bitmap file format.

6.2. Analysis: the Closed Canopy Stand

6.2.1. Orthoimage of the Closed Canopy Stand

An orthoimage was generated using the LH DPW 770 from the 1:10,000 scale black and white photographs, at 0.5m resolution (Figure 6.1). The DEM used to

generate the orthoimage was the analytical stereoplotter (AS) canopy elevation model (that is, canopy heights with respect to a map datum).

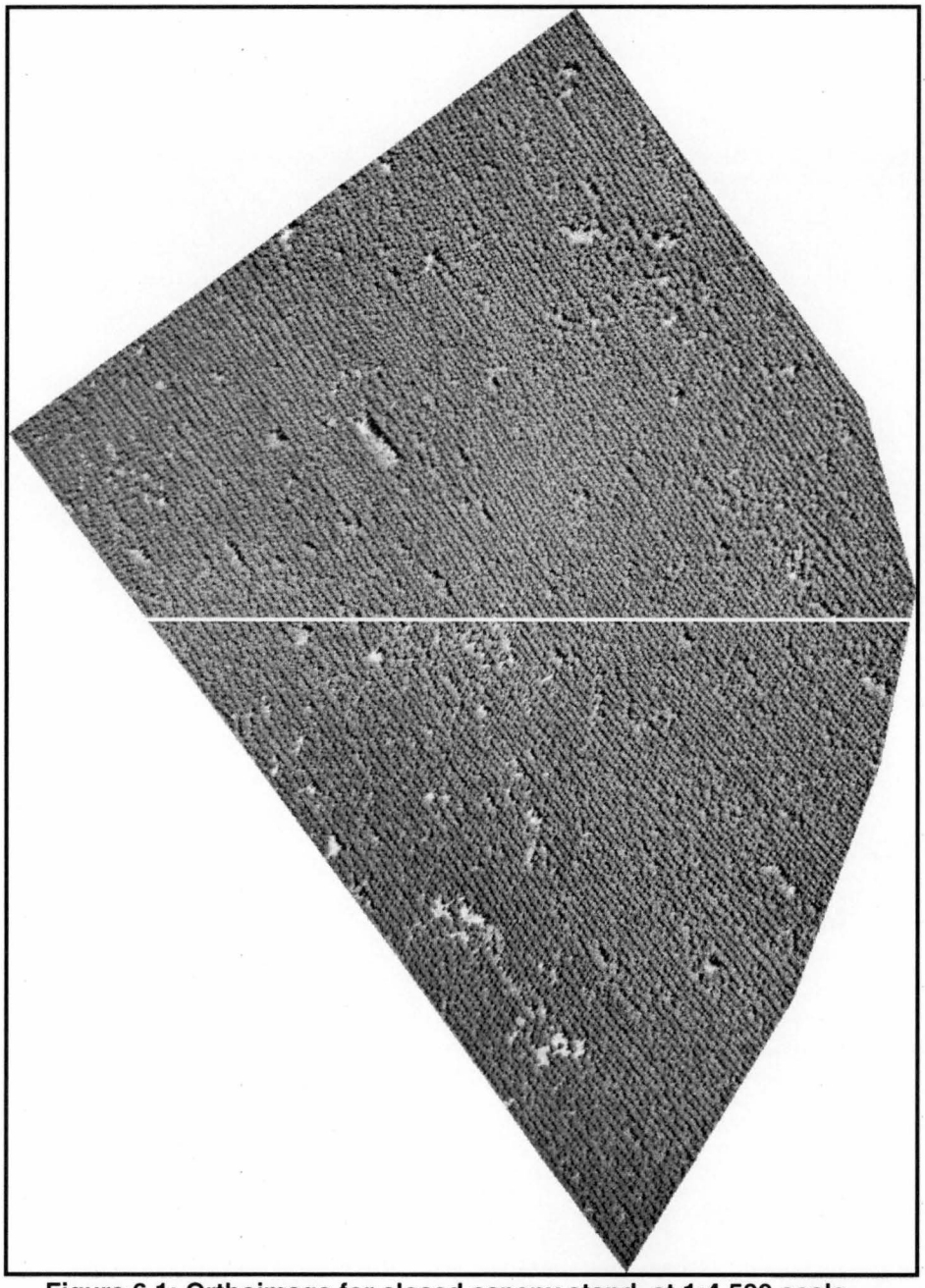

Figure 6.1: Orthoimage for closed canopy stand, at 1:4,500 scale approximately; and a line indicating the location of derived height profiles.

The closed canopy stand contained 1000–1250 thirteen-year-old trees per hectare, and the canopy was closed or approaching closure. However, there were failed areas within the stands, clearly visible in Figure 6.1. These patches are less visible when looking at larger scale photographs (ie. 1:5,000) due to camera viewing angle, which limits the penetration through the canopy.

In the closed canopy stand, viewing the stereo images was relatively easy at all image resolutions and for all film types and scales. The proportion of visible ground that appeared in the images was small in comparison to the canopy surface and tree heights were relatively uniform. Therefore, there were few abrupt changes in the canopy surface, resulting in comfortable stereo viewing.

6.2.2. Analytical Stereoplotter Data

As noted in Chapter 4, two sets of analytical stereoplotter canopy height data were obtained. These were the 1996 and 1999 data sets. The 1996 analytical stereoplotter data were used to assess only the 1996 1:15,000 data (colour), which had been extracted from the same aerial photographs, whereas the 1999 analytical stereoplotter canopy height models were used to analyse the 1998/1999 1:10,000 and 1:5,000 data.

Both 1996 and 1999 data sets were extracted from the same analytical stereoplotter, a Zeiss Planicomp P2, but two different operators were employed. Hence, a consequent possibility of systematic differences should be considered when comparing the two data sets. The results for both data sets are summarised in Table 6.1 and the images of both models are shown in Figure 6.2 and Figure 6.3.

Image Types	AS 1996		AS 1999		AS 1999–AS 1996		
	Mean (m)	σ (m)	Mean (m)	σ (m)	Mean (m)	σ (m)	ρ
Raw Data	5.8	±1.0	11.2	±1.3	5.4	±0.8	0.78
MTT Data	6.5	±1.0	12.3	±1.3	5.8	±0.7	0.81

Table 6.1: Statistical results for analytical stereoplotter raw and MTT data for 1996 and 1999 data (closed canopy stand). ρ = correlation coefficient.

As indicated in Table 6.1, it can be seen that in three years the trees in the closed canopy stand had grown more than five metres on average. This is greater than expected, based on the current growth model [Candy 1989b]. According to the growth model, in three years the trees would be expected to grow by a factor of 1.35, or about two metres on average. The ground truthing was undertaken in 1999 and has confirmed the reliability of the 1999 analytical stereoplotter data. So it seems likely that the 1996 analytical stereoplotter data may be underestimating the actual tree heights at that date. Further, the different photoscales and viewing and illumination conditions need to be considered as well as possible systematic

differences due to the two different operators.

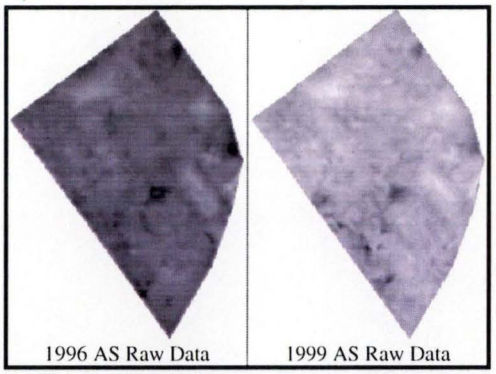

Figure 6.2: Analytical stereoplotter raw data (closed canopy stand). Gray scale: 0–20m [dark–light].

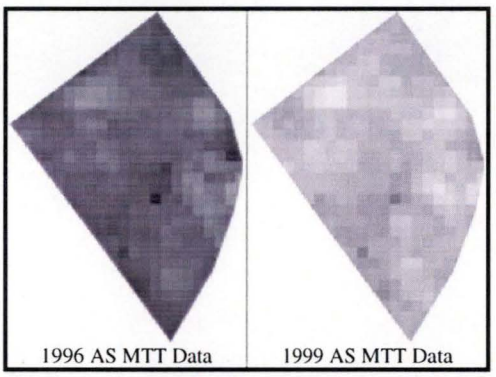

Figure 6.3: Analytical stereoplotter MTT data (closed canopy stand). Gray scale: 0–20m [dark–light].

The correlation (ρ) between the 1996 and 1999 raw analytical plotter data was high. The correlation between the MTT filtered data sets was even higher, but the mean difference was significantly increased ($P<0.0001$). This correlation can be used as evidence that the growth rate was relatively uniform across the plantation stand. This is supported by visual inspection of the height distributions shown in the images above.

When comparing the analytical MTT data against the DPW MTT data, it is expected that the MTT filter will have increased the tree heights. The analytical stereoplotter data were filtered using the MTT filter so that the structure of the surface can be compared and the statistical differences derived.

6.2.3. Analysis: Raw and Filtered Tree Heights

The 1:15,000 colour data are illustrated in Figure 6.4. Canopy heights derived from raw DPW data are illustrated in Figure 6.5. Canopy heights filtered using the

median, adaptive wavelet, and adaptive Fourier filters can be seen in Figures 6.6 to 6.8.

Visual inspection suggests that all raw data sets produced similar tree height distributions, except for the 1:10,000 scale colour data, where some parts of the model differ substantially. The height data also visually compares well with the orthoimage (Figure 6.1). The black and white infrared data for both the 1:5,000 and 1:10,000 scale photography clearly illustrate plantation row direction, while only the colour infrared and black and white at 1:5,000 show these patterns.

In the case of the 1:10,000 scale colour data, the quality of one image of the stereopair was poor, especially in some areas of the closed canopy. In these areas, the individual trees could not be clearly identified due to blurring. Various image enhancement techniques were investigated but none improved the image quality. Therefore, the 1:10,000 scale colour data will not be discussed in detail in this chapter but the statistical results will be included to indicate its characteristics.

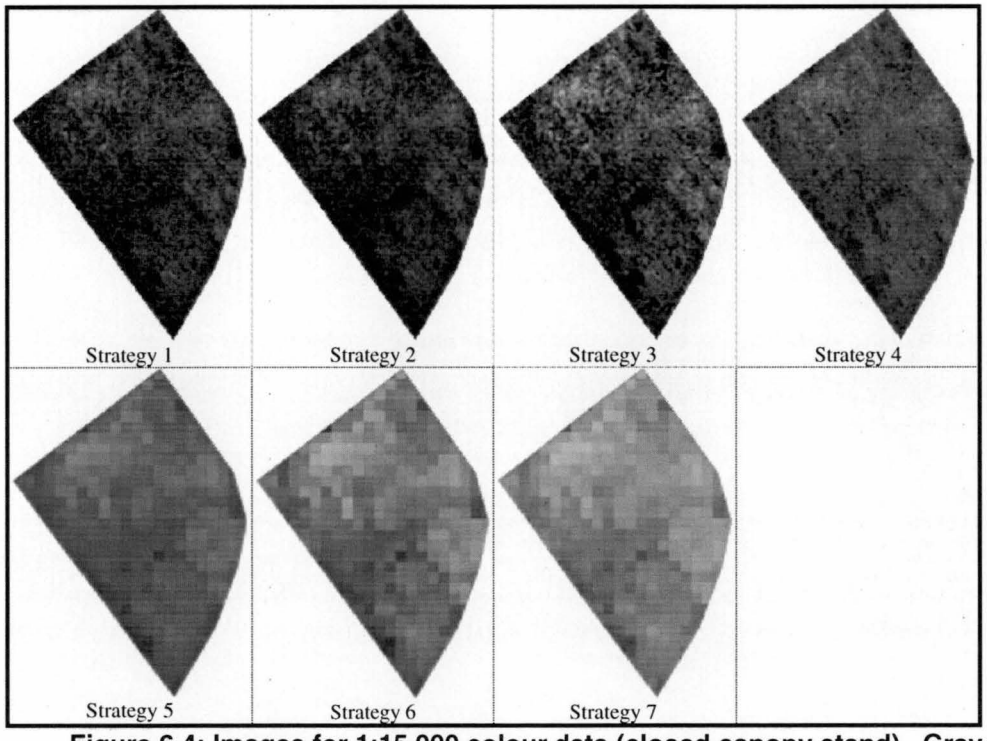

Figure 6.4: Images for 1:15,000 colour data (closed canopy stand). Gray scale: 0–20m [dark–light].

The following filters were applied to the raw data for Strategies 2–4:

- a median filter (Strategy 2): 7 × 7 pixels;
- an adaptive wavelet filter (Strategy 3): Daubechies–6 level 2; and

- an adaptive Fourier filter (Strategy 4): radius of 0.25 of the shorter image dimension.

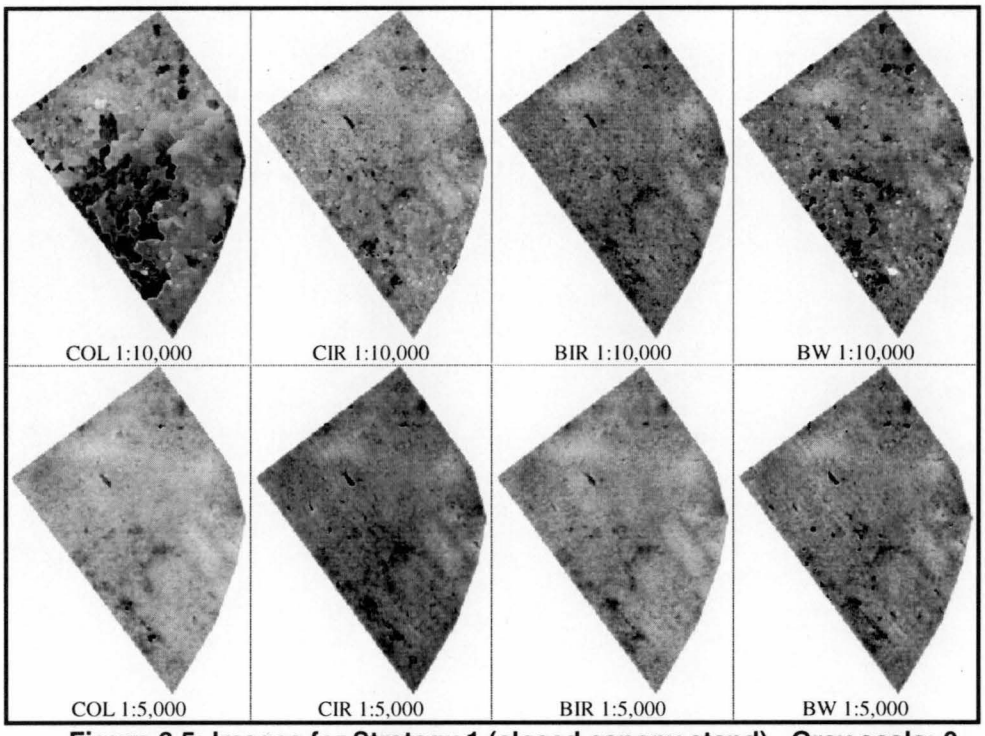

Figure 6.5: Images for Strategy 1 (closed canopy stand). Gray scale: 0–20m [dark–light].

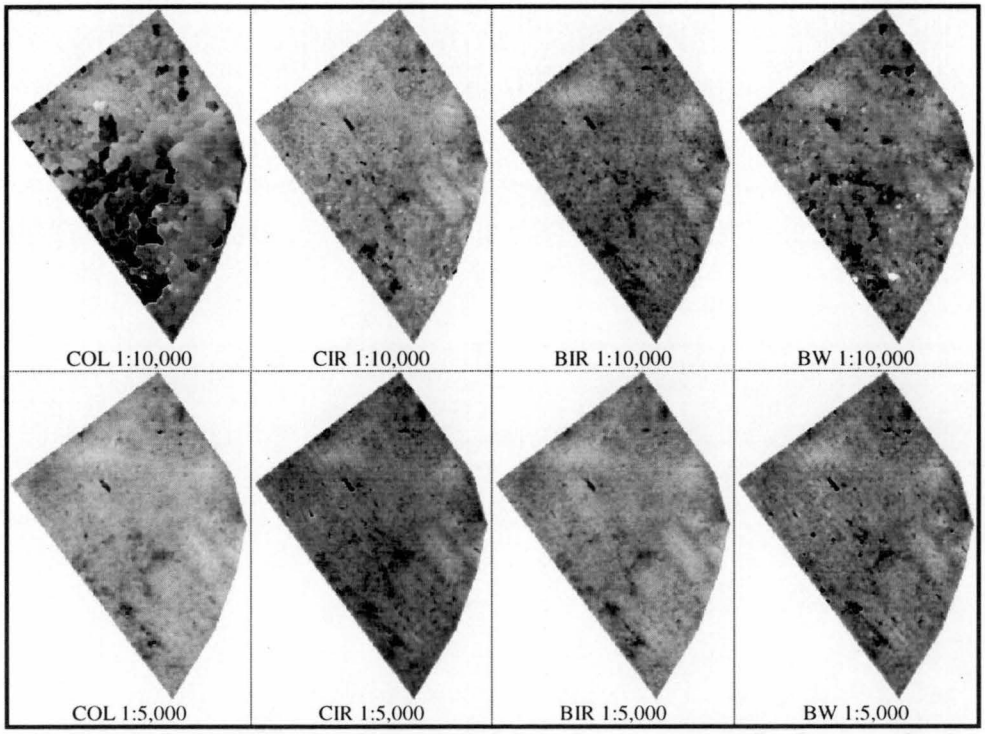

Figure 6.6: Images for Strategy 2 (closed canopy stand). Gray scale: 0–20m [dark–light].

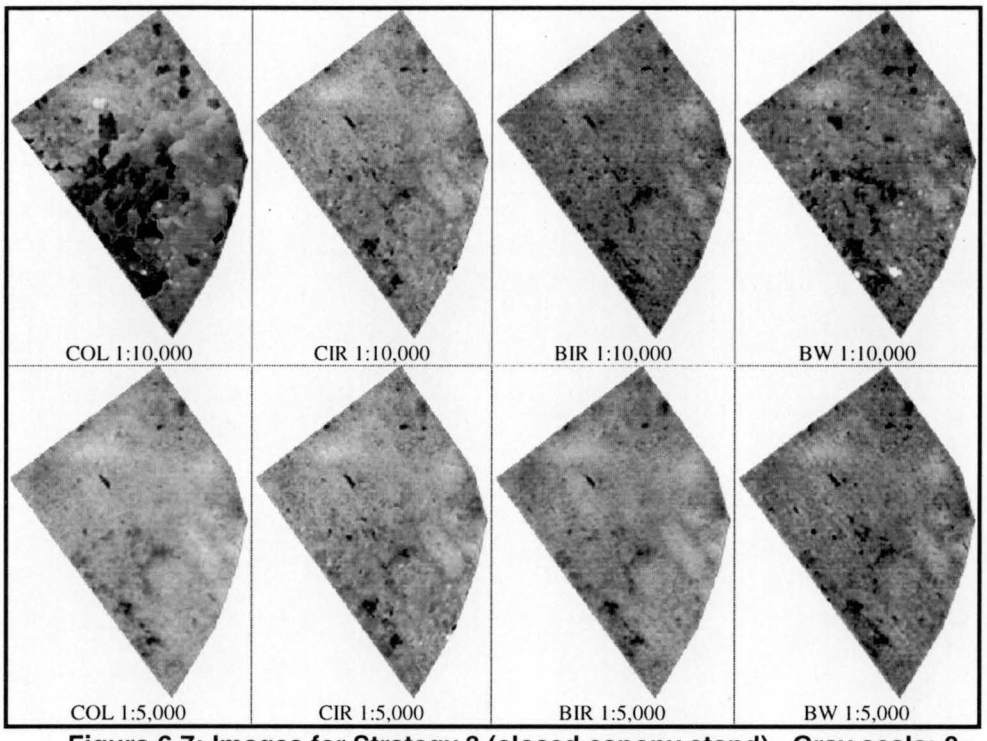

Figure 6.7: Images for Strategy 3 (closed canopy stand). Gray scale: 0–20m [dark–light].

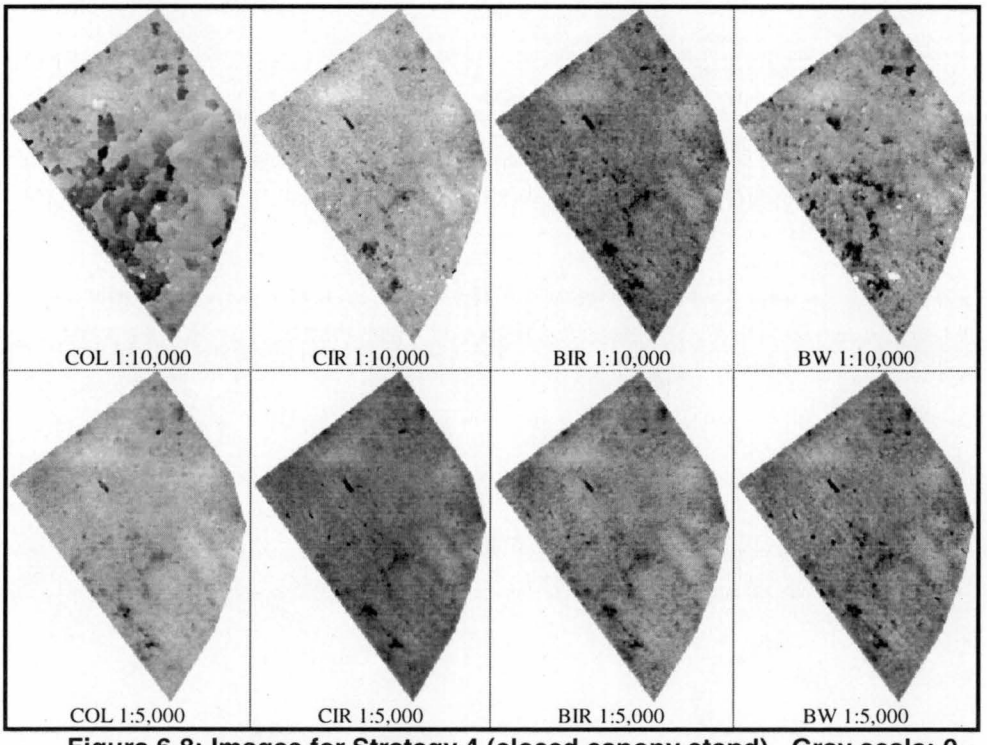

Figure 6.8: Images for Strategy 4 (closed canopy stand). Gray scale: 0–20m [dark–light].

The analysis of the DPW and analytical stereoplotter data and the absolute differences between them are summarised in Table 6.2.

μ=mean σ=standard deviation D=DPW–AS ρ=correlation		BW 5000	BW 10000	BIR 5000	BIR 10000	CIR 5000	CIR 10000	COL 5000	COL 10000	COL 15000
Strategy 1 Raw Data	μ (m)	7.3	7.2	8.7	7.0	5.7	9.3	10.4	7.2	4.9
	σ (m)	±1.6	±2.1	±1.6	±1.8	±1.6	±1.9	±1.7	±3.0	±2.1
	μ_D (m)	-2.1	-2.2	-1.3	-2.3	-3.0	-1.0	-0.4	-2.5	-0.8
	σ_D (m)	±2.3	±2.5	±1.5	±2.4	±2.9	±0.9	±0.9	±3.3	±1.7
	ρ	0.64	0.60	0.70	0.68	0.70	0.69	0.69	0.59	0.59
	<1m	0.3	1.0	8.3	0.2	0.0	22.3	56.7	6.3	42.7
	1–2m	3.2	3.2	26.3	1.7	0.0	34.1	30.7	13.2	31.6
	2–4m	50.2	45.0	56.3	44.3	6.9	38.0	11.5	28.5	21.2
	4–8m	44.8	46.5	9.1	52.2	90.0	5.0	1.0	35.6	4.5
	>8m	1.5	4.3	0.1	1.6	3.0	0.7	0.1	16.3	0.0
Strategy 2 Median	μ (m)	7.3	7.1	8.8	7.0	5.7	9.3	10.4	7.2	5.0
	σ (m)	±1.5	±2.0	±1.5	±1.7	±1.5	±1.8	±1.6	±7.1	±2.0
	μ_D (m)	-2.1	-2.2	-1.3	-2.2	-3.0	-1.1	-0.4	-2.5	-0.8
	σ_D (m)	±2.2	±2.5	±1.4	±2.3	±2.9	±1.3	±0.8	±3.2	±1.5
	ρ	0.69	0.63	0.76	0.73	0.75	0.71	0.78	0.60	0.62
	<1m	0.1	0.5	5.2	0.0	0.0	20.2	59.0	5.6	44.8
	1–2m	1.3	2.0	26.9	0.7	0.0	37.1	30.8	13.5	32.5
	2–4m	53.1	46.2	62.0	45.1	4.1	38.5	9.5	29.0	19.2
	4–8m	44.4	47.6	5.9	53.2	93.9	3.7	0.7	35.7	3.5
	>8m	1.2	3.7	0.0	1.0	2.0	0.5	0.1	16.2	0.0
Strategy 3 Wavelet	μ (m)	7.2	7.1	8.7	7.0	5.7	9.3	10.4	7.1	4.9
	σ (m)	±1.6	±2.1	±1.5	±1.7	±1.5	±1.8	±1.7	±3.0	±2.0
	μ_D (m)	-2.1	-2.2	-1.3	-2.3	-3.0	-1.0	-0.4	-2.5	-0.8
	σ_D (m)	±2.2	±2.5	±1.5	±2.3	±2.9	±1.4	±0.9	±3.2	±1.5
	ρ	0.69	0.64	0.74	0.72	0.75	0.70	0.75	0.61	0.62
	<1m	0.1	0.6	5.2	0.0	0.0	20.2	58.0	5.9	43.7
	1–2m	1.5	2.3	25.5	0.8	0.0	36.0	30.2	12.6	31.9
	2–4m	50.9	45.0	62.1	43.2	4.3	38.3	10.3	28.5	21.4
	4–8m	46.4	48.8	7.1	54.8	93.4	5.2	1.5	37.5	3.0
	>8m	1.1	3.3	0.1	1.1	2.2	0.3	0.0	15.5	0.0
Strategy 4 Fourier	μ (m)	8.5	10.2	9.2	8.3	7.5	12.4	11.6	10.2	5.9
	σ (m)	±1.4	±2.0	±1.4	±1.5	±1.2	±1.6	±1.4	±2.6	±1.3
	μ_D (m)	-1.5	-0.5	-1.1	-1.6	-2.0	0.6	0.2	-0.5	0.2
	σ_D (m)	±1.6	±1.3	±1.3	±1.7	±2.0	±1.0	±0.7	±1.6	±1.1
	ρ	0.67	0.62	0.72	0.70	0.73	0.68	0.75	0.60	0.60
	<1m	3.3	51.4	14.9	1.6	0.1	37.8	67.9	41.4	12.9
	1–2m	20.3	30.0	36.8	15.9	1.7	40.6	27.9	29.2	30.9
	2–4m	65.9	14.2	44.8	66.9	60.9	20.7	4.0	19.9	51.6
	4–8m	10.1	4.0	3.4	15.4	37.0	0.8	0.2	9.0	4.7
	>8m	0.4	0.3	0.0	0.2	0.2	0.1	0.0	0.5	0.0

Table 6.2: Statistical results and absolute difference distribution (%) of DPW data from analytical stereoplotter data (closed canopy stand).

The means and standard deviations of the differences between the DPW raw data (Strategy 1) and the analytical stereoplotter raw data were encouraging for all models. In the best case, the μ_D was 0.4m (using the 1:5,000 scale colour) and the

σ_D was ±0.9m (using the 1:5,000 scale colour and the 1:10,000 scale colour infrared), and in the worst case, the μ_D was 3.0m and the σ_D was ±2.9m (both using the 1:5,000 scale colour infrared). The DPW canopy heights consistently underestimated the analytical stereoplotter data ($P<0.001$) but otherwise correlated well ($\rho>0.6$). The distribution of the absolute differences was also encouraging, except for the 1:5,000 scale colour infrared models in which more than 90% of the points had an error of 4–8m. In contrast, the correlation coefficient between the 1:5,000 scale colour infrared and analytical stereoplotter data was slightly higher than the other models ($P<0.01$). This suggests that there are systematic errors in the process of the automatic DCM extraction.

The median filter (Strategy 2) significantly reduced the means of the differences between the DPW raw data and the analytical stereoplotter raw data for the 1:10,000 scale black and white model ($P\approx0$), but significantly increased the means for the 1:5,000 scale black and white infrared, and the 1:15,000 scale colour models ($P\approx0$). The means for other models were not changed. The correlation coefficients between the DPW and analytical stereoplotter data were slightly improved for all models ($P<0.01$), but not the absolute differences.

The adaptive wavelet filter (Strategy 3) significantly reduced the means of the differences between the DPW raw data and the analytical stereoplotter raw data for both the 1:10,000 and 1:5,000 scale black and white models ($P<0.001$). The means for other models were not changed. Similar to the median filter, the correlation coefficients between the DPW and analytical stereoplotter data were slightly improved for all models ($P<0.01$), but not the absolute differences.

The adaptive Fourier filter (Strategy 4) produced results that had different characteristics from the other two filters. Without exception, the adaptive Fourier filter significantly increased the means of the original data ($P\approx0$), and consequently reduced the mean differences between the DPW data and the analytical stereoplotter data. The correlation coefficients between all DPW models and the analytical stereoplotter data were slightly increased ($P<0.01$). The most significant improvement was the absolute differences between the DPW data and the analytical stereoplotter data, in particular for the 1:5,000 scale colour infrared model, in which the number of points having an error of less than 4m was

improved significantly from 6.9% to 60.9%.

The height distributions for all models are presented in Figure 6.9, and skewness and kurtosis data are shown in Table 6.3.

The distributions for both the 1996 and 1999 analytical stereoplotter data sets were slightly skewed to the left and more sharply peaked than a normal distribution. The analytical stereoplotter data can be expected to have identified fewer short trees and fewer tall trees since the sample size is smaller and located on a systematic grid. This needs to be considered when comparing the data sets.

The distributions for all DPW data were slightly more skewed to the left than the analytical stereoplotter data, except for the 1:10,000 scale black and white, in which the distribution is symmetric (kurtosis=0.0) and were more sharply peaked than a normal distribution. The similarity can be seen in more detail when comparing image profiles derived from each canopy height model. Figure 6.10 and Figure 6.11 show height profiles along a representative line (constant y coordinate) of the height data set. This line is illustrated in Figure 6.1.

The adaptive Fourier filter appears to preserve the general surface trend most reliably. In smaller-scale models (ie. The 1:10,000 and 1:15,000 scales), the height profiles from the adaptive Fourier filtered data are higher than the other two filters, while the profiles are similar in height for all of the 1:5,000 models.

Image Name	Strategy 1		Strategy 2		Strategy 3		Strategy 4	
	Skewness	Kurtosis	Skewness	Kurtosis	Skewness	Kurtosis	Skewness	Kurtosis
AS 1996	-0.1	1.7						
AS 1999	-0.2	1.3						
BW 5000	-1.1	3.5	1.2	4.5	-1.1	3.6	-1.1	3.6
BW 10000	0.0	10.0	0.0	11.3	0.0	9.8	0.0	9.7
BIR 5000	-0.6	1.6	-0.6	1.9	-0.6	1.7	-0.6	1.6
BIR 10000	-0.7	2.1	-0.7	2.3	-0.7	2.0	-0.7	2.0
CIR 5000	-0.7	2.6	-0.8	3.0	-0.7	2.6	-0.7	2.6
CIR 10000	-0.7	5.1	-0.7	5.4	-0.7	4.2	-0.7	4.2
COL 5000	-0.8	5.5	-0.8	2.9	-0.7	2.3	-0.8	2.4
COL 10000	-0.7	0.1	-0.7	0.0	-0.7	0.0	-0.7	0.0
COL 15000	-0.2	0.3	-0.2	0.2	-0.2	2.7	-0.2	0.2

Table 6.3: Height distribution characteristics for Strategies 1–4 and analytical stereoplotter data (closed canopy stand). For a symmetrical distribution, skewness=0, and for a normal distribution shape, kurtosis=0.

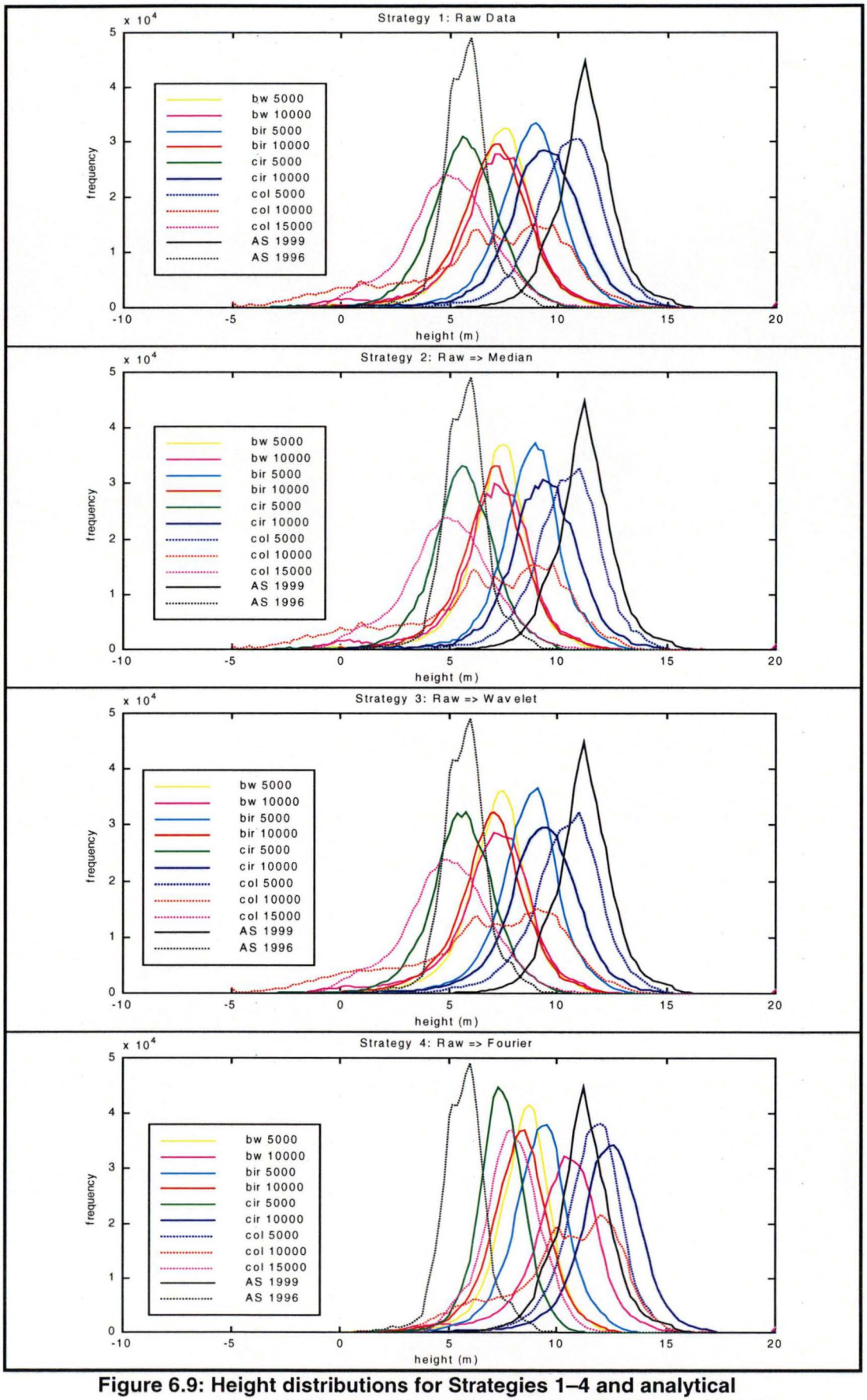

Figure 6.9: Height distributions for Strategies 1–4 and analytical stereoplotter data (closed canopy stand). Tree height data have been rounded to the nearest 0.2m.

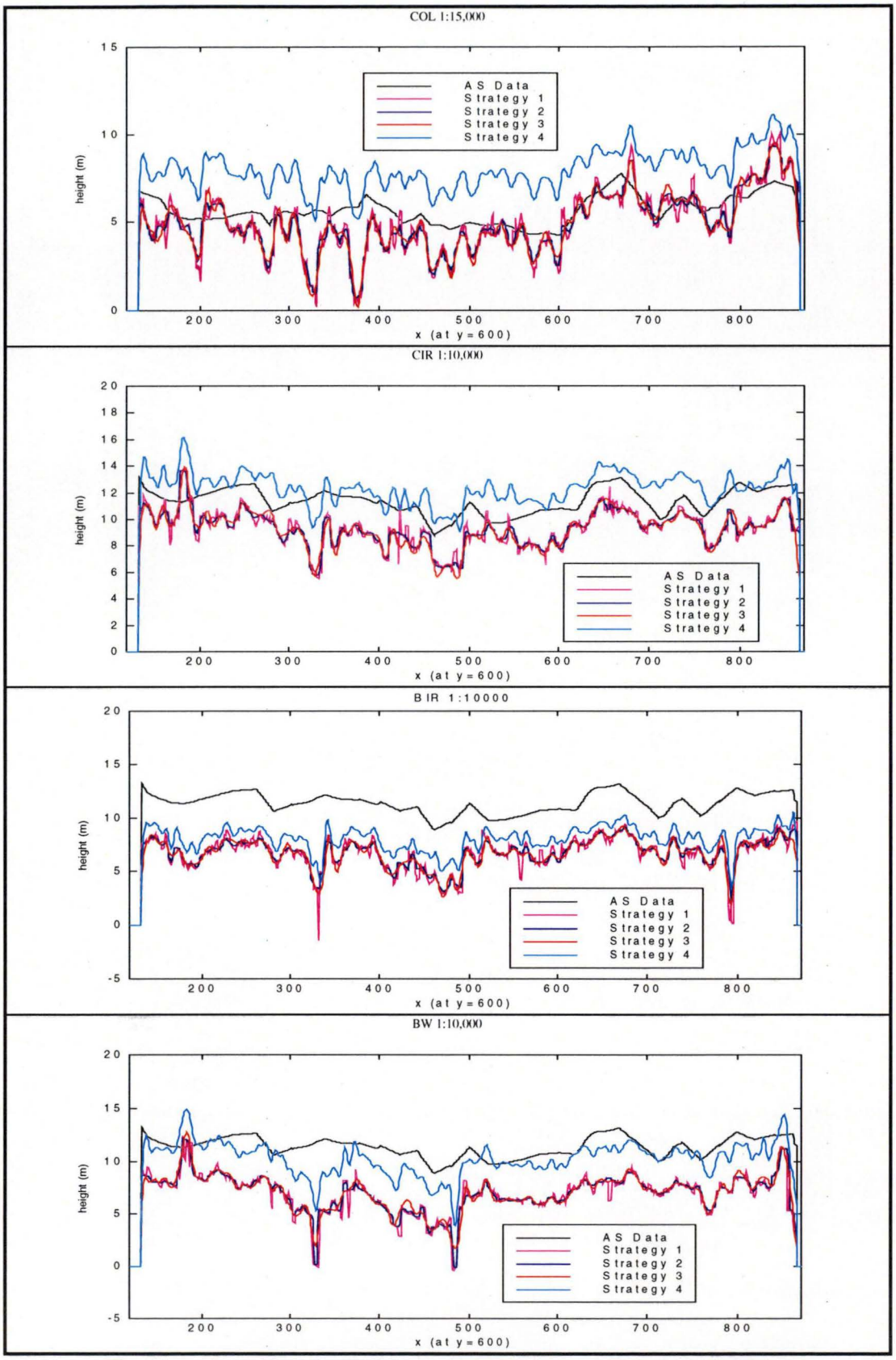

Figure 6.10: Height profiles for 1:15,000 and 1:10,000 models (closed canopy stand). Analytical stereoplotter data for 1:15,000 model is the 1996 data.

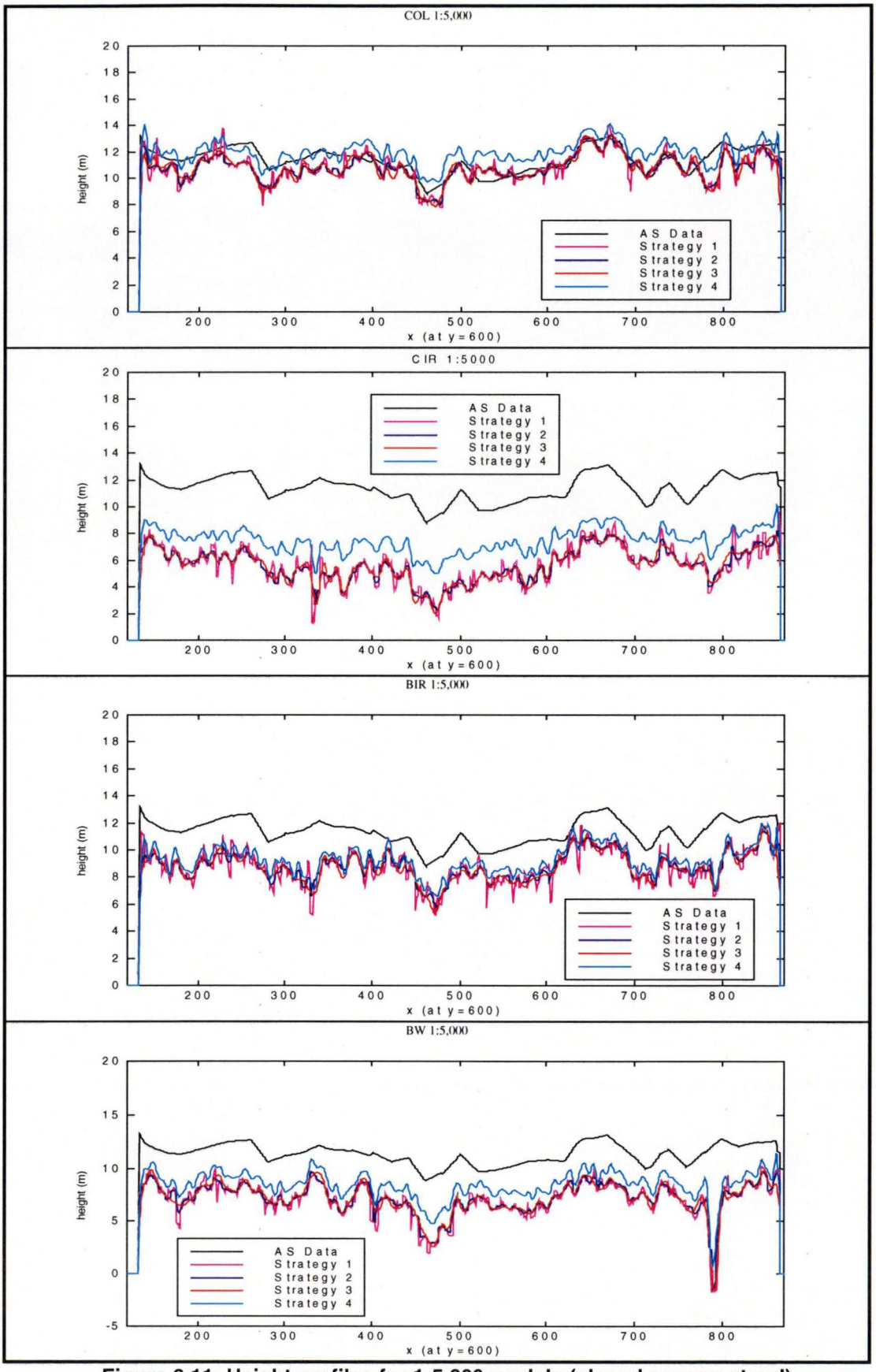

Figure 6.11: Height profiles for 1:5,000 models (closed canopy stand).

6.2.4. Analysis: Mean Tallest Tree Heights

For strategies 5–7, a 20m×20m (40×40 pixels for a pixel size of 0.5m) MTT filter was applied to the images. Figures 6.12 to 6.14 show the images of the MTT models for Strategies 5–7. The results of the MTT models and the absolute differences from the analytical stereoplotter MTT data are summarised in Table 6.4.

μ=mean σ=standard deviation D=DPW MTT–AS MTT ρ=correlation		BW 5000	BW 10000	BIR 5000	BIR 10000	CIR 5000	CIR 10000	COL 5000	COL 10000	COL 15000
Strategy 5 Median→MTT	μ(m)	9.6	12.0	10.4	9.2	8.2	13.8	12.6	11.9	6.8
	σ(m)	±0.9	±1.9	±1.1	±1.1	±0.9	±1.2	±1.0	±1.9	±1.1
	μ_D(m)	-1.4	-0.1	-1.0	-1.6	-2.2	0.8	0.2	-0.2	0.4
	σ_D(m)	±1.4	±1.3	±1.1	±1.6	±2.1	±1.0	±0.5	±1.0	±0.9
	ρ	0.86	0.84	0.84	0.85	0.85	0.77	0.85	0.68	0.68
	<1m	1.2	63.8	11.1	0.0	0.0	25.3	82.8	51.7	0.1
	1–2m	13.0	31.5	43.7	3.9	0.0	52.5	17.1	33.6	77.0
	2–4m	83.0	2.7	45.1	86.4	43.3	21.0	0.0	13.5	20.7
	4–8m	2.8	1.1	0.0	9.7	56.7	1.1	0.0	1.2	2.3
	>8m	0.0	0.8	0.0	0.0	0.0	0.0	0.0	0.0	0.0
Strategy 6 Wavelet→MTT	μ(m)	9.7	12.5	10.6	9.4	9.0	13.9	12.7	12.1	7.2
	σ(m)	±0.9	±1.9	±1.0	±1.1	±0.8	±1.2	±1.0	±1.8	±1.7
	μ_D(m)	-1.4	0.1	-0.9	-1.5	-1.7	0.8	0.2	-0.1	0.7
	σ_D(m)	±1.4	±1.3	±1.0	±1.5	±1.7	±1.0	±0.5	±1.0	±1.3
	ρ	0.86	0.84	0.82	0.84	0.84	0.78	0.85	0.67	0.63
	<1m	1.4	72.7	17.7	0.0	0.0	22.4	79.7	51.0	52.5
	1–2m	19.0	22.8	49.2	9.1	2.4	51.5	19.7	36.8	30.4
	2–4m	77.9	2.9	33.1	84.5	81.0	25.5	0.6	11.5	16.9
	4–8m	1.7	0.8	0.0	6.4	16.6	0.6	0.0	0.6	3.4
	>8m	0.0	0.8	0.0	0.0	0.0	0.0	0.0	0.0	0.0
Strategy 7 Fourier→MTT	μ(m)	10.0	12.4	10.7	9.8	8.6	14.1	12.9	12.2	7.1
	σ(m)	±0.9	±1.9	±1.1	±1.1	±0.9	±1.2	±1.0	±1.9	±1.1
	μ_D(m)	-1.2	0.1	-0.8	-1.3	-1.9	0.9	0.3	0.0	0.6
	σ_D(m)	±1.2	±1.3	±1.0	±1.3	±1.9	±1.1	±0.6	±1.0	±0.9
	ρ	0.86	0.83	0.83	0.84	0.85	0.76	0.85	0.67	0.62
	<1m	3.1	71.1	20.3	0.0	0.0	17.2	71.8	49.1	69.9
	1–2m	34.6	22.3	51.7	25.1	0.3	44.7	26.0	38.4	24.2
	2–4m	62.0	4.0	28.1	72.6	68.8	36.4	2.1	11.5	5.9
	4–8m	0.3	1.1	0.0	2.2	30.9	1.7	0.0	0.9	0.0
	>8m	0.0	0.8	0.0	0.0	0.0	0.0	0.0	0.0	0.0

Table 6.4: Statistical results and absolute difference distribution (%) of DPW data from analytical stereoplotter data for Strategies 5-7 (closed canopy stand).

In the closed canopy stand, the MTT filter significantly increased the mean height of all canopy height models ($P<0.001$). This consequently reduced the absolute differences from the analytical stereoplotter data where more than 80% of

points (except for the 1:5,000 scale colour infrared after Strategies 5 and 7) had an error of less than 4m.

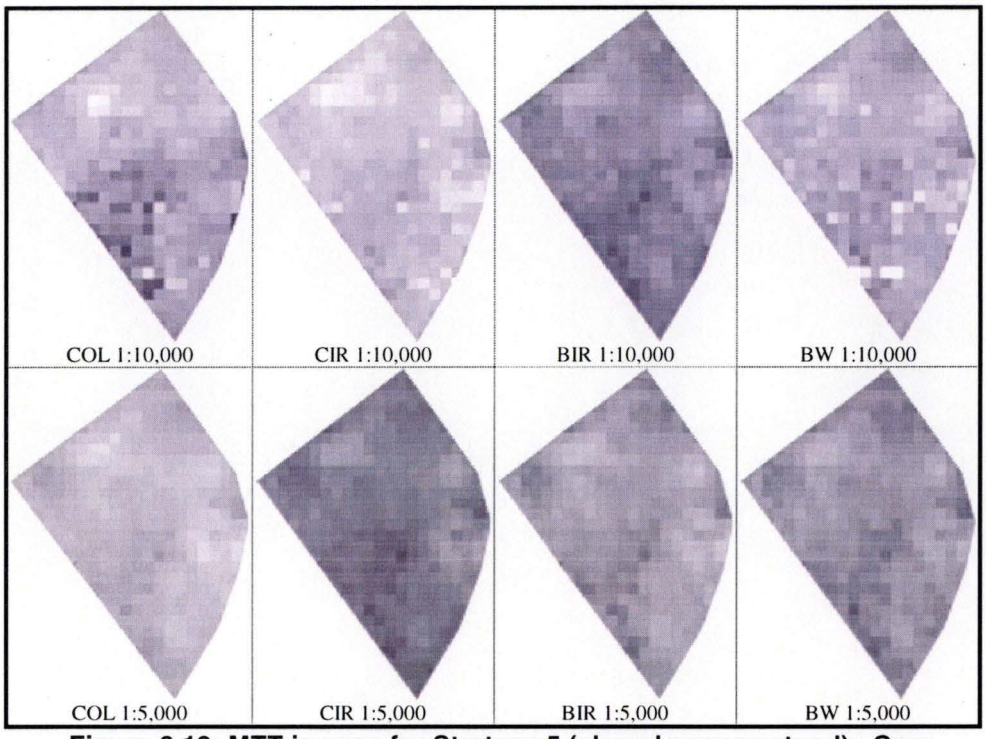

Figure 6.12: MTT images for Strategy 5 (closed canopy stand). Gray scale: 0–20m [dark–light].

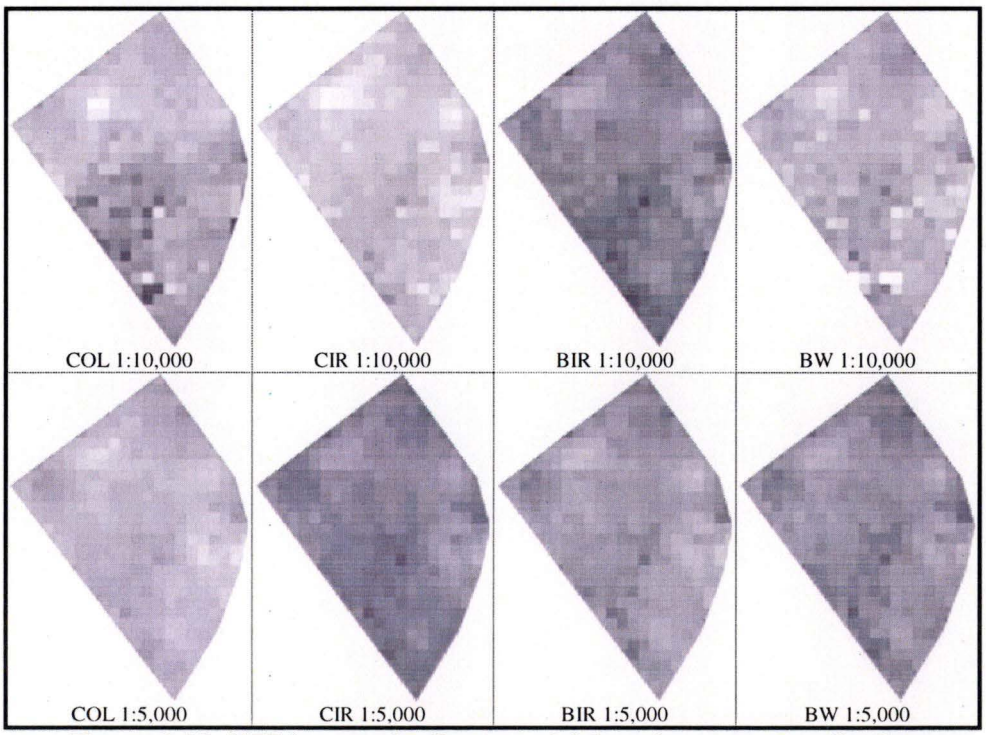

Figure 6.13: MTT images for Strategy 6 (closed canopy stand). Gray scale: 0–20m [dark–light].

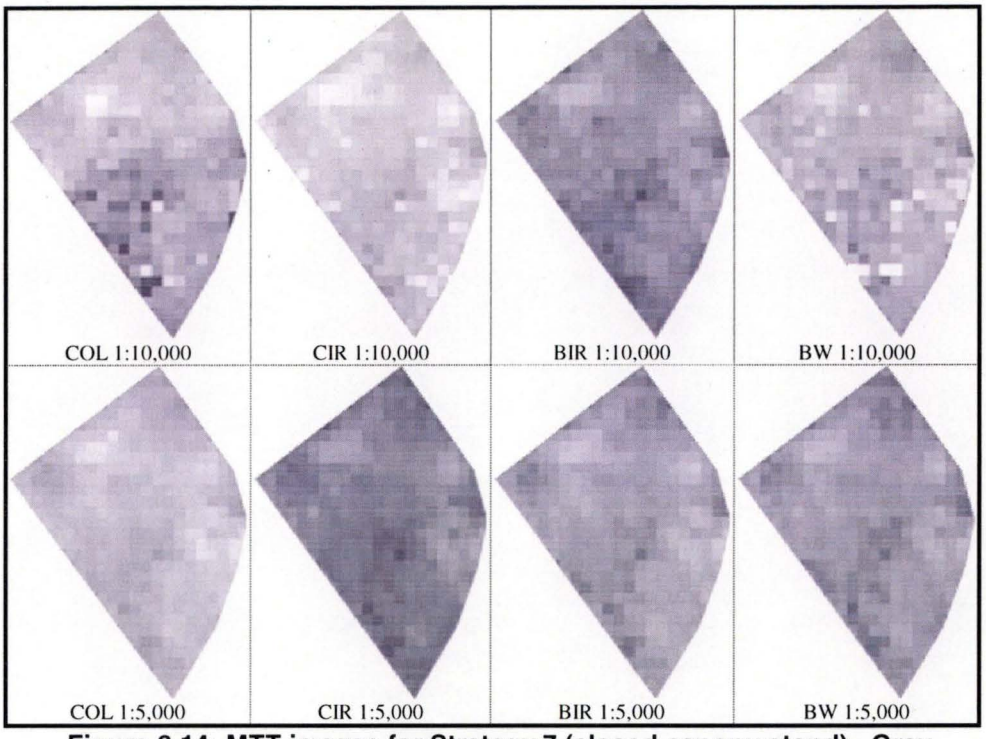

Figure 6.14: MTT images for Strategy 7 (closed canopy stand). Gray scale: 0–20m [dark–light].

For the 1996 data, the 1:15,000 scale colour data slightly overestimated the analytical stereoplotter data by 0.4m to 0.7m on average. The MTT filter reduced the mean difference significantly for the Fourier filtered image from 2.2m to only 0.6m (Strategy 7). The absolute differences for Strategy 7 were better than the other two MTT models where more than 90% of points had an error of less than 2m.

Some models underestimated the analytical stereoplotter data (ie. The 1:5,000 scale black and white, the 1:10,000 and 1:5,000 scale black and white infrared, and the 1:5,000 scale colour infrared) and others overestimated the analytical stereoplotter data. The major improvement was the 1:5,000 scale colour infrared models where the mean differences were reduced significantly from –3.0m to –1.7m. The correlation coefficients between all models and the analytical stereoplotter model were increased significantly ($P<0.001$). The height distributions are shown in Figure 6.15 and the skewness and kurtosis data are summarised in Table 6.5. Image profiles for each model derived from Strategies 5 to 7 are shown in Figure 6.16 and Figure 6.17.

Image Name	Strategy 5		Strategy 6		Strategy 7	
	Skewness	Kurtosis	Skewness	Kurtosis	Skewness	Kurtosis
AS 1996	0.5	0.7				
AS 1999	0.2	0.9				
BW 5000	0.3	1.0	0.2	1.2	0.1	2.3
BW 10000	4.6	3.8	5.0	4.3	4.7	4.7
BIR 5000	0.3	0.8	0.3	1.0	0.1	1.5
BIR 10000	0.2	0.8	0.2	0.9	0.2	1.4
CIR 5000	0.3	0.3	0.3	0.5	0.2	1.1
CIR 10000	0.7	7.5	0.7	6.9	0.4	8.1
COL 5000	0.1	0.6	0.1	1.1	-0.1	2.7
COL 10000	-0.4	0.4	-0.4	0.4	-0.4	0.5
COL 15000	0.2	-0.2	0.1	-0.2	0.1	0.2

Table 6.5: Height distribution characteristics for the MTT data (closed canopy stand).

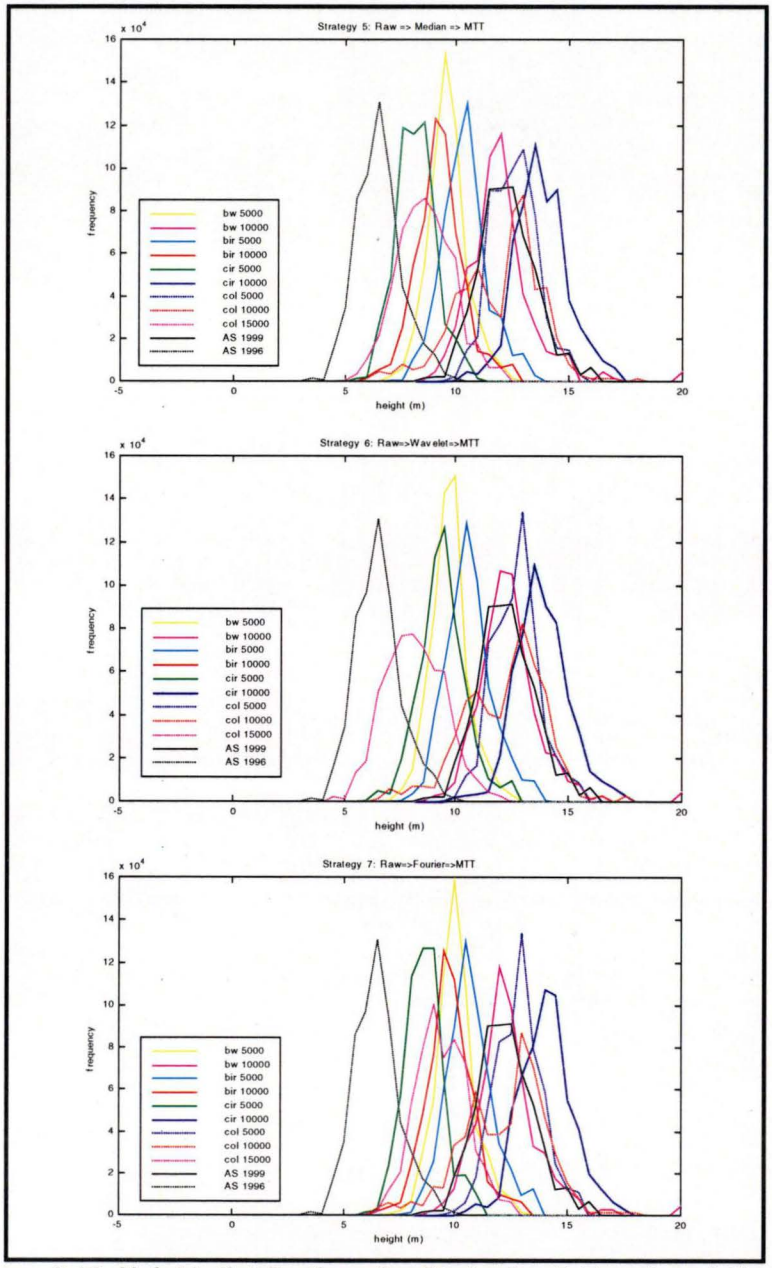

Figure 6.15: Height distributions for Strategies 5–7 and analytical stereoplotter data (closed canopy stand). Tree height data are rounded to the nearest 0.2m.

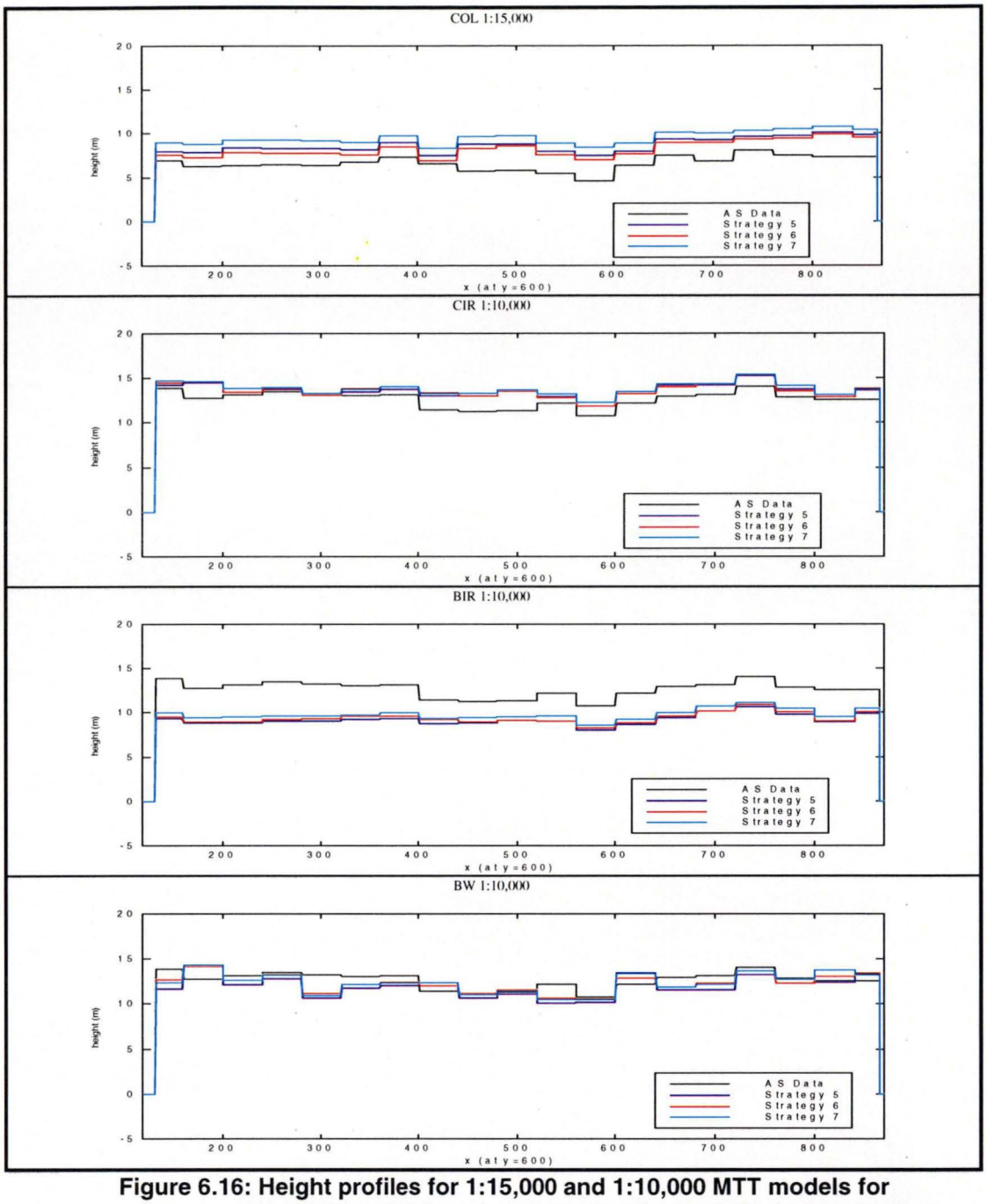

Figure 6.16: Height profiles for 1:15,000 and 1:10,000 MTT models for Strategies 5–7 (closed canopy stand). Analytical stereoplotter data for 1:15,000 model is the 1996 data.

Following application of the MTT filter, the height distribution was slightly skewed to the right for all models, except for the 1:5,000 scale colour. As before, the distributions were more sharply peaked than a normal distribution. The MTT filter has excluded heights representing the shortest 94% of observations from the data set, and meaned the heights representing the tallest 6% of observations. The changes in the distribution are consistent with the anticipated effects of the filter. Visual inspection indicates that the height profiles for Strategies 5 to 7 are similar

and compare well with the analytical stereoplotter data.

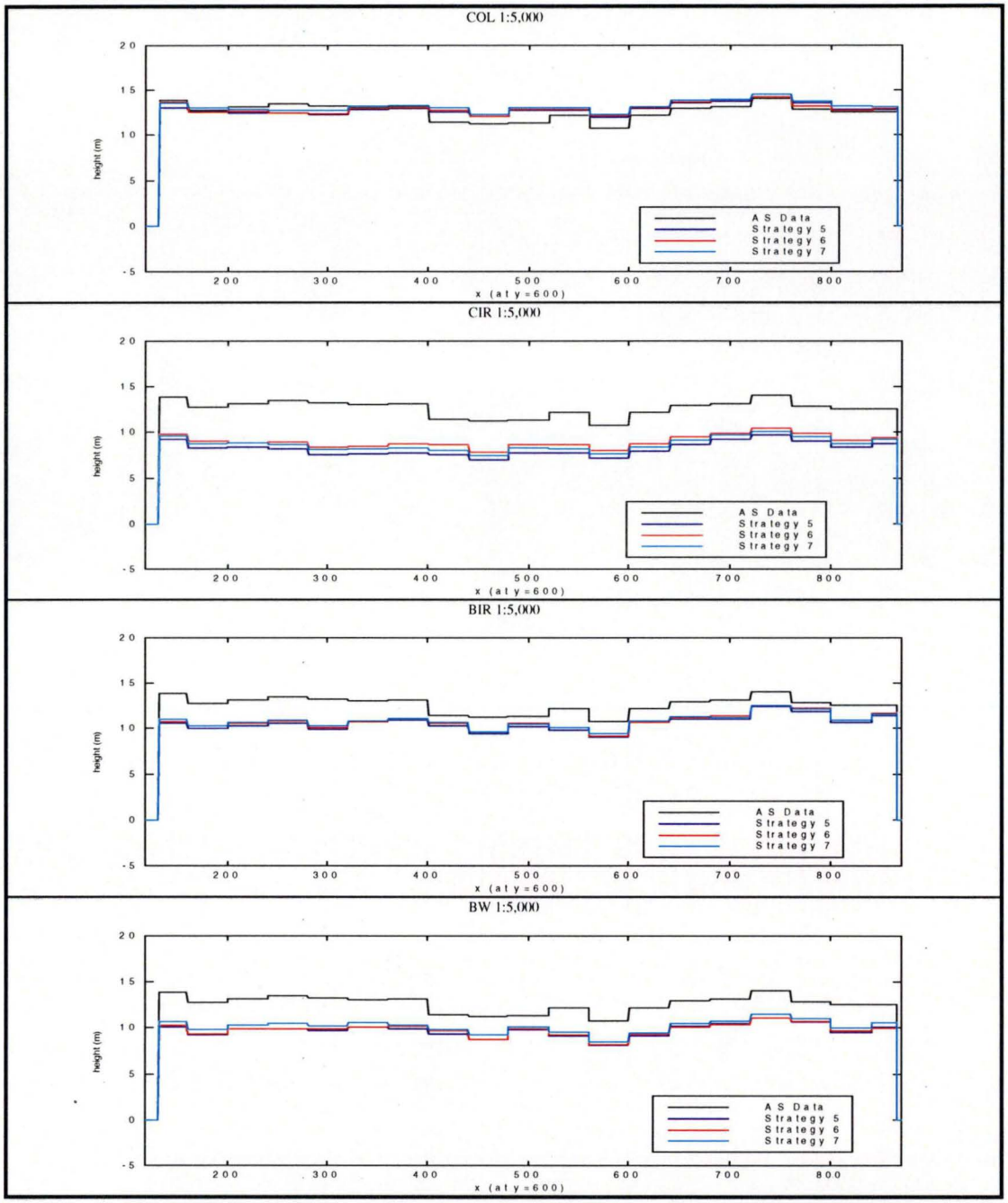

Figure 6.17: Height profiles for 1:5,000 MTT models for Strategies 5–7 (closed canopy stand).

6.3. Analysis: the Thinned Stand

6.3.1. Orthoimage of the Thinned Stand

The method for deriving the orthoimage for the thinned stand was similar to the

closed canopy stand. The orthoimage is shown in Figure 6.18.

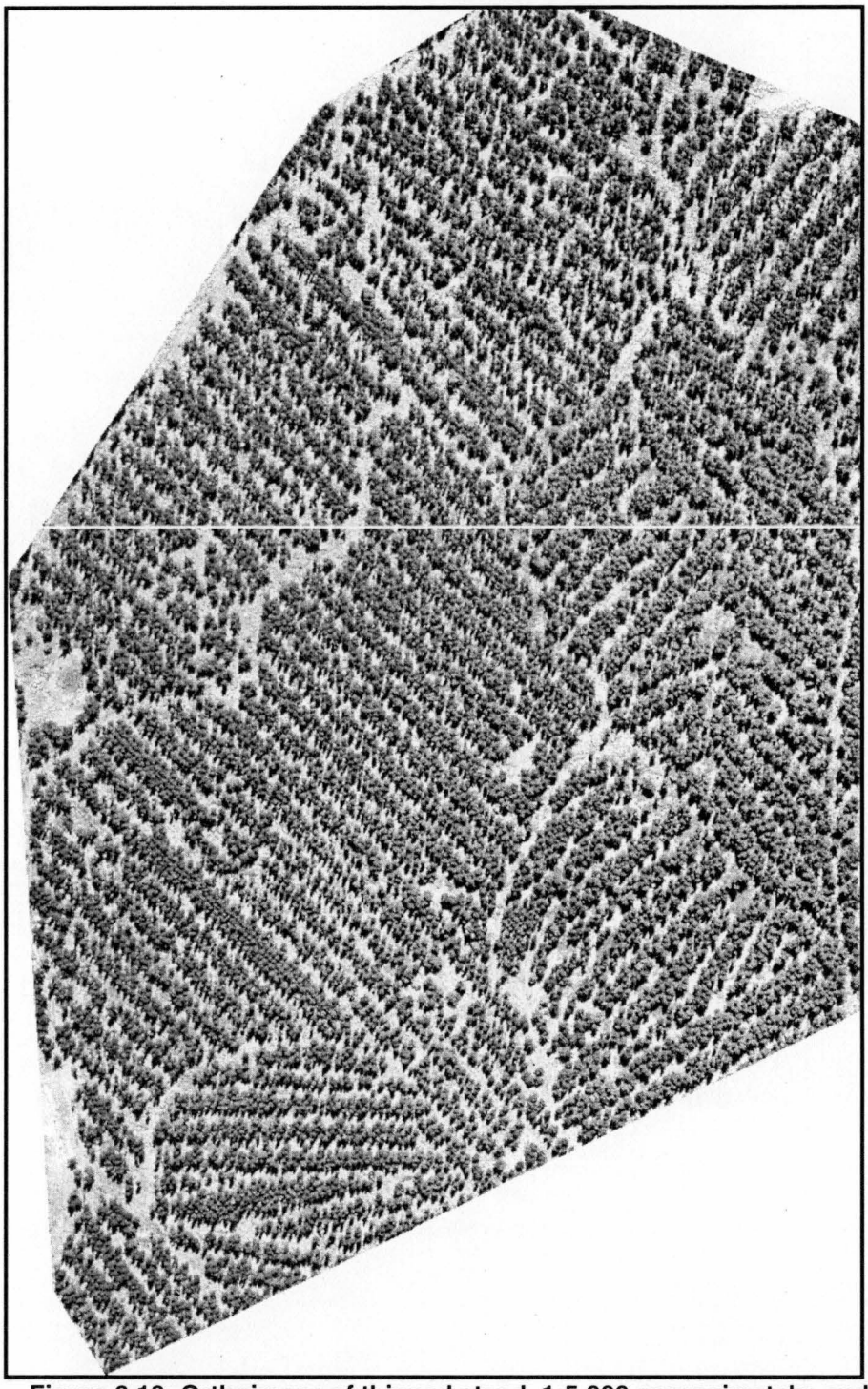

Figure 6.18: Orthoimage of thinned stand, 1:5,000 approximately; and a line indicating the location of derived height profiles.

The plantations consisted of eighteen-year-old trees that were thinned in late 1995. As shown in Figure 6.18, the trees had been thinned in various different directions, and thus the thinning had produced an irregular stand structure.

6.3.1.1. Stereo Viewing

In most cases, the thinned stand were very difficult to view in stereo. When the plantations were thinned, the lower part of some trees became visible and their images differed greatly in the left and right photographs because of viewing angle. Dark shadows appearing on the ground made it difficult to comfortably view the bare ground between trees.

Similar problems have been reported by Carson *et al.* (1996). Stereo viewing is made difficult when viewing bare ground between the trees because it has the same shape in the left and right images but corresponds to different positions on the ground (Figure 6.19).

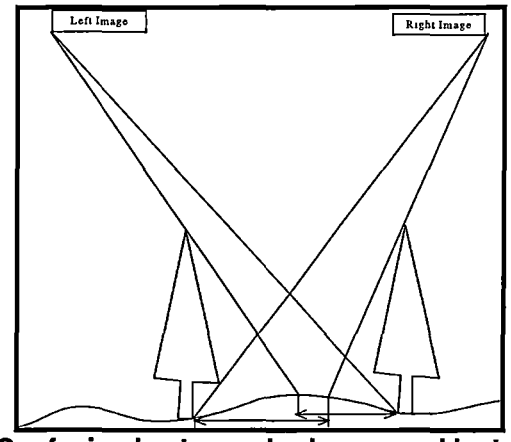

Figure 6.19: Confusion in stereo viewing caused by tall trees. Arrows indicate the two different locations of bare ground, which may appear to have the same shape. [Adapted from Carson *et al.* 1996].

6.3.1.2. Canopy Height Models

Image matching errors may be expected because of the same geometric effects that degraded stereo viewing. If the errors in the resulting DCHMs are related to measurements of ground surface rather than tree tops then it can be hypothesised that these errors will be minimised by applying filters that:

- threshold and remove data below an anticipated minimum tree height, in this case accomplished with the MTT filter; or
- remove data that falls at a horizontal location that is not associated with a tree or canopy cover.

6.3.2. Analysis Before Applying NDVI–Threshold

6.3.2.1. Analytical Stereoplotter Data

For the thinned canopy stands, the analytical stereoplotter data were extracted using the same methods as for the closed canopy stand. The results of the raw and MTT data are summarised in Table 6.6, and the images of both raw and MTT models are shown in Figure 6.20. As seen in Figure 6.20, measurements at a low sampling rate (10m) eliminated the thinning patterns of the thinned plantation.

	Mean (m)	σ(m)
AS raw data	18.7	±2.9
AS MTT data	20.7	±2.3

Table 6.6: Statistical results for analytical stereoplotter raw and MTT data before thresholding (thinned stand).

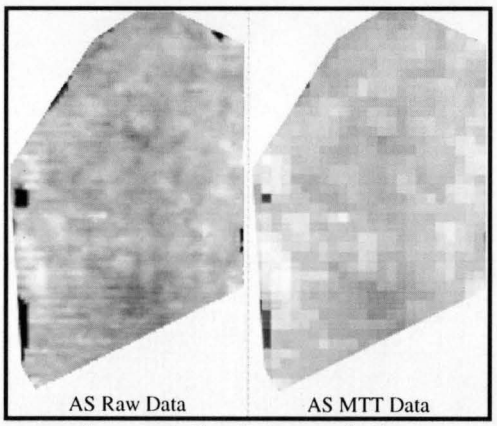

Figure 6.20: Images for analytical stereoplotter raw and MTT data before thresholding (thinned stand). Gray scale: 0–30m [dark–light].

6.3.2.2. Analysis: Raw and Filtered Tree Heights

The filter defined for Strategies 2 to 4 were applied to the raw data (Table 5.2). The resulting canopy height models for Strategies 1 to 4 are illustrated in Figures 6.21 to 6.24. Visual inspection indicates that the canopy structures for the raw data – the thinning directions in particular – can be seen clearly in some models but less clearly in others. All of the 1:5,000 models appear to extract the canopy structure well, while only the 1:10,000 scale black and white infrared model shows these patterns.

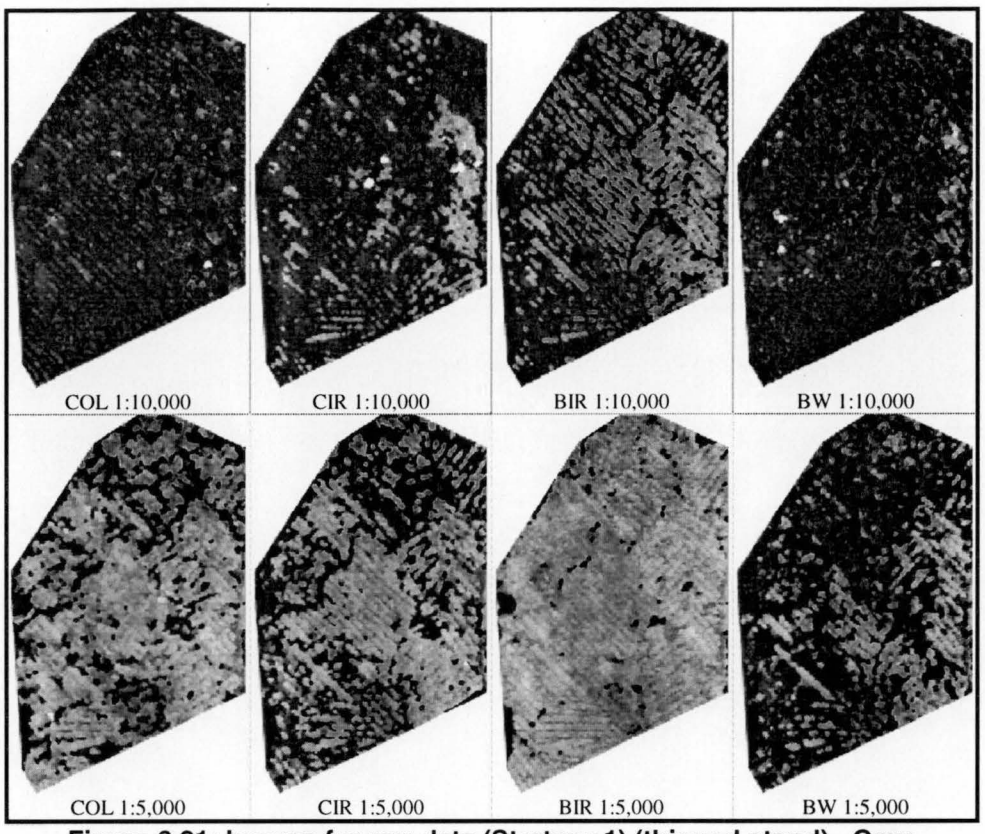

Figure 6.21: Images for raw data (Strategy 1) (thinned stand). Gray scale: 0–30m [dark–light].

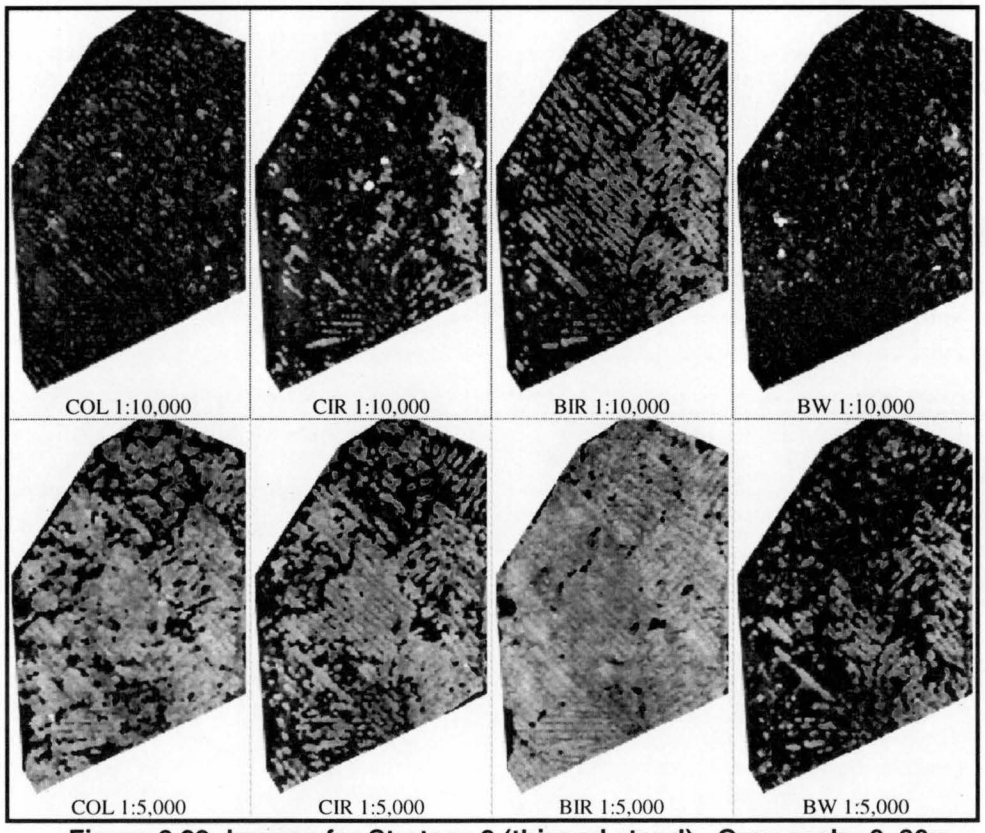

Figure 6.22: Images for Strategy 2 (thinned stand). Gray scale: 0–30m [dark–light].

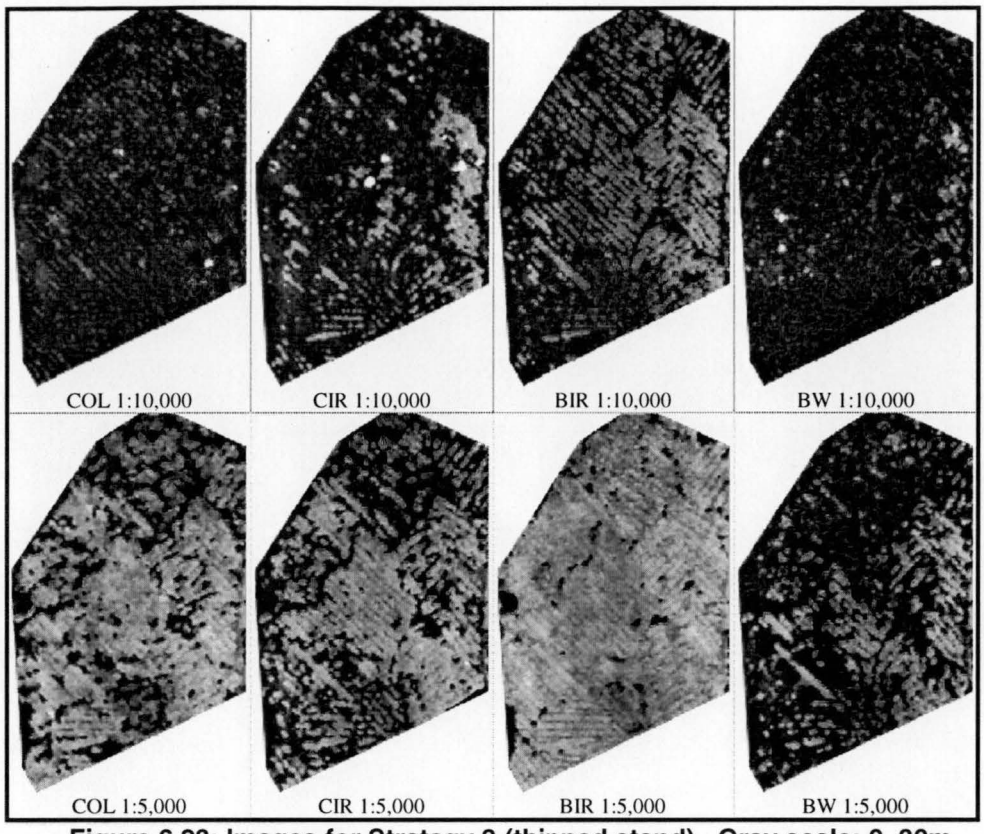

Figure 6.23: Images for Strategy 3 (thinned stand). Gray scale: 0–30m [dark–light].

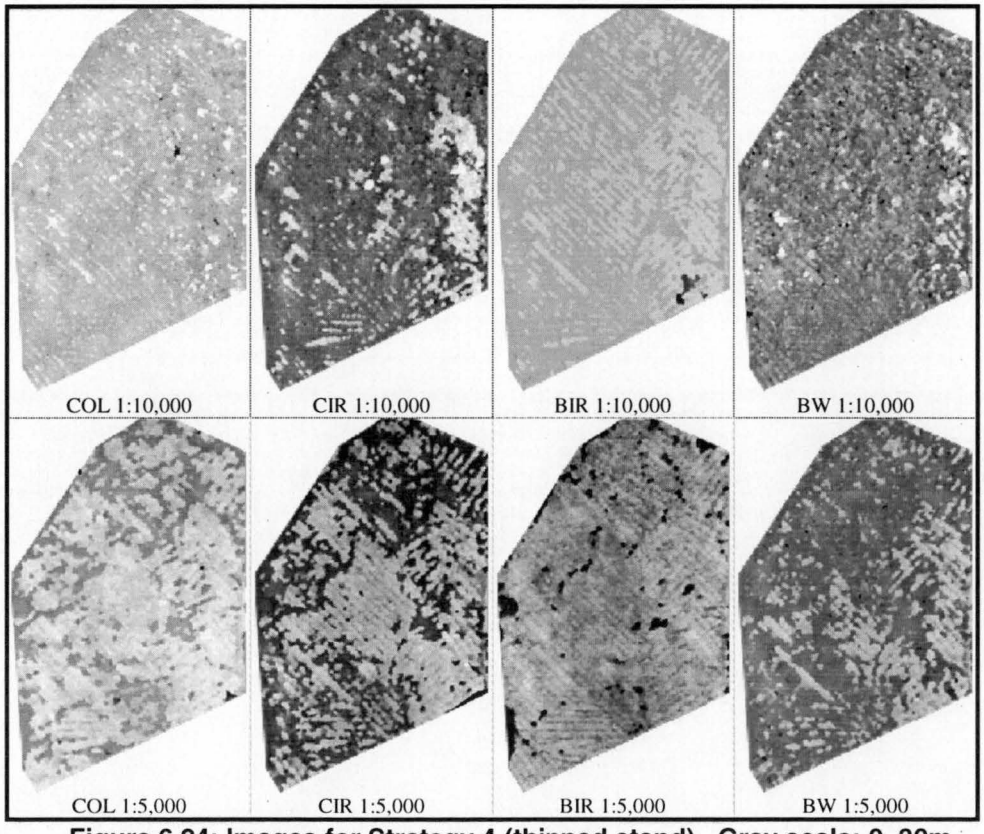

Figure 6.24: Images for Strategy 4 (thinned stand). Gray scale: 0–30m [dark–light].

The results for Strategies 1 to 4 and their differences from the analytical stereoplotter data are summarised in Table 6.7. The height distributions of all models are illustrated in Figure 6.25.

μ = mean σ = standard deviation D = DPW–AS ρ = correlation		BW 5000	BW 10000	BIR 5000	BIR 10000	CIR 5000	CIR 10000	COL 5000
Strategy 1 Raw Data	μ(m)	5.7	2.4	12.5	4.8	7.7	5.1	9.7
	σ(m)	±2.4	±3.9	±4.1	±6.8	±6.7	±5.5	±7.0
	μ_D(m)	-14.5	-16.4	-6.2	-13.9	-11.1	-13.6	-9.1
	σ_D(m)	±5.8	±4.3	±3.3	±6.7	±6.6	±5.5	±6.6
	ρ	0.27	0.23	0.61	0.23	-0.05	0.24	0.04
	<1m	0.6	0.4	1.7	0.2	1.4	1.3	3.9
	1–2m	0.9	0.4	3.2	0.6	2.7	1.6	5.6
	2–4m	4.2	0.7	16.6	2.5	12.5	5.5	16.5
	4–8m	14.5	3.0	58.7	23.7	27.1	8.1	30.4
	>8m	79.8	95.4	19.9	72.9	56.2	83.5	43.6
Strategy 2 Median	μ(m)	4.2	2.3	12.5	4.8	7.7	5.1	9.7
	σ(m)	±5.7	±3.7	±4.1	±6.6	±6.7	±5.3	±6.9
	μ_D(m)	-14.5	-16.4	-6.2	-13.9	-11.1	-13.6	-9.1
	σ_D(m)	±5.6	±4.1	±3.3	±6.6	±6.6	±5.4	±6.5
	ρ	0.28	0.23	0.64	0.23	-0.05	0.25	0.04
	<1m	0.5	0.4	0.9	0.2	1.1	1.1	3.3
	1–2m	0.7	0.4	1.9	0.5	2.2	1.4	5.2
	2–4m	3.5	0.7	11.7	1.5	12.4	5.4	16.9
	4–8m	14.9	3.0	47.4	24.3	28.2	8.3	31.2
	>8m	80.3	95.4	38.1	73.4	56.2	83.9	43.4
Strategy 3 Wavelet	μ(m)	4.5	2.6	12.5	5.2	7.8	5.2	9.9
	σ(m)	±5.2	±3.4	±3.9	±5.4	±6.2	±5.1	±6.3
	μ_D(m)	-14.2	-16.1	-6.2	-13.5	-10.9	-13.5	-8.9
	σ_D(m)	±5.2	±3.9	±3.0	±5.3	±6.0	±5.1	±5.9
	ρ	0.29	0.24	0.64	0.28	-0.05	0.26	0.04
	<1m	0.6	0.4	1.3	0.2	1.4	1.3	3.2
	1–2m	0.9	0.4	2.5	0.6	2.4	1.5	4.9
	2–4m	3.1	0.7	14.6	2.3	10.6	3.8	15.6
	4–8m	12.4	2.2	63.1	18.7	26.0	8.2	30.6
	>8m	83.0	96.3	18.5	78.1	59.6	85.2	45.7
Strategy 4 Fourier	μ(m)	13.1	14.3	14.3	18.4	12.5	13.3	19.8
	σ(m)	±3.1	±3.0	±3.4	±1.5	±5.2	±4.3	±3.6
	μ_D(m)	-5.6	-4.5	-4.5	-0.3	-6.3	-5.5	1.0
	σ_D(m)	±3.6	±3.7	±2.8	±2.9	±5.2	±4.6	±3.8
	ρ	0.28	0.24	0.63	0.24	-0.05	0.25	0.03
	<1m	8.0	5.9	4.1	33.0	14.3	4.9	14.9
	1–2m	7.2	7.0	8.1	26.8	11.8	5.4	16.2
	2–4m	12.8	21.3	34.0	30.4	15.0	12.5	35.9
	4–8m	45.3	53.0	46.6	7.8	17.8	45.5	30.7
	>8m	26.8	12.7	7.3	2.0	41.1	31.7	2.3

Table 6.7: Statistical results and absolute difference (DPW–AS) distribution (%) for Strategies 1–4 (thinned stand).

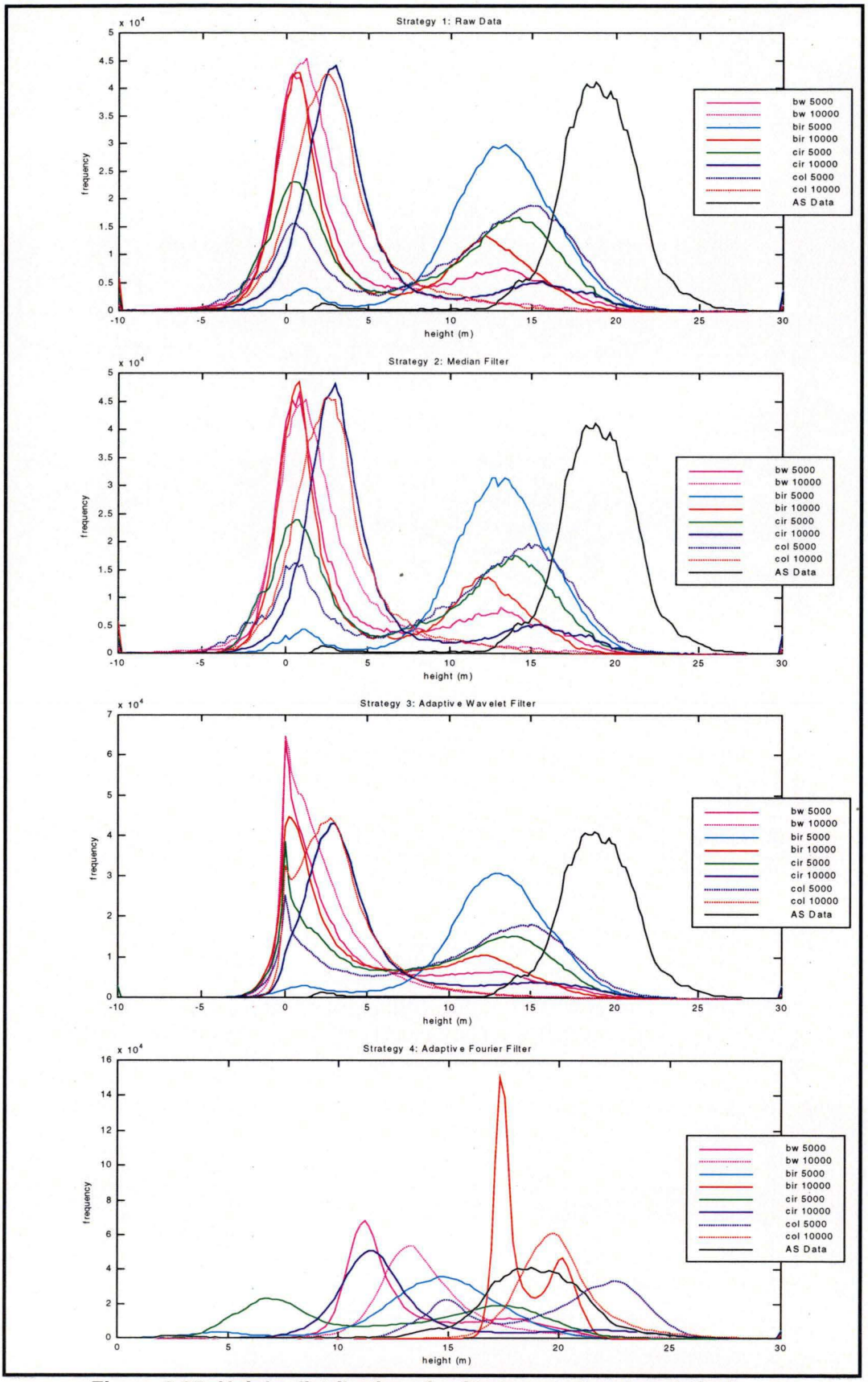

Figure 6.25: Height distributions for Strategy 1–4 and analytical stereoplotter data (thinned stand). Tree heights were rounded to the nearest 0.2m.

The height distributions for Strategies 1 to 3 models are bi–modal. The left peak represent terrain measurements, whereas the right peak represents the height distributions of the canopy surface. The adaptive Fourier filter (Strategy 4) produced canopy height models in which the left peak for most models has been shifted significantly to the right and right peaks shifted slightly to the right. This is indicative of the smoothing effect of the Fourier filter. Due to the bi–modal distribution, comparing the distributions' kurtosis and skewness data is inappropriate. The task is to separate the canopy data from the terrain data.

6.3.2.3. Analysis: Mean Tallest Tree Heights

The MTT filter, provided the array is sufficiently large, should operate only on data representing tree heights and thus exclude data in the left–hand data set of the bi–modal distribution at the same time as computing mean tallest tree. The size of the MTT filter applied to Strategies 5 to 7 was 25m×25m (50×50 pixels). The images of the MTT models for Strategies 5 to 7 are shown in Figures 6.26 to 6.28.

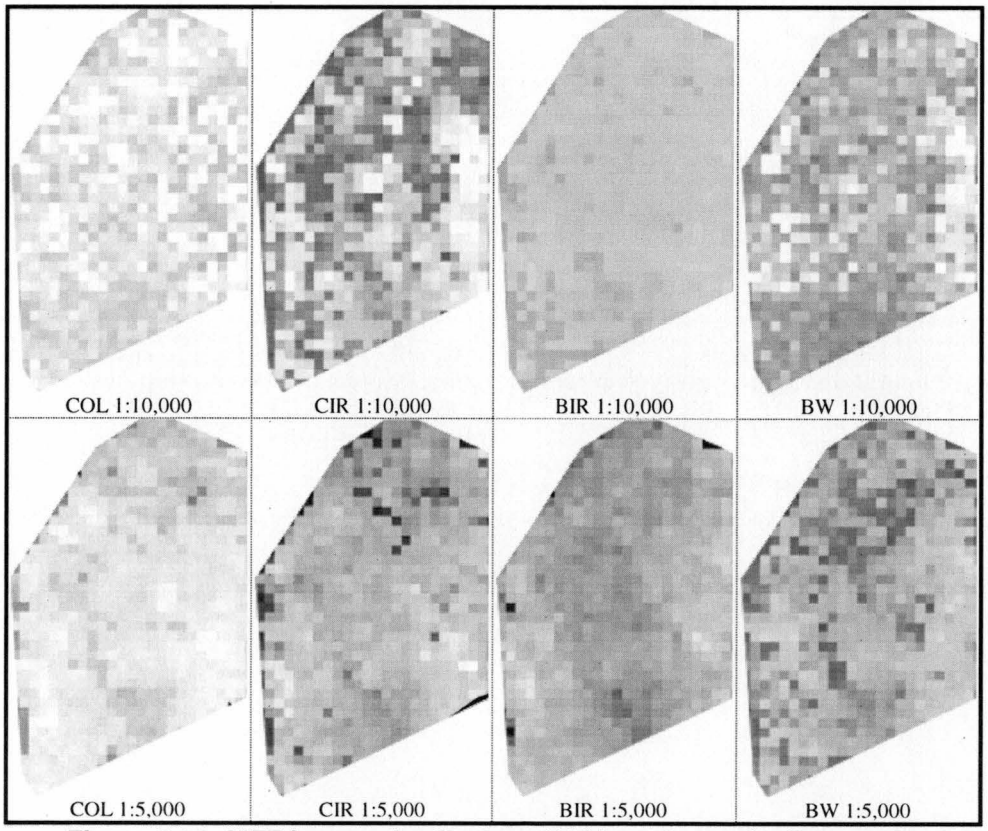

Figure 6.26: MTT images for Strategy 5 (thinned stand). Gray scale: 0–30m [dark–light].

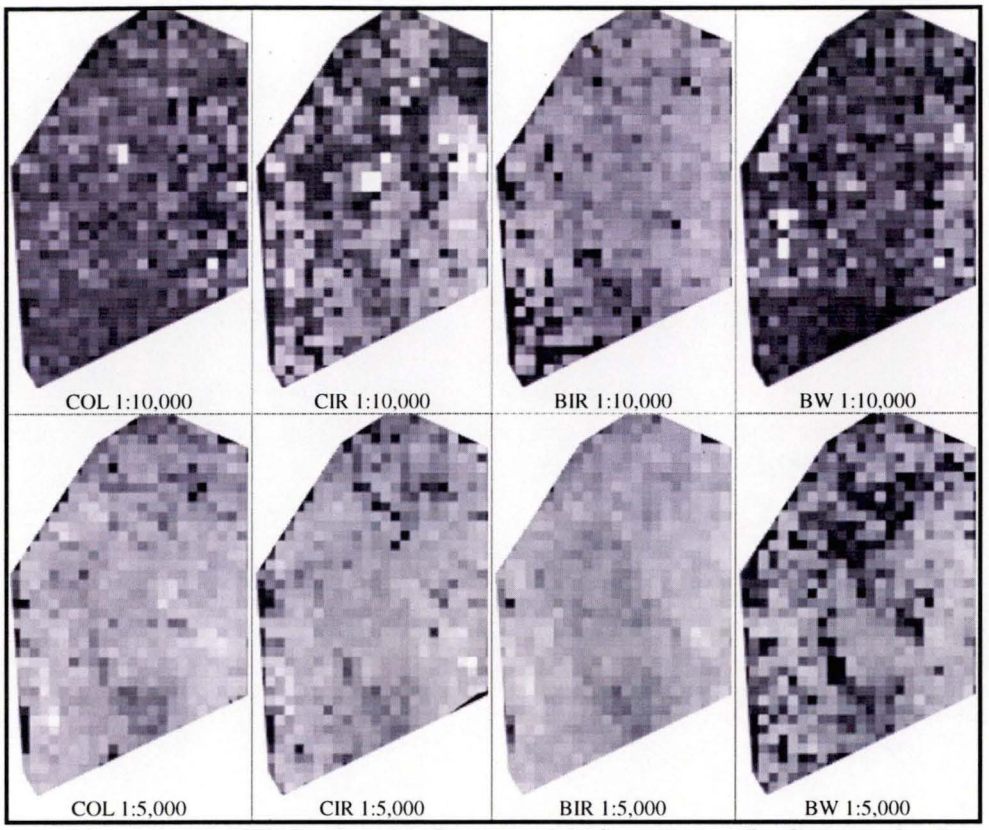

Figure 6.27: MTT images for Strategy 6 (thinned stand). Gray scale: 0–30m [dark–light].

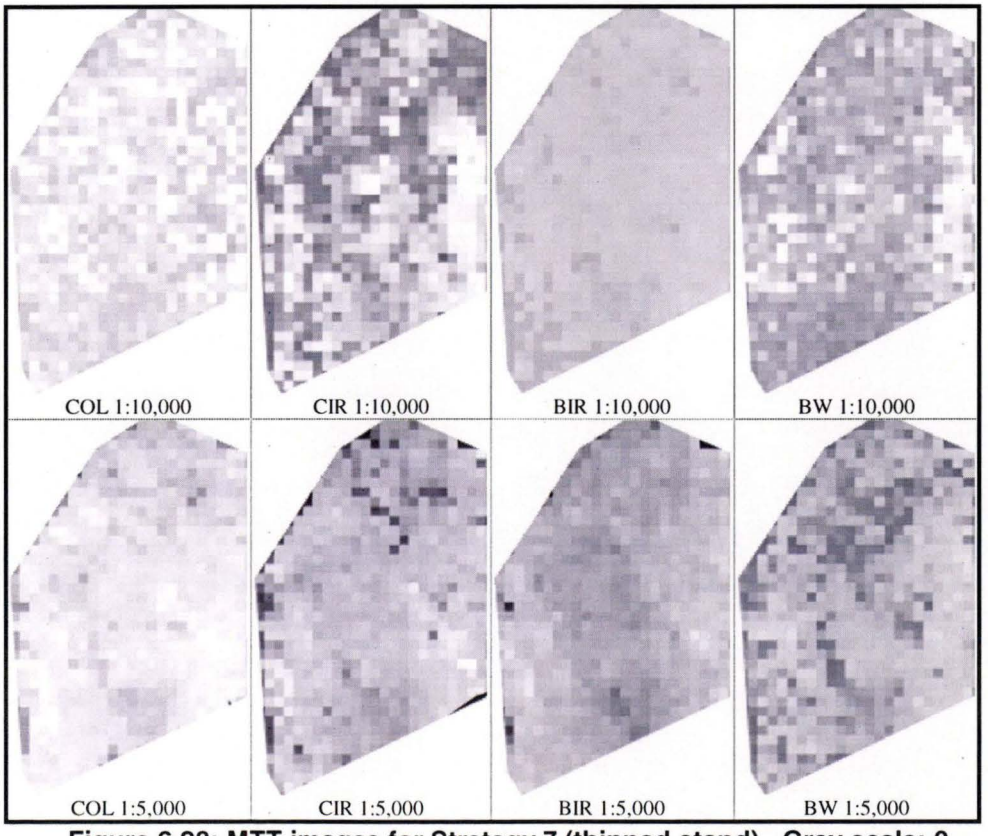

Figure 6.28: MTT images for Strategy 7 (thinned stand). Gray scale: 0–30m [dark–light].

Visual inspection suggests that the MTT-derived DCHMs for Strategies 5 and 7 correlate well with the analytical stereoplotter data. Comparison of the DPW and analytical stereoplotter data and the absolute differences between the DPW and analytical stereoplotter data are summarised in Table 6.8.

μ = mean σ = standard deviation D = DPW - AS ρ = correlation		BW 5000	BW 10000	BIR 5000	BIR 10000	CIR 5000	CIR 10000	COL 5000
Strategy 5 Median→MTT	μ(m)	17.4	19.2	17.4	20.3	18.4	19.2	23.2
	σ(m)	±2.9	±3.9	±2.2	±0.9	±3.0	±5.4	±2.1
	μ_D(m)	-3.3	-1.5	-3.3	-0.4	-2.3	-1.5	2.5
	σ_D(m)	±3.0	±3.7	±1.5	±2.1	±2.8	±5.3	±2.1
	ρ	0.43	0.44	0.83	0.42	0.52	0.31	0.57
	<1m	19.7	20.5	3.3	41.3	29.8	14.6	15.3
	1-2m	23.6	19.1	10.6	31.9	24.9	16.2	16.1
	2-4m	25.3	34.1	57.0	19.2	28.9	26.7	44.9
	4-8m	21.9	23.1	28.6	7.2	10.8	31.9	23.5
	>8m	9.5	3.3	0.5	0.4	5.6	10.6	0.3
Strategy 6 Wavelet→MTT	μ(m)	12.1	8.4	16.2	13.1	15.4	12.4	16.4
	σ(m)	±5.4	±5.0	±2.6	±4.2	±4.0	±6.8	±4.0
	μ_D(m)	-8.6	-12.3	-4.5	-7.6	-5.3	-8.4	-4.3
	σ_D(m)	±5.1	±4.7	±1.6	±3.9	±3.5	±6.6	±3.3
	ρ	0.41	0.44	0.83	0.42	0.48	0.22	0.54
	<1m	0.4	0.7	0.9	0.0	1.7	2.5	8.7
	1-2m	1.1	0.4	4.2	0.0	4.9	5.3	13.2
	2-4m	15.7	1.8	31.8	5.3	34.0	15.7	33.3
	4-8m	40.1	9.4	61.6	65.1	44.0	24.0	32.8
	>8m	42.7	87.7	1.6	29.6	15.3	52.5	12.0
Strategy 7 Fourier→MTT	μ(m)	17.6	19.4	17.6	20.4	18.8	19.5	23.4
	σ(m)	±2.9	±4.0	±2.2	±1.0	±3.2	±5.6	±2.1
	μ_D(m)	-3.1	-1.3	-3.1	-0.3	-1.9	-1.2	2.7
	σ_D(m)	±3.0	±3.8	±1.5	±2.1	±2.9	±5.5	±2.1
	ρ	0.41	0.45	0.84	0.43	0.49	0.33	0.55
	<1m	25.9	19.2	4.9	40.7	38.1	12.3	14.1
	1-2m	20.7	20.9	14.0	32.6	23.7	13.0	13.0
	2-4m	21.7	35.0	56.0	19.6	23.2	30.6	43.1
	4-8m	22.8	22.1	24.6	6.8	9.6	34.2	29.5
	>8m	8.9	2.8	0.5	0.4	5.3	9.8	0.3

Table 6.8: Statistical results and absolute difference (DPW - AS) distribution (%) for Strategies 5–7 (thinned stand).

In comparison with the analytical stereoplotter MTT data, the means and standard deviations of the DPW MTT data were encouraging for Strategies 5 and 7. The minimum μ_D and σ_D were –0.3m and ±1.5m (both using the 1:5,000 scale black and white infrared). The maximum μ_D were –3.3m (using the 1:5,000 scale black

and white and the 1:5,000 scale black and white infrared of Strategy 5) and 3.3m (using the 1:10,000 scale colour of Strategy 7) and the maximum σ_D was ±5.6m (using the 1:10,000 scale colour infrared of Strategy 7). The correlation coefficients of the 1:5,000 scale black and white infrared were high for all strategies ($\rho>0.8$).

In comparison with the non-MTT filtered data discussed in the previous section, the MTT filter significantly reduced the absolute differences for all model in Strategies 5 and 7 ($P<0.0001$) but less significantly in Strategy 6 ($P<0.01$). In Strategies 5 and 7, points having an error of >8m had been reduced significantly, for example, from 41% to only 5.3% (using the 1:10,000 scale colour infrared of Strategy 4).

The similarity of models produced using Strategies 5 and 7 are apparent, with no significant difference between the parameters ($P\approx0$). The similarities are also demonstrated by the height distribution graphs (Figure 6.29) and the example image profiles for each model (Figure 6.30 and Figure 6.31). The line indicating the location of derived height profiles is shown in Figure 6.18. It is clear also that the MTT filter has greatly reduced or removed the bi–modal distribution.

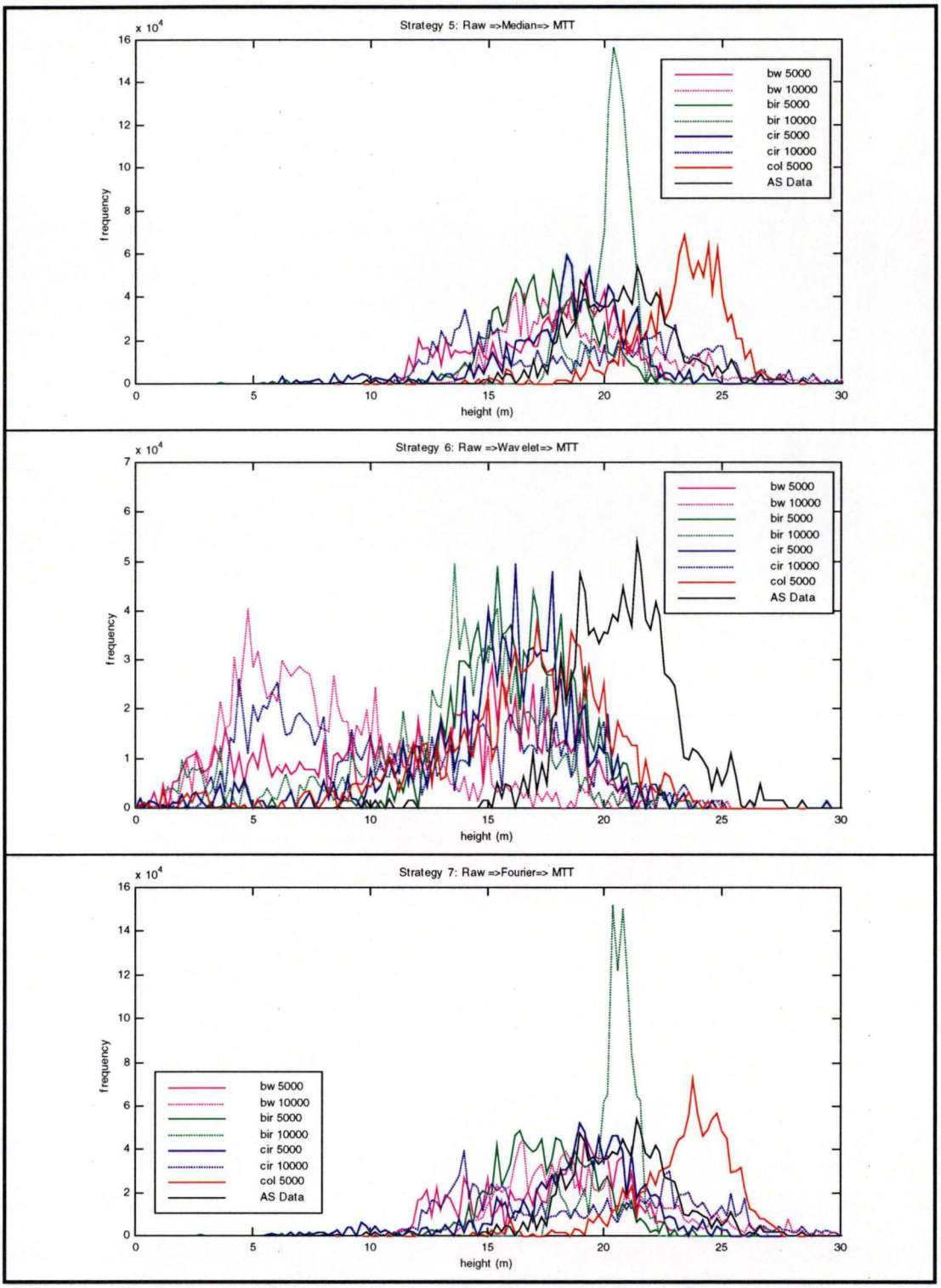

Figure 6.29: Height distributions for Strategies 5–7 (thinned stand).

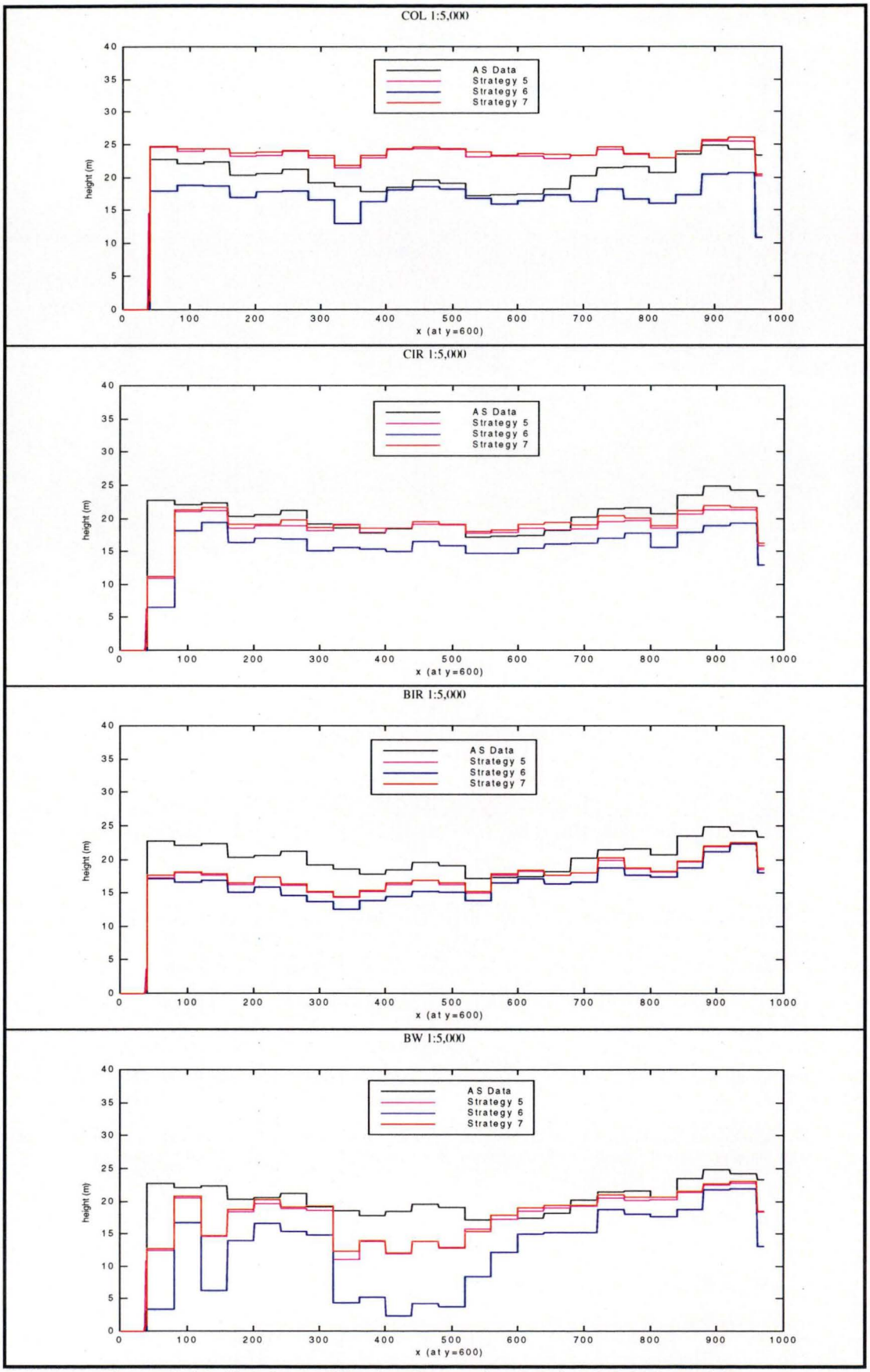

Figure 6.30: Height profiles for Strategies 5–7 for 1:5,000 models (thinned stand).

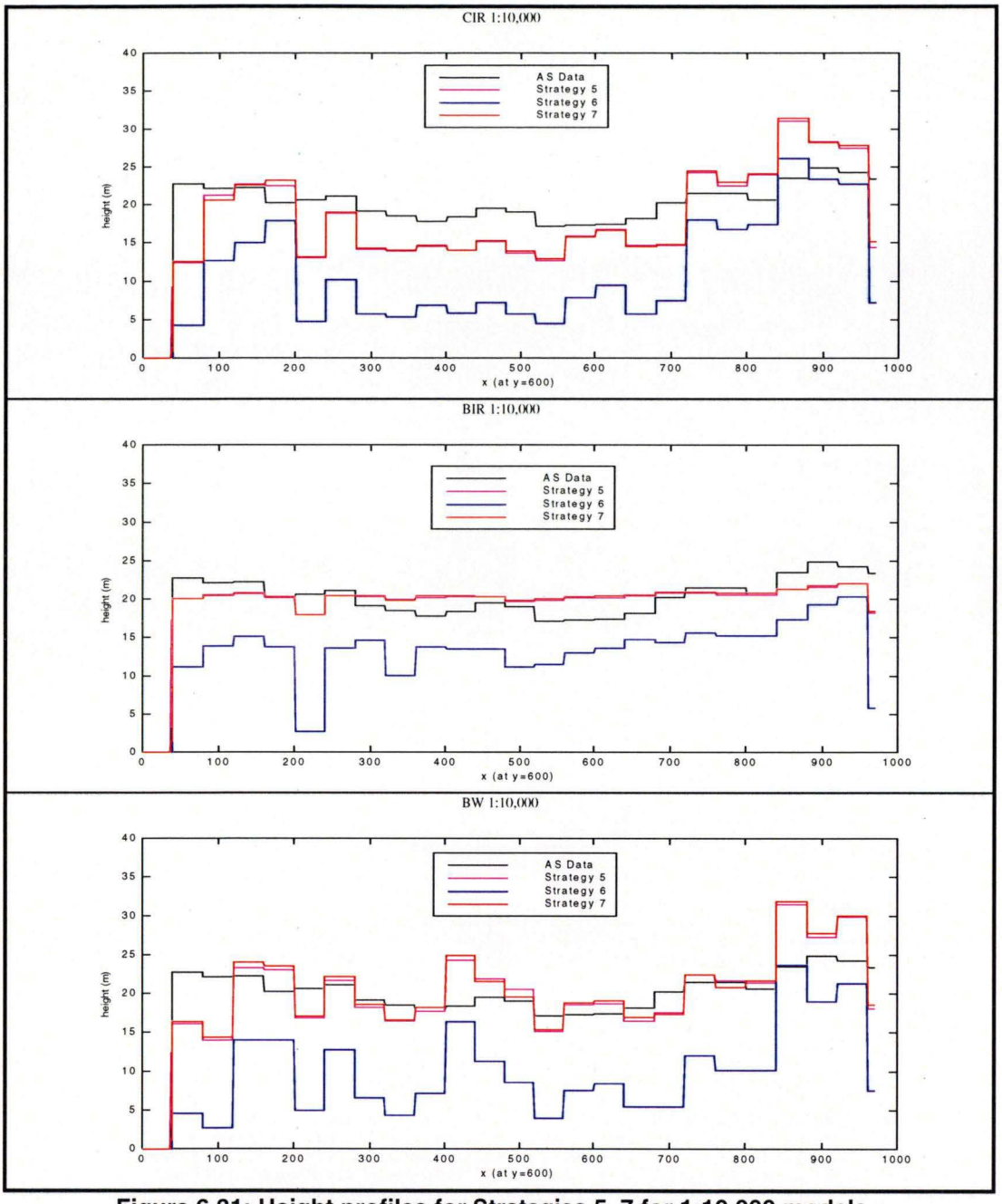

Figure 6.31: Height profiles for Strategies 5–7 for 1:10,000 models (thinned stand).

6.3.3. Analysis After Applying an NDVI–Threshold

6.3.3.1. Filters

The pixel values resulting from an NDVI computation range from –1 to 1. The canopy cover was extracted from the NDVI image having pixel values between 0.4 and 1.0 based on an interactive threshold. A binary image was generated with ones representing the canopy cover and zeros representing the non-canopy cover. The

resulting data is illustrated in Figure 6.32, with approximately 40% of the pixels having been identified as canopy.

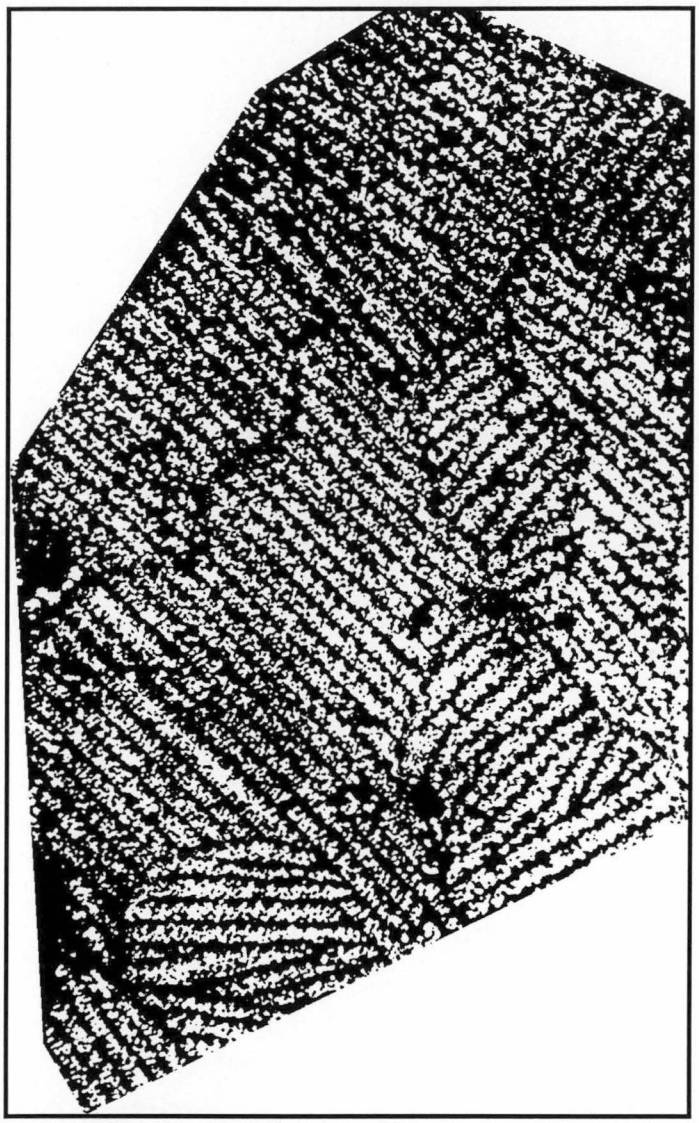

Figure 6.32: NDVI thresholding image.

The NDVI threshold was applied to all canopy height models with each element of the filter multiplied by the corresponding element in the canopy height model converting to zero all heights at points not identified as canopy.

6.3.3.2. Analytical Stereoplotter Data

The results for the analytical stereoplotter data are summarised in Table 6.9. The raw data and MTT data after application of the NDVI-threshold are illustrated in Figure 6.33.

In comparison to the original analytical stereoplotter data, the filter significantly increased the mean height of the analytical stereoplotter raw and MTT data

(P<0.0001). The standard deviation of the MTT data was significantly increased (P<0.0001).

Raw Data		MTT Data	
Mean (m)	σ (m)	Mean (m)	σ (m)
19.1	±2.3	20.0	±2.9

Table 6.9: Statistical results for analytical stereoplotter after NDVI–threshold.

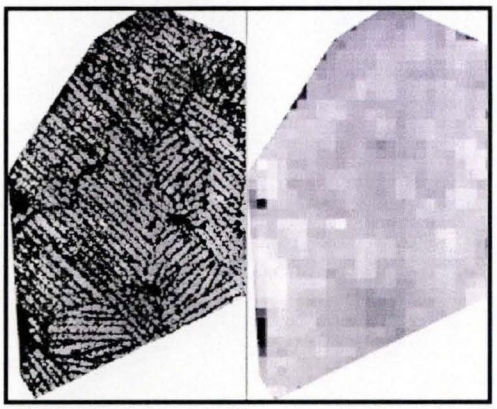

Figure 6.33. Analytical stereoplotter raw data and MTT data after NDVI-thresholing (0–30m [dark–light]).

6.3.3.3. Analysis Before Applying a Mean Tallest Tree Filter

The NDVI threshold was used to filter DPW data following Strategies 1 to 4 (Table 5.2). The images of the DPW data after NDVI–threshold (Strategies 8 to 11) are shown in Figures 6.35 to 6.38. The results for Strategies 8 to 11 and their differences from the analytical stereoplotter data are summarised in Table 6.10. The height distribution graphs are illustrated in Figure 6.38.

The bi–modal distributions are still clearly apparent in all models except, again, the 1:5,000 scale black and white infrared. There are two contributing factors. The NDVI filter relies on accurate georeferencing of the canopy, particularly when it is applied to photography other than the 1:10,000 colour infrared from which the filter was derived. Small errors in geolocation between rows will result in the exclusion of the canopy heights and the inclusion of the terrain heights. Further, inspection of image profiles for the raw and filtered tree height data indicates that there are many points within rows with low elevations being derived within and between trees along a row, which will not be excluded from the height model by the NDVI filter because of both georeferencing and resolution limits. An erosion filter was applied to the binary data illustrated in Figure 6.32 in case this included additional terrain,

without significant improvement. The MTT filter is therefore still required in order to extract meaningful data. These considerations suggest that more reliable methods to distinguish tree crown are required. Crown recognition algorithms are being developed and tested in a separate research project at the Centre.

μ = mean σ = standard deviation D = DPW - AS ρ = correlation		BW 5000	BW 10000	BIR 5000	BIR 10000	CIR 5000	CIR 10000	COL 5000
Strategy 8 Raw→NDVI	μ(m)	5.8	2.7	13.4	6.9	9.8	6.3	11.6
	σ(m)	±6.6	±4.4	±3.4	±7.4	±6.5	±6.3	±6.5
	μ_D(m)	-13.3	-16.4	-5.7	-12.2	-9.4	-12.8	-7.6
	σ_D(m)	±6.3	±4.4	±2.8	±7.2	±6.4	±6.1	±6.2
	ρ	0.29	0.26	0.59	0.24	0.24	0.27	0.32
	<1m	0.3	0.1	1.6	0.1	1.3	1.1	5.4
	1-2m	0.9	0.1	3.5	0.2	3.4	2.1	7.8
	2-4m	6.7	0.5	19.8	3.5	17.6	8.6	21.1
	4-8m	21.3	3.4	59.5	36.2	34.4	11.8	32.2
	>8m	70.8	95.9	15.6	60.0	43.4	76.4	33.4
Strategy 9 Median→NDVI	μ(m)	5.8	2.7	13.4	6.9	9.8	6.2	11.5
	σ(m)	±6.4	±4.4	±3.3	±7.2	±6.4	±6.1	±6.4
	μ_D(m)	-13.4	-16.4	-5.7	-12.2	-9.4	-12.9	-7.6
	σ_D(m)	±6.1	±4.4	±2.6	±7.0	±6.3	±5.9	±6.1
	ρ	0.30	0.26	0.61	0.24	0.24	0.27	0.32
	<1m	0.2	0.1	1.1	0.1	0.8	0.8	4.6
	1-2m	0.5	0.1	2.7	0.1	2.6	1.6	7.4
	2-4m	5.7	0.5	19.0	2.0	17.6	8.4	21.8
	4-8m	22.4	3.4	63.7	37.5	35.8	12.0	33.1
	>8m	71.2	95.9	13.5	60.4	43.2	77.2	33.1
Strategy 10 Wavelet→NDVI	μ(m)	6.1	3.1	13.4	7.3	9.9	6.4	11.7
	σ(m)	±5.9	±3.7	±3.2	±5.6	±6.0	±5.8	±5.8
	μ_D(m)	-13.0	-16.1	-5.7	-11.8	-9.2	-12.8	-7.4
	σ_D(m)	±5.6	±3.8	±2.5	±5.4	±5.8	±5.6	±5.5
	ρ	0.31	0.29	0.62	0.30	0.25	0.28	0.35
	<1m	0.4	0.1	1.1	0.1	1.4	1.2	4.7
	1-2m	0.9	0.1	2.9	0.3	3.1	1.8	6.9
	2-4m	5.2	0.4	18.1	3.3	15.6	5.9	20.4
	4-8m	19.0	2.5	64.5	29.4	33.3	12.1	32.7
	>8m	74.6	96.9	13.4	66.9	46.7	79.0	35.2
Strategy 11 Fourier→NDVI	μ(m)	14.0	14.6	15.1	18.9	14.1	14.2	20.8
	σ(m)	±3.5	±3.4	±2.8	±1.6	±5.1	±5.0	±3.4
	μ_D(m)	-5.1	-4.6	-4.1	-0.2	-5.0	-4.9	1.6
	σ_D(m)	±3.6	±3.5	±2.3	±2.5	±5.1	±5.0	±3.4
	ρ	0.30	0.27	0.61	0.25	0.24	0.26	0.33
	<1m	12.6	6.9	4.8	34.7	20.1	7.0	13.9
	1-2m	10.3	7.8	9.5	27.8	16.2	7.3	15.1
	2-4m	15.0	22.0	37.7	29.9	17.9	15.3	36.7
	4-8m	39.2	49.9	43.8	6.6	16.7	41.5	33.1
	>8m	22.9	13.4	4.3	0.9	29.0	29.0	1.1

Table 6.10: Statistical results and absolute difference (DPW–AS) distribution (%) after NDVI–thresholding (Strategies 8–11).

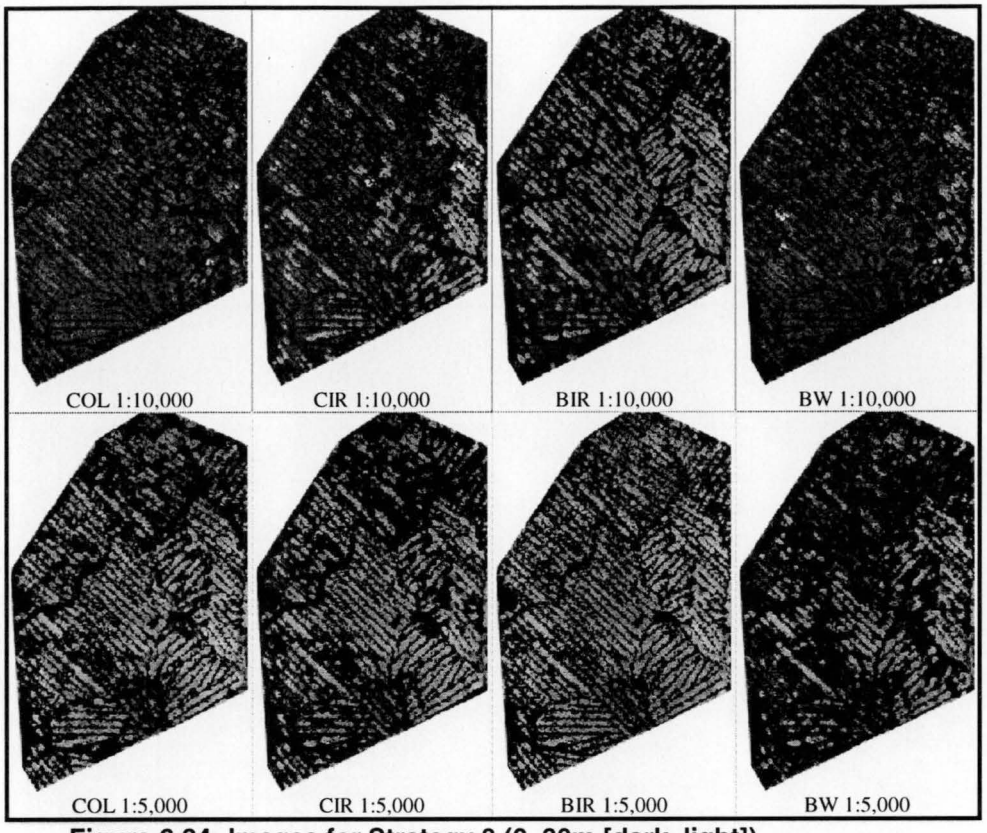

Figure 6.34: Images for Strategy 8 (0–30m [dark–light]).

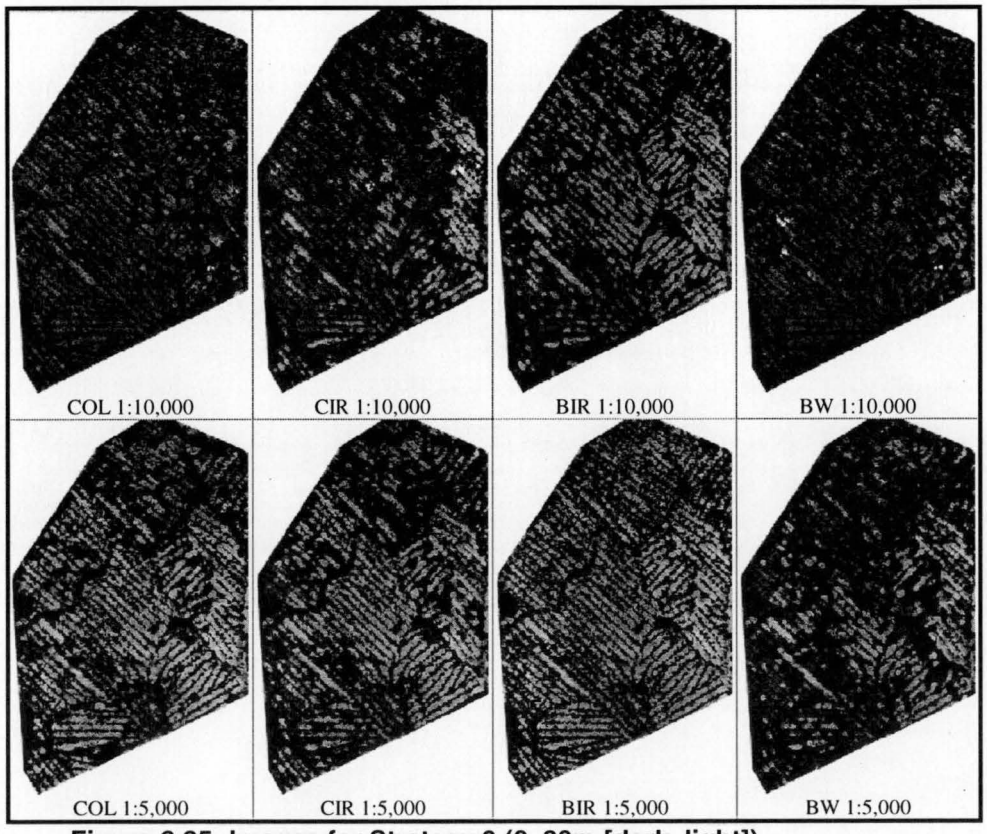

Figure 6.35: Images for Strategy 9 (0–30m [dark–light]).

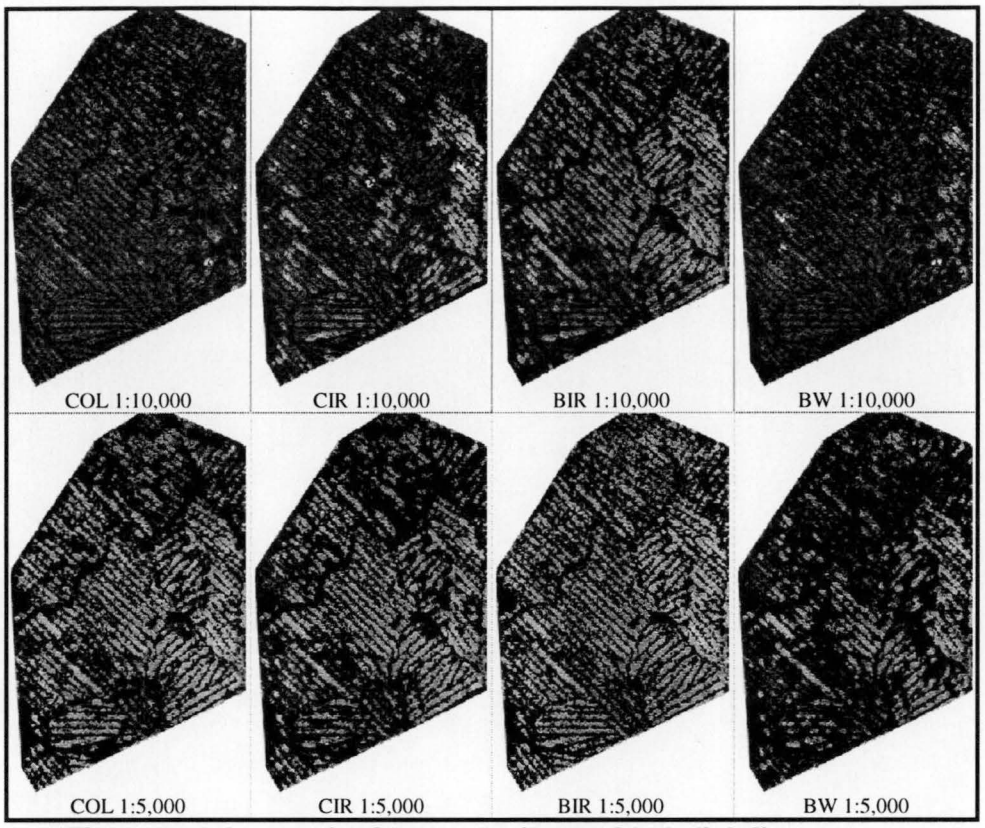

Figure 6.36: Images for Strategy 10 (0–30m [dark–light]).

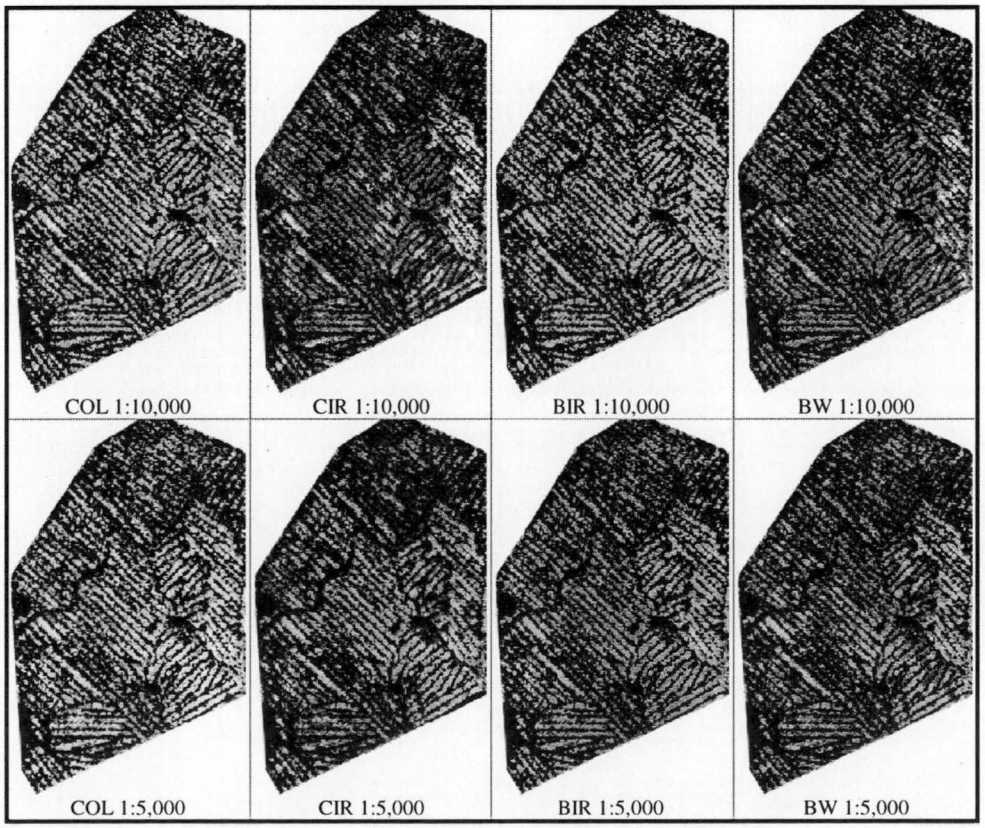

Figure 6.37: Images for Strategy 11 (0–30m [dark–light]).

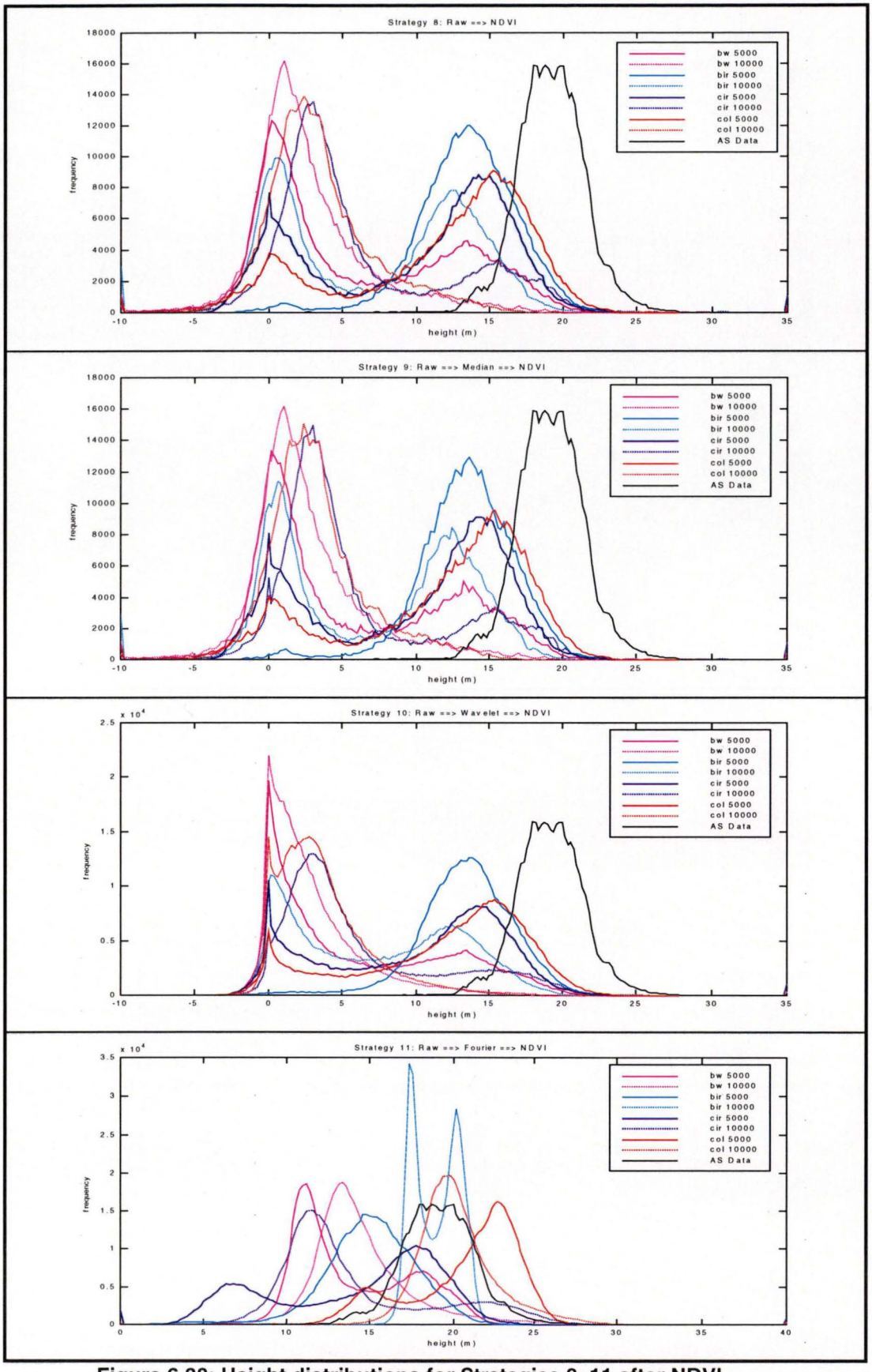

Figure 6.38: Height distributions for Strategies 8–11 after NDVI–thresholding.

6.3.3.4. Analysis After Applying a Mean Tallest Tree Filter

The DPW data following the application of the NDVI threshold were filtered using the MTT filter for Strategies 12 to 14 (Table 5.2). The size of the MTT filter was 25m×25m (50×50 pixels). The resulting images are shown in Figures 6.40 to 6.42. Comparison of the DPW and analytical stereoplotter data and their differences are summarised in Table 6.11. The height distributions are illustrated in Figure 6.42.

The results for Strategy 12 compare well with Strategy 13. This is supported by visual inspection of the images and height distributions. In comparison to the DPW MTT data before the application of the NDVI threshold, visual inspection of the images and height distributions, and investigation of the statistical results indicates that the results for Strategies 12 and 13 compare well with Strategy 6, and that the results for Strategy 14 compare well with Strategies 5 and 7, with no significant difference between the parameters ($P<0.0001$). The similarities are also demonstrated by the example image profiles for each model, as illustrated in Figure 6.43 and Figure 6.44.

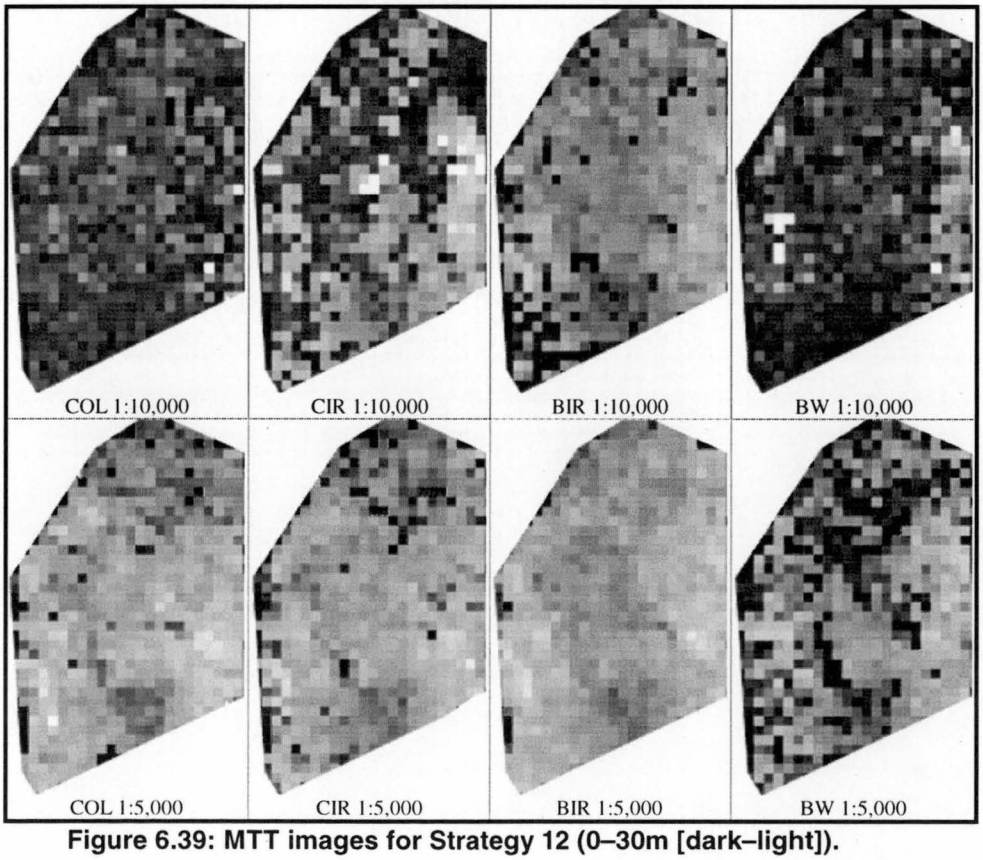

Figure 6.39: MTT images for Strategy 12 (0–30m [dark–light]).

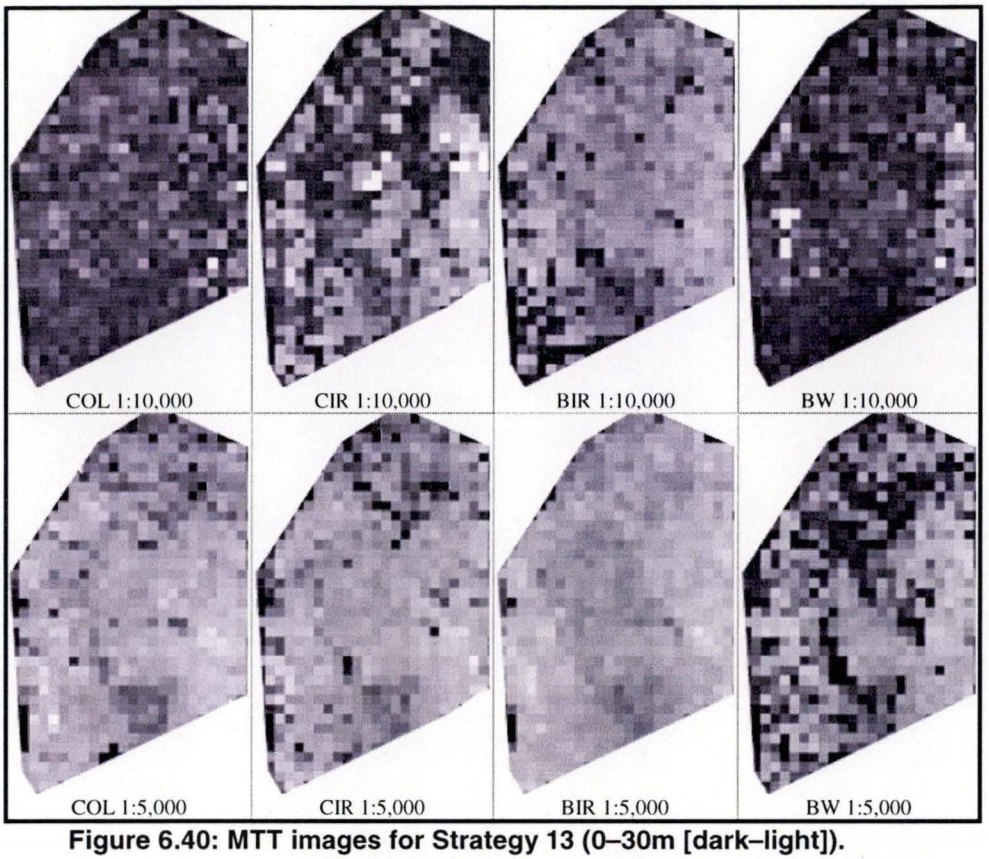

Figure 6.40: MTT images for Strategy 13 (0–30m [dark–light]).

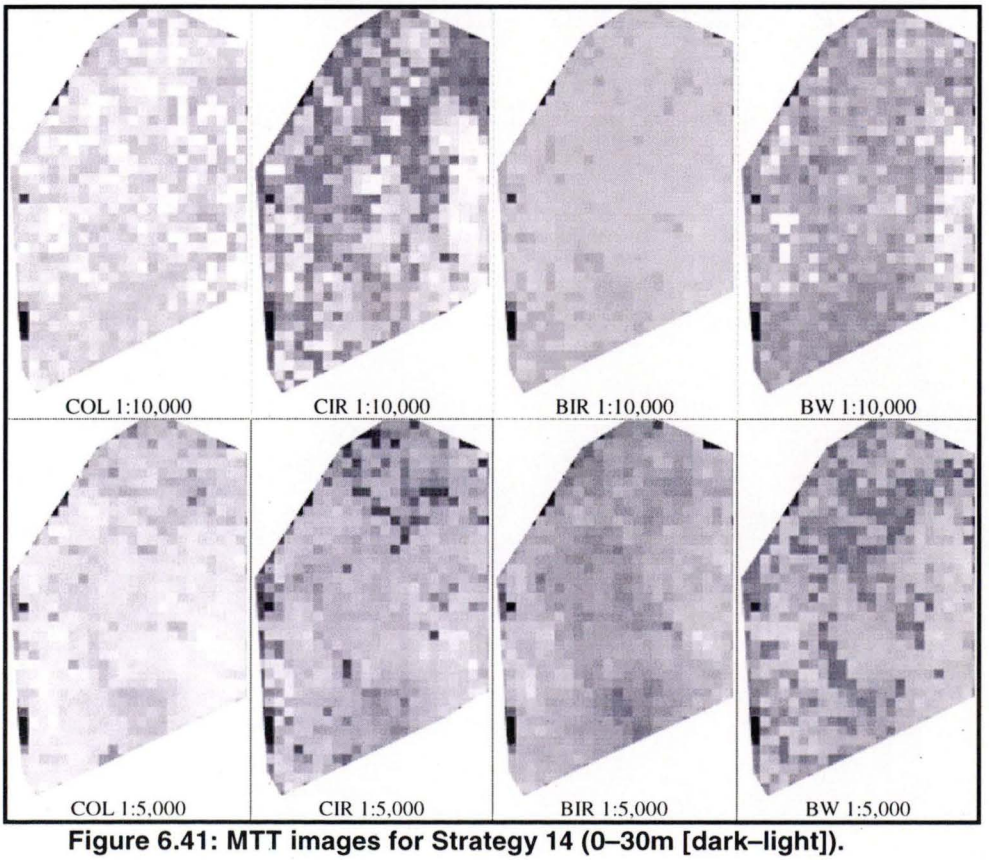

Figure 6.41: MTT images for Strategy 14 (0–30m [dark–light]).

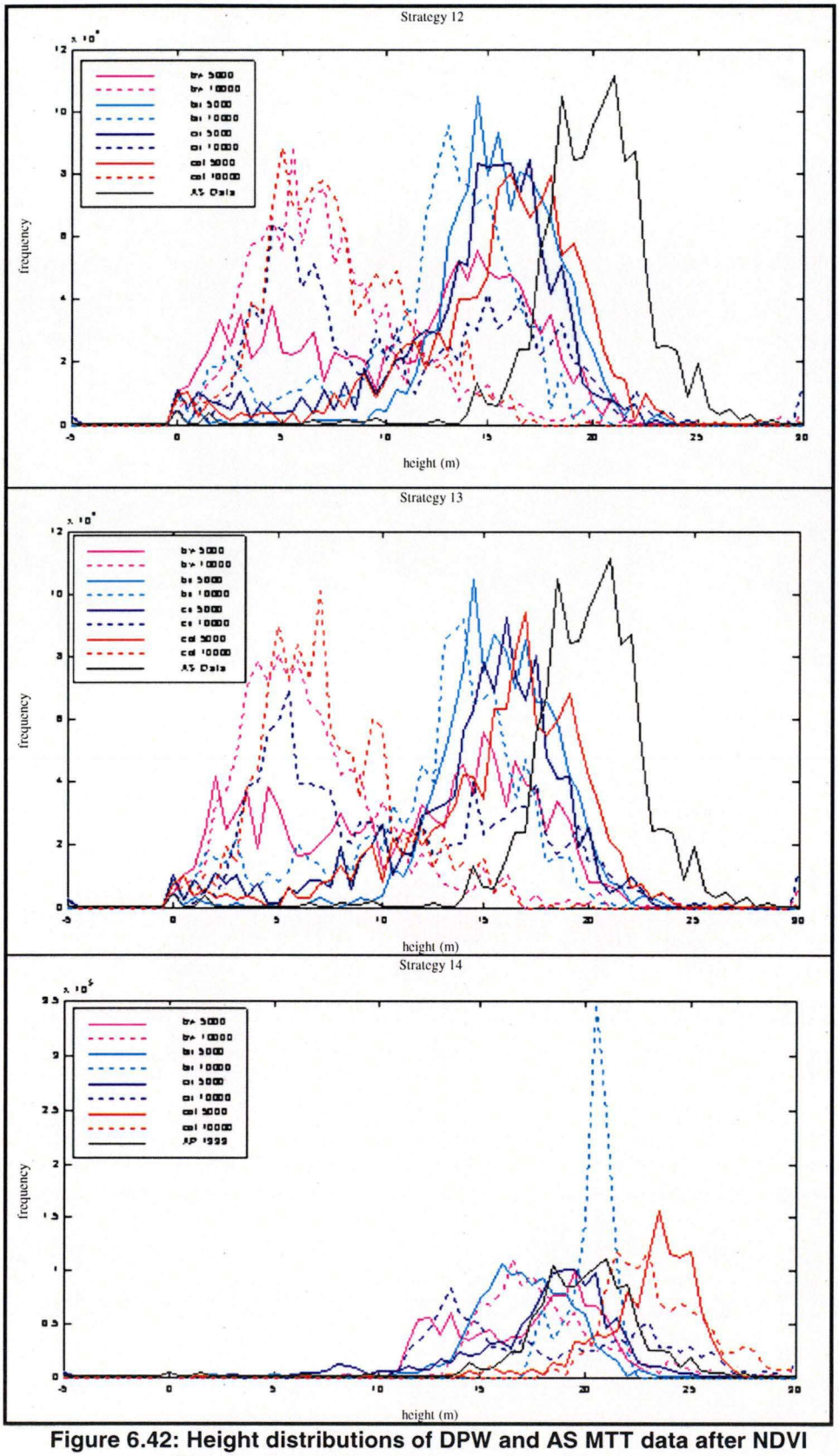

Figure 6.42: Height distributions of DPW and AS MTT data after NDVI filter for Strategies 12–14.

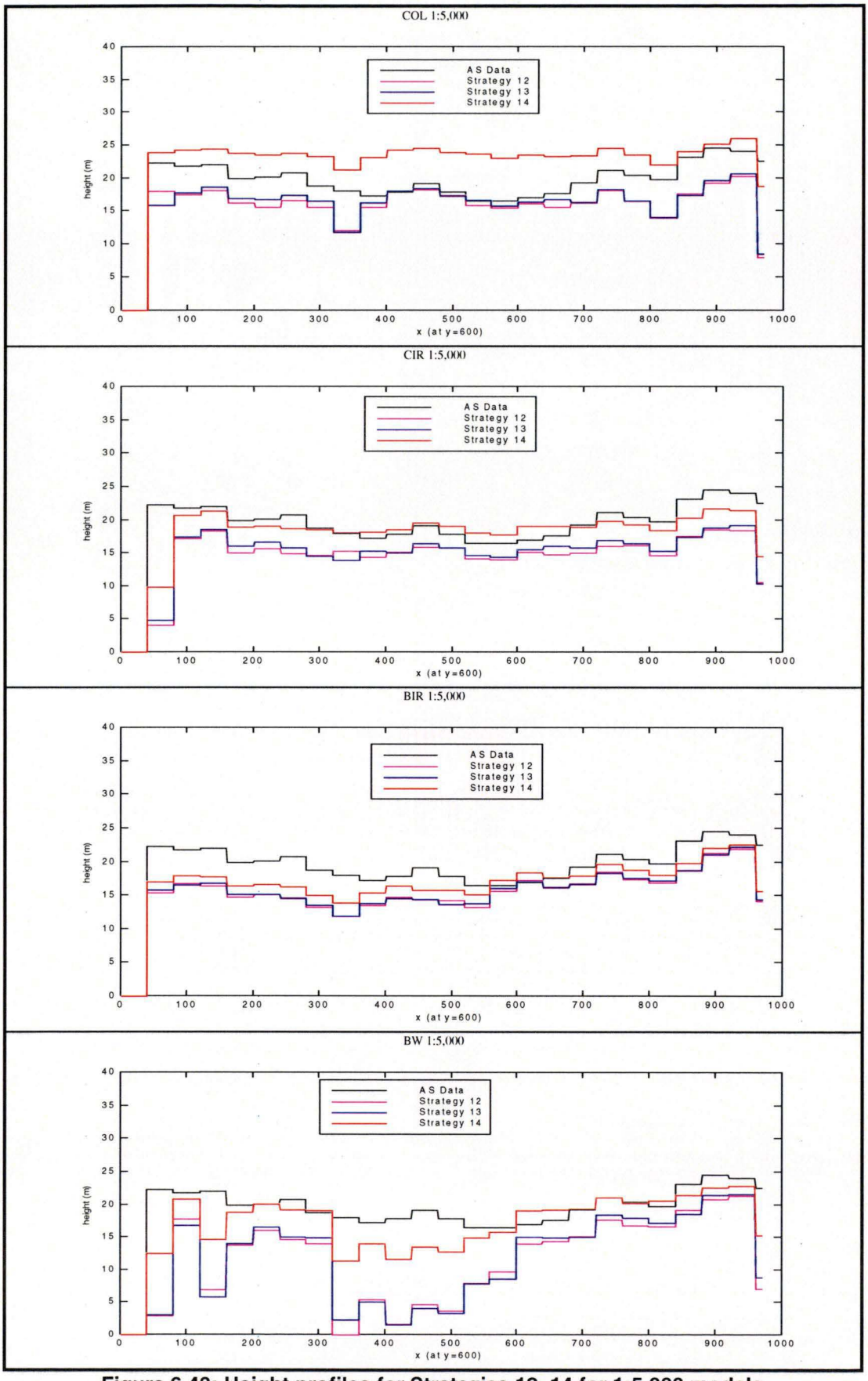

Figure 6.43: Height profiles for Strategies 12–14 for 1:5,000 models (thinned stand) after NDVI–threshold.

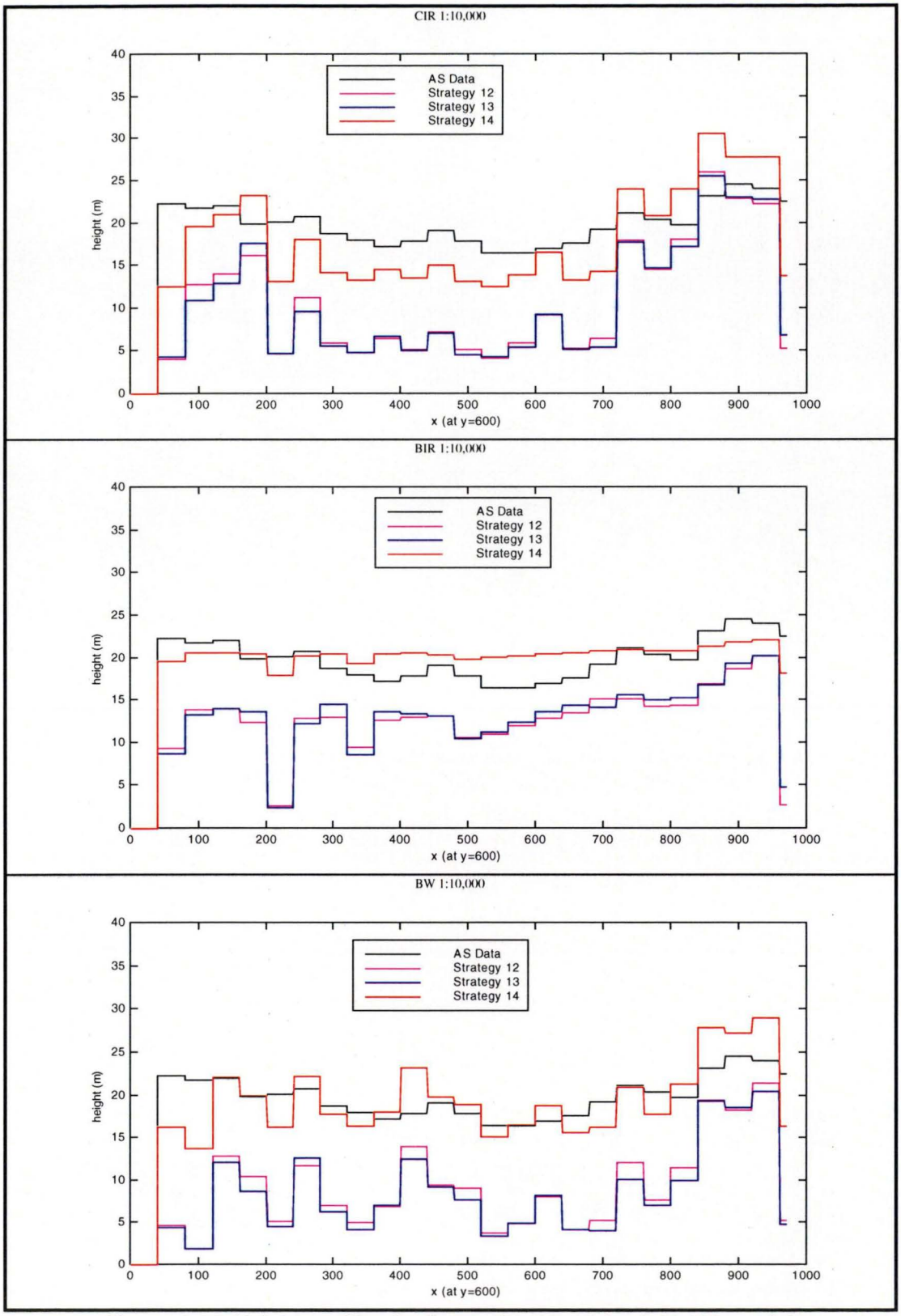

Figure 6.44: Height profiles for Strategies 12–14 for 1:10,000 models (thinned stand) after NDVI–threshold.

μ = mean σ = standard deviation D = DPW - AS ρ = correlation		BW 5000	BW 10000	BIR 5000	BIR 10000	CIR 5000	CIR 10000	COL 5000
Strategy 12 Median→NDVI→MTT	μ(m)	10.9	7.5	15.6	12.1	14.1	11.1	15.3
	σ(m)	±5.6	±4.7	±2.9	±4.4	±4.4	±6.5	±4.4
	μ_D(m)	-9.0	-12.4	-4.4	-7.9	-5.8	-8.9	-4.6
	σ_D(m)	±5.2	±4.5	±1.6	±4.0	±3.9	±6.3	±3.5
	ρ	0.40	0.39	0.85	0.47	0.51	0.30	0.60
	<1m	0.6	0.2	2.1	1.4	1.2	1.8	7.7
	1-2m	0.7	0.4	3.2	0.9	4.3	4.7	12.1
	2-4m	11.3	1.0	32.3	3.3	29.1	15.4	31.3
	4-8m	44.0	9.1	57.3	66.4	48.3	24.7	35.2
	>8m	43.5	89.2	5.1	28.0	17.2	53.4	13.7
Strategy 13 Wavelet→NDVI→MTT	μ(m)	11.0	7.0	15.6	12.3	14.3	11.1	15.5
	σ(m)	±5.7	±4.7	±3.0	±4.5	±4.6	±6.5	±4.5
	μ_D(m)	-8.9	-13.0	-4.3	-7.7	-5.6	-8.9	-4.5
	σ_D(m)	±5.3	±4.5	±1.6	±4.1	±4.0	±6.3	±3.6
	ρ	0.40	0.37	0.84	0.47	0.50	0.30	0.59
	<1m	1.0	0.5	1.8	0.1	2.6	3.6	10.9
	1-2m	1.6	0.1	4.2	0.2	6.6	5.1	13.7
	2-4m	15.3	1.2	34.6	6.7	31.7	15.6	30.4
	4-8m	35.9	6.7	57.5	61.6	40.0	19.9	31.0
	>8m	46.1	91.5	1.9	31.3	19.1	55.9	14.0
Strategy 14 Fourier→NDVI→MTT	μ(m)	16.9	18.1	17.0	20.1	17.9	18.3	22.8
	σ(m)	±3.4	±4.0	±2.7	±1.9	±3.9	±5.6	±3.0
	μ_D(m)	-3.1	-1.9	-2.9	0.1	-2.1	-1.7	2.8
	σ_D(m)	±3.2	±3.6	±1.5	±2.2	±3.4	±5.3	±2.3
	ρ	0.52	0.50	0.86	0.68	0.55	0.36	0.70
	<1m	28.4	18.5	7.1	36.5	37.3	11.5	10.9
	1-2m	18.5	20.4	15.8	31.4	22.9	11.0	14.2
	2-4m	20.3	34.2	56.7	25.5	21.9	28.0	39.6
	4-8m	23.7	24.3	20.0	6.5	10.6	38.7	35.1
	>8m	9.2	2.6	0.4	0.2	7.3	10.9	0.2

Table 6.11: Statistical results and absolute difference (DPW–AS) distribution (%) for thinned stand after NDVI–thresholding filter (Strategies 12–14).

6.4. Summary

In the closed canopy stand, tree height modelling was relatively easy and the results were encouraging. The digital photogrammetric data compared well with the analytical stereoplotter data for most models. The median and adaptive wavelet filters produced similar results, but neither significantly improved the raw data,

whereas the adaptive Fourier filter produced canopy height models that reliably preserved the general surface trend and significantly increased the mean height of the raw data. The mean tallest tree filter reduced the differences and improved the correlation between the digital photogrammetric and analytical stereoplotter data for all models in all strategies (5–7).

In the thinned stand, the results were less satisfactory. The median and adaptive wavelet filters did not improve the raw data. The adaptive Fourier filter produced canopy height models that preserved the general surface trend and significantly increased the mean height of the raw data. Application of the mean tallest tree filter to the thinned stand, following either the median or adaptive Fourier filter, improved the correlation and reduced the absolute differences between the digital photogrammetric data and the analytical stereoplotter data.

The NDVI threshold did not appear to improve the results due to errors in georeferencing and resolution limits. Application of the mean tallest tree filter improved the NDVI filtered data, in a manner comparable to the previous data sets. This was shown in the statistical results, images, and height profiles.

The following conclusion can be drawn:

- in closed canopy stand, canopy height can be reliably mapped using 1:5,000 or 1:10,000 photography and either colour, black and white, colour infrared, or black and white infrared, film;
- in the thinned stand, the digital photogrammetric data were comparable to the analytical stereoplotter data but only after the application of an appropriate mean tallest tree filter.

The analytical stereoplotter data used to provide a reference canopy elevation model will contain random and systematic errors. Differences in tree height measurements by two different operators were evident. This suggest that there is still a need to provide limited field measured data to check either digital or analytical photogrammetric data.

Chapter 7. Improving Automatically Derived Digital Photogrammetric Data

7.1. Introduction

This chapter presents a method for improving the automatically derived photogrammetric tree heights using a small set of manually measured photogrammetric tree heights. The chapter is divided into three parts. The first part (Section 7.2) describes the method used to improve the automatically derived photogrammetric data; the second part (Section 7.3) describes its application to the closed canopy stand; and the third part (Section 7.4) describes its application to the thinned stand.

7.2. Methodology

In order to improve the digital photogrammetric data, a linear relationship between the automatically derived photogrammetric data and manually measured photogrammetric data was defined by:

$$ManualPhotoData = m \times AutomaticPhotoData + c.$$

Then, for each model the parameters m and c were applied to the whole data sets, giving

$$CorrectedPhotoData = m \times AutomaticPhotoData + c.$$

A scale factor (m) was included, but constrained to values between 0.9 and 1.1, as there was no reason to expect a substantial scale error, and this constraint provided a simple method of ensuring a clean data set. The refined DPW data were then compared against the corresponding analytical stereoplotter data using the methods described in Chapter 6.

Approximately 10 to 20 tree heights were measured manually using the DPW 770 in both the closed canopy stand and thinned stand. Heights obtained from the automatically derived photogrammetric coverage were plotted against their corresponding manually measured photogrammetric height, and a linear regression used to define the relationship between them. If the computed gradient was outside the specified range then data points which differed from the mean by more than 1σ were systematically removed until the constraint was satisfied. This simple rule was implemented as an automatic routine and proved to be robust. In both stands, only the photogrammetric data following the median, adaptive wavelet, and adaptive Fourier filters were tested, as these were already shown to provide the best data.

7.3. Analysis: the Closed Canopy Stand

For the closed canopy stand, ten representative heights were measured at location which were well distributed across the stands. Between two and four of these heights were removed in each model because they were detected as outliers[1]. The relationships between the automatically derived photogrammetric tree height (automatic data) and manually measured photogrammetric tree height (manual data) are shown in Figures 7.1 to 7.3.

The correlation between the automatic and manual data was high for all models in all strategies in the closed canopy stand. The correlation ranged from 0.79 (using the 1:10,000 scale black and white infrared following the adaptive wavelet filter) to 0.98 (using the 1:5000 scale colour following the adaptive Fourier filter). Two models produced a gradient significantly outside the 0.9 and 1.1 limit. These were the 1:10,000 and 1:5,000 scale black and white models ($m \approx 0.7$ in both cases following the adaptive Fourier filter). These two models were not further processed. However, it is not impossible to remeasure these points or to measure new points so that the final gradient can fall within the limits.

[1] Note that the "outliers" should not be considered errors in the automatically derived data, but a consequence of comparing point data in both data sets at sub-metre horizontal precision.

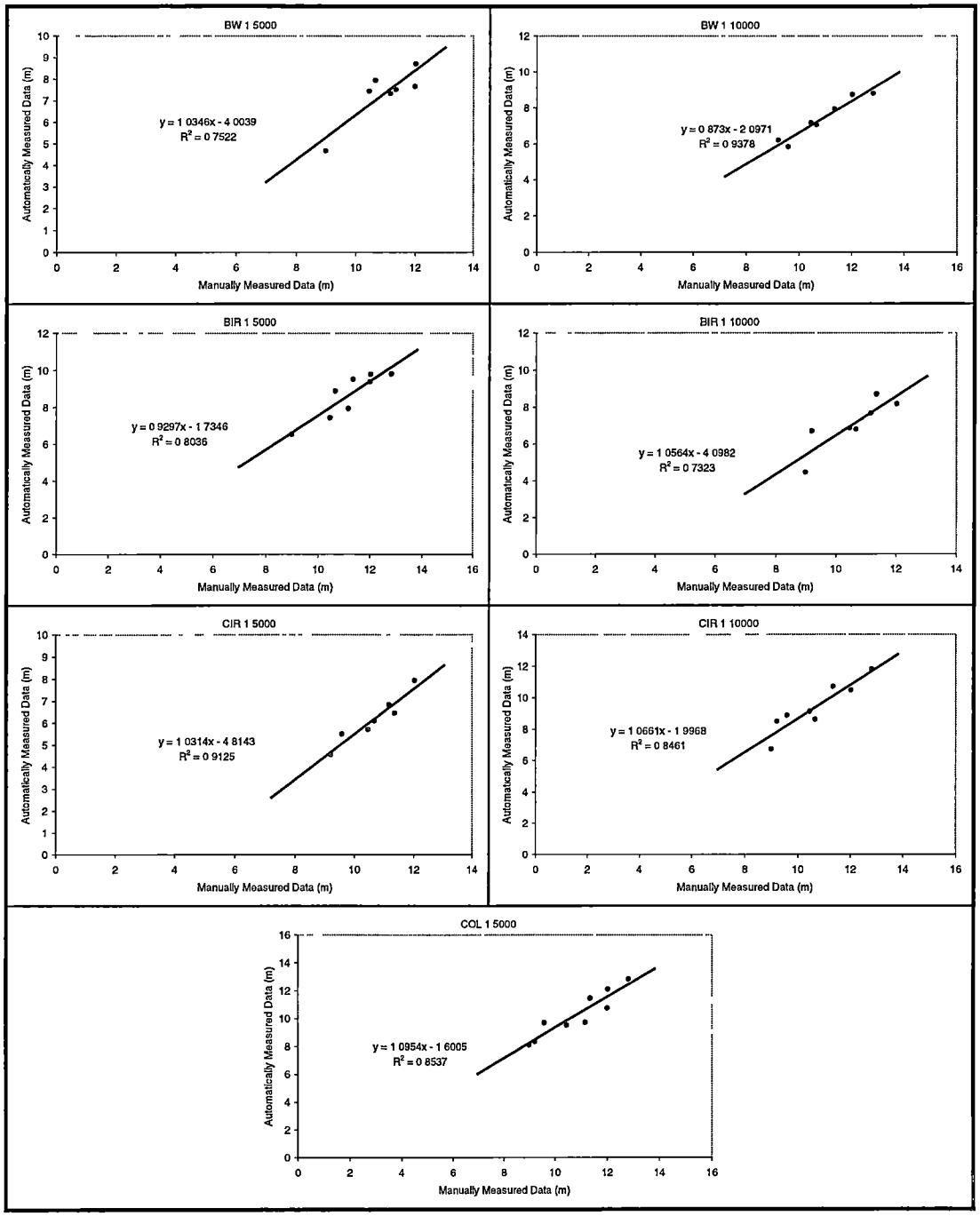

Figure 7.1: Relationship between the automatic and manual photogrammetric data in the closed canopy stand following the median filter (Strategy 2).

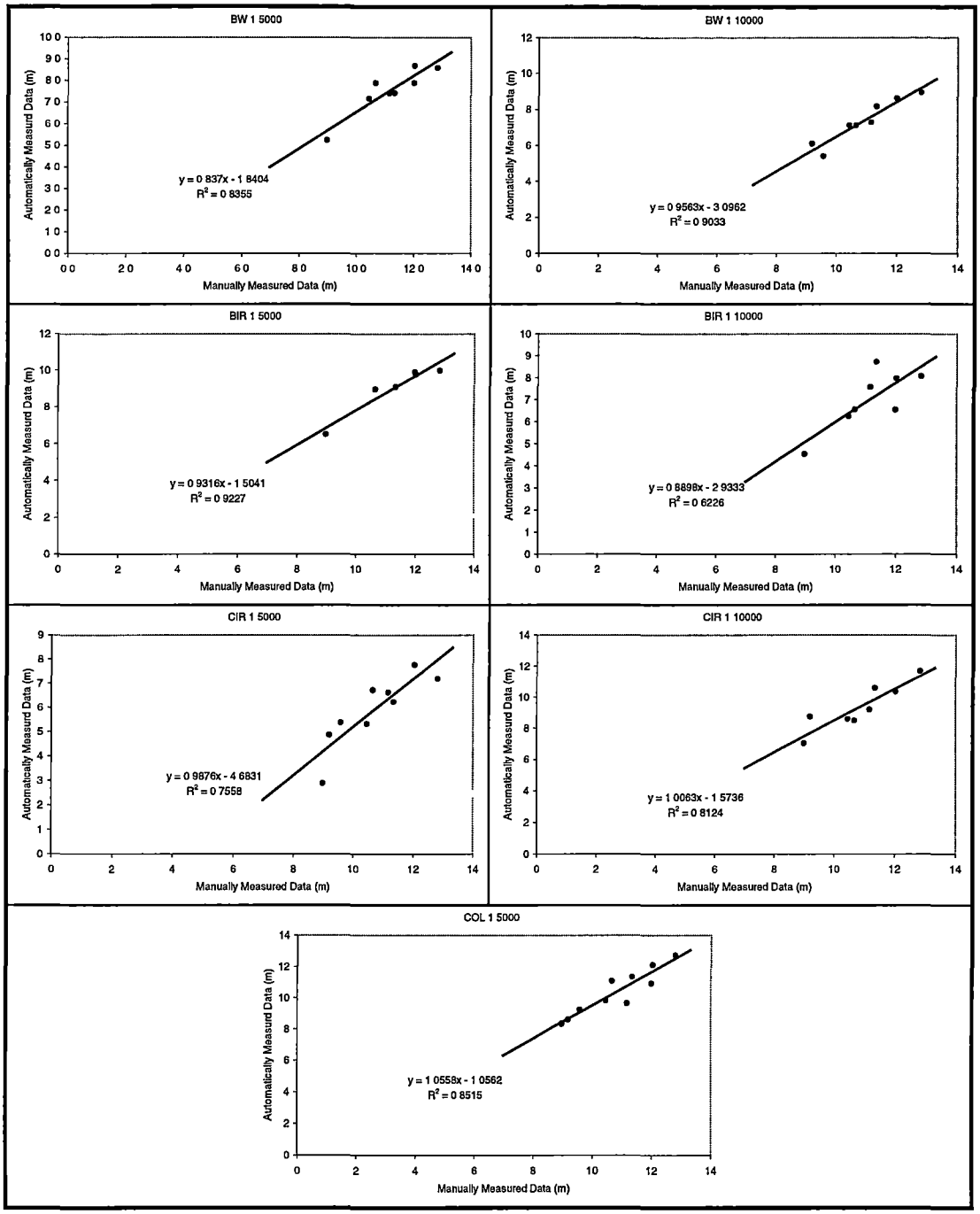

Figure 7.2: Relationship between the automatic and manual photogrammetric data in the closed canopy stand following the adaptive wavelet filter (Strategy 3).

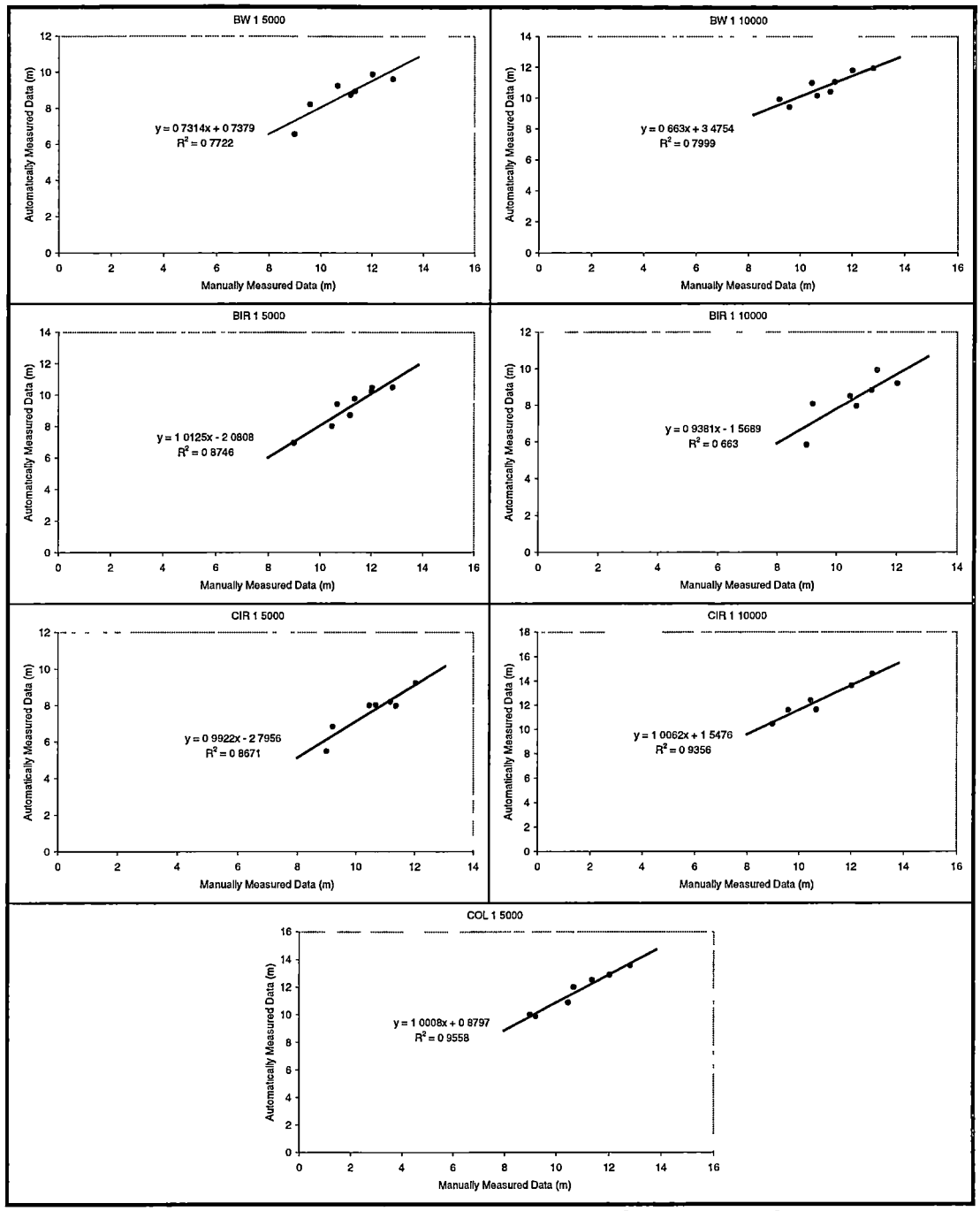

Figure 7.3: Relationship between the automatic and manual photogrammetric data in the closed canopy stand following the adaptive Fourier filter (Strategy 4).

The linear equations representing the relationship between the automatic and manual data can be applied to the digital photogrammetric data for tree height refinement because of these high correlations. The results are summarised in Table 7.1. The height distributions are illustrated in Figure 7.4.

μ=mean σ=standard deviation D=DPW–AS ρ=correlation		BW 5000	BW 10000	BIR 5000	BIR 10000	CIR 5000	CIR 10000	COL 5000
Strategy 2 Raw→Median→Linear Correction	μ(m)	10.8	10.4	11.3	10.5	10.1	10.6	11.0
	$\pm\sigma$(m)	1.6	2.6	1.6	1.6	1.6	1.7	1.5
	μ_D(m)	-0.4	-0.8	0.1	-0.7	-1.1	-0.6	-0.3
	$\pm\sigma_D$(m)	1.2	2.0	1.0	1.1	1.1	1.2	0.9
	ρ	0.69	0.63	0.76	0.73	0.75	0.71	0.78
	<1m	69.8	55.7	69.7	61.6	48.5	64.0	74.0
	1–2m	23.5	26.7	25.4	26.8	35.4	27.1	22.4
	2–4m	5.4	11.6	4.6	10.3	15.0	7.4	3.2
	4–8m	1.2	4.9	0.4	1.3	1.0	1.4	0.3
	>8m	0.1	1.0	0.0	0.0	0.1	0.1	0.0
Strategy 3 Raw→Wavelet→Linear Correction	μ(m)	10.8	10.6	11.0	11.1	10.4	10.8	10.8
	$\pm\sigma$(m)	2.0	2.3	1.6	2.0	1.6	1.8	1.6
	μ_D(m)	-0.5	-0.7	-0.3	-0.1	-0.8	-0.4	-0.4
	$\pm\sigma_D$(m)	1.4	1.8	1.1	1.4	1.1	1.3	1.1
	ρ	0.69	0.64	0.74	0.72	0.74	0.70	0.75
	<1m	62.2	57.7	68.5	59.7	58.5	64.3	69.8
	1–2m	26.5	25.6	24.8	29.2	29.9	25.9	24.1
	2–4m	9.0	11.8	5.9	9.6	10.5	8.0	5.1
	4–8m	1.9	4.4	0.8	1.4	1.0	1.7	0.9
	>8m	0.3	0.5	0.0	0.1	0.1	0.1	0.0
Strategy 4 Raw→Fourier→Linear Correction	μ(m)			11.2	10.5	10.3	10.7	10.7
	$\pm\sigma$(m)			1.4	1.6	1.2	1.6	1.4
	μ_D(m)			-0.1	-0.8	-0.9	-0.5	-0.5
	$\pm\sigma_D$(m)			1.0	1.2	0.9	1.2	1.0
	ρ			0.72	0.70	0.73	0.68	0.75
	<1m			70.9	59.7	56.0	65.7	69.2
	1–2m			24.3	27.5	33.0	25.6	25.0
	2–4m			4.6	11.5	10.5	7.3	5.3
	4–8m			0.3	1.3	0.6	1.2	0.5
	>8m			0.0	0.0	0.0	0.1	0.0

Table 7.1: Statistical results and absolute difference distribution (%) between DPW data and analytical stereoplotter data after tree height refinement for the closed canopy stand.

Refinement using the linear correlation between the automatic and manual data significantly reduced the mean differences (μ_D) between the DPW and analytical stereoplotter data for all models in all strategies ($P<0.0001$). In the best case, the μ_D was –0.1m (using the 1:5,000 scale black and white infrared following the adaptive wavelet filter and the 1:10,000 scale black and white infrared following the adaptive wavelet filter) and 0.1m (using the 1:5,000 scale black and white infrared following the median filter); and in the worst case, the μ_D was –1.1m (using the 1:5,000 scale colour infrared following the median filter). All DPW data consistently underestimated the analytical stereoplotter data, except for the 1:5,000

scale black and white infrared model following the median filter. This is probably caused by a small systematic difference between the manual height observations made on the DPW and the height observations made on the analytical stereoplotter.

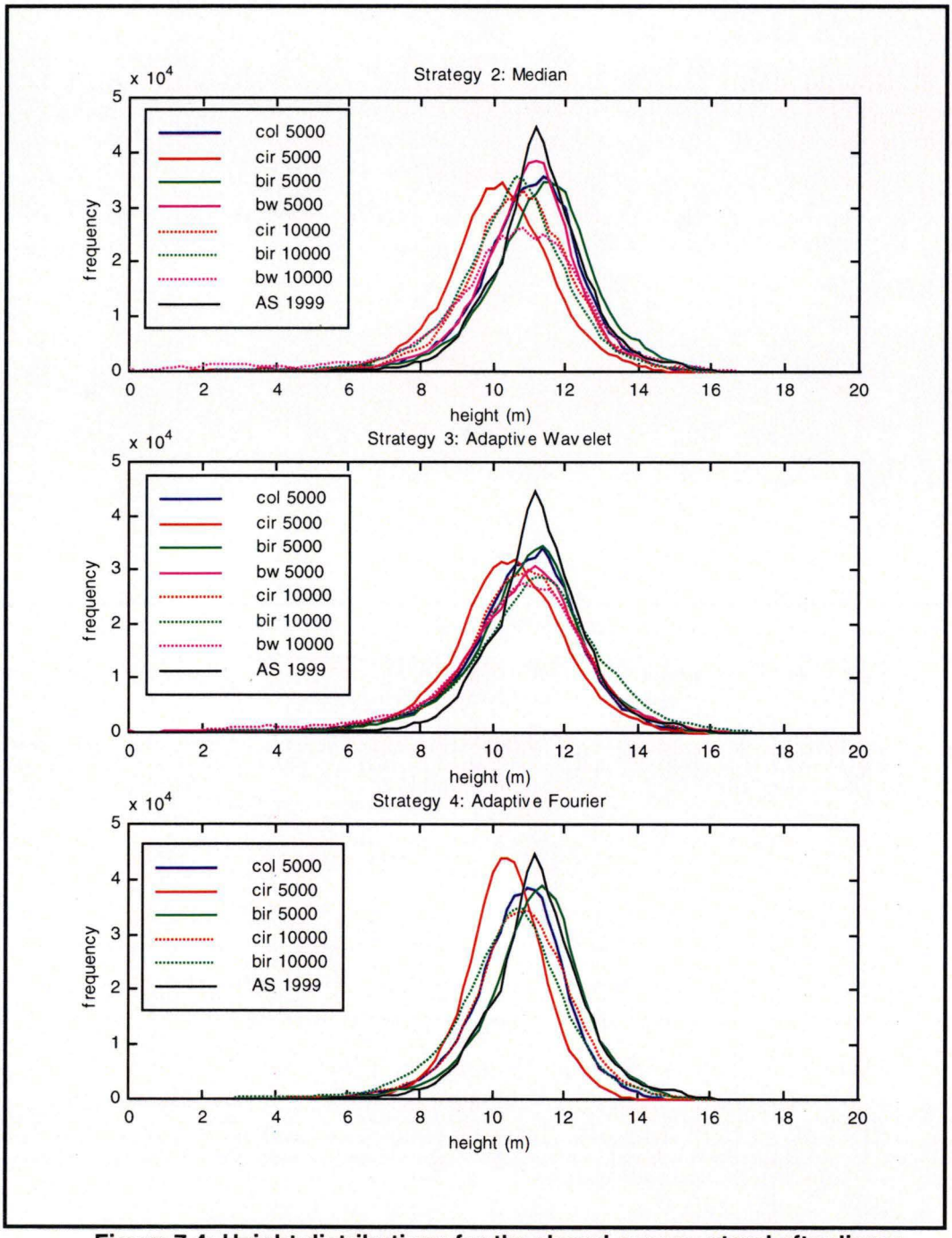

Figure 7.4: Height distributions for the closed canopy stand after linear transformation. Tree height data have been rounded to the nearest 0.2m.

The correlation between the DPW and analytical data was not changed significantly because the gradients of the linear equations were limited within 1 ±

0.1; however, the absolute differences between the DPW and analytical stereoplotter data were significantly improved. The number of points having an error of less than 2m ranged from 82% (using the 1:10,000 scale black and white following the median filter) to more than 96% (using the 1:5,000 scale colour following the median filter). The improvement in the mean difference and absolute difference is illustrated in the height distributions (Figure 7.4) and example image profiles (Figure 7.5 and Figure 7.6).

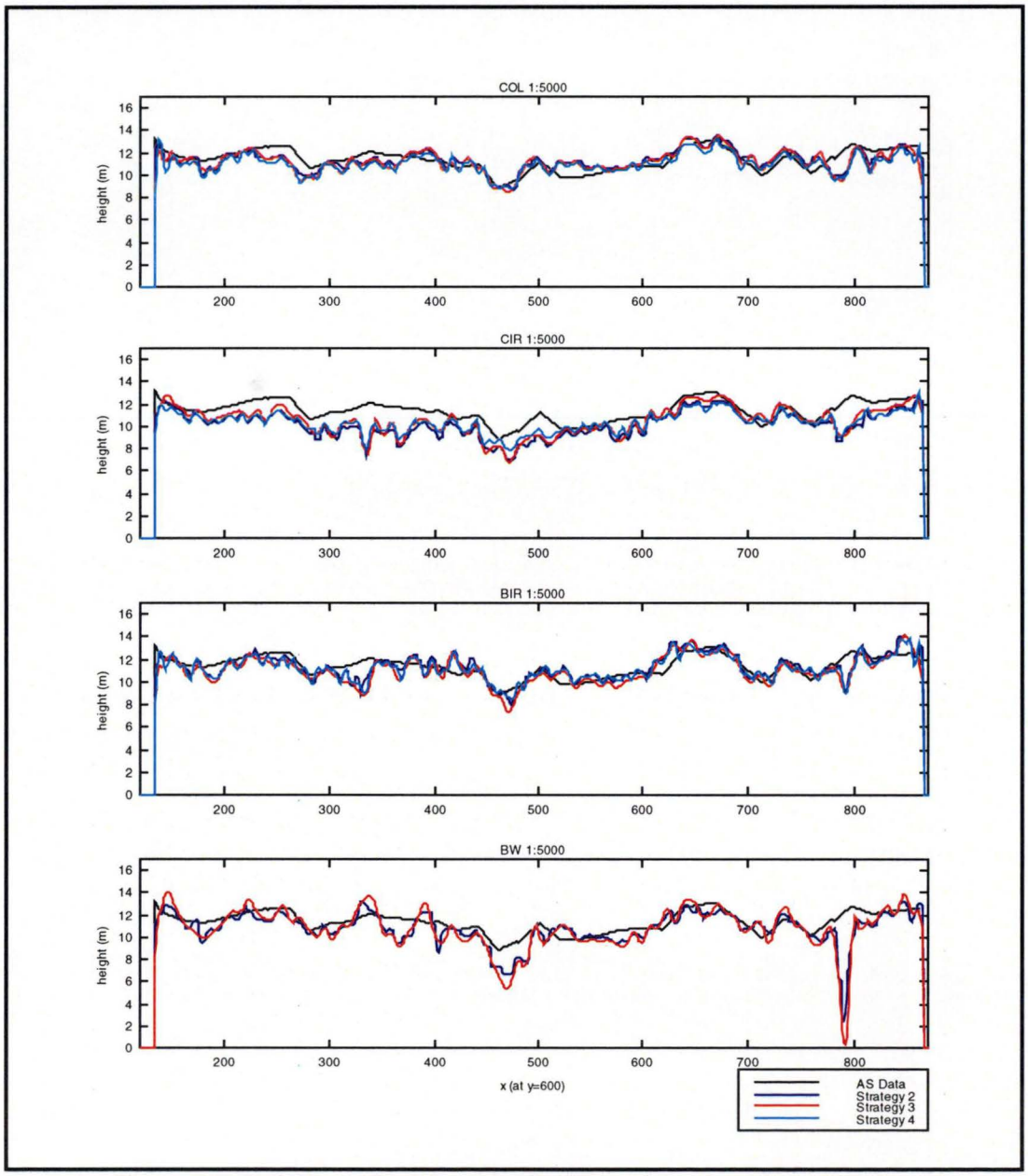

Figure 7.5: Height profiles for the 1:5,000 models after tree height refinement (closed canopy stand).

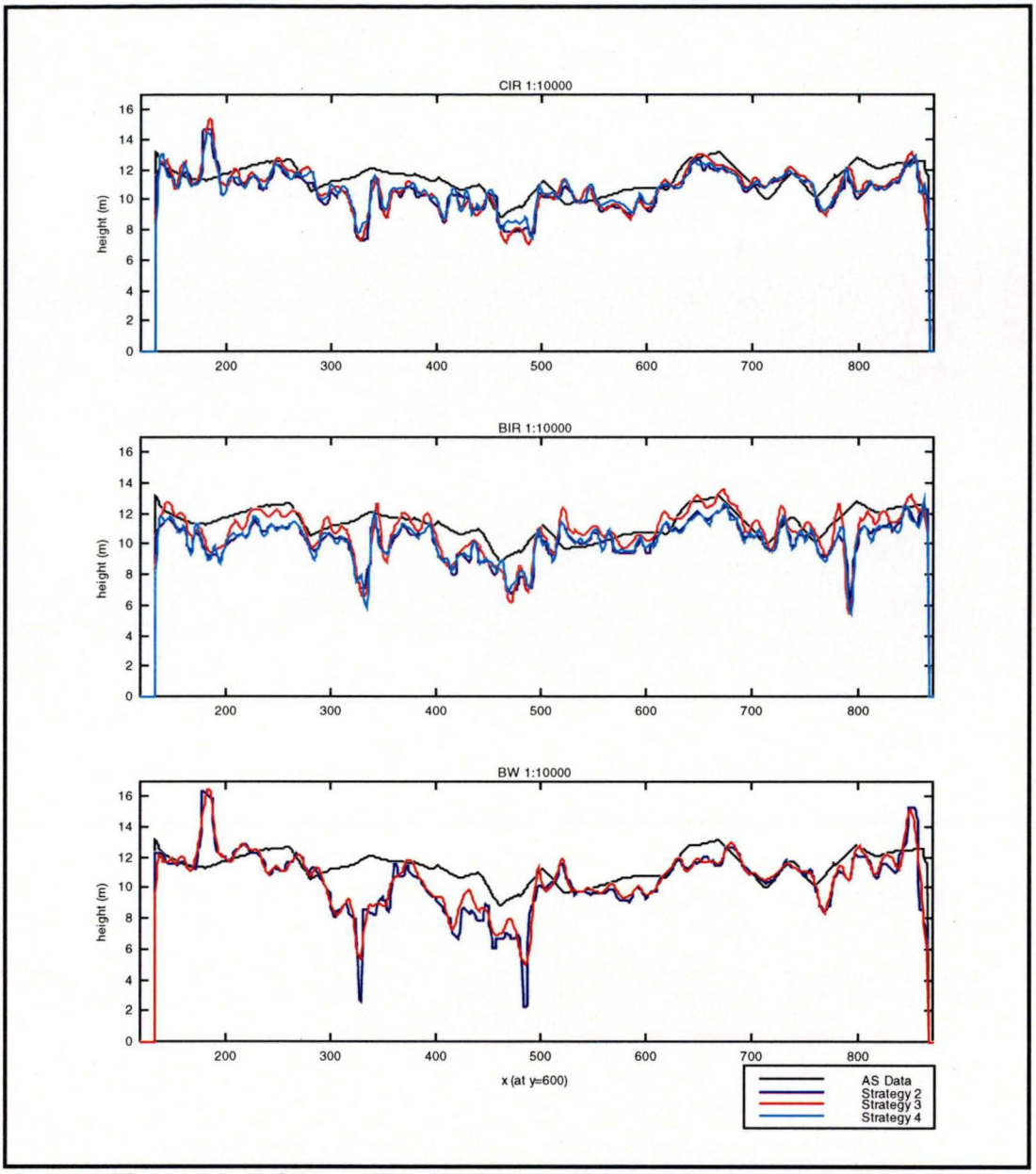

Figure 7.6: Height profiles for the 1:10,000 models after tree height refinement (closed canopy stand).

The height distributions and height profiles of all DPW models following all strategies were comparable and consistent with the analytical stereoplotter data. Again, all models appear to preserve the general surface trend reliably. Tree height refinement using a limited number of manually measured heights produced reliable results, comparable with the analytical stereoplotter data. MTT data for the refined closed canopy heights is not shown here, but clearly will correspond at least as well.

7.4. Analysis: the Thinned Stand

Eighteen representative tree heights were measured for the thinned stand. More tree heights were measured to anticipate the more complex canopy surface. Between four and ten of these points were detected as outliers and were removed, with most of the 1:10,000 models containing many outliers. The relationships between the automatic and manual data are shown in Figures 7.7 to 7.9.

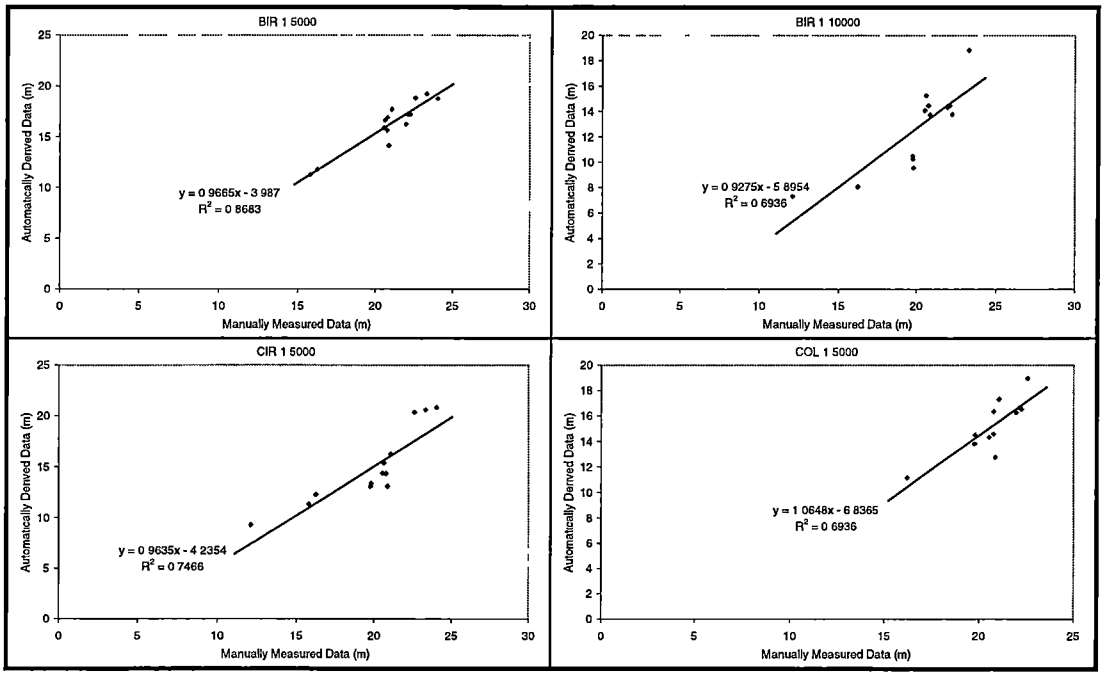

Figure 7.7: Relationship between the automatically derived and manually measured photogrammetric data in the thinned stand following the median filter (Strategy 2).

In the thinned stand, the correlations between the automatic and manual data were high but only using the following models:

- Strategy 2:
  - 1:5,000 scale black and white infrared,
  - 1:10,000 scale black and white infrared,
  - 1:5,000 scale colour, and
  - 1:5,000 scale colour infrared;
- Strategy 3 :
  - 1:5,000 scale black and white infrared,
  - 1:5,000 scale colour infrared, and
  - 1:5,000 scale colour;
- Strategy 4:
  - 1:5,000 scale black and white,
  - 1:5,000 scale black and white infrared, and
  - 1:5,000 scale colour infrared.

Therefore, the linear equations representing the relationship between the automatic and manual data were applied only for these models. The results are summarised in Table 7.2.

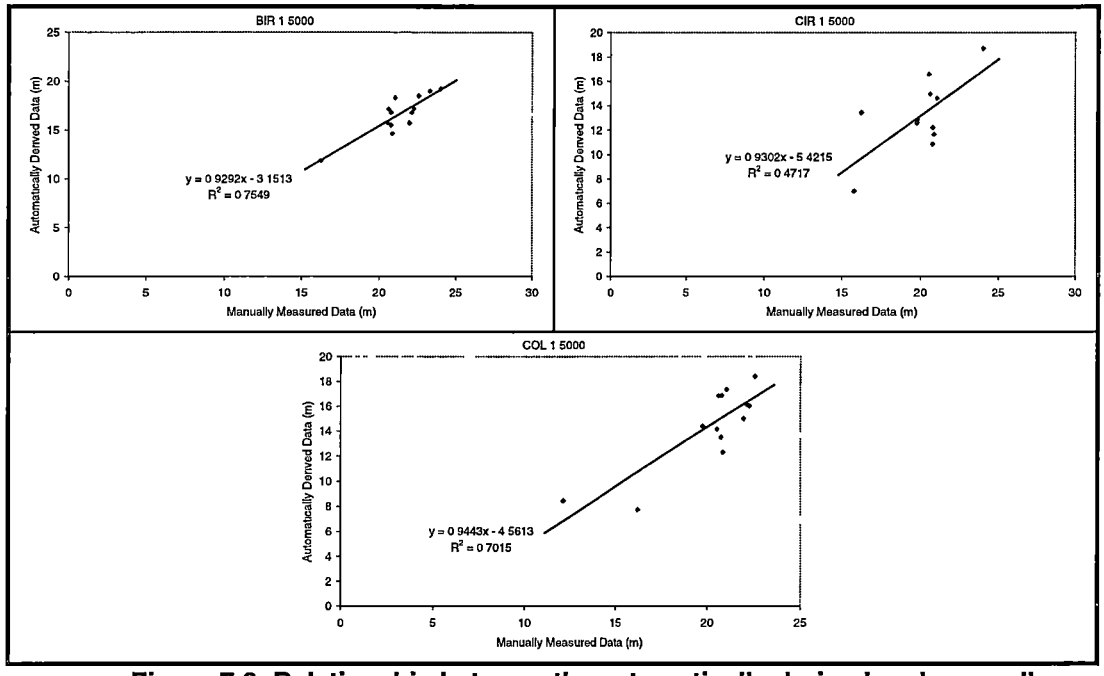

Figure 7.8: Relationship between the automatically derived and manually measured photogrammetric data in the thinned stand following the adaptive wavelet filter (Strategy 3).

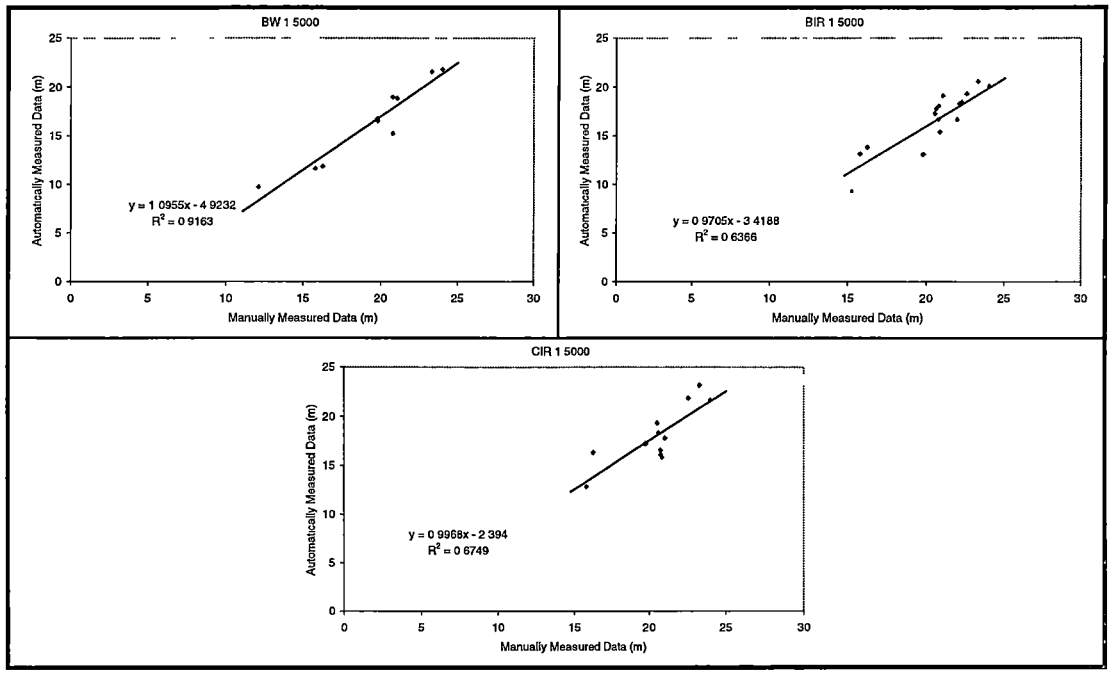

Figure 7.9: Relationship between the automatically derived and manually measured photogrammetric data in the thinned stand following the adaptive Fourier filter (Strategy 4).

μ=mean σ=standard deviation D=DPW–AS ρ=correlation		BW 5000	BIR 5000	BIR 10000	CIR 5000	COL 5000
Strategy 2 Raw→Median→Linear Correction	μ (m) ±σ (m)		13.9±6.6	11.5±7.1	12.3±6.9	15.5±6.5
	μ_D (m) ±σ_D (m)		-0.2±3.7	-7.2±7.0	-6.4±6.7	-3.2±6.1
	ρ		0.90	0.23	0.27	0.35
	<1m		23.0	12.6	16.8	17.8
	1–2m		19.3	10.6	13.7	16.7
	2–4m		22.1	10.8	15.2	24.2
	4–8m		32.1	9.5	10.3	15.2
	>8m		3.4	56.4	44.1	26.1
Strategy 3 Raw→Wavelet→Linear Correction	μ (m) ±σ (m)		16.9±4.1		14.3±6.6	15.3±6.7
	μ_D (m) ±σ_D (m)		-1.9±3.2		-4.5±6.5	-3.4±6.2
	ρ		0.64		0.28	0.37
	<1m		28.0		11.0	15.3
	1–2m		24.3		11.1	14.9
	2–4m		30.5		20.2	23.9
	4–8m		12.6		20.5	19.0
	>8m		4.6		37.2	26.9
Strategy 4 Raw→Fourier→Linear Correction	μ (m) ±σ (m)	8.3±5.2	18.2±3.5		14.9±5.2	
	μ_D (m) ±σ_D (m)	-10.4±5.2	-0.5±2.8		-3.8±5.3	
	ρ	0.28	0.63		0.27	
	<1m	4.1	37.9		15.4	
	1–2m	5.0	28.1		14.5	
	2–4m	9.2	24.0		19.9	
	4–8m	10.1	7.1		20.9	
	>8m	71.7	3.0		29.3	
Strategy 5 Raw→Median→Linear Correction→MTT	μ (m) ±σ (m)		21.1±2.5	20.7±3.9	20.5±3.6	22.0±3.2
	μ_D (m) ±σ_D (m)		0.5±1.5	0.1±3.5	-0.1±3.1	1.4±2.7
	ρ		0.82	0.44	0.52	0.57
	<1m		54.0	30.4	38.1	21.4
	1–2m		29.9	28.1	26.0	23.6
	2–4m		14.2	30.6	26.5	39.3
	4–8m		1.9	4.6	6.2	14.1
	>8m		0.1	6.3	3.2	1.6
Strategy 6 Raw→Wavelet→Linear Correction→MTT	μ (m) ±σ (m)		21.2±2.6		22.9±3.9	22.7±3.7
	μ_D (m) ±σ_D (m)		0.6±1.6		2.3±3.4	2.1±3.1
	ρ		0.81		0.51	0.55
	<1m		50.4		10.8	17.8
	1–2m		30.2		12.6	16.1
	2–4m		16.6		41.6	36.6
	4–8m		2.7		32.5	27.4
	>8m		0.1		2.5	2.1
Strategy 7 Raw→Fourier→Linear Correction→MTT	μ (m) ±σ (m)	16.2±4.2	21.9±2.1		21.6±2.9	
	μ_D (m) ±σ_D (m)	-4.4±3.9	1.3±1.4		1.0±2.6	
	ρ	0.40	0.81		0.51	
	<1m	12.5	36.1		23.8	
	1–2m	21.4	33.4		29.8	
	2–4m	28.7	27.6		36.6	
	4–8m	17.5	2.8		7.9	
	>8m	19.9	0.1		1.9	

Table 7.2: Statistical results and absolute difference distribution (%) between DPW data from analytical stereoplotter data after tree height refinement for the thinned stand.

Again, comparing the statistical results at this stage is not useful because the DPW data still contained terrain measurements. The more useful way is to compare the height profiles of each model (Figure 7.10). Visual inspection shows that the canopy surface for all DPW data was comparable with the analytical

stereoplotter data, except for the 1:5,000 scale black and white model.

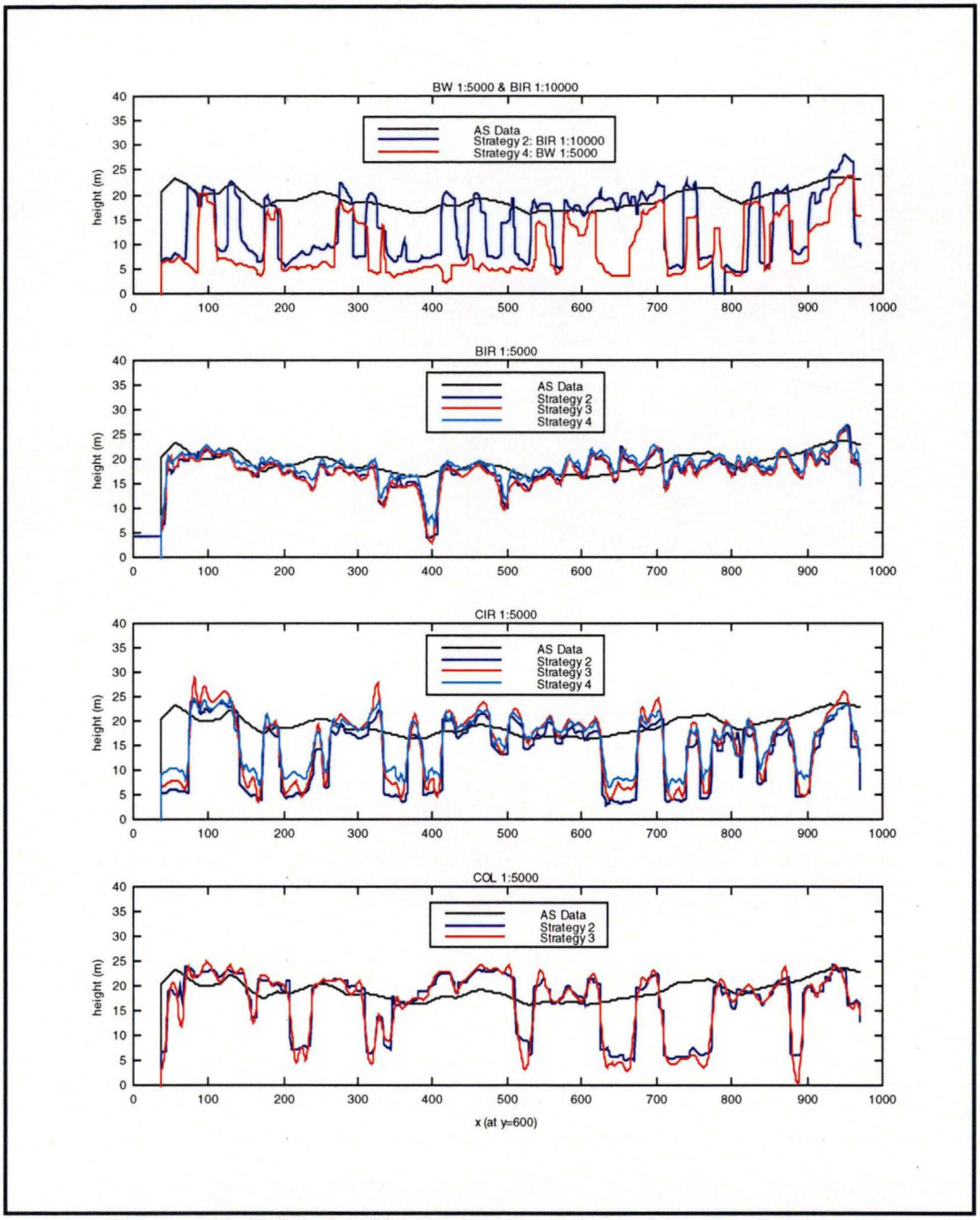

Figure 7.10: Height profiles for the filtered raw data after linear correction (thinned stand).

For the thinned stand, the same MTT filter (25m×25m or 50×50 pixels) was applied to the refined photogrammetric data. The results are summarised in Table 7.2. The height distributions are presented in Figure 7.11 and example image profiles are given in Figure 7.12.

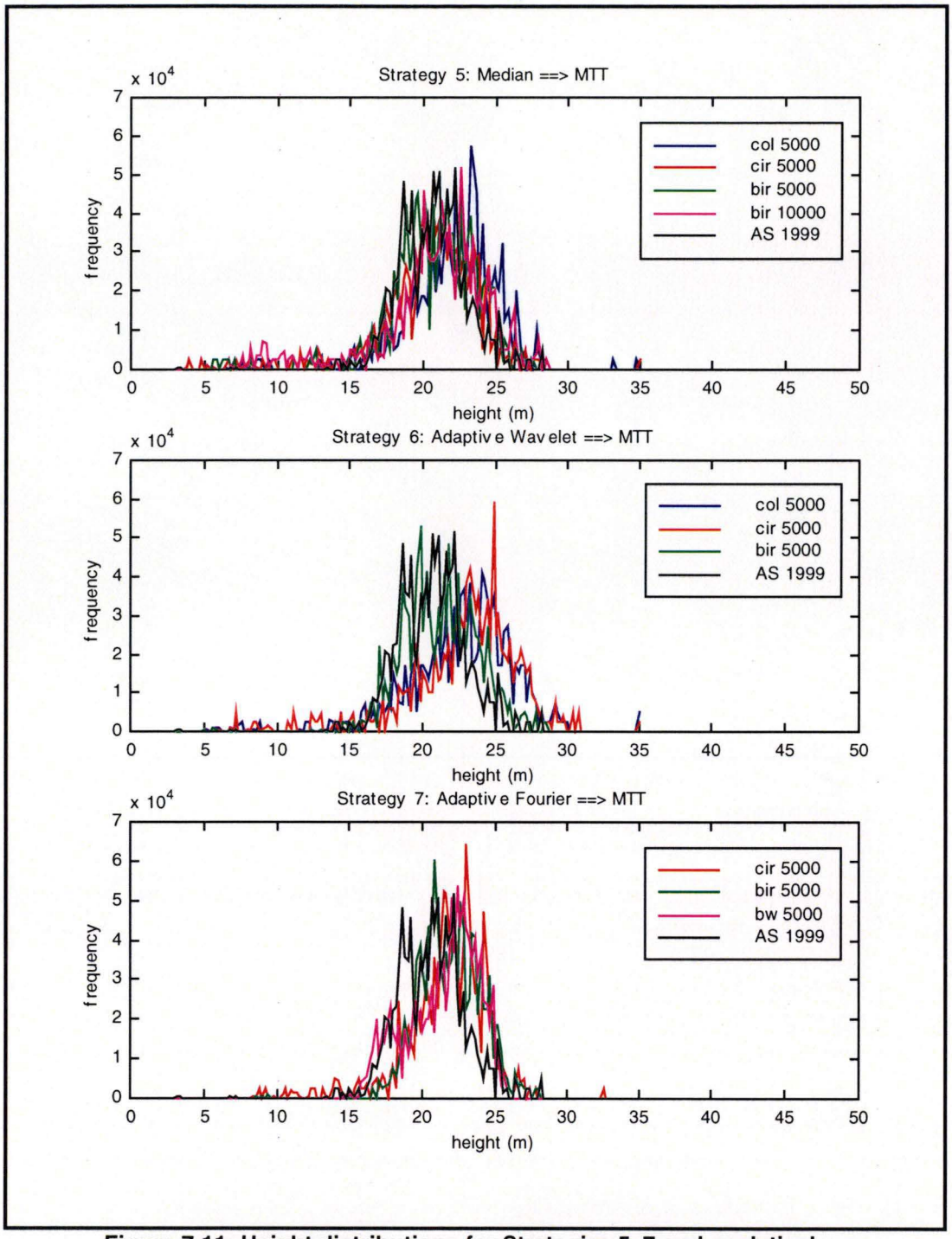

Figure 7.11: Height distributions for Strategies 5–7 and analytical stereoplotter MTT data in the thinned stand after linear transformation. Tree height data have been rounded to the nearest 0.2m.

As expected, the MTT filter increased significantly the mean heights of the DPW data in all strategies, and reduced the standard deviations of the DPW data and the mean differences between the DPW and analytical stereoplotter data. The correlation between the DPW and analytical stereoplotter data was also improved significantly, with the black and white infrared having the highest correlation

(ρ>0.80).

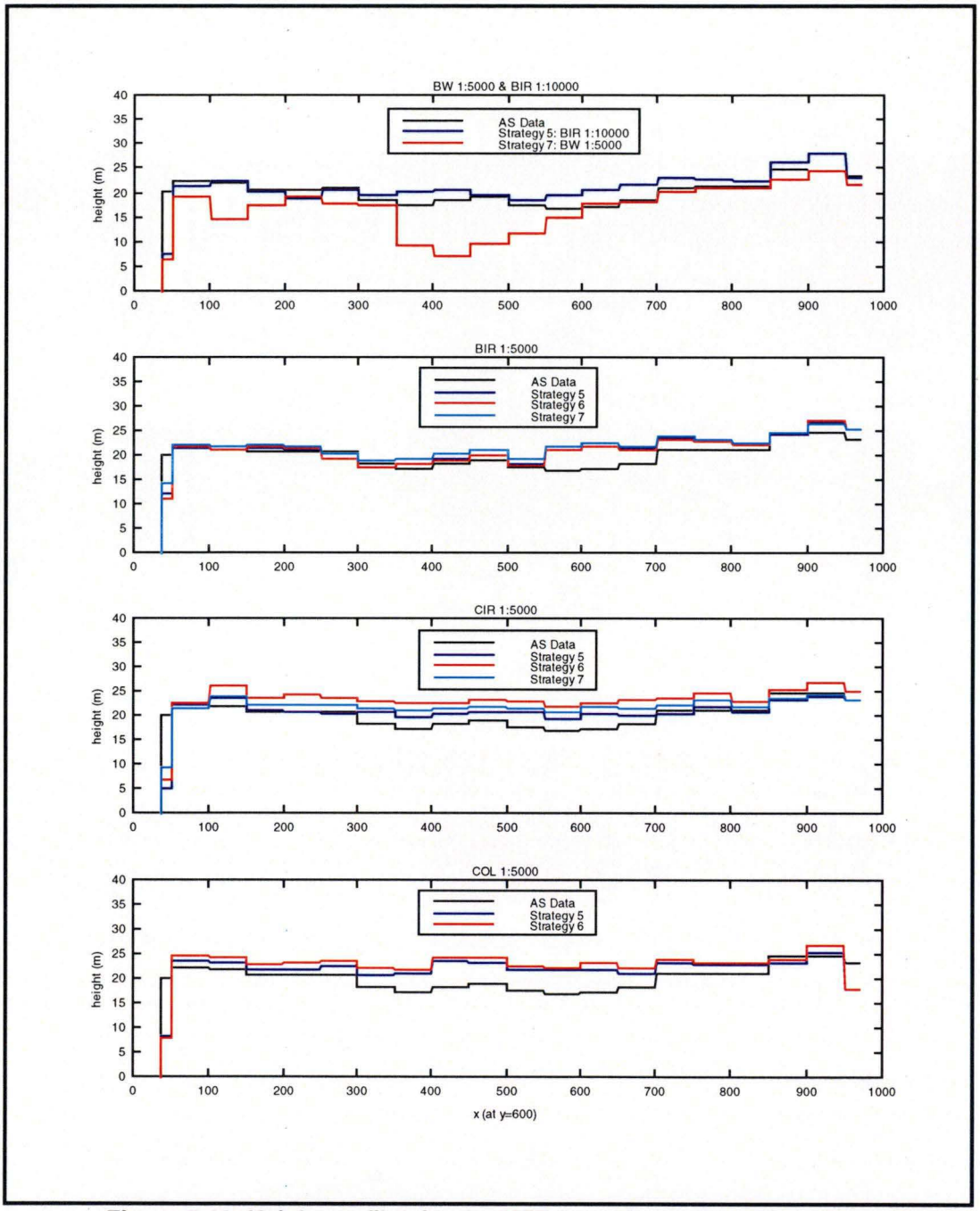

Figure 7.12: Height profiles for the MTT data after tree height refinement (thinned stand).

Following the MTT filter, all DPW data were comparable to the analytical stereoplotter MTT data, except for the 1:5,000 scale black and white model. All DPW MTT data overestimated the analytical stereoplotter data, except for the 1:5,000 scale colour infrared following the median filter which underestimated the analytical MTT data by 0.1m. The amount of overestimation ranged from 0.1m

(using the 1:10,000 scale black and white infrared) to 2.3m (using the 1:5,000 scale colour infrared following the adaptive wavelet filter).

Visual inspection of the height distributions indicates that all DPW MTT data following the median and adaptive Fourier filters, and the 1:5,000 scale black and white infrared following the adaptive wavelet filter were similar to the analytical stereoplotter MTT data.

Visual inspection of the image profiles indicates that the DPW MTT data were similar to the analytical stereoplotter MTT data, again, except for the 1:5,000 scale black and white model.

7.5. Summary

A method for improving automatically derived tree height using a limited number of tree heights measured manually on the DPW has been developed.

In the closed canopy stand, the correlations between the automatically derived and manually measured photogrammetric tree heights were high and within the gradient limit for almost all models. A maximum of ten points measured across the area was sufficient to model the linear correlation between the automatically derived and manually measured photogrammetric data. The results after tree height refinement were good for almost all models, with tree heights shown to be comparable with the analytical stereoplotter data.

In the thinned stand, the correlations between the automatically derived and manually measured photogrammetric tree heights were high and within the gradient limit for most of the 1:5,000 models, but not for most of the 1:10,000 models. The eighteen points used to model the relationship between the automatic and manual data were sufficient. All of the 1:5,000 models, except the black and white model, produced results which were comparable with the analytical stereoplotter data, particularly following the MTT filter.

Chapter 8. Summary and Conclusions

8.1. Review of Research Objectives and Methodology

The objectives of this study, as stated in Chapter 1, were to determine whether high resolution scanned aerial photographs can be used to estimate canopy height in a Radiata pine plantation, and to develop methods to represent the extracted data in a form that can contribute to forest inventory and management. To achieve these objectives, the research has been constructed in four steps:

1. Extraction of a DEM over pine plantation forests

While the limitations of using automatic area based matching in a complex forest canopy were acknowledged, the potential benefits of generating a dense DEM with a 100% coverage were considered to make photogrammetric techniques worthy of consideration. A digital photogrammetric workstation, the Leica-Helava DPW 770, that uses area based image matching techniques, was used to generate digital canopy height data using different photo scales and film types.

2. Extraction of canopy height models

Canopy height models were derived by subtracting a digital terrain model from the corresponding photogrammetrically derived digital canopy data. The DTM was generated using GPS in the closed canopy stand, and both photogrammetric and terrestrial surveying techniques in the thinned stand. Terrain data can also be collected using alternative methods such as historical photography prior to plantation, radar, or laser technology.

3. Post–processing of DPW data

Various different filters, and combination of filters, were employed to remove outliers, to smooth the digital data, and to extract tallest tree data. These filters

were a median filter, adaptive wavelet filter, adaptive Fourier filter, mean tallest tree filter, and an NDVI filter.

In order to measure the accuracy of the raw and filtered DPW data, reference canopy height data was derived using an analytical stereoplotter. While the limitations of using a human operator on an analytical stereoplotter to measure tree height, and the difference in sampling rates between the digital photogrammetric data and analytical stereoplotter data were acknowledged, the reference data derived from the analytical stereoplotter were capable of providing comparative data over the whole plantation rather than just a sample. The accuracy of the analytical stereoplotter data was confirmed using field measurements.

4. **Improving photogrammetric data using a limited number of manually measured photogrammetric measurements**

In order to remove systematic errors from the digital photogrammetric data, a limited number of tree heights were manually measured using the DPW. The parameters that represent the linear relationship between the automatically derived photogrammetric data and manually measured photogrammetric data were applied to the photogrammetric data.

8.2. Summary of Results

For the closed canopy stand, the digital photogrammetric data compared well with the analytical stereoplotter for all types of film and photographic scales. The best results were obtained using the 1:5,000 scale colour photography, a median filter, and a linear transformation of the filtered data using at least 6 manually measured photogrammetric heights.

For the thinned stand, the 1:5,000 scale colour and the 1:5,000 scale black and white infrared films produced the most reliable results. In combination with a Fourier filter, mean tallest tree filter, and linear transformation of the measured heights using at least 6 manually measured photogrammetric heights, the results were most consistent and comparable with the analytical stereoplotter. Useful mean tallest tree estimates can be derived from the photogrammetric data, however improved crown identification algorithms are required in order to provide reliable information at higher spatial resolutions.

8.3. Conclusions and Recommendations for Future Work

The results indicate that high resolution scanned aerial photography can be used to estimate canopy height in Radiata pine plantations, and can contribute to forest inventory and management. As a result of this study, some conclusions can be drawn about the use of a digital photogrammetric workstation for mapping tree heights within a pine plantation with respect to the objectives, methodology and limitations of the research:

1. Tree heights in a closed canopy and open canopy Radiata pine plantation can be mapped using a digital photogrammetric workstation and high resolution scanned aerial photography provided that the raw photogrammetric data is appropriately postprocessed.
2. Images derived from colour and black and white infrared film perform better than black and white and colour infrared. Colour photography is routinely acquired by forest managers and provides cost advantages, and so is likely to be the preferred choice. Images derived from 1:5,000 scale photography performed better than 1:10,000 scale photography.
3. The selection of optimum postprocessing filter varies and needs to be determined by the operator through comparison with manual photogrammetric measurements or ground truth data.
4. In comparison with analytical stereoplotter data, in the best case – in the closed canopy stands – accuracy of 0.4m (mean absolute error) was achieved using the 1:5,000 scale colour imagery.
5. Additional linear corrections applied to the filtered data using manually measured data produced tree heights more comparable with the analytical data.

However, due to limited time and funding, there are aspects that warrant further investigation, or at least need to be considered when mapping tree height using a digital photogrammetric workstation:

1. It would be worthwhile further investigating the influence of different image matching algorithms and variation of the matching parameters on the height data derived from, particularly, the 1:5,000 colour

photography. Matching algorithms that make greater use of feature based techniques to constrain the area based matching (such as VirtuoZo) may perform better in the thinned stand.

2. The approach taken in this research has been to employ standard photogrammetric techniques and rely on postprocessing to derive reliable data. The techniques developed therefore can be easily and immediately applied in practice. An interesting further investigation would be to employ preprocessing, such as an NDVI classification of colour infrared film, to segment the pine trees within each image, and then to limit image matching to these regions.
3. Of the competing measurement technologies, airborne scanning laser appears to hold the most immediate promise. It seems highly unlikely that there would be sufficient canopy penetration in the closed Radiata pine plantation to make it a viable option; however it might be expected to perform well in open or thinned stand. It would be worthwhile testing a scanning laser over the plantation used in this research in order to compare the two technologies and to assess their potentially complimentary roles.

****

References

IAPRS *International Archives for Photogrammetry and Remote Sensing*

PERS *Photogrammetric Engineering and Remote Sensing*

RSE *Remote Sensing of Environment*

Acker S. 2000. Personal communication with Assistant Professor, Senior Research, Dept. of Forest Science, Oregon State University, USA (contributing author in Means *et al* (1999)). March, 2000.

Ackermann F and Krzystek P. 1995. New investigations into the technical performance of automatic DEM generation. *Proc. ASPRS/ACSM Annual Convention*, Charlotte NC 1995, Vol. 2: 488–500.

Ackermann F. 1988. Digital terrain models of forest areas by airborne laser profiling. *In: High Precision Navigation: Integration of Navigational and Geodetic Methods. Proc. of an International Workshop.* Stuttgart and Altensteig, May 1988: 239–250.

Ackermann F. 1996. Some consideration about feature matching for the automatic generation of digital terrain models. *Official Publication OEEPE.* 33: 231–240.

Aldred AH and Bonnor GM. 1985. Application of airborne lasers to forest surveys. Petawawa National Forestry Institute, Chalk River, Ontario. Inf. Rep. PI–X–51. 62pp.

Aldred AH and Kippen FW. 1967. Plot volumes from large–scale 70mm air photographs. *Forest Science.* 13(4): 419–426.

Allison GW. 1956. The accuracy of tree height measurements on various qualities of aerial photographs. *Forestry Chronicle.* 32: 444–450.

Anderson GL, Hanson JD and Haas RH. 1993. Evaluating Landsat Thematic Mapper derived vegetation indices for estimating aboveground biomass on semiarid rangelands. *RSE.* 45: 165–175.

Andrews GS. 1936. Tree heights from air photographs by simple parallax measurements. *Forestry Chronicle.* 12(2): 152–197.

Anger CD, Mah S, and Babey SK. 1994. Technological enhancement to the compact airborne spectrographic Imager (CASI). *Proc. First Int. Airborne Rem. Sens. Conf. and Exh.*. Sept. 11–15, Strasbourg, France. 2: 205–213.

Antonini M, Barlaud M, Mathieu P, and Daubechies I. 1992. Image coding using the wavelet transform. *IEEE Trans. On Image Processing*. Vol. 1: 205–220.

Avery TE and Canning J. 1973. Tree measurements on large–scale aerial photographs. *Can.For.Serv., For.Manage.Inst., Inf.Rep. FMR–X–40.* 43pp.

Babey SK and Anger CD. 1993. Compact airborne spectrographic imager (CASI): a progressive review. *Proc. SPI.E.* 1937: 152–163.

Baltsavias E. 1998. Photogrammetric film scanners. *Geomatics Info Magazine.* July 1998. 12: 55–61.

Baltsavias EP and Käser C. 1998. DTM and orthoimage generation – A thorough analysis and comparison of four digital photogrammetric systems. Paper presented at the ISPRS Com. IV Symposium, 7.–10. September, Stuttgart, Germany. In IAPRS, Vol. 32, Part 4, pp. 42–51.

Baltsavias EP, Li H, Stefanidis A, Sinning M and Mason S. 1996. Comparison of two digital photogrammetric systems with emphasis on DTM generation: Case study glacier measurement. *IAPRS.* Vol. XXXI, Part B2, Vienna 1996: 104–109.

Barnard ST and Thompson WB. 1980. Disparity analysis of images. *IEEE–PAMI.* Vol 2 (4): 333–340.

Bercha FG, Currie DH and Dechka JA. 1990. Multi–sensor airborne forest inventory system. *Proc. 23rd Int. Symp. Rem.Sens.* ERIM, Ann Arbor. II: 603–608.

Biging GS, Congalton RG and Murphy EC. 1991. A comparison of photo interpretation and ground measurements of forest structure. *in: Technical papers ACSM–ASPRS annual conv., Baltimore 1991. Vol. 3; Rem.Sens. (ACSM/ASPRS).* 6–15.

Blair JB, Rabine DL and Hofton MA. 1999. The Laser Vegetation Imaging Sensor: a medium–altitude, digitisation–only, airborne laser altimeter for mapping vegetation and topography. *ISPRS J of Photogram. and Rem. Sens..* 54: 115–122.

Bolstad PV and Stowe T. 1994. An evaluation of DEM accuracy: elevation, slope and aspect. *PERS.* 60: 1327–1332.

Bradshaw FJ and Chandler RJ. 1978. Full coverage at large scale. *Proc. American Society Photogram. Sym. On Rem. Sens. for Vegetation Damage Assessment,* Seattle, Washington, 267–290.

Bradshaw FJ. 1974. Large scale colour photography as an aid to detecting jarrah dieback. *Proc. American Society Photogram. and Rem. Sens. and Photo Interpretation,* Banff, Alberta. 439–448.

Brigham, EO. 1988. *The Fast Fourier Transform and Its Applications.* Prentice Hall. Englewood Cliffs, New Jersey. 448 pp.

Brown RJ. 1987. Preparing for satellite microwave systems for renewable resource management. *Geocarto International.* 3: 31–37.

Bryan ML. 1981. Urban landuse classification using synthetic aperture radar. *Proc. PECORA VII Symp.* Sioux Falls, South Dacota, Oct. 18–21. Pp. 124–143.

Candy SG. 1989a. Compatible tree volume and variable–form stem taper models for Pinus radiata in Tasmania. *New Zealand J. of Forestry Science.* 19(1): 97–111.

Candy SG. 1989b. Growth and yield models for Pinus radiata in Tasmania. *New Zealand J. of Forestry Science.* 19(1): 112–133.

Cappelini V, Alparone L, Galli G, Lange P, Mecocci A, Menichetti L, Capanni G and Carla R. 1991. Digital processing of stereo images and 3–D reconstruction techniques. *Int. J. Rem. Sens..* 12(3): 477–490.

Carron LT. 1968. *An Outline of Forest Mensuration with Special Reference to Australia.* Australian National University Press, Canberra 1968: 86–93.

Carson W, Miller S and Walker A. 1996. Automated forest inventory using a digital photogrammetric workstation. Presented at the *Second Int. Airborne Rem. Sens. Conf. and Exhibition,* San Francisco, California. 24–27 June 1996: 7pp.

Chisholm L and Louis J. 1998. Forest moisture stress mapping using pixel unmixing and multispectral imagery. *Proc. 9th Australasian Rem. Sens. Photogram. Conf..* Sydney, Australia 20–24 July 1998. 9pp.

Congalton RG and Biging GS. 1992. A pilot study evaluating ground reference data collection efforts for use in forest inventory. *PERS.* 58: 1669–1671.

Coulson SN. 1996. SAR interferometry with ERS. *Earth Space Review.* 5(1): 9–16.

Danson FM. 1987. Preliminary evaluation of the relationships between SPOT–1 HRV data and forest stand parameters. *Int. J. Rem. Sens.* 8: 1571–1575.

Daubechies I. 1988. *Commun. Pure and Applied Math.* 41: 909–996.

Davis L and Steentrup M. 1987. Genetic algorithms and simulated annealing: an overview. In: *Genetic Algorithms and Simulated Annealing,* Research notes in artificial intelligence. Edited by Lawrence Davis, Cambridge, Massachusetts. Morgan Kaufmann Pub., Los Altos, CA : 1–11.

DeVore RA , Jawerth B and Lucier BJ. 1992. Image compression through wavelet transform coding. *IEEE Trans. Inform. Theory.* 38(2): 719–746.

Dickinson A and Webb J. 1999. Personal communication with personnel of Fletcher Challenge Paper Australia, New Norfolk, Tasmania, Australia. November.

Dobson MC, Ulaby FT, Pierce LE, Sharik TL, Bergen KM, Kellndorfer J, Kendra JR, Li E, Lin YC, Nashashibi A, Sarabandi K and Siquiera P. 1995. Estimation of forest biophysical characteristics in Northern Michigan with SIR–C/X–SAR. *IEEE Trans. On Geoscience and Rem. Sens..* 33(4) 877–895.

Donoho DL and Johnstone IM. 1994. Ideal spatial adaptation by wavelet shrinkage. *Biometrika.* 81: 425–455.

Donoho DL. 1993. Nonlinear wavelet methods for recovery of signals, densities, and spectra from indirect and noisy data. *Different Perspectives on Wavelets, Proc. of Symposia in Applied Mathematics.* Vol 47, I. Daubechies ed Amer. Math. Soc., Providence, R.I. pp. 173–205.

Donoho DL. 1995. De–noising by soft–thresholding. *IEEE Trans. Inf. Theory.* Vol. 41: 613–627.

Elachi C. 1987. *Introduction to the Physics and Techniques of Remote Sensing.* Wiley, New York. 413pp.

Elhassan IM and Ali AE. 1995. Radargrammetry with Almaz SAR imagery. *Geomatics Research Australasia.* 62: 63–92.

Elvidge CD. 1990. Visible and near infrared reflectance characteristics of dry plant materials. *Int.J.Rem. Sens..* 11(10): 1775–1795.

Fent L, Hall RJ and Nesby RK. 1995. Aerial films for forest inventory: optimising film parameters. *PERS.* 61(3) 281–289.

Ferrazzoli P and Guerriero L. 1995. Radar sensitivity to tree geometry and wood volume – a model analysis. *IEEE Trans. on Geoscience & Rem. Sens..* 33(2): 360–371.

Förstner W. 1982. On the geometric precision of digital correlation. *IAPRS,* Symposium Helsinki, Commission III. 24(3): 176–189.

Förstner W. 1986. A feature–based correspondence algorithm for image matching. *IAPRS.* 26(3/3): 150–166.

Franklin SE. 1994. Discrimination of subalpine forest species and canopy density using digital CASI, SPOT, PLA and Landsat TM data. *PERS.* 60(10): 1233–1241.

Gabriel AK, Goldstein RM and Zebker HA. 1989. Mapping small elevation changes over large areas: differential radar interferometry. *J. Geophys. Res.* 94: 9183–9191.

Gagnon PA, Agnard JP and Nolette C. 1993. Evaluation of a softcopy photogrammetry system for tree plot measurements. *Canadian J. of Forest Research.* 23: 1781–1785.

Gambill CW, Wiant HV Jr, and Yandle DO. 1985. Optimum plot size and BAF. *Forest Science.* 31(3): 587–594.

Gillis MD and Leckie DG. 1996. Forest inventory update in Canada. *Forestry Chronicle.* 72: 138–156.

Gonzalez RC. 1987. *Digital Image Processing.* Addison–Wesley Pub. Company, Inc. 503pp.

Gooch MJ, Chandler JH and Stojic M. 1999. Accuracy assessment of digital elevation models generated using the Erdas Imagine OrthoMAX digital photogrammetric system. *Photogram. Record.* 16(93): 519–531.

Grün AW and Baltsavias EP. 1987. High precision image matching for digital terrain model generation. *Photogrammetria.* 42(3): 97–102.

Grün AW. 1989. Digital photogrammetric processing systems: current status and prospects. *PERS.* 55(5): 581–586.

Hagberg JO, Ulander LMH and Askne J. 1995. Repeat–pass SAR interferometry over forested terrain. *IEEE Transactions on Geoscience & Rem. Sens..* 33(2): 331–340.

Hannah MJ. 1989. A system for digital stereo image matching. *PERS.* 55(12): 1765–1770.

Heipke C. 1992. A global approach for least squares image matching and surface reconstruction in object space. *PERS.* 58(3): 317–323.

Helava UV. 1976. Digital correlation in photogrammetric instruments. *IAPRS.* Congress Helsinki, Com. II, Vol. 21. 26pp.

Helava UV. 1988. Object space least squares correlation. *IAPRS.* 27(B2): 297–302.

Held A and Billings S. 1998. Automatic tree crown recognition and counting from high–resolution casi data. *Proc. 9th Australasian Remote Sensing Photogrammetry Conference.* Sydney, Australia 20–24 July 1998. 5pp.

Henke–Reed MB and Cheng SNC. 1993. Cloth texture classification using the wavelet transform. *J. of Imaging Science and Technology.* 37(6): 610–614.

Horgan G. 1998. Wavelet for SAR image smoothing. *PERS.* 64(12): 1171–1177.

Hosking G. 1994. Airborne video for resource monitoring – a new technology takes off. *What's new in Forest Research,* No. 233. New Zealand Forest Research Institute, Rotorua, NZ. 5pp.

Howard JA. 1990. *Remote Sensing of Forest Resources. Theory and applications.* Chapman & Hall. London. 420pp.

Hyyppä J and Hallikainen M. 1996. Applicability of airborne profiling radar to forest inventory. *RSE.* 57: 39–57.

Imhoff ML. 1995. Radar backscatter and biomass saturation – ramification for global biomass inventory. *IEEE Transactions on Geoscience & Remote Sensing.* 33(2): 511–518.

Jaakkola S and Saukkola P. 1979. Timber volume estimation and cutting opportunity mapping using multispectral remote sensing techniques. *Photogram. J. of Finland.* 8(1): 1–56.

Jacobs DM, Evans DL and Ritchie JC. 1993. Laser profiler and aerial video data for forest assessments. *Proc. ACSM/ASPRS Annual Convention,* New Orleans, LA, Feb. 15–18, *ASPRS,* Vol. II: 135–142.

Johnson EW. 1954. Shadow–height computations made easier. *Journal of Forestry.* 52: 438–442.

Johnson EW. 1958. Effect of photographic scale on precision of individual tree measurement. *Photogram. Eng..* 24(1): 142–152.

Kendall MG and Stuart A. 1969. *The Advanced Theory of Statistics.* Vol. 1, Charles Griffin and Co.Ltd., London. 439pp.

King DJ and Vlcek J. 1990. Development of multispectral video system and its application in forestry. *Canadian Journal Remote Sensing.* 16(1): 15–22.

Kippen FW and Sayn–Wittgenstein L. 1964. Tree measurement on large–scale, vertical, 70–mm air photographs. *Canada, Dept. of Forestry, Publication No. 1053.* 16pp.

Kirkpatrick S, Gelatt CD and Vecchi MP. 1983. Optimisation by simulated annealing. *Science.* 220: 671–680.

Korning J and Thomsen K. 1994. A new method for measuring tree height in tropical rain forest. *Journal of Vegetation Science.* 5(1): 139–140.

Kovats M. 1997. A large–scale aerial photographic technique for measuring tree heights on long–term forest installations. *PERS.* 63(6): 741–747.

Krabill WB, Collins JG, Link LE, Swift RN and Butler ML. 1984. Airborne laser topographic mapping results. *PERS.* 50(6): 685–694.

Kreyszig, E. 1972. *Advanced Engineering Mathematics.* John Wiley and Son.

866pp.

Lewis R. 1990. *Practical Digital Image Processing*. Ellis Horwood Ltd. 1990: 238pp.

Li Z. 1992. Variation of the accuracy of digital terrain models with sampling interval. *Photogrammetric Record.* April 1992. 14(79): 113–128.

Liew AWC, Law NF, and Nguyen DT. 1997. Multiple resolution wavelet restoration. *IEEE Proc.: Vision, Image and Signal Processing.* 144(4): 199–206.

Light DL. 1996. Film camera or digital sensors? The challenge ahead for digital imaging. *PERS.* 62(3): 285–291.

Lillesand TM and Kiefer RW. 1994. *Remote Sensing and Image Interpretation.* Wiley and Sons. New York. 750pp.

Lohmann P, Luken C and Picht G. 1990. Digital photogrammetric workstation. *IAPRS.* 28(2): 283–294.

Long, Y. 1994. *Integrating Satellite and Ancillary Data to Predict Site Quality.* Thesis submitted for the degree of Doctor of Philosophy of the Australian National University. August 1994: 252 pp.

Lowe I, Oswald B, Coleman TI, Tadesse W, Everitt JH, Escobar DE and Davis MR. 1995. Comparison of conventional ground sampling and remote sensing techniques for mapping forest vegetation. *Proc., 15th Biennial Workshop on Colour Photography and Videography in Resource Assessment.* Terre Haute, Indiana, May 2–3, American Society of Photogrammetry and Remote Sensing. 31–52.

Lyons EH. 1967. Forest sampling with 70mm fixed air–based photography from helicopters. *Photogrammetria.* 2: 213–231.

Mallat S and Zhong S. 1992. Characterisation of signals from multiscale edges. *IEEE Trans. Pattern Machine Intelligence.* 14: 710–732.

Mallat S. 1989a. Multifrequency channel decomposition of images and wavelet models. *IEEEE Trans.Acoust. Speech Signal Process.* 37(12): 2091–2110.

Mallat S. 1989b. IEEE Trans. Pattern Machine Intelligence. 11: 674–693.

Mason B Jr. 1953. The hotspot in wide–angle photographs. *Photogramm. Eng.* 19: 619–625.

Massonnet D, Briole P, and Arnaud A. 1995. Deflation of Mount Etna monitored by spaceborne radar interferometry. *Nature.* 375: 567–570.

Massonnet D, Rossi M, Carmona C, Adragna F, Peltzer G, Feigl K, and Rabaute T. 1993. The displacement field of the Landers earthquake mapped by radar interferometry. *Nature.* 364: 138–142.

Matlab Version 5.2.0.3084. 1998. The MathWorks, Inc.

McColl WD, Neville RA and Till SM. 1983. Multi–detector Electro–optical Imaging Scanner MEIS II. *Proc. 8th Canadian Symp. Remote Sensing,* Montreal, Quebec, May 3–6: 71–79.

Means JE, Acker SA, Harding DJ, Blair JB, Lefsky MA, Cohen WB, Harmon ME and McKee WA. 1999. Use of large–footprint scanning airborne Lidar to estimate forest stand characteristics in the Western Cascades of Oregon. *RSE.* 67: 298–308.

Medioni G and Nevatia R. 1985. Segment–based stereo matching. *Computational and Graphical Image Processing.* 31: 2–18.

Miller SB and Devenecia K. 1992. Automatic elevation extraction and the digital photogrammetric workstation. In *ASPRS Technical Papers, 1992 ASPRS–ACSM Annual Convention, Albuquerque.* February, Vol. 1: 572–580.

Milne A, Morgan G and Orr T. 1996. SAR data in the Northern Territory. *The Australian GIS Applic. Journal.* 15: 21–24.

Naesset E. 1997a. Estimating timber volume of forest stands using airborne laser scanner data. *RSE.* 61:246–253.

Naesset E. 1997b. Determination of mean tree height of forest stands using airborne laser scanner data. *ISPRS J. of Photogram. & Rem. Sens..* 52: 49–56.

Nelson R, Case D, Horning N, Anderson V and Pillai S. 1987. Continental land cover assessment using Landsat MSS data. *RSE.* 21 : 61–68.

Nelson R, Krabill W and Maclean G. 1984. Determining forest canopy characteristics using airborne laser data. *RSE.* 15: 201–212.

Nelson R, Krabill W and Tonelli J. 1988. Estimating forest biomass and volume using airborne laser data. *RSE.* 24: 247–267.

Neville RA, Marois R, Schwartz and Till SM. 1992. Wide–angle high–resolution line–imager prototype flight test results. *Applied Optics.* 31(18): 3463–3472.

Nielsen U. 1997. Operational resource data collection using large–scale aerial photography. *Proc. of the First American Symposium on Small Format Aerial Photography.* ASPRS. October 14–17, 1997: 37–44.

Nilsson M. 1996. Estimation of tree heights and stand volume using an airborne Lidar system. *RSE.* 56: 1–7.

Nilsson NJ. 1982. *Principles of Artificial Intelligence.* Tioga Publishing Company, Palo Alto, CA. 476p.

Paine DF. 1981. *Aerial Photography and Image Interpretation for Resource Management.* John Wiley & Sons. New York. 571p.

Pearl J. 1984. Heuristics: Intelligent Search Strategies for Computer Problem Solving. Addison–Wesley, Reading, MA. 382p.

Pertl A. 1985. Digital Image correlation with an analytical plotter. *Photogrammetria.* 40: 9–19.

Pilard M and Epelboin Y. 1998. Multiresolution analysis for the restoration of noisy x–ray topographs. *Journal of Applied Crystallography.* 31(1): 36–46.

Pitt DG, Wagner RG, Hall RJ, King DJ, Leckie DG and Runesson U. 1997. Use of remote sensing for forest vegetation management: A problem analysis. *The Forestry Chronicle.* 73(4): 459–477.

Poso S, Häme T and Paananen R. 1984. A method of estimating the stand characteristics of a forest compartment using satellite imagery. *Silva Fennica.* 18(3): 261–292.

Poso S, Paananen R and Similä M. 1987. Forest inventory by compartment using satellite imagery. *Silva Fennica..* 21:69–94.

Ranson KJ and Sun G. 1994. Mapping biomass of a Northern forest using

multifrequency SAR data. *IEEE Transactions on Geoscience & Remote Sensing.* 32(2): 388–395.

Reich RM and Hussin YA. 1993. Estimating average stand biomass for a regional forest inventory using radar backscatter. *ITC Journal.* 1: 82–87.

Reutebuch SE and Ahmed KM. 1997. Monitoring stand development within the Mt. St. Helens blast zone using a twin–camera helicopter boom. *Proc. of the First American Symposium on Small Format Aerial Photography.* ASPRS. October 14–17, 1997: 173–185.

Rieger W. 1996. Accuracy of slope information derived from DEM–data. In Kraus K and P Waldhäeusl, editor. *IAPRS* (Vol. 31, Part B4, Commission IV), Vienna: Austrian Society of Surveying and Geoinformation, 690–695.

Rignot EJ, Zimmermann R and van Zyl JJ. 1995. Scapeborne applications of P band imaging radars for measuring forest biomass. *IEEE Transactions on Geoscience & Remote Sensing.* 33(5): 1162–1169.

Rosenfeld A and Kak AC. 1982. *Digital Picture Processing.* Second Edition Volume I. Academic Press. 435pp.

Rosenholm D. 1987a. Least squares matching method: some experimental results. *Photogrammetric Record.* 12(70): 493–512.

Rosenholm D. 1987b. Multi–point matching using least–squares technique for evaluation of three–dimensional models. *PERS.* 31(3): 223–239.

Sader SA, Waide RB, Lawrence WT and Joyce AT. 1989. Tropical forest biomass and successional age class relationships to a vegetation index derived from Landsat TM data. *RSE.* 28: 143–156.

Sayn–Wittgenstein L and Aldred AH. 1967. Tree volumes from large–scale photos. *Photogrammetric Engineering.* 33(1): 69–73.

Schenk T, Li JT, and Toth C. 1991. Toward an autonomous system for orienting digital stereo pairs. *PERS.* 57(8): 1057–1064.

Schott, JR. 1997. *Remote Sensing: The image Chain Approach,* Oxford University Press, New York, 1997. Pp 148–153.

Schowengerdt RA. 1997. *Remote Sensing: Models and Methods for Image Processing.* Academic Press, San Diego, CA, USA. 522pp.

Shapiro LG and Haralick RM. 1987. Relational matching. *Applied Optic.* 26(10): 1845–1851.

Simhadri KK, Iyengar SS, Holyer RJ, Lybanon M, and Zachary JM. 1998. Wavelet–based feature extraction from oceanographic images. *IEEE Trans. on Geoscience & Rem.Sens.* 36(3): 767–778.

Slymaker DM, Jones KML, Griffin CR and Finn JT. 1995. *Mapping Deciduous Forests in New England Using Aerial Videography and Multi–temporal Landsat TM Imagery.* Amherst, Massachusetts: Dept. of Forestry and Wildlife Management, University of Massachusetts, 15pp.

Smith MJ and Smith DG. 1996. Operational experiences of digital photogrammetric systems. *IAPRS.* Vol. XXXI, Part B2. Vienna 1996: 357–362.

SOCET SET® User's Manual. 1996.

Spencer RD. 1979. Fixed–base large scale photographs for forest sampling.

Photogrammetria. 35: 117–140.

Starck JL and Bijaoui A. 1992. *Signal Processing*. 35: 195–211.

Stojic M, Chandler J, Ashmore P and Luce J. 1998. The assessment of sediment transport rates by automated digital photogrammetry. *PERS*. 64(5) 387–395.

Strahler AH and Li X. 1981. An invertible coniferous forest canopy reflectance. *Proc. 15th Int. Symp. Rem. Sens. Environ.*, Ann Arbor, Michigan, ERIM. 1237–1244.

Strang G. 1992. Wavelets. *American Scientist*. Vol. 82: 250–255.

Sun GQ and Ranson KJ. 1995. A three–dimensional radar backscatter model for forest canopies. *IEEE Transactions on Geoscience & Remote Sensing*. 33(2): 372–382.

Susilawati S and Weir MJ. 1990. GIS application in forest land management in Indonesia. *ITC Journal*. Vol. 3: 236–244.

Titus SJ and Morgan DJ. 1985. Tree height: can large–scale photo measurements be more accurate than field measurements? *Forestry Chronicle*. 61(3): 214–217.

Turner BJ, Moore DM and Skidmore AK. 1987. Forest management applications of SPOT data in Australia. *Proc. SPOT–1 Image Utilisation, Assessments, Results Symposium*, Paris, France.

Van Halsema E and Hanssen R. 1996. Radar interferometry: A new tool for accurate height modelling. *GIM International Journal for Geomatics*. January 1996: 27, 29, and 31.

Van Zyl JJ. 1996. Keynote – Radar – Success stories and future prospects. Proceeding of the 8th Australasian Remote Sensing Conference, 26–29 March 1996, Canberra, Australia: 19–25.

Vosselman G. 1992. *Lecture Notes in Computer Science: Relational Matching*. Springer–Verlag Berlin Heidelberg 1992: 628p.

Vosselman G. 1994. Use of tree search in digital photogrammetry. *IAPRS*. 30(3/2): 886–893.

Wang Z, Krupnip A, Zong J, and Schenk T. 1993. An iterative image/object space matching strategy for determining surface points. *In: Looking to the Future with an Eye on the Past, ACSM/ASPRS Conference Proceedings*: 392–401.

Wang Z. 1990. *Principles of Photogrammetry (With Remote Sensing)*. Press of Wuhan Technical University of Surveying and Mapping, Publishing House of Surveying and Mapping, Beijing. 575pp.

Weaver HJ. 1983. *Application of Discrete and Continuous Fourier Analysis*. A Wiley–Interscience publication. John Wiley & Sons, US. 375pp.

Wehr A and Lohr U. 1999. Airborne laser scanning–an introduction and overview. *ISPRS J. of Photogram. & Rem. Sens.*. 54: 68–82.

Weishampel JF, Sun G, Ranson KJ, LeJeune KD and Shugart HH. 1994. Forest textural properties from simulated microwave backscatter: The influence of spatial resolution. *RSE*. 47: 120–131.

Welch R. 1968. Film transparencies vs paper prints. *Photogr. Eng.*. 34: 490–501.

Wilson BA. 1996. Estimating coniferous forest structure using SAR texture and

tone. *Canadian J. of Remote Sensing*. 22(4): 382–389.

Worley DP and Landis GH. 1954. The accuracy of height measurements with parallax instruments on 1:12,000 photographs. *Photogrammetric Engineering*. 20(5): 823–829.

Wright R. 1993. Airborne videography: principles and practice. *Photogrammetric Record*. 14(81): 447–457.

Wrobel B. 1991. Least squares methods for surface reconstruction from images. *ISPRS J. of Photogram. and Rem. Sens.* 46: 67–84.

Young RK. 1993. *Wavelet theory and its applications*. Kluwer Academic Publishers, Boston. 223pp.

Zhang J, Zhang Z, Shen W and Wang Z. 1996. Virtuozo digital photogrammetry system and its theoretical foundation and key algorithms. *IAPRS*. Vol. XXXI, Part B2. Vienna 1996: 424–429.

Zhang Z. 1989. A new approach of epipolar–line image matching – bridging mode. Acta Geodetica et Cartographic Sinica 1989 (English version): 34–45.

Zhang Z. 1990. Extension of the concept of feature bridging mode method and global image matching. *Proc. of the Symposium of Progress in Data Analysis*. ISPRS Comm. III. Wuhan, China: 1106–1120.

APPENDIX

Graphical User Interface

The following screen images illustrate the graphical user interface developed for the post-processing routines.

Main menu

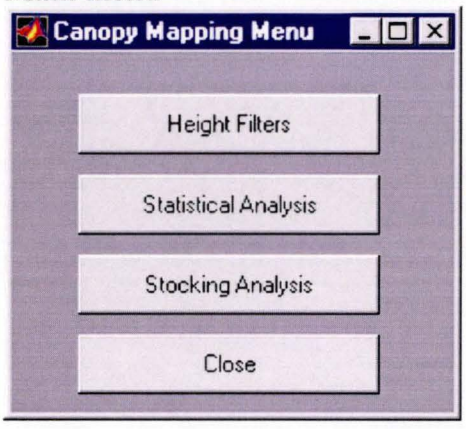

Tree Height Filter Menu

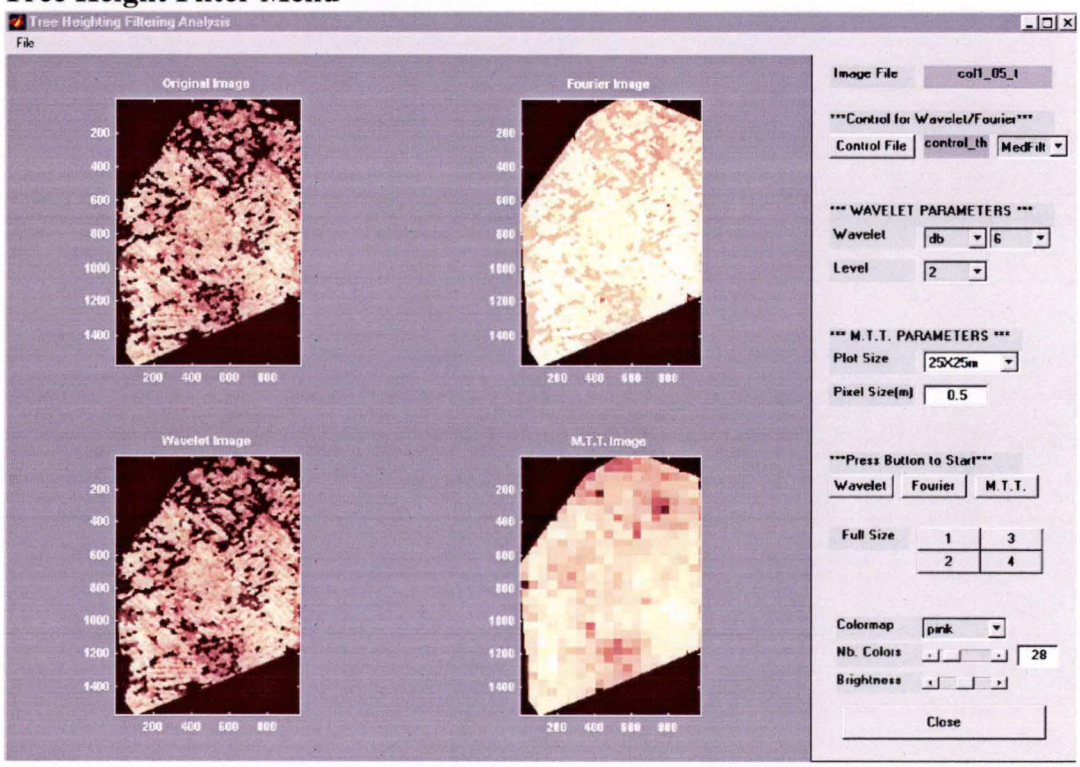

Analysis: Image Profiles

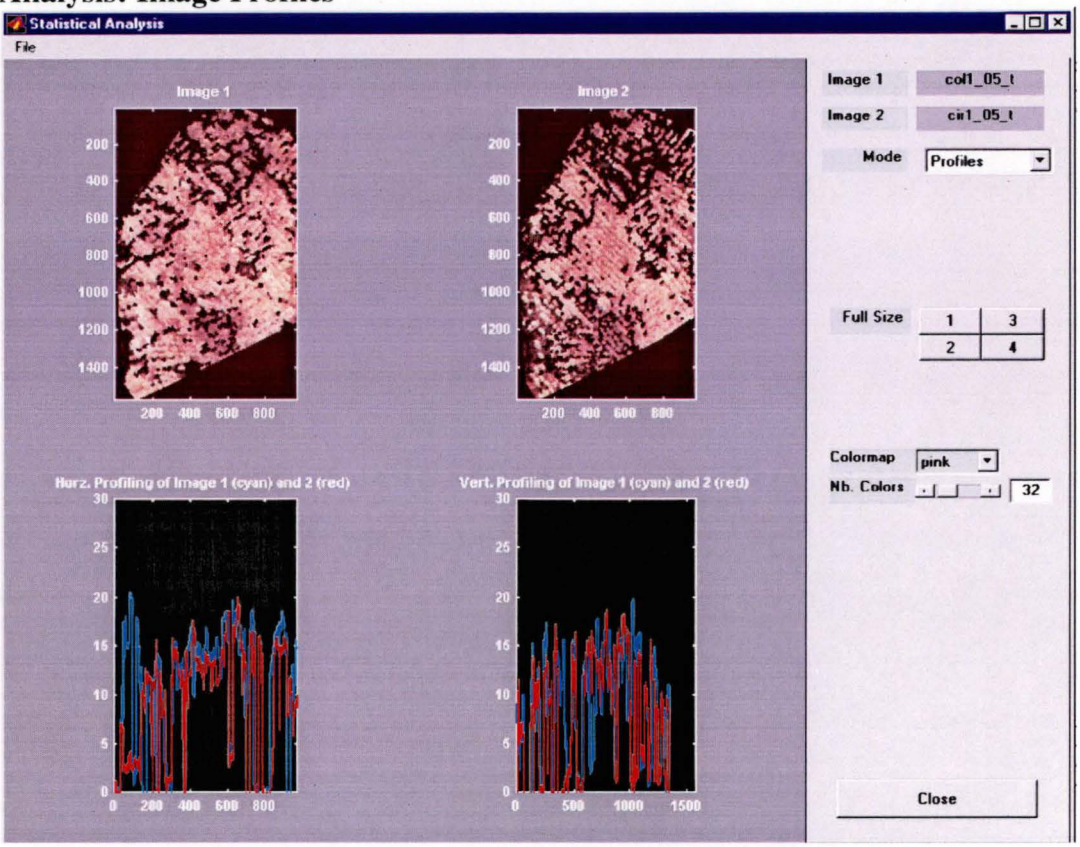

Analysis: Zooming

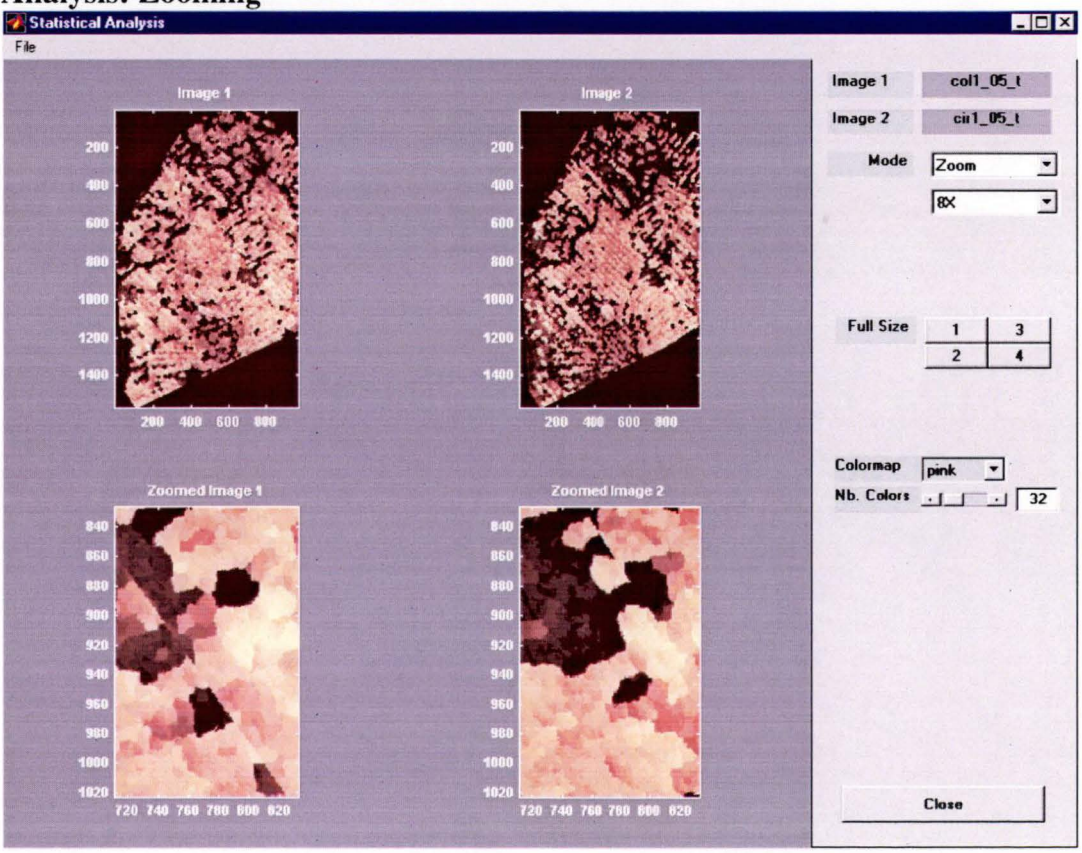

APPENDIX

List of Figures

APPENDIX

List of Tables